THE UNIVERSITY
of EDINBURGH

This thesis has been submitted in fulfilment of the requirements for a postgraduate degree (e.g. PhD, MPhil, DClinPsychol) at the University of Edinburgh. Please note the following terms and conditions of use:

This work is protected by copyright and other intellectual property rights, which are retained by the thesis author, unless otherwise stated.
A copy can be downloaded for personal non-commercial research or study, without prior permission or charge.
This thesis cannot be reproduced or quoted extensively from without first obtaining permission in writing from the author.
The content must not be changed in any way or sold commercially in any format or medium without the formal permission of the author.
When referring to this work, full bibliographic details including the author, title, awarding institution and date of the thesis must be given.

Transcriptional Analysis of Astrocytes Reveals Protective Functions during Remyelination

Irene Molina-González

Doctor of Philosophy
THE UNIVERSITY OF EDINBURGH
2020

ABSTRACT

In Multiple Sclerosis (MS), the insulating membrane that ensheaths axons termed myelin, is lost by a process known as demyelination. Initial regeneration of myelin, termed remyelination, restores neuronal function. However, remyelination failure with disease leads to a loss of cognitive, sensory and motor functions. There are no currently approved therapies aimed at inducing remyelination, highlighting the need to investigate new targets that can promote this process. Astrocytes are the most abundant glial cell type in the central nervous system (CNS). They are known to support myelin formation in development and its maintenance during adulthood, yet their roles during remyelination are controversial and remain poorly understood.

The work from this thesis explores the changes in astrocytes at the cellular and molecular level during remyelination. Using two different *in vivo* models of toxin-induced demyelination, I have found that astrocytes during remyelination undergo a series of changes in numbers, reactivity (assessed by GFAP, vimentin, nestin and NFIA), and morphology, which indicate a temporal regulation of reactivity. Interestingly, I observed that astrocytes increase in reactivity at the time at which the myelin-forming cells, termed oligodendrocytes, differentiate to remyelinate axons. These findings suggest that astrocytes are important for regulating remyelination. To explore this, unbiased RNA-sequencing of astrocyte translating mRNA, isolated using translational ribosome affinity purification (TRAP), was used to identify changes in their gene expression. I found that astrocytes upregulate genes indicative of neuroprotective functions early after demyelination, characterised by the

upregulation of the Nrf2 pathway. Subsequently, at the time of oligodendrocyte differentiation, astrocytes downregulate Nrf2 signalling and activate cholesterol biosynthesis, which is essential during myelination. Here, I hypothesised whether Nrf2 is an critical regulator of astrocyte functions that are important for remyelination. Hence, I used a transgenic mouse model in which Nrf2 is overexpressed in reactive astrocytes. The results suggested that upon sustained Nrf2 overexpression, cholesterol biosynthesis in astrocytes is impaired and consequently remyelination is poor.

This study identifies a mechanism by which astrocytes regulate their functions after demyelination to control the timing of remyelination. These findings are of translation relevance, given that some MS therapies are thought to act via Nrf2 activation.

LAY SUMMARY

Myelin is the insulation surrounding nerves that ensures their health and function and is needed for intellect, sensation, and movement. After damage of myelin, regeneration of myelin can take place to restore nerve function. Nonetheless, this process is impaired in some neurodegenerative diseases like Multiple Sclerosis. There are no approved therapies than can encourage the regeneration of myelin to stop the progression of these diseases, highlighting the need to find new ways in which myelin regeneration can be supported.

Astrocytes are the most abundant type of cell in the brain. Although during development, they are known to support the formation of myelin, their roles after damage are poorly understood. This PhD project has focused on investigating the functions of astrocytes in promoting the regeneration of myelin. To do so, I have used mouse models in which efficient regeneration of myelin takes place after inducing damage with a toxin. Using these models, I found that astrocytes undergo dynamic changes in numbers and activation and that these precede the onset of myelin regeneration. These findings suggested that astrocytes may be necessary for initiating and controlling this process. To understand this, I used an approach named RNA-sequencing, that enables reading a type of genetic material (RNA) which is converted to protein, the central molecules within a cell that regulate specific functions. By using this methodology, I discovered that early after myelin damage, astrocytes adopted roles suggestive of protection, characterised by an increase in as activation of a pathway called Nrf2. Before the onset of myelin regeneration,

astrocytes decreased the levels of activity of the Nrf2 pathway and increased the production of fats. Myelin is a fatty structure, and astrocytes are the main producers of fats in the adult brain. I then asked whether Nrf2 activity could be important in controlling the functions of astrocytes during myelin regeneration. To do so, I used a mouse model where astrocytes constant high activity of Nrf2 and explored the effects on myelin regeneration. I observed that in this model, astrocytes decreased the production of fats, and consequently, myelin regeneration was poor. These findings could help us understand how myelin fails in Multiple Sclerosis since this involves high levels of Nrf2 activity in brain lesions that regenerate poorly. This study could thus contribute to developing new ways to promote myelin regeneration.

Declaration of Original Work

I declare that the work included in this thesis is my own original work and, unless otherwise indicated, and I am the unique author of this thesis. This work has not been submitted for any other degree or professional qualification. Work included from other authors has been appropriately adapted and referenced. I am co-author of the publications included at the end of this thesis, which include an article review that I wrote and a research paper in which I contributed. Sections from Chapter 1 in this thesis were included in this submitted review (Molina-González and Miron. *Neurosciences letters,* 2019).

Irene Molina-González

Acknowledgements

First of all, I would like to thank you, **Veronica**, for how a fantastic supervisor you have been. I admire you in so many aspects, and not just for being a great mentor, but also, and what is more important to me, for the great person that you are; you always see the best in everyone and make them believe in their potential. During my PhD, you have always been there, checking, advising, providing great ideas and feedback for my project with endless patience, and even now, while writing my thesis, you have been here to encourage me so I could give my best. And, an infinite thanks for always checking up on my English and making sure that my word addictions were not going too far (besides, in addition, nonetheless…)!!! I will take all these excellent examples to build upon a great career.

Secondly, I feel so grateful for all the Miron group members that have helped me along all my PhD, **Claire, Graeme, Lindsey, Niamh, Ayisha, Ally, Rebecca,** and **Amy**. It has been an amazing experience to work with you all in such a friendly, fun, and great environment. And thanks **Amy, Ally** and **Rebecca** for being also wonderful friends and sharing great and fun moments with killer caipirinhas, aggressive Bob Ross painting evenings, delicious brunch and dinners, and buying so many therapeutic plants!

I also own a huge thanks to my second supervisor **Prof Siddharthan Chandran**, for the great ideas, feedback, and guidance that have provided me to get such an exciting direction for this excellent PhD project. Moreover, to all the **Chandran group** for the

excellent feedback provided during the lab meetings. I would also like to give a big thanks to the **Hardingham group**, especially to **Prof Giles Hardingham, Owen**, and **Zoeb** for the enormous help with the TRAP, bioinformatics, and significant input that have provided for building such a good project.

To the **ffrench-Constant** and **Williams lab**, since I have enjoyed the lab meetings on Wednesday, learning so much from myelin experts, and obtained excellent contributions for my project. I also feel very grateful for the fantastic postgraduate committee I have had during my PhD, **Dr Rob Mitchel, Prof Niki Gray,** and **Prof Anna Williams**, for their supportive contributions, comments, and input.

I would like to express my gratitude to the **Animal facility (LF2) staff**, especially to **Mike** and **Duncan**, for helping with the animals and always making sure that anything I needed for my experiments was available. Also, to the **CALM facility staff** (**Rolly Wiegand** and **Trudi Gillespie**) and **Daniel Soong** for their help with the imaging set up and technical support. To **Linda Ferguson** for her best advice on PCR machines, and also to the **Pollard lab** for always being helpful around in the lab.

I wanted to thanks to my little Spanish family here in Edinburgh, **Manu, Sara, Clara,** and **Joan**. Thank you for making me feel like home, for being my family here. And for all these great moments with our elaborated Roast dinners, nasty Santa's presents…

To **my friends from Girona**, for your fun visits to Edinburgh but also for the great moments in Girona, for caring about me and being great friends. I would like to also thanks my good and old friends (and almost my sisters) **Lucía, Alejandra Martí, Alejandra Molina** and **Anna** for always being there to support me. To my lovely

cousins **Inés** and **Marta** four your visits for also being my friends and so special to me.

I would particularly like to thanks to my real family in Spain, **Papá, Mamá, Alejandra** and **Paco**, for your unconditional support and love, because I would not have been able to do this and be who I am without you. 'Muchas gracias, **Papá y Mamá**, porque haber conseguido esto os lo debo a vosotros'. And, especially to you, **Mario**, for supporting me in my best and worst moments during this PhD, and always, for making everything so that I can be the happiest person, and because you make it possible.

Lastly, I would like thanks to the **MS Society** for funding this project; without it, it would not have been possible the realisation of this exciting project.

TABLE OF CONTENTS

LIST OF TABLES

LIST OF FIGURES

1. CHAPTER: INTRODUCTION

1.1. Myelin and Remyelination

1.1.1. Myelination

Myelin is a high-lipid content membrane specialisation of oligodendrocytes in the central nervous system (CNS) and of Schwann cells in the peripheral nervous system (PNS) that wraps axons. In contrast to Schwann cells, oligodendrocytes can form several myelin sheaths along axons [1, 2]. Myelin forms regular segments along the axons, called internodes, separated by myelin-free regions termed nodes of Ranvier. At the nodes of Ranvier, clusters of voltage-dependent sodium (Na+) channels on the axonal membrane enables efficient and fast propagation of action potentials along myelinated fibres [3, 4]. This efficient saltatory conduction enables sensory, motor and higher-order cognitive functions. More recently, it has been demonstrated that myelin is crucial for providing trophic and metabolic support to axons through the transport of metabolites such as lactate, which is transformed into adenosine triphosphate (ATP) via the Krebs cycle [5, 6].

Developmental myelination is controlled spatially and temporally by extrinsic and intrinsic signals [7]. In the CNS, neural stem cells and radial glial cells give rise to oligodendrocytes precursor cells (OPCs), which differentiate into pre-myelinating oligodendrocytes and finally into myelinating mature oligodendrocytes. Oligodendrocyte development is regulated by complex transcriptional programming. In the brain, OPCs, characterised by expression of the chondroitin sulfate proteoglycan (NG2) [8], arise from neuroepithelium of ventricular zones [9]. Neural

stem cell progenitors mature into OPCs by the upregulation of several transcription factors including oligodendrocyte transcription factor (Olig)1/2, homeodomain factor (Nkx)2.2/6, achaete-scute complex homolog (Mash)1, myelin transcription factor (MyT)1 and Sry-type HMG box (Sox)8/9/10 [9, 10]. Then, pre-myelinating oligodendrocytes downregulate Olig1, sonic hedgehog (Shh), Mash1, MyT1 and Sox8/9 [9-11]. Terminal oligodendrocyte differentiation is regulated by the expression of myelin regulatory factor (Myrf), osterix (Sp)7 and Chromodomain Helicase DNA Binding Protein (Chd)7 [11]. Mature oligodendrocytes then upregulate genes to form myelin sheaths, including myelin-associated glycoprotein (MAG), myelin basic protein (MBP), myelin oligodendrocyte glycoprotein (MOG) and proteolipid protein (PLP)[9, 12].

Oligodendrocyte specification starts during late gestation in rodents [7], and developmental myelination initiates after birth and is complete around the third postnatal week [13]. In humans and primates, this process is delayed, with robust myelination occurring in the first year after birth. Myelination is not completed until sexual maturation in non-human primates and the third decade in humans [14]. It has also been demonstrated that myelin changes take place during adulthood due to learning [15].

Oligodendrocytes are highly dynamic cells that have the fascinating capacity to extend their membrane around 6,500-fold of their surface area in order to myelinate [5, 8]. Interestingly, in some areas, one oligodendrocyte can myelinate up to 80 axons [7]. Myelination is a highly metabolically demanding process that

requiring nutrients from axons and other glial cells in the environment to meet the energy demand.

1.1.2. Remyelination

Demyelination is the process by which damage of myelin takes place. Different types of insult inducing demyelination include inflammation, viral infection, acquired metabolic defects, and hypoxic-ischemia [16]. Demyelination results in nude axons that can atrophy and degenerate due to the lack of metabolic support and protection from insult and inflammation.

Remyelination is the regenerative process, whereby oligodendrocytes form new myelin sheaths after demyelination, restoring neuronal function [17-19]. During remyelination, OPCs migrate into demyelinated lesions, proliferate, and then differentiate into oligodendrocytes to form new myelin sheaths [20] (Figure 1.1). Recent findings suggest that remyelination may also be mediated by surviving mature oligodendrocytes already present in the lesion that re-ensheath axons [21, 22]. However, these last findings are still under debate, and the presence of mature oligodendrocytes could reflect areas that have not been fully demyelinated [22].

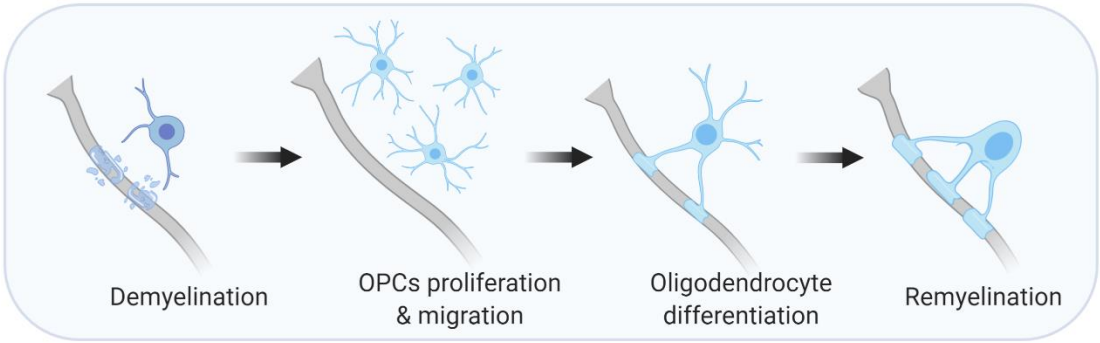

Figure 1.1. Main phases of remyelination. Following a demyelinating insult, OPCs migrate to the demyelinated lesion and proliferate, then differentiate into myelin-producing cells, and remyelinate. **OPCs:** Oligodendrocyte precursor cells.

Although remyelination and developmental myelination share common processes [23], yet they are not identical. Myelin internodes formed during remyelination are thinner and shorter to the ones formed during myelination [17]. This difference may reflect a change in the environment, such as the immune response, or intrinsic changes within the oligodendrocyte lineage with ageing or following damage [17]. The importance of myelin and remyelination is exemplified by the consequences of its destruction and failure, respectively, in neurological disorders.

1.1.3. Multiple Sclerosis

Multiple Sclerosis (MS) is the most common inflammatory neurodegenerative disease affecting young adults. There are three different clinical presentations of MS. Relapse remitting MS (RRMS) has the highest prevalence, characterised by transient episodes in which new demyelinating plaques are formed reflected by disability, followed by recovery phases [24]. Over half of the patients presenting with RRMS will develop secondary progressive MS (SPMS), characterised by continuous neurodegeneration and worsening of the clinical symptoms [25, 26]. Lastly, in primary progressive MS (PPMS), patients present slow and continuous neurological degeneration from diagnosis, without recovery phases [25]. Furthermore, MS is a heterogeneous disease in which different lesion types exist within patients; including active (characterised by a loss of myelin, active remyelination, immune cell infiltration), chronic active (presence of ongoing damage and remyelination in the rim of the lesion, and phagocytes containing myelin debris), chronic inactive (no remyelination, axonal degeneration and glial scar), and fully remyelinated lesions [27, 28].

There are 2.2 million people (30.1 cases per 100,000 population) with MS worldwide, with an increase of 10.4% cases since 1990. The highest prevalence is found in North America (164.6 cases per 100,000 population) followed by Western Europe (127 cases per 100,000 population) and the lowest in Sub-Saharan Africa (2.8 cases per 100,000 population) and Oceania (2 cases per 100,000 population) [29]. The Scottish population has one of the highest rates of MS, with 8.76 in 100,000 new

cases per year [30]. Observational studies associate high prevalence with latitude, increasing the prevalence of MS by 1.03 times per degree of latitude [29].

There are more women than men with MS, with a general ratio of 2:1 (2.3:1 in favour of women in Scotland) [29, 30]. Hormones may be a factor that increases the risk of MS. Sex steroids have been suggested as modulator of the inflammatory response. Reproductive hormones increased during pregnancy, like oestrogen, progesterone, glucocorticoids and prolactin can increase the number of T-regulatory cells (T-reg), which are supportive for remyelination [31], and decrease MS pathology [32, 33]. *In vitro,* hormones have an effect on oligodendrocyte responses, where oestrogen promotes oligodendrocyte proliferation, whereas oestrogen or progesterone mediates differentiation [34]. Nonetheless, the effects of hormone therapy in humans is controversial, where often confounding factors lead to weak evidence of effect [35-37].

Genetic factors have also been suggested to contribute to MS. The genetic risk to develop MS increases from 1 in 1,000 in the normal population to 1 in 4 in identical twins [38]. The major histocompatibility class (MHC) II human leukocyte antigen (HLA) haplotype *DRB1*15:01* gene is the highest genetic risk factor for MS [38]. *HLA DRB1* encodes for a peptide expressed in antigen-presenting cells (APC), mainly monocytes. It is responsible for regulating activation of cluster of differentiation (CD)4+ T cells, associated with the immunopathogenesis of MS [39]. Nonetheless, genomic studies have identified over 50 non-HLA genetic factors that influence the risk to develop MS [40].

Migrant studies have reinforced the importance of an environmental component as a factor for the causation of MS [41]. Three main environmental factors have been described, including vitamin D deficiency, Epstein Barr virus infection and cigarette smoking. These all have been shown to have immunomodulatory effects, causing demyelination [42, 43].

1.1.3.1. Theories for remyelination failure in MS

De novo (new lesions) and repeated lesions can form in RRMS and progressive MS (PMS) patients, the latter more common in progressive forms of MS [44]. Both types of lesions can remyelinate, but this is rarely completed as assessed by imaging analysis [45-47]. Nonetheless, in progressive MS, remyelination often fails, which is considered to contribute to irreversible axonal dysfunction and loss, which in turn leads to severe disability [16, 47].

OPC deficiency has been proposed as one mechanism that could explain remyelination failure. OPCs are the most proliferative cells in the adult brain in mammals [8]. These cells are essential for the turnover and maintenance of myelin in the CNS [8, 48, 49]. After demyelination, other glial cells like astrocytes and microglia release factors, e.g. fibroblast growth factor 2 (FGF-2) or transglutaminase-2 (TG2), that stimulate OPC proliferation [50-52]. Evidence points to OPC proliferation as being required for CNS remyelination [53]. Non-dividing OPCs can be present in demyelinated areas [54], where a lack of growth factors may not allow

them to survive or differentiate to finally remyelinate [55]. A second hypothesis for remyelination failure is impairment in OPC migration to reach the demyelinating plaques. For example, OPC migration is inhibited during development by Sema3A, a secreted factor of the semaphorin family, which acts on the receptor neuropilin-1 [56], and chronic active MS lesions contain higher levels of Sema3A compared to active lesions [57].

Another possible explanation for remyelination impairment is the failure of oligodendrocyte differentiation. Over 70% of MS chronic lesions have pre-myelinating oligodendrocytes indicating a block in remyelination [58]. Some factors have been identified, which can prevent oligodendrocytes from reaching a complete, mature state. The leucine-rich repeat and immunoglobulin-like domain-containing Nogo receptor-interaction protein 1 (LINGO-1), expressed by both oligodendrocytes and axons, is a potent inhibitor of oligodendrocyte differentiation [59, 60]. Blocking LINGO-1 leads to increased oligodendrocyte differentiation during developmental myelination [60] and enhanced remyelination, axon regeneration and functional recovery in a chronic demyelinating model, experimental autoimmune encephalomyelitis (EAE) [61-64]. Moreover, a tight and transient regulation of Wnt signalling controls OPC differentiation during myelination and remyelination [65]. Wnt dysregulation and sustained activation leads to hypomyelination in development and is associated with remyelination failure in MS[66]. Other identified inhibitors of oligodendrocyte differentiation in remyelination have consisted of hyaluronan accumulation [67], bone morphogenic protein (BMP) signalling [68] and

activation of notch receptors [69]. Recent studies have suggested that oligodendrocyte heterogeneity could be a reason for limited remyelination, where a switch to a population with less myelinating capacity and immune characteristics has been suggested to predominate in patients with MS [70, 71].

Remyelination failure may also result from impaired functioning of supporting cells. For instance, the clearance of myelin debris by phagocytes, such as microglia/macrophage, is required for remyelination [72-74]. Continuous demyelination impairs microglial/macrophage functions [75], by exhausting their capacity to phagocytose, leading to accumulation of myelin debris and preventing oligodendrocyte differentiation [74, 76]. Models of ageing have shown that in this context, demyelination severity is not affected in age. However, microglia and macrophages accumulate myelin fragments and cholesterol crystals, which leads to senescence and immune dysfunction, affecting remyelination efficiency [74, 75]. Impaired remyelination in age can be due to intrinsic factors of cells of the oligodendrocyte lineage [77]. Aged oligodendrocyte progenitors present a delay in colonising demyelinated areas, and decreased expression of the transcription factor MyT1 (important for differentiation) leading to reduced remyelination capacity [78]. Epigenetic control of gene expression is altered with ageing, in which an accumulation of transcriptional inhibitors could prevent differentiation [79].

1.1.3.2. Therapeutics for Multiple Sclerosis

There are 16 FDA (Food and drug administration) approved therapies to treat MS, which act by dampening inflammation and slowing neurodegeneration [80, 81]. Available therapies have immunomodulatory effects and are only effective during the relapse-remitting phase. β-interferons and glatiramer acetate were the first treatments used to treat MS [82]. β-interferons block blood-brain barrier (BBB) leakage to prevent peripheral immune cell infiltration, whereas glatiramer acetate prevents T-cell activation. These treatments, although having a low risk for side effects, only reduce relapses by a 30% [83]. More effective drugs have since been developed, which reduce relapses by around 70%, like dimethyl fumarate, mavenclad, alemtuzumab, ocrelizumab and natalizumab [83]. Nonetheless, risk of side effects is generally correlated to the efficacy of the therapy at preventing relapses.

Some treatments effective at reducing relapses are now being tested for their capacity to reduce progression. Ocrelizumab is being assessed for PMS [25], targeting CD20 to deplete B-cells [80], significantly reducing relapses compared to β-interferon [84], and moderately reducing progression compared to placebo [80]. Compared to alemtuzumab, which is also highly effective at reducing relapses, it has very mild risk of developing side effects [85]. Another therapy, dimethyl fumarate (DMF), is now being tested in PMS, and is highly effective at preventing relapses, and has a low risk of side effects [86]. DMF acts by dampening oxidative stress due to activation of the nuclear factor (erythroid-derived 2)-like 2 (Nrf2) pathway [87] expressed primarily by

astrocytes [88, 89], and has immunomodulatory effects on macrophages and T-cells [90, 91]. It has been suggested that DMF might prevent demyelination [92], and promote oligodendrocyte differentiation [89]; however, its role in promoting remyelination has not been assessed. Indeed, there are no currently approved therapies that are aimed at enhancing remyelination. However, there are potential pro-remyelination therapeutic candidates in clinical trial and pre-clinical phases (Table 1.1). In future, a combination of therapeutics that target inflammation and remyelination should be considered. Furthermore, further work is required to understand how efficient remyelination occurs in order to identify suitable pro-remyelination therapies, including elucidating the indirect contribution of other glial cells.

Table 1.1| Potential clinical remyelinating/neuroprotective candidates and ongoing trials

Treatment	MS type	Target	Brief description	Phase
Pre-clinical trials				
IR4X4204	MS	Retinoid X receptor (RXR)- γ	Promotes differentiation of CD+4 T cells into inducible regulatory T cells (iTreg). Promotes oligodendrocyte precursor differentiation [93, 94]	Not yet performed
Kappa opioid	MS	Kappa opioid receptor (KOR)	Promotes survival and oligodendrocyte differentiation [95].	Not yet performed
Ongoing trials				
Anti-LINGO-1	RRMS	LINGO-1	Inhibits LINGO-1 inducing oligodendrocyte differentiation and promoting remyelination [96, 97].	Phase II ClinicalTrials.gov Identifier: NCT03222973
Olexisome	RRMS	Components of the mitochondrial permeability	Cholesterol-like compound. Prevents opening the PTP due to oxidative stress and confers neuroprotection.	Phase I ClinicalTrials.gov Identifier: NCT01808885

		transition pore (PTP)	Increases number of oligodendrocytes [81, 96, 98].	
Testosterone	RRMS	Androgen receptor	Induces a shift from pro-inflammatory T-helper type 1 (Th1) to anti-inflammatory T-helper 2 (Th2) [99]. Promotes an increase in cells of the oligodendrocyte lineage and remyelination[81].	Phase II ClinicalTrials.gov Identifier: NCT03910738
GSK239512	RRMS	Histamine H3 receptor blocker	Promotes remyelination [47].	Phase II ClinicalTrials.gov Identifier: NCT01772199
Clemastine	RRMS	Histamine H1 receptor blocker	Oligodendroglial differentiation via muscarinic receptor antagonism [100].	Phase II ClinicalTrials.gov Identifier: NCT02040298
Lipoic acid	PMS	Reactive oxygen species (ROS)	Antioxidant effects. Reduces inflammation [25, 101].	Phase II ClinicalTrials.gov Identifier: NCT03161028
Quetiapine fumarate	RRMS/ PMS	Nrf2	Confers neuroprotection. Prevents demyelination [97].	Phase I/II ClinicalTrials.gov Identifier: NCT02087631
Biotin (MD1003)	PMS	B vitamin family coenzyme	Stimulates fatty acid synthesis. Increase of myelin production through an increase of adenosine triphosphate (ATP) production [25, 95, 102].	Phase III ClinicalTrials.gov Identifier: NCT02936037
Anti-semaphorin 4D	MS	Semaphorin (Sema)-4D	Blocks interaction of Sema-4D and its receptors. Hence, blocks inhibition of OPC migration and differentiation [103].	Phase I ClinicalTrials.gov Identifier: NCT01764737
Bexarotene	RRMS	Pan RXR agonist	Promotes oligodendrocyte differentiation [93, 95, 100].	Phase II

Repurposed				
Simvastatin	SPMS	T-cells Nrf2	Initially indicated for high cholesterol (hydroxymethylglutaryl-CoA reductase (Hmgr) inhibitor). Modulates the shift of Th1 to Th2. Prevents oxidative stress by activating Nrf2 [97].	Phase II ClinicalTrials.gov Identifier: NCT00647348
Ibudilast	PMS	Prevents cell death	Confers neuroprotection [104].	Phase II ClinicalTrials.gov Identifier: NCT01982942
Domperidone	SPMS	Hormone prolactin	Initially indicated for treating nausea and vomiting. Increases prolactin hormone. Improves remyelination [97].	Phase II ClinicalTrials.gov Identifier: NCT02308137

1.2. Astrocytes

Astrocytes are CNS-resident cells characterised by a star-shaped cell body, and are the most abundant neuroglial cell type in the brain. Astrocytes form a mesh in the CNS contacting the vasculature, neurons and oligodendrocytes. This is a highly heterogeneous population defined by diverse morphologies and region-specific functions. Astrocytes are specialised in different homeostatic and metabolic functions in order to meet the needs of their neighbouring cells both in white and grey matter [105].

These cells play essential roles during development and adulthood. For instance, they are crucial to support developmental myelination but also myelin turnover during the life span. Moreover, they have an essential role in supporting synaptogenesis, and in the regulation of synapses [106-108]. Astrocytes are active players in the control of synaptic transmission since they are in contact with the pre-synaptic and the post-synaptic terminals, forming the tripartite synapses [109].

Their end-feet surround the cerebral vasculature and are critical components involved in the formation and control of the BBB [110]. Astrocytes supply nutrients to the brain, as they are in direct contact with the basal lamina [111]. For instance, they can take up glucose from the blood vessels to feed neurons or act as storage for glycogen [111]. Furthermore, astrocytes control cerebral blood flow via secretion of vasoactive molecules [112, 113]. Astrocytes can also be involved in ion and pH homeostasis via water and ion channels [114].

These cells also have neuroprotective functions, providing antioxidant support and regulating immune responses after insult [105, 115]. In addition, demyelination affects astrocyte homeostasis and activation, which in turn induces changes in OPCs. Astrocytes activated by injury can release factors that promote the rapid proliferation and differentiation of OPCs. Hence, this type of glia has been a focus of study in the context of white matter re/myelination and MS.

1.2.1. Astrocytes in development

Various markers are used to identify astrocytes such as the expression of transcription factors, upregulation of intermediate filaments and detection of other specific proteins. Nonetheless, their study has been challenging due to the lack of specific markers, most prominent during development [115]. The glial fibrillary acidic protein (GFAP) is an intermediate filament, which has been the most popular marker used to detect astrocytes. However, GFAP only labels a small subset of astrocytes in physiological conditions (around 30%), and it is expressed only at low levels in grey matter [116]. Another limitation of the use of GFAP is that some neuronal progenitors and radial glia also express it [117]. Other markers used to detect astrocytes consist of S100 calcium-binding protein-β (s100β), aquaporin 4 (Aqp4), and the glutamate transporters, glutamate aspartate transporter-1 (GLAST) and glutamate transporter soluble carrier family 1, member 2 (GLT-1). However, these markers can also be expressed, although at lower levels, in other cells such as OPCs (s100β, GLT-1 and GLAST) and ependymal cells (Aqp4) [118]. Aldehyde Dehydrogenase 1 Family

Member L1 (Aldh1l1) has been accepted as the most specific pan-astrocytic marker [119], and although there is a lack of antibodies that successfully detect this protein, reporter lines for Aldh1l1 can be used to overcome this limitation. Moreover, recently, Sun *et al.* (2017) identified the transcription factor Sox9 as a specific nuclear pan-astrocytic marker in the adult brain outside neurogenic regions [120].

Macroglia, consisting of astrocytes and oligodendrocytes, and neurons share origins from the neuroepithelial cell. In the ventricular zone (VZ), neural precursors differentiate into radial glia which then turn into neurons and macroglia. Neurogenesis and gliogenesis take place during a tightly control period during development, in which neurogenesis precedes the gliogenesis phase [121]. Nuclear factor I A (NFIA) and Sox9 are master regulators of gliogenesis, and their upregulation controls the switch from neurogenesis to gliogenesis [122, 123]. Then, the upregulation of the transcription factor Zinc finger- and BTB domain-containing protein 20 (Zbtb20) defines the astrocytic fate, just before oligodendrocyte generation [124]. In the mouse, astrogenesis begins between embryonic days (E)16-18 in the brain and E12.5 in the spinal cord [121].

After the formation of astrocytes, they populate the brain, migrating with the support of radial glia. Astrocytes then reach different areas where they adopt specific functions to fulfil the needs of the respective brain region. The maturation of astrocytes to obtain specialised physiological functions involves several changes in morphology, connectivity and electrophysiological properties [121, 125]. Different neural precursors with specific molecular profiles in different regions could give rise

to distinct astrocyte populations [126]. The main types of astrocytes described consist of fibrous astrocytes located in white matter, protoplasmic in grey matter, Müller glia in the retina, Bergmann and velate glia in the cerebellum, ependymal astrocytes, marginal and perivascular astrocytes [127, 128].

1.2.2. Astrocytes in developmental CNS myelination

Fibrous astrocytes are characterised by their small cell bodies and elongated shape aligning with myelinated axons [129]. Compared to grey matter astrocytes, they express higher levels of GFAP. The roles of astrocytes in white matter have been less studied, but evidence suggests they are supportive during developmental myelination and adulthood.

During myelination, astrocytes support the formation of the myelin sheath by oligodendrocytes, which is a highly metabolically demanding process (Figure 1.2). Cultured oligodendrocytes purified from developing rat optic nerve in the presence of astrocytes were able to differentiate and extend their processes along the axon, a process that was not observed in the absence of astrocytes [130]. Moreover, mice deficient in GFAP have dysmyelination, non-myelinated axons and disrupted BBB integrity [131].

Astrocytes also secrete factors that promote oligodendrocyte differentiation. Conditioned media from astrocytes increases OPC differentiation measured by an increase in the expression of MBP [132]. This effect was mediated through pro-

differentiating factors like ciliary neurotrophic factor (CNTF) and tissue inhibitor metalloproteinase-1 (TIMP-1) [132-135]. The energy demands of oligodendrocytes also depends on astrocyte-derived lipids. Astrocytes contribute to lipid biosynthesis and supply these to oligodendrocytes during myelination in development, a mechanism that has been suggested to be mediated through horizontal transfer [136]. Nonetheless, further studies are needed to confirm the mechanism underpinning this process. In addition, astrocytes and oligodendrocytes can communicate through chemokine signalling. Astrocytic release of chemokine (C-X-C motif) ligand 1 (CXCL1) acts on the C-X-C chemokine receptor type 2 (CXCR2) on oligodendroglial cells to promote differentiation and myelin formation *in vivo* [137]. Moreover, immunofluorescence and ultrastructural analysis shows that most of the nodes of Ranvier are in contact with astrocytic processes [138]. The contact of astrocytes with nodes of Ranvier is essential for nodal formation and maintenance [139].

For myelin development and stabilisation, the coupling of astrocytes to oligodendrocytes occurs through two types of heterodimeric gap-junction connections, regulating ion and water homeostasis, and energy supply [140-142]. These consist of connexin 30 (Cx30) and connexin 43 (Cx43) present in astrocytes, coupled to connexin 32 (Cx32) and connexin 47 (Cx47) in oligodendrocytes, respectively [142]. Lack of Cx47 and Cx30 prevents oligodendrocyte-astrocyte coupling, which causes myelin abnormalities, consisting of myelin vacuoles and thinner myelin sheaths, reduced number of oligodendrocytes, and severe gliosis in

white matter areas, which reduces survival in these mice. Importantly, these animals can still form astrocyte-astrocyte connections through Cx32 and oligodendrocyte-oligodendrocyte coupling through Cx43 [143], highlighting that astrocyte to oligodendrocyte connectivity is crucial for myelin development and preservation.

Failure and dysfunction of these connections can be observed in human myelin disorders. One such example is the autosomal recessive hypomyelinating disorder Pelizaeus-Merzbacher-like disease, in which a mutation in the *GJC2* gene that encodes for Cx47 [144] impairs Cx43/Cx47 coupling [145]. There is further evidence for the role of astrocytes during myelination and its maintenance from leukodystrophies in which astrocyte pathology leads to myelin disruptions [146]. Alexander's disease is a neurodegenerative disease characterised by severe myelin alterations caused by a mutation in the gene encoding for GFAP [147]. Furthermore, the leukodystrophy Niemann-Pick type C (NPC) is caused by a mutation in the gene *NPC-1* (NPC intracellular cholesterol transported-1) that is predominantly expressed in astrocytes and causes failure in cholesterol storage and metabolism [148]. Mutations in this gene causes premature death in humans and animal models, with neuropathological features including demyelination and axonal loss [149]. In mice lacking NPC-1, the specific expression of this protein in astrocytes was sufficient to at least partially restore myelination, although ultrastructural analyses were not performed [150].

Another example in which astrocyte dysfunction leads to myelin pathology is the rare genetic disease Pyruvate carboxylase [148, 151, 152]. Pyruvate carboxylase

is an enzyme mostly found in the mitochondria of astrocytes in the CNS, and it is essential for controlling processes like glucogenesis, lipogenesis and insulin secretion [151]. Patients affected with pyruvate carboxylase deficiency present generalised myelin defects in the CNS due to a failure in myelin formation [152, 153].

Astrocytes are also crucial for controlling myelin development after perinatal CNS insult. In a mouse model of premature hypoxic-ischemic brain injury, transplantation of immature human induced pluripotent stem cells (iPSC)-derived astrocytes rescued hypomyelination of the corpus callosum and promoted behavioural recovery [132]. Moreover, conditional ablation of astrocytic signal transducer and activator of transcription 3 (STAT3), aggravated myelin injury. STAT3 signalling in astrocytes is essential for restricting transforming growth factor beta-1 (TGFβ1) production by microglia, which in turn regulates oligodendrocyte differentiation, and is critical for providing neuroprotection [154].

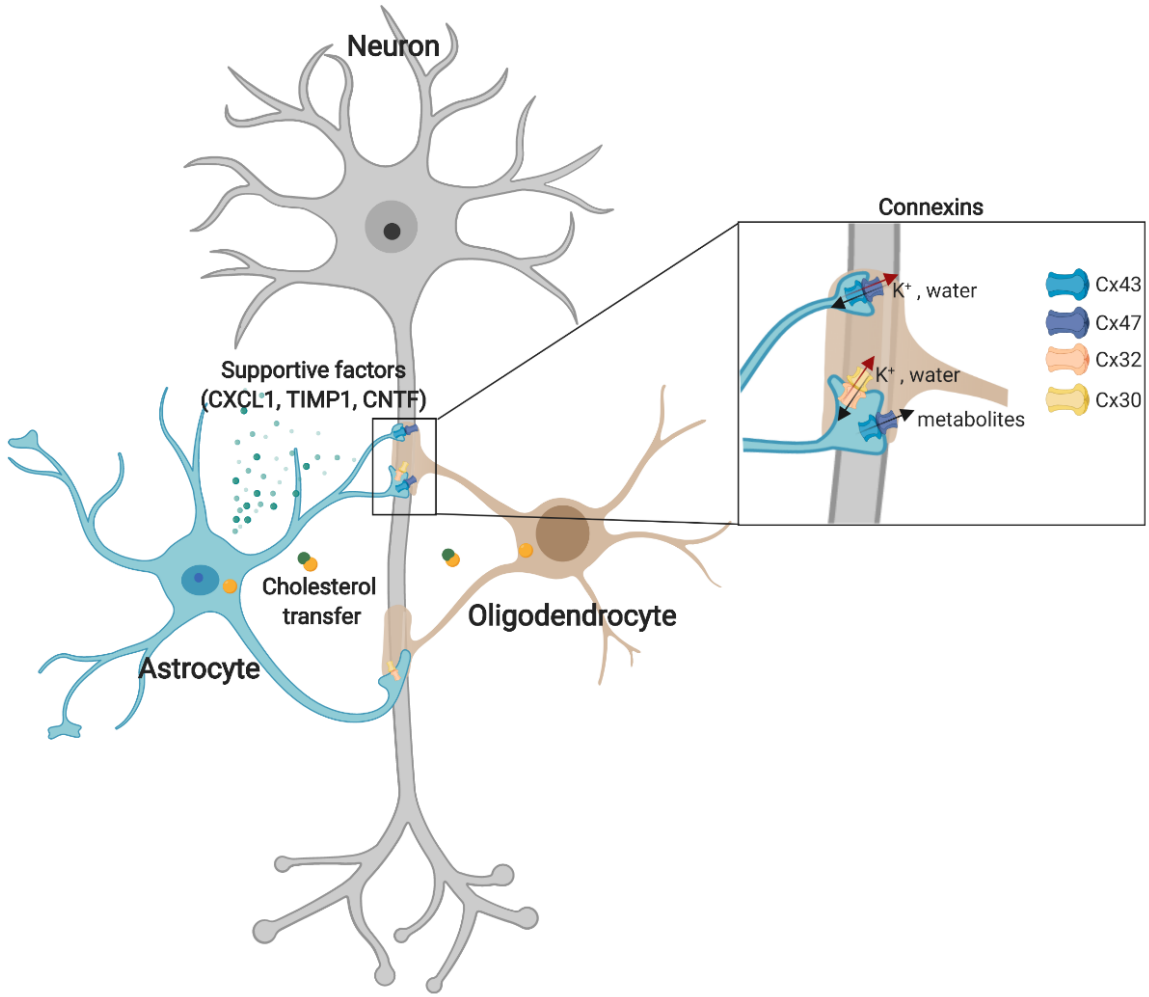

Figure 1.2. Astrocytes are important players during myelin formation in development. Astrocytes mediate myelination through the release of factors like C-X-C motif ligand 1, CXCL1, tissue inhibitor of metalloproteinase 1 (TIMP1), and ciliary neurotrophic factor (CNTF), transfer of cholesterol, and via direct coupling through connexins (Cx) necessary for potassium (K+), water and metabolite transport (taken from Molina-González *et al.* 2019).

Despite the existing evidence for the implication of astrocytes in myelination, there are still open questions that need to be addressed in order to fully understand the role of astrocytes in myelin formation. Do astrocytes in different areas of white matter have different roles in myelination? [155] Does the direction of ion and water

flow through gap-junctions matter for myelin formation and maintenance? [156] Can transplantation of cells restore astrocyte dysfunction in human neurodevelopmental disorders? [157].

1.2.3. Astrocytes in myelin damage and remyelination in the adult CNS

Astrocytes continue to contribute to myelin homeostasis and remodelling during adulthood. In physiological conditions, astrocyte processes are in contact with myelinated fibres [158]. Evidence shows that within areas of disrupted myelin in normal adult animals, astrocyte processes accumulate lysosomes which contain lipid droplets or membrane-like debris [158]. These findings would suggest that oligodendrocyte-astrocyte contacts are required for myelin turnover and maintenance. Furthermore, reduction of exocytosis in astrocytes is associated with myelin paranodal loop detachment, increased nodal gap length, and thinning of myelin in the optic nerve. Hence, pointing to the importance of astrocytes in maintaining myelin in homeostasis [139].

Astrocytes also play a role after demyelination. Evidence is often controversial showing either supportive or detrimental functions that may be explained by different astrocyte phenotypes responsible for regulating different responses.

1.2.3.1. Astrocytes phenotype regulation

After insult, astrocytes change their activation by a complex process known as reactive astrogliosis. This process consists of a series of changes in transcription, function, increase in proliferation, and alteration in morphology including hypertrophy and upregulation of intermediate filaments (such as GFAP, synemin, vimentin and nestin) [116, 159, 160].

Additionally, astrocytes adopt diverse phenotypes depending on the severity of the insult. The simplistic phenotype characterisation macrophages as 'M1' (pro-inflammatory) and 'M2' (pro-repair) has been adapted to astrocytes [161]; in an ischemic mouse model, astrocytes polarised towards an 'A2 phenotype', defined to be a repair phenotype due to the upregulation of neurotrophic factors and beneficial cytokines. Contrarily, in the same study, they showed that astrocytes in a lipopolysaccharide (LPS) model, adopted pro-inflammatory functions, which were defined as 'A1 phenotype' [161].

Microglia are also crucial for regulating astrocyte phenotypes after insult. LPS promotes the expression and secretion of inflammatory molecules by microglia [interleukin (IL)-1α, tumour necrosis factor (TNF)-α, and complement complex-1q (C1q)], which in turn regulates an 'A1 phenotype' and expression of complement-3 (C3) by astrocytes, also seen in human neuropathological tissue like MS [162]. Opposite to this, microglia were shown to induce a protective phenotype in astrocytes by the downregulation of the P2Y purinoceptor 1 (P2YR1), which

facilitated the formation of the scar and reduced neuronal damage in a model of traumatic brain injury [163]. In addition, pro-inflammatory microglia were shown to mediate astrocyte death by necroptosis in a model of spinal cord injury, which was required for repair [164]. This process may be a protective mechanism to prevent damage due to excessive astrogliosis [165].

Astrocyte phenotypic regulation is highly complex and is likely regulated in a context-dependent manner. For instance, opposed to the concept of A1 being a detrimental phenotype, in a model of prion disease, the inhibition of A1 astrocyte formation accelerated the disease course and increased its severity, and lead to a mixed A1/A2 astrocyte phenotype. After demyelination, astrocytes beneficial or detrimental roles may depend on the severity of the demyelinated lesion, the level of inflammation and their interaction with other cells. Regenerative and damaging functions of astrocytes are described and discussed in the following sections.

1.2.3.2. Regenerative and protective functions of astrocytes

Due to the implication of the requirement for astrocytes in myelin formation in development and maintenance in adulthood, it can be considered that astrocytes are also crucial for promoting remyelination after insults (Figure 1.3.A). One of the first evidence for the direct effect of astrocytes on remyelination *in vivo* was in a model of spinal cord focal demyelination, where astrocytes were transplanted into the demyelinating area [166]. In this study, the transplantation of astrocytes

promoted remyelination by host oligodendrocytes [166]. These effects may have been mediated by the secretion of supportive factors that promoted remyelination. For example, in an *in vivo* model of viral induced-demyelination, astrocytes were shown to express CNTF during the remyelinating phase [167], shown to support oligodendrocyte differentiation. In the cuprizone model, in which demyelination is achieved by providing cuprizone to the mouse diet astrocytes secrete the glycoprotein osteopontin during remyelination, which promotes myelin generation in an oligodendrocyte-neuron co-culture model [168].

Moreover, astrocytes may regulate remyelination through the control of cholesterol metabolism. In instances of poor remyelination (EAE, and in MS optic chiasm), astrocytes were shown to downregulate genes for cholesterol biosynthesis [169]. In adulthood, astrocytes are the primary cells producing and delivering cholesterol, via apolipoprotein E (ApoE)[170]. The treatment of EAE mice with CS-6253, a compound that increases cholesterol efflux to extracellular ApoE, increased expression of cholesterol synthesis genes and consequently decreased the severity of disability [169]. Furthermore, dietary cholesterol promoted remyelination in two models of demyelination [171]. This effect could be in part due to cholesterol influencing astrocyte phenotype to support remyelination through modulating the secretion of factors to oligodendrocytes like FGF-2 [171]. However, the outcome of manipulating different targets in the lipid metabolism pathway in astrocytes may depend on disease progression and timing of administration. For instance, depletion of the fatty acid binding protein 7 (FABP-7), a chaperon for long fatty acids that

regulates lipid metabolism, in EAE showed that, although there was increased inflammation and earlier presentation of symptoms, it attenuated disease severity late in the disease course [172].

Myelin debris inhibits oligodendrocyte differentiation and remyelination [173, 174]. Astrocytes can regulate microglia attraction, through the release of CXCL10 [72, 175, 176], an interaction shown to be required for clearing of myelin debris and remyelination in the cuprizone model [72]. Moreover, the phagocytosis of myelin debris by microglia can be regulated by astrocytes through angiopoietin-like 4 (ANGPL4), an inhibitor of lipoprotein-lipase. ANGPL4 is expressed by astrocytes in MS lesions, and a reduction in astrocytes *in vitro* induced myelin clearance by microglia/macrophages, which was then suggested to be required to enable remyelination [177].

Astrocyte expression of GFAP may also influence their function in remyelination. In the cuprizone model, mice overexpressing GFAP had reduced neuronal damage and demyelination potentially due to decreased activation of nuclear factor kappa-light-chain enhancer of activated B cells (NF-κB) in astrocytes [175]. Accordingly, in the same model, astrocyte depletion was achieved by injecting ganciclovir into a GFAP-thymidine kinase transgenic, which causes non-inflammatory apoptosis of GFAP+ cells [72]. This model of ablation causes 60-70% of GFAP+ astrocytes to die [72]. Importantly, in this model, when depletion of astrocytes was performed at 4 weeks after cuprizone-induced demyelination, it was sufficient to impair remyelination [72]. This could suggest that different populations of astrocytes

may have different roles during remyelination, where the 30-40% of remaining astrocytes were not supportive of repair, as indicated by decreased numbers of proliferating oligodendrocytes and mature oligodendrocytes and impaired remyelination [72].

1.2.3.3. Damaging functions of astrocytes

After demyelination, astrocytes have also been shown to inhibit remyelination (Figure 1.3.B). Blakemore and colleagues (2003) observed that OPCs transplanted into demyelinated lesions remyelinated axons more often in astrocyte-free regions, suggesting that astrocytes inhibit remyelination [178]. However, demyelination was achieved by injecting the DNA-intercalating agent ethidium bromide, which creates a lesion free of OPCs and astrocytes, and a day later X-irradiation was performed to confirm the full ablation of astrocytes [178]. Therefore, this type of demyelination is severe and could have promoted an inflammatory environment in the surrounding tissue that could have influenced astrocyte phenotype in a manner not favourable for repair. In this study, they also explored the effect of transplanting astrocytes into the X-irradiated ethidium bromide lesion, on remyelination [178]. They observed that although minimal, some remyelinated axons were present alongside transplanted astrocytes. Hence, the authors suggested that the impairment in remyelination could have been mediated due to other mechanisms that could indirectly have affected astrocytes responses [178].

This could also explain the difference between Franklin *et al.* (1991), in which acute demyelination permitted transplanted astrocytes to promote remyelination [166]. Supporting the postulate that chronic and severe demyelination could influence astrocyte responses, the ablation of astrocytes after chronic cuprizone administration, which prevents remyelination, increased the number of cells of the oligodendrocyte-lineage [176]. Nonetheless, an increase in the number of oligodendrocytes is not necessarily reflective of repair as no evidence of new myelin formation was shown to confirm remyelination.

Astrocytes could potentially impair remyelination through the production of factors that prevent beneficial responses from the oligodendrocyte lineage. For instance, fibronectin is an extracellular matrix component, which is expressed by astrocytes and has been correlated with disease severity in EAE [172]. Reactive astrocytes also express high levels of endothelin-1 (ET-1), an endogenous inhibitor of remyelination that is highly expressed after demyelination [179]. ET-1 induces Jagged1 in astrocytes and activates Notch in OPCs after LPC-induced demyelination. Blocking ET-1 inhibited expression of Notch by OPCs in demyelinating lesions, and enhanced remyelination [179].

Astrocytes respond to signals in their environment, coming from other cells that can promote further damage. For instance, astrocyte-microglia communication is critical for regulating the severity of oligodendrocyte and myelin damage. Supporting this, Rothhammer and colleagues (2018) showed that microglia are essential in regulating astrocyte signalling and EAE pathogenesis [180]. Transforming

grow factor (TGF)-α derived from microglia was shown to act on the epithermal growth factor receptor (ErbB1) on astrocytes and reduce EAE pathogenesis. In contrast, microglial-derived vascular endothelial growth factor(VEGF)β triggered vascular endothelial growth factor receptor (VEGFR)-1 signalling in astrocytes and worsened EAE [180]. Moreover, oligodendrocyte death *in vitro* mediated by LPS-treated microglia was shown to require the presence of astrocytes, as oligodendrocytes did not die in their absence [181]. Astrocytes could also confer a pro-inflammatory state in microglia. Astrocytes in MS release advanced glycation end-products, whose receptors are on macrophages/microglia, which may induce nuclear factor (NF)-κB activation and proinflammatory cytokine release, potentially promoting MS pathology [182].

Astrocytes are essential for regulating immune cell functions after myelin insult. Mayo *et al.* (2014) observed the effect of depleting astrocytes at different stages in EAE [183]. Depleting astrocytes in the acute phase resulted in worsening of the clinical score, whereas it was improved when they were depleted in the progressive stage [183]. Transcriptomic analysis of astrocytes in the progressive phase revealed that *B4GALT6* (Beta-1,4-Galactosyltransferase 6 gene), the gene encoding for Lactosylceramide (LacCer), was highly upregulated [183]. Importantly, the B4GALT6/LacCer pathway in astrocytes regulates the expression of C-C motif chemokine ligand 2 (CCL2), which controls the recruitment of inflammatory monocytes into the CNS, and granulocyte-macrophage colony-stimulating factor (GM-CSF), which modulates microglial activation [183], suggesting a role in crosstalk

with myeloid cells. B4GALT6/LacCer was also found to be more highly expressed in MS lesions compared to normal-appearing white matter (NAWM) and controls [183].

Astrocytes are critical in regulating the BBB, and as such, they have a crucial role in controlling the entrance of peripheral immune cells into the CNS. Astrocyte detachment from the vasculature leads to BBB dysfunction, which coincides with areas of T-cell infiltration and inflammation in cortex and white matter [184]. Moreover, astrocytes regulate the entrance of peripheral immune cells into the brain and spinal cord through the release of chemoattractant molecules [185]. Interleukin (IL)-17 expression in astrocytes is critical for the recruitment of leukocytes [186]. Moreover, knocking out CCL2 in astrocytes in the EAE model decreased T-cell and macrophage infiltration in spinal cord white matter, which decreased microglia activation and axonal degeneration [185].

Transcriptomic analysis of astrocytes in EAE revealed that they upregulate genes indicative of inflammation [169]. Astrocytes can act as APCs for T-cell activation [187], and express adhesion molecules like the vascular cell adhesion molecule (VCAM)-1 that facilitate the entrance of lymphocytes through the BBB [188]. Astrocytes also regulate the activity of T-cells through the upregulation of CD39, which is an enzyme increased in inflammation and has a role in converting ATP into the immunosuppressive factor adenosine [189]. Moreover, knocking out NF-κB in GFAP+ astrocytes resulted in a reduction of infiltrated T-cells into the spinal cord during the acute and chronic phases of EAE independent of BBB disruption, which led to a reduction of myelin pathology and improved clinical outcomes [190]. Astrocytes

may influence remyelination by regulating inflammation through phagocytic capacity. It has been proposed that astrocytes could act as APCs and release cytokines to recruit immune cells after phagocytosis [191-193]. That raises the question as to whether astrocyte phagocytosis of myelin debris could be an early pathological mechanism in myelin disorders [192].

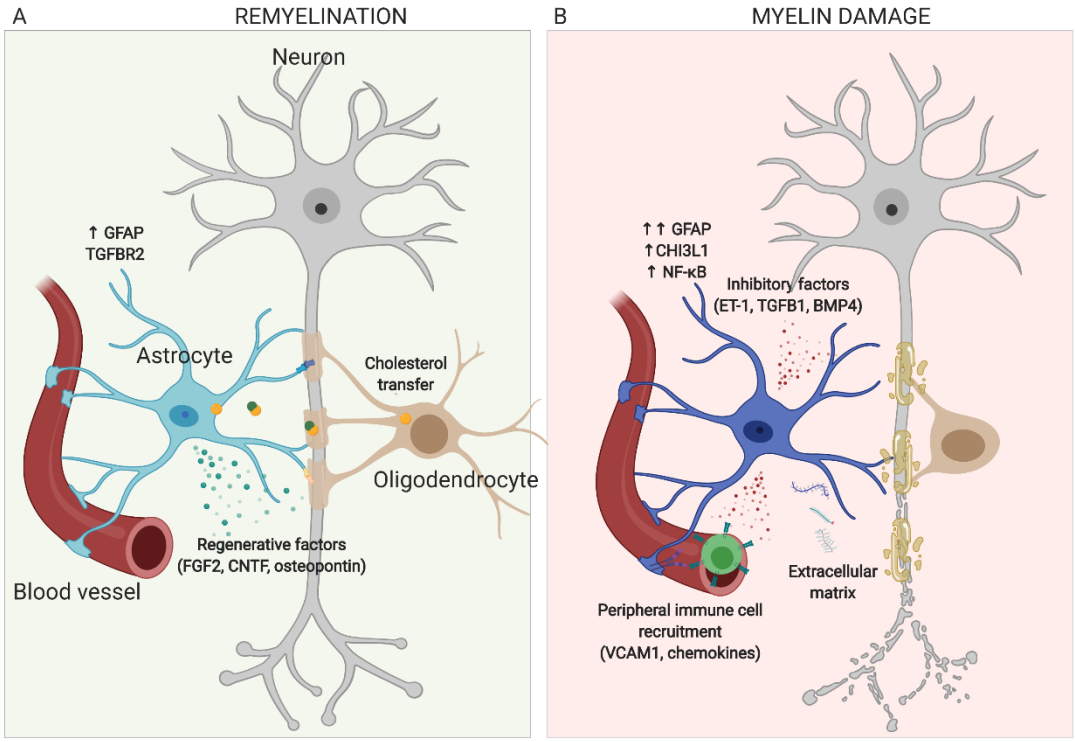

Figure 1.3. Astrocytes play both supportive and damaging functions after demyelination. **A.** Astrocytes upregulate glial fibrillary acidic protein (GFAP) and transforming growth factor receptor (TGFR)-β2 during myelin repair. To support remyelination, they transfer cholesterol (via ApoE) and secrete regenerative factors like fibroblast growth factor (FGF)-2, ciliary neurotrophic factor (CNTF), and osteopontin. **B.** Astrocytes express high levels of GFAP, increase chitinase 3 like 1 (CIH3L1), and nuclear factor kappa-light-chain enhancer of activated B cells (NF-κB) signalling during myelin damage. Astrocytes can promote demyelination and impair remyelination via the secretion of inhibitory factors like

endothelin-1 (ET-1), transforming growth factor beta-1 (TGFβ1), bone morphogenic protein-4 (BMP-4), and extracellular matrix components. They mediate the recruitment of peripheral immune cells (lymphocytes and macrophages) by the secretion of chemokines and expression of vascular cell adhesion protein 1 (VCAM1) (taken from Molina-González *et al.* 2019).

1.2.3.4. Astrocytes in Multiple Sclerosis

It has long been believed that MS is a disease in which reactive T-cells mediate demyelination. However, in some instances, demyelination can be observed in the absence of peripheral immune cells. For instance, after immunomodulatory therapy that prevent peripheral cell infiltration and activation, new demyelination can still take place. Hence, glial cells have been recently investigated as potential mediators of MS pathology.

A hallmark of MS has been defined as the demyelinated plaque accompanied by reactive glial scar formation. After inflammation and demyelination, highly proliferating astrocytes adopt a hypertrophic morphology and start overlapping their processes in an atypical form, resulting in glial scarring [194]. Both beneficial and detrimental properties have been defined. For example, the glial scar is required for axonal regrowth in a model of severe spinal cord injury via the secretion of repair supporting molecules [195]. More recently, it was observed that in remyelinating lesions of rat EAE, astrocytes presenting characteristics of the glial scar coincided with the expression of factors previously shown to have pro-differentiating effects on oligodendrocytes [196]. Nonetheless, although the suggested benefit in limiting

inflammation in demyelinated lesions [191, 194, 197], it may also limit the migration of oligodendroglial cells, thereby impeding repair [198].

Several studies have supported the view that astrocytes may have supportive functions in promoting remyelination in MS. Gene expression analysis of astrocytes in MS NAWM showed that they adopted a neuroprotective role, indicated by upregulation of genes involved in the control of iron homeostasis and neurotrophic support [199]. The regulation of iron metabolism by astrocytes has been shown to regulate remyelination; conditional deletion of the iron efflux transporter ferroportin (fpn) in astrocytes (using a Cre-driver targeting GLAST+ astrocytes) in a model of toxin induced-demyelination caused remyelination failure and decreased OPC proliferation [51]. Astrocytes have also been shown to regulate microglia phenotype in MS and other myelin disorders and iron transport regulation by astrocytes could be important for regulating microglia functions. A depletion of fpn in astrocytes decreases microglial secretion of TNFα and IL-1β during remyelination [51]. Furthermore, treating cultured astrocytes with TNFα and IL-1β increases mRNA encoding FGF2, insulin growth factor (IGF)-1 and TGFβ, factors supportive of oligodendrocyte differentiation [51].

In NAWM of MS patients, astrocytes upregulate genes that regulate oxidative responses [199]. Astrocytes have antioxidant roles, mediated through the activation of Nrf2 [200, 201]. Nrf2 activation has been observed to be neuroprotective in some neurological disorders [202]. In the cuprizone model, conditional activation of Nrf2 driven by the GFAP promoter prevented oligodendrocyte loss and demyelination

[92]. Nrf2 activation may need to be tightly regulated to have protective effects, as sustained levels may be detrimental and causative of cancer [202]. In addition, its expression in MS brain seems to vary in the different cell types, being highly expressed in degenerating cells [203], potentially as an attempt to prevent oxidative injury.

Astrocyte-oligodendrocyte connections are lost in chronic MS and EAE [204]. This would indicate a loss of connection that would support the maintenance of myelin and remyelination. Masaki *et al.* (2013) aimed to investigate the link between Cx pathology in acute and chronic MS, Neuromyelitis Optica (NMO), and NMO spectrum disorder (NMOSD), in which lesions were classified as demyelinating, chronic active, and chronic inactive [205]. They observed a loss of Cx43 in demyelinating areas of NMO, NMOSD and MS, which consequently lead to a Cx43/Cx47 (astrocyte to oligodendrocyte) connection loss [205]. Loss of Cx43 was associated with actively progressive disease and oligodendrocyte pathology and degenerating astrocytes [205]. The frequency of loss of Cx43 was higher in patients with a rapidly progressive disease that had died after two years of onset [205]. Hence, astrocyte-oligodendrocyte connexin loss could be associated with the severity of the disease due to the failure to maintain myelin integrity.

After a demyelinating insult, astrocytes can modulate the extracellular matrix and prevent remyelination (Figure 1.3.B.). In MS, astrocytes upregulate the expression of extracellular matrix components such as fibronectin, chondroitin sulfate proteoglycans, and hyaluronic acid, which inhibit oligodendrocyte

differentiation and impair remyelination [67, 206-209]. Astrocytes also secrete factors that promote inflammation and demyelination. BMP are a family of proteins that have a role in regulating inflammatory processes and have been studied in the context of demyelination. BMP4 overexpression increases astrocyte density, but decreases oligodendrocyte numbers in development [210], and is highly expressed by astrocytes during cuprizone-demyelination [211]. Noggin, a BMP4 antagonist, promotes oligodendrocyte differentiation and remyelination in the cuprizone model [211]. Importantly, BMP4 expression is upregulated in chronic-inactive MS lesions, which have no repair capacity, in reactive astrocytes, negatively correlating with remyelination potential [212].

Gene expression analysis of astrocytes in MS revealed that the functions of astrocytes could be lesion-dependent (Figure 1.3.A). Expression of TGFβ1 in astrocytes correlates with the development of astrogliosis, and its expression is associated with inhibited oligodendrocyte differentiation in the periplaques of the spinal cord in MS [213]. On the contrary, astrocytes in remyelinated MS lesions express the TGFβ-receptor2 (TGFβ-R2), but this is downregulated in chronic active MS lesions, thereby, associating its expression with a protective phenotype [214].

Astrocyte activation and morphology varies in MS, depending on the lesion type and the disease stage (Figure 1.3). Hence, studies have proposed the presence of different markers generally expressed by astrocytes as potential biomarkers for MS. For instance, *CHI3L1* could be used as an indicator for PMS [215], but its function remains controversial. Astrocytes express *CHI3L1* at the rim of chronic active lesions,

but it is downregulated in all the other lesion types [214]. Moreover, GFAP levels in the cerebrospinal fluid (CSF) have been associated with highly active inflammation in relapse-remitting MS (RRMS) and clinically isolated syndrome (CIS), in which GFAP levels are correlated with the levels of chronic inflammation load [216]. Moreover, GFAP levels are elevated in CSF of PPMS [217].

1.3. Aims of thesis

Astrocytes have been shown to have critical roles in the development and maintenance of myelin, yet their contribution to remyelination, and the molecular mechanisms underpinning this potential role, are not clear. Indeed, no transcriptomic analysis of astrocytes during remyelination have been conducted. My PhD project aims to characterise astrocyte responses and perform unbiased transcriptomic analysis of astrocytes during efficient remyelination in order to reveal their potential regenerative functions and identify novel therapeutic strategies to promote remyelination in disease.

Hypothesis; Astrocytes are dynamic cells that are supportive of remyelination.

Aims;

1. *Characterise astrocyte responses during remyelination.*
2. *Identify the molecular mechanisms underpinning the role of astrocytes by RNA sequencing.*
3. *Manipulate astrocytic functions and assess impact on remyelination.*

2. CHAPTER: METHODS

2.1. Animals and ethics

Animal experiments were of moderate severity, approved by and performed under United Kingdom Home Office project licences issued under the Animals (Scientific Procedures) Act 1968. Animals were housed in groups of 5 in a 12:12h light: dark cycle with free access to food and water. A minimum of three animals were used per condition in each experiment unless otherwise stated.

C57Bl/6J were purchased from Jackson Laboratories. Animals were used at the age of 2-3 months or 9-12 months for the ageing study. Tg(Aldh1l1-EGFP/Rpl10a)JD130 (ASRIBO) mice were re-derived by Prof Giles Hardingham's lab, The University of Edinburgh. This BAC-TRAP line expresses an eGFP-tag on the large ribosomal subunit protein L10a, targeted to the translational start site of the *Aldh1l1* gene. ASRIBO mice were used at the age of 2-3 months or 9-12 months for ageing study. GFAP-Nrf2.2 mice were provided by Prof Jeffrey Johnson, University of Wisconsin. The hGFAP-Nrf2 transgene was constructed as previously described [218] and transgenic mice were generated by pronuclear microinjection using fertilised eggs of the FVB/N strain. Mice were then bred in-house onto a C57/Bl6 background by Dr Jill Fowler, The University of Edinburgh. These mice overexpress Nrf2 in astrocytes, which is driven by the GFAP promoter. GFAP-Nrf2.2 mice were used at the age of 2-3 months.

2.2. Genotyping

2.2.1. DNA extraction

DNA for genotyping was extracted from ear tissue which was incubated in 100 µl of 50 mM NaOH and centrifuged for 90 seconds (sec) at 10,000 rpm. Samples were incubated at 100ºC for 7 minutes (min) then placed on ice for 10 min, and frozen until use.

2.2.2. Polymerase chain reaction (PCR)

GoTaq®Green Master Mix (Promega) for PCR was used according to the manufacturer's instructions. Briefly, 1µl of DNA template was mixed with 1X GoTaq®Green Master Mix, 0.25 µM of forward primer, 0.25 µM of reverse primer (Table 2.1 & 2.2) and nuclease-free water to a volume of 25 µl. PCR reactions used the following cycle parameters; 5 min at 95 ºC for initial denaturation, 35 cycles of 30 sec at 95 ºC for denaturation, 30 sec at 54 ºC for annealing and 30 sec at 72 ºC for extension, 5 min at 72 ºC for final extension and samples then held at 4 ºC. PCR products were run on a 2% agarose gel in Tris-borate-EDTA (TBE).

Table 2.1 | GFAP-Nrf2 genotyping primer sequence:

Gene	**Forward**	**Reverse**
Nrf2	5'-GCCTGAGAGCTGTAGGCC C–3'	5'-GGAATGGAAAATAGCTCCTGCC-3'
Gfap	5'-CTTCATAAAGCCCTCGCATC-3'	5'-TCTTGCCTCCAAAGGATGTC-3'

* Sequence obtained from Vargas *et al.* 2008 [218].

Table 2.2 | ASRIBO genotyping primer sequence:		
Gene	**Forward**	**Reverse**
Transgene	5'-CTGTCATCAGTCTTCACATCCAC-3' (*Aldh1l1*)	5'-CTGAACTTGTGGCCGTTTAC-3' (*Gfp*)
Internal positive control	5'-AGTGGCCTCTTCCAGAAATG-3'	5'-TGCGACTGTGTCTGATTTCC-3'

* Sequence obtained from The Jackson Laboratory

2.3. *In vivo* stereotaxic demyelination

Mice were anaesthetised with isoflurane and demyelinating lesions induced by stereotaxically injecting 0.5 mg/ml of lysolecithin (LPC) (egg-yolk, Sigma Aldrich L4129) diluted in sterile phosphate-buffered saline (PBS) into the corpus callosum with a Hamilton syringe (Figure 3.1.A). Sham lesions were induced by injecting sterile PBS. Coordinates for injection corresponded; 0.5 mm mediolateral from middle line, 1.2 mm rostral to bregma, and 1.4 mm depth to brain surface at bregma. Mice were sacrificed for immunofluorescence by intracardially perfusing with 4% paraformaldehyde (PFA) at 3, 7, 10, 14, and 21 days post-injection (DPI), or by carbon dioxide (CO_2) asphyxiation at 3, 7, 10 DPI for translational ribosome affinity purification (TRAP) experiments.

2.4. Cuprizone model

Cuprizone demyelination on mice was performed and provided by Tanja Kuhlmann, University of Münster provided tissue. Briefly, 8 weeks mice were fed with 0.2% (w/w) cuprizone diet for 5 weeks, and then switched to a normal diet until 10 weeks (Figure 3.6.A). Mice were sacrificed under deep anaesthesia by intracardially perfusing with PBS at 3, 5, 7 and 10 weeks. Brains were then fixed overnight with 4% PFA and then paraffin-embedded. Cuprizone sections quantified were within bregma 0 and bregma-2, according to the anterior-posterior axis of the mouse brain atlas [219].

2.5. Immunofluorescence

2.5.1. Tissue processing for OCT embedding

Mouse brain tissue was post-fixed overnight with 4% PFA, and cryoprotected in sucrose (15% and then 30%), before OCT (VWR, 361603E) embedding on dry ice. Sections were cut at 10 µm thickness on a cryostat. Sections were cut from bregma 0 to bregma -2, according to the anterior-posterior axis of the mouse brain atlas [219].

2.5.2. Deparaffinisation

Paraffin-embedded sections were pre-heated at 60°C in a hybridisation oven for 20 min. Slices were then immersed thrice for 5 min in Histo-clear II, twice for 5 min in Ethanol Absolute, and 5 min in each 95% Ethanol, 5 min in 70% Ethanol and distilled water.

2.5.3. Staining

Heat inactivated antigen retrieval (HIER) was achieved by microwaving the sections at medium power in 10 mM citrate buffer (pH 6.0) and heating for 20 min at 60°C, followed by three washes of PBS for 5 min. Slices were blocked in 5% heat-inactivated horse serum and 0.3 % Triton-X in PBS for 1 hour (h) at room temperature and then primary antibodies were applied, diluted in blocking solution and left overnight at 4°C in a humid chamber. Following three washes with PBS for 5 min, secondary antibodies diluted in blocking solution were applied for 2h at room temperature in a humid chamber. Hoechst (Sigma-Aldrich) was applied, followed by three washes in PBS, and slices were mounted onto glass slides and coverslipped with Fluoromount G (Cambridge Biosciences, 0100-01).

Antibodies to be used for this study are listed in Table 2.3.

Table 2.3 | Antibodies for immunostaining:		
Antibody	**Dilution**	**Provider – Catalog number**
Rat anti-myelin basic protein (MBP)	1:100	Bio-Rad antibodies - MCA409S
Chicken anti-glial fibrillary acidic protein (GFAP)	1:500	BioLegend – PCK-591P
Rabbit anti- glial fibrillary acidic protein (GFAP)	1:500	Dako – Z0334
Rabbit anti-Sox9	1:500	Sigma-Aldrich – AB5535
Mouse anti-nestin	1:100	Abcam – ab6142
Mouse anti-vimentin, clone LN-6	1:100	Sigma-Aldrich – MAB1681
Rabbit anti-nuclear factor IA (NFIA)	1:250	Abcam – ab228897
Rabbit anti-Ki67	1:100	Sigma-Aldrich – AB9260
Chicken anti-neurofilament H (NF-H)	1:100	Covance – PCK-592P05
Mouse anti-neurofilament H (NF-H)	1:1000	EnCor – MCA-9B12
Mouse anti-myelin associated glycoprotein (MAG), clone 513	1:100	Sigma-Aldrich – MAB1567
Mouse anti-myelin oligodendrocyte glycoprotein (MOG)	1:100	Sigma-Aldrich – MAB5680
Mouse anti-APC (CC-1)	1:100	Abcam – ab16794
Rabbit anti-Olig2	1:100	Sigma-Aldrich – AB9610
Rabbit anti-Heme oxygenase 1 (Hmox1)	1:100	Enzo – ADI-SPA-895-D
Goat anti-NQO1	1:100	Abcam – ab2346
Rabbit-HMGCS1	1:500	Invitrogen – PA5-29488
Rabbit-FDPS	1:100	Invotrogen – PA5-28228
Secondary antibodies; Alexa Fluor®-conjugated antibody	1:500	Life Technologies

2.6. Image acquisition and analysis

Z-stacks of images were obtained using an Olympus 3i Spinning Disk confocal microscope (30x silicone objective) using SlideBook 6 software. For astrocyte counts, TIFF files from max projections were imported to Image J, and the images were converted to 8-bit fluorescence RGB tiff and thresholded. For nuclear counts, watershed segmentation on binary images was used to separate objects and then images were analysed. Two fields of view were quantified per section within the right hemisphere of the corpus callosum, then the mean was calculated and converted to mm^2. For the analysis of myelin, the mean grey value was analysed in two regions of

interest within the right hemisphere of the corpus callosum, and from this, the mean background grey value of two regions of interest outside the corpus callosum were subtracted; the results were plotted as myelin protein intensity. For counting astrocytes positive for Hmgcs1, Fdps, Hmox1 and Nqo1, Imaris 9.0.0 software was used. TIFF files were converted to Imaris files using ImarisFileConverter 9.0.0. and images in z-stacks were analysed. To analyse the number of positive cells, a colocalisation channel was created using ImarisColoc and analysed using ImarisSurfaces. Two regions of interest of 450 µm x 450 µm were selected for analysis within the right hemisphere corpus callosum. Thresholding was done using absolute intensity. The size of each surface (named particle) was adjusted so that each was approximately the size of a cell.

For each image analysis, two different regions of interest were measured, and the mean was obtained. Three sections per animal were analysed and the mean was obtained, which is indicated as an 'n'.

2.7. BAC-Aldh1l1-translational ribosome affinity purification

Translational ribosome affinity purification (TRAP) protocol was performed according to Heiman *et al.* (2014)[220]. Briefly, magnetic beads (Dynabeads, Invitrogen) were coupled to anti-eGFP antibodies (Htz-GFP-19F7 and Htz-GFP-19C8, Memorial-Sloan Kettering Monoclonal Antibody Facility) and tissue lysates were prepared. The injured hemisphere of the corpus callosum was dissected using a brain

matrix and brain sections were homogenised in tissue-lysis buffer [20 mM HEPES RNase-free (Affymetrix), 10 mM Magnesium Chloride RNase-free ($MgCl_2$, Applied Biosystems), 150 mM Potassium chloride RNase-free (KCl, Applied Biosystems), 0.5 mM DL-Dithiothreitol (DTT, Sigma-Aldrich), 100 mg/ml cycloheximide (CHX) (Sigma Aldrich), 10µl/ml RNasin (Promega), and 10µl/ml Superasin (Applied Biosystems) in RNase free water). Lysates were centrifuged at 2,000 g for 10 min at 4°C. A 1/9 volume of 300 mM 1,2-diheptanoyl-*sn*-glycero-3-phosphocholine (DHPC, Avanti Polar Lipids) was added to supernatants. Following a 5 min incubation, lysates were centrifuged at 20,000 g for 20 min at 4°C. A small fraction of the supernatant was saved at this point as 'input' sample. The rest of the supernatant was added to the anti-eGFP-coated-magnetic beads and incubated overnight at 4°C in rotation. Beads were collected with a magnet, washed 4 times in high-salt wash buffer [20 mM HEPES, 10 mM $MgCl_2$, 350 mM KCl, 0.5 mM DTT, 1% Nonidet P-40 (NP-40, AG Scientific), and 100 µg/mL CHX] and then resuspended in 100 µl of Nanoprep Lysis Buffer with β-ME (Stratagene Absolutely RNA Kit).

2.8. RNA extraction and bioanalysis

Input and TRAP samples were processed for RNA extraction. RNA extraction was achieved by using the Agilent Nanoprep kit following the manufacturer's protocol. Quality of the samples was measured by the use of an Agilent Bioanalyzer, using the Agilent RNA 6000 PICO assay protocol. Samples selected had an RNA integrity number (RIN)>7.

2.9. Quantitative polymerase chain reaction (qPCR)

Complementary DNA (cDNA) for qPCR was obtained using SuperScriptTM VILOTM cDNA Synthesis Kit (Invitrogen). The FastStart Universal SYBR Green Master Mix (ROX) (Roche, *04913850001)* was used, and qPCR was run on a QuantStudio 5 Real-Time PCR System.

2.10. RNA sequencing

Samples were sent to Cambridge Genomic Services for Next-Generation Sequencing. For Library preparation the SMART-Seq v4 Ultra Low input RNA kit according to manufacturer's protocol (Takara Bio USA). The sequencing was run on a NextSeq 550 system (Illumina) on a 150 cycle high-output run paired-end read (30K reads).

2.11. Bioinformatics

Bioinformatics was carried out by Dr Owen Dando from Prof Giles Hardingham's Lab, The University of Edinburgh. For each sample, 75 base pair paired-end reads were mapped to the primary assembly of the mouse (mm10) reference genome contained in Ensembl release 93 [221]. Alignment was performed with STAR version 2.5.3a [222]. Tables of per-gene read counts were generated from the mapped reads with featureCounts version 1.5.2 [223]. Differential expression analysis was then

performed using DESeq2 (R package version 1.18.1) [224]. Sample heatmaps and PCA plots were produced using variance-stabilized per-gene read counts.

In order to account for variable amounts of background mRNA contamination in these TRAP-seq samples the presence of a set of cell-type-specific genes which should not be expressed in astrocytes were quantified, including microglial-specific genes (Sfpi1 and Aif1), oligodendrocyte-specific genes (Sox10 and Mbp) and neuronal-specific genes (Syp and Rbfox3). For each cell-type-specific gene, its expression in FPKM (fragments per kilobase per million mapped reads) in each sample was divided by its maximum FPKM in any sample, giving, for each gene, a per-sample measure of background contamination (with a value between 0 and 1). Per-gene contamination values for the six genes correlated well across samples.

An average was taken over the six genes to give a per-sample contamination measure, C, with a value between 0 and 1. For every other gene, the correlation of its gene expression with C over all samples was calculated, giving a per-gene measure, R, of the likelihood of a gene's apparent presence in the data as being due to background mRNA contamination.

To determine how likely it was to get high values of R by chance, a fake gene expression data set containing the FPKM values from our data was created with the values scrambled between samples for each gene (in which case, this fake gene expression should not be correlated with C). From this fake data, the R value for each scrambled gene was created, deriving a null distribution of R values. In the real data,

a Z-score for each gene indicating how far its own R value was from the mean of this null distribution in units of standard deviations of the null distribution was calculated. Hence, any gene whose Z-score that was greater than 2 excluded from the gene ontology enrichment and gene set analyses, thus removing significant GO terms and GSA gene sets whose presence was likely due to non-astrocytic background mRNA expression.

2.12. Pathway analysis

Pathway analysis was performed using Ingenuity Pathway Analysis software (QIAGEN). The list of genes and their FPKM for the control, sham (3 DPI), and demyelinating conditions (3, 7 and 10 DPI) with a cut off of 5 FPKM, were analysed in IPA to identify canonical pathways, top biological functions, top upstream regulators and top toxicity functions. Parameters included 'species=mouse' and 'confidence=experimentally observed'.

Gene ontology and pathway networks were explored using the plugging ClueGO v.2.5.4 for Cytoscape v.3.7.1 software. The top 200 significantly upregulated genes at each time point (3, 7 and 10 DPI) were used for the analysis. *Mus Musculus* annotation was used. Ontologies/Pathways selected corresponded to GO-Biological processes, KEGG pathways and WikiPathways. Statistical significance was analysed by two-sided hypergeometric test, and Bonferroni step down correction. Grouping was based on highest significance and GO-term fusion.

2.13. Cluster analysis

Cluster analysis performed using Graphia Professional (KAJEKA) in three-dimensional (3D) layout, using the top 5000 highly expressed genes in control and comparing FPKM values to 3, 7 and 10 DPI. A 0.8 Pearson correlation threshold was applied. Pearson correlation measures the association between two different variables. In this study, Pearson correlation related to the similarity between nodes, which represent genes [225]. Markov clustering algorithm (MCL) with inflation value of 2.0 was applied. MCL clustering, groups genes according to similarities in their expression pattern and forms clusters. Inflation is a factor which defines how clean and robust the clusters are (1.7 to 2.2 correspond to optimal values) [225]. Clusters were set to contain ≥4 nodes. Graphs of different clusters were plotted against the mean centred FPKM, where the mean is centred to 0, meaning that the average of the FPKM values for each cluster is calculated and then the average is subtracted to the average of each group (CT, 3, 7 and 10 DPI). The graphs were scaled by the software from 1 to -1.

2.14. Statistical analysis

Samples were blinded prior to quantification. Statistical analysis was performed by the use of GraphPad Prism 7 software. Shapiro-Wilk were applied to analyse the data for Gaussian distribution, and then statistical analysis was performed using the parametric tests (student's t-test or ANOVA) when normal distributed, and the non-

parametric test (Kolmogorov-Smirnoff test or Kruskal-Wallis test) when not normally distributed. When two independent variables were compared (eg. treatment and time) a two-way ANOVA was applied. Data was represented as mean ± standard error of means (s.e.m.). *P* values <0.05 were considered statistically significant and are indicated in figures legends.

3. CHAPTER: CHARACTERISATION OF ASTROCYTE RESPONSES DURING REMYELINATION

3.1. Introduction

Fibrous astrocytes are crucial for developmental myelination and homeostasis of white matter during adulthood [129]. After an insult, astrocytes become reactive. In acute situations, temporary astrocyte reactivity counteracts damage and limits inflammation to restore homeostasis. In contrast, in chronic injury, continuous astrogliosis can promote further damage, thereby limiting repair [226].

The opposite functional regulation of astrocytes after demyelination comes from studies in MS and experimental models of demyelination. These have shown that reactive astrocytes can have several detrimental functions, and thus impair remyelination. Astrocytes can secrete unfavourable factors that inhibit the differentiation of OPC into new myelin forming-oligodendrocytes. As astrocytes also are in contact with the BBB, they control the entrance of peripheral immune, which can aggravate myelin damage [184, 185]. Reactive astrogliosis can lead to the formation of glial scar, a significant component of chronic inactive MS lesions [27], and impair the migration of oligodendrocyte progenitors to the lesion [198]. Contrarily, astrocytes can promote remyelination by secreting factors that promote new myelin sheath formation by oligodendrocytes [51, 227]. They can attract microglia to phagocytose myelin debris, required for remyelination [72]. Moreover, they are essential for limiting inflammation and oxidative stress by mediating antioxidant functions [92, 199].

These differences observed in the astrocyte responses towards oligodendrocyte differentiation and remyelination could result from changes in activation and responses over time. However, the responses of astrocytes (i.e. reactivity, numbers, proliferation) during the course of efficient remyelination have never been fully characterised. Here, I assessed astrocyte behaviour in two models of remyelination.

3.2. Results

3.2.1. Characterisation of astrocytes after LPC-demyelination

3.2.1.1. GFAP+ astrocytes increase during oligodendrocyte differentiation

To characterise astrocyte responses during remyelination, I used a model of focal demyelination where remyelination occurs in temporal isolation of demyelination, allowing characterisation of astrocyte responses during remyelination alone (Figure 3.1.A-B). In this model, the myelin toxin lysolecithin (LPC) is stereotaxically injected into the white matter tract the corpus callosum. After LPC-induced demyelination, remyelination takes place within a well-characterised time-window, where proliferation and recruitment of OPCs occurs after 3-4 days post-injection (DPI), oligodendrocyte precursor differentiation occurs between 7-10 DPI, and remyelination takes place between 14-21 DPI (Figure 3.1.A-B). Hence, I first confirmed de- and re-myelination in this model by staining for myelin basic protein (MBP).

I then assessed astrocyte reactivity during remyelination, using GFAP as a pan-reactivity marker. I observed that in comparison to PBS-injected controls ('sham') and non-lesioned controls, demyelinated lesions showed an increase in GFAP+ reactive astrocytes over the course of remyelination, peaking during the phase of oligodendrocyte differentiation and early remyelination (7-14 DPI) (Figure 3.1. C-D). GFAP+ astrocytes were subsequently reduced when remyelination was completed at 21 DPI. Moreover, early after demyelination, astrocytes adopted a hypertrophic morphology characteristic of a reactive state, compared to the clear separation of

cell bodies along the corpus callosum seen in undemyelinated and sham controls (Figure 3.1. C).

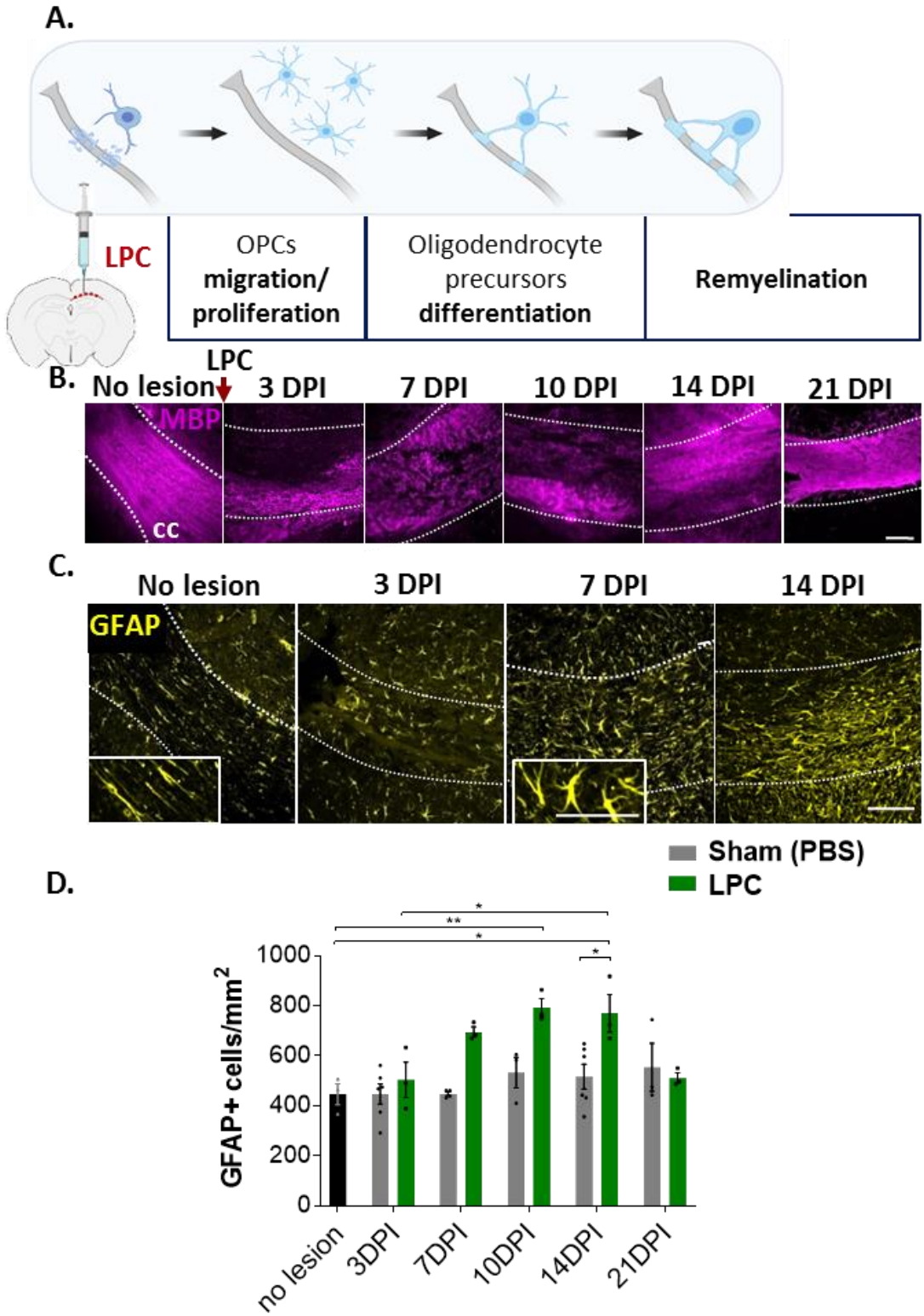

Figure 3.1. Reactive astrocyte numbers peak during oligodendrocyte differentiation and onset of remyelination. A. Schematic representation of the focal demyelination model, where the toxin LPC is injected into the corpus callosum**. B.** Main phases of the LPC model are shown by MBP staining (magenta) in the corpus callosum (indicated with dashed lines) in a control animal (no lesion), at 3DPI (OPC migration/proliferation phase), 7 and 10 DPI (oligodendrocytes precursor differentiation phase), and 14 and 21 DPI (remyelination phase). **C.** Representative images of GFAP+ astrocytes in lesions (yellow). Scale bar; 100µm. White box shows a magnified view of different astrocyte morphologies. Scale bar; 50 µm. **D.** Quantification of GFAP+ astrocytes in Sham animals (injected with PBS) and lesioned animals (injected with LPC). Error bars indicate s.e.m. of the number (n) of animals. n=3-6 animals. Significance was determined by using one-way ANOVA with multiple comparisons and Tukey posthoc test. *P<0.05, **P<0.01. **OPCs;** oligodendrocytes precursor cells. **LPC;** Lysolecithin. **MBP;** Myelin basic protein. **CC;** Corpus callosum. **DPI;** days post-injection. **GFAP;** Glial fibrillary acidic protein.

3.2.1.2. Sox9+ astrocytes decrease early after LPC-demyelination

I next assessed astrocyte numbers during remyelination using the transcription factor Sox9 as a pan-astrocyte marker [120]. I observed that Sox9+ cells decreased significantly at 3 DPI compared to the Sham and non-lesion controls (Figure 3.2.A-B). The number of Sox9+ cells were rapidly recovered by 7 DPI, reaching similar levels to those observed in control and not significantly changing during the rest of the remyelination process (Figure 3.2.B). To determine the proportion of astrocytes that become reactive during remyelination, I assessed the proportion of

Sox9+ astrocytes which are GFAP+ (Figure 3.2.C). This ratio was close to 1.0 at 3 DPI, indicating that the majority of astrocytes became reactive after demyelination (Figure 3.2.C). The proportion of reactive astrocytes subsequently decreased during early remyelination (14 DPI) and reached basal levels when remyelination was completed (21 DPI) (Figure 3.2.C).

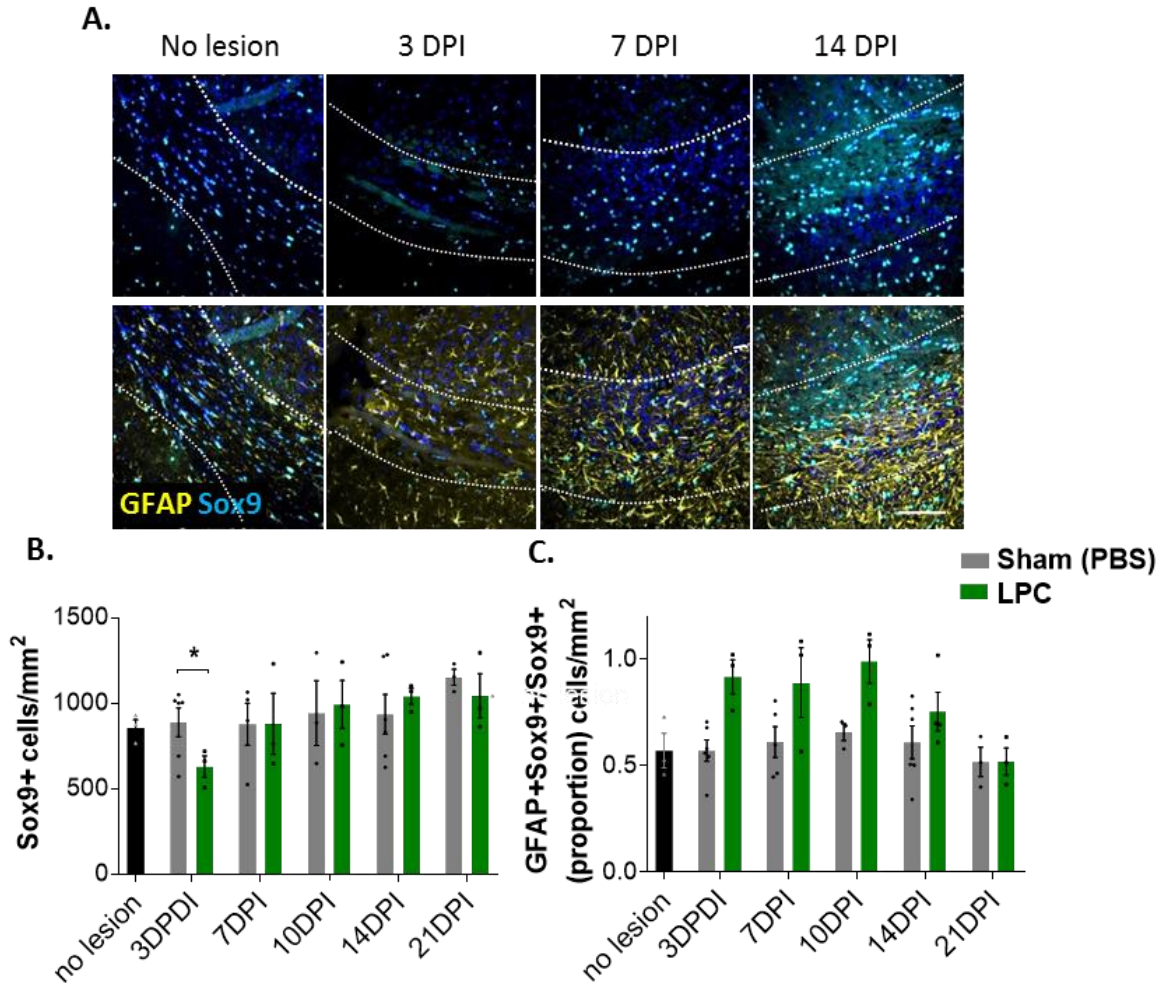

Figure 3.2. Dynamic changes in the proportion of astrocytes, which are reactive during remyelination. A. Representative images of all astrocytes (Sox9+; cyan) which are reactive (GFAP+; yellow). Cell nuclei are stained with Hoechst (Blue). Scale bar; 100 µm. **B.** Quantification of Sox9+ astrocytes in Sham animals (injected with PBS) and lesion animals

(injected with LPC). Significance was determined by using the Kruskal-Wallis test with multiple comparisons and Dunn's test correction. **C.** Quantification of the proportion of GFAP+Sox9+/Sox9+ cells (ratio) in Sham animals (injected with PBS) and lesion animals (injected with LPC). Significance was determined using one-way ANOVA with multiple comparisons and Tukey posthoc test. Error bars indicate s.e.m. of the number (n) of animals. n=3-6 animals. *P<0.05.

3.2.1.3. Vimentin+ and Nestin+ astrocytes increase during remyelination

To confirm the changes in reactive astrocytes during remyelination, I investigated additional markers for reactivity: nestin and vimentin (Figure 3.3.). I found that vimentin+ GFAP+ astrocytes increased at the time of oligodendrocyte differentiation (7 DPI) with a small but not significant drop at 10 DPI, and a significant increase during early remyelination (14 DPI) compared to non-lesioned controls (Figure 3.3.A and C). Similarly, Nestin+ GFAP+ cells were gradually increased after demyelination, reaching a significant peak at 14 DPI compared to non-lesioned animals (Figure 3.3.B and D). Vimentin and nestin positive GFAP+ cells reached basal levels when remyelination was completed (21 DPI). No significant changes were observed in the sham controls for both markers.

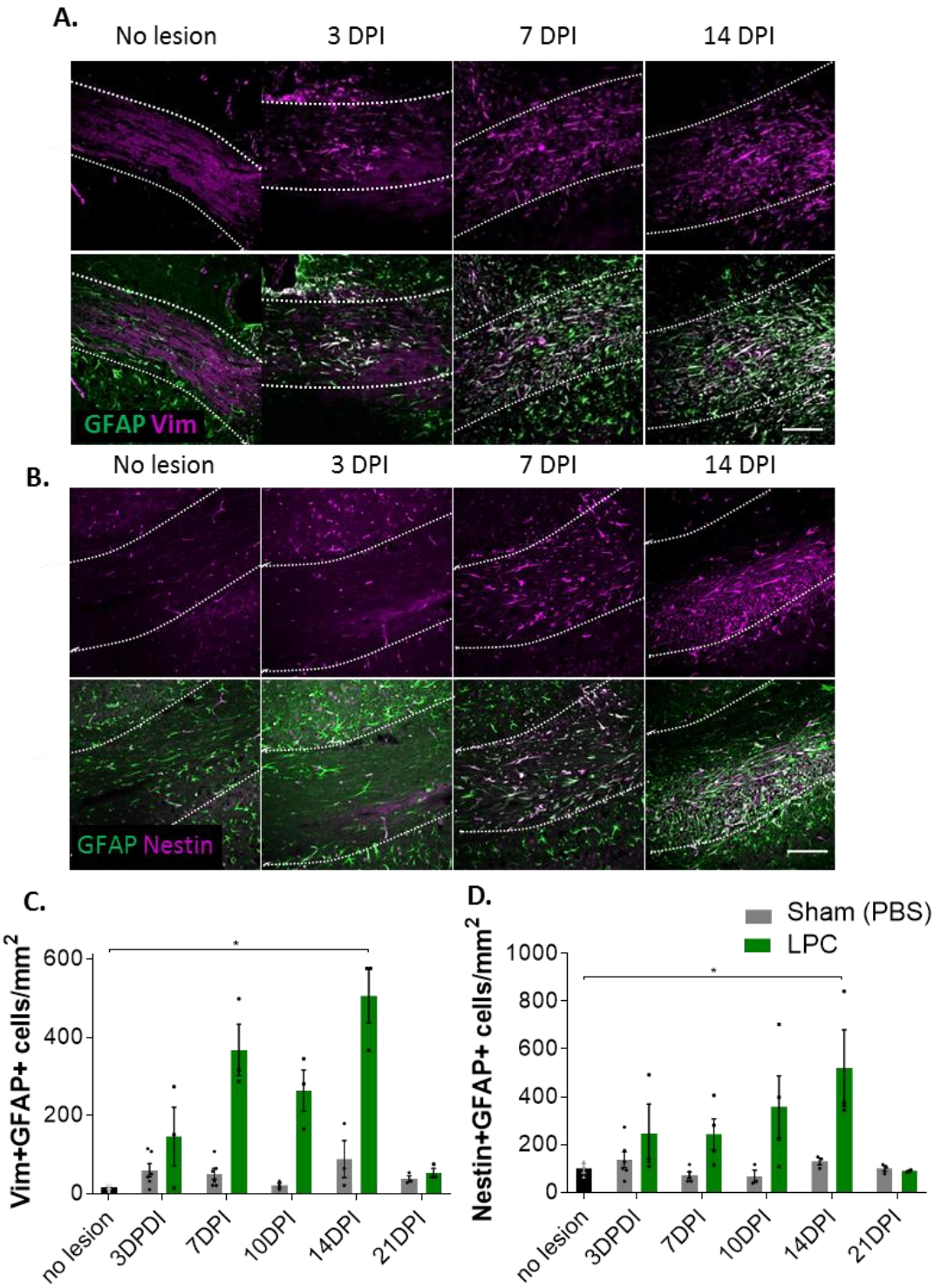

Figure 3.3. Reactive astrocytes express vimentin and nestin during oligodendrocyte differentiation and onset of remyelination. A and B. Representative images of GFAP+ astrocytes (green) co-stained with vimentin (A), or nestin (B) (magenta). Scale bar; 100 µm.

C. Quantification of Vim+GFAP+ astrocytes in Sham animals (injected with PBS) and lesion animals (injected with LPC). Significance was determined using the Kruskal-Wallis test with multiple comparisons and Dunn's test correction. **D.** Quantification of Nestin+GFAP+ astrocytes in Sham animals (injected with PBS) and lesion animals (injected with LPC). Significance was determined using one-way ANOVA with multiple comparisons and Tukey posthoc test. Error bars indicate s.e.m. of the number (n) of animals. n=3-6 animals. *P<0.05. **Vim;** Vimentin.

3.2.1.4. GFAP+ astrocyte proliferate early in remyelination

Given that I observed an increase in GFAP+ astrocytes during remyelination, I next asked whether this reflected increased proliferation by using the proliferation marker Ki67. I observed that reactive astrocytes which were proliferating (GFAP+ Ki67+) significantly increased during the oligodendrocyte differentiation phase (7-10 DPI) and the numbers were maintained during early remyelination (14 DPI) compared to the sham and non-lesioned controls (Figure 3.4). The increase in proliferative astrocytes coincided with the increase in reactive astrocyte numbers (Figure 3.1.C-D). Proliferating reactive astrocytes returned to normal levels when remyelination was completed at 21 DPI.

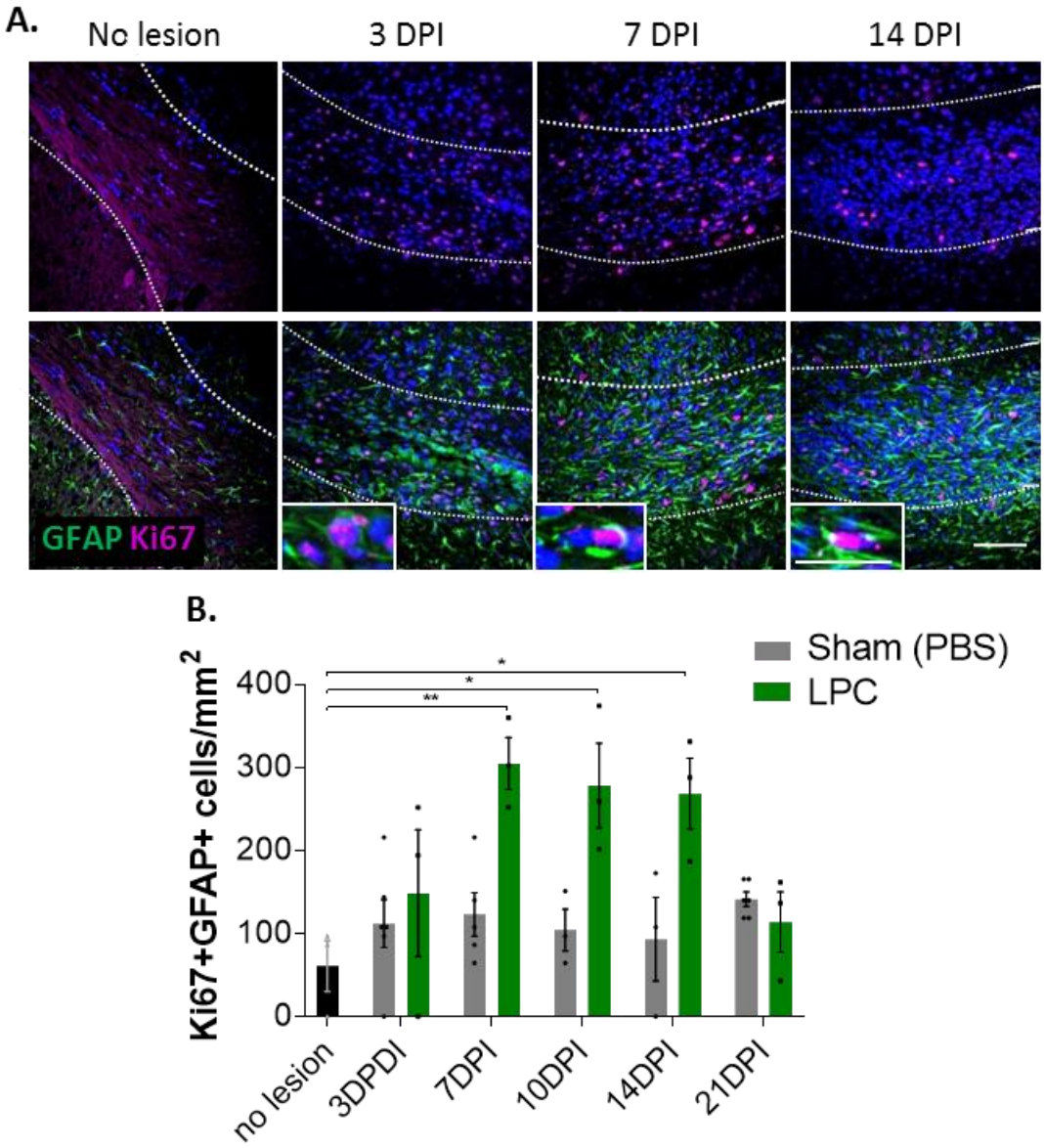

Figure 3.4. GFAP+ astrocytes proliferate during oligodendrocyte differentiation and remyelination phases. Representative images of proliferative astrocytes identified with Ki67 (magenta) and GFAP+ (green). Cell nuclei are stained with Hoechst (Blue). Scale bar; 100 µm. White boxes show magnified views of proliferative reactive astrocytes (Ki67+GFAP+). Scale bar; 25 µm. **B.** Quantification of Ki67+GFAP+ astrocytes in Sham animals (injected with PBS) and lesion animals (injected with LPC). Significance was determined using one-way ANOVA

with multiple comparisons and Tukey posthoc test. Error bars indicate s.e.m. of the number (n) of animals. n=3-6 animals. *P<0.05.

3.2.1.5. NFIA is increased in reactive astrocytes during remyelination

I then investigated whether astrocytes could be derived from progenitors by staining for an astrocyte progenitor marker NFIA, a transcription factor expressed in glial progenitors that controls the formation of astrocytes in development [122]. I observed that NFIA expression in reactive astrocytes significantly increased at the onset of remyelination (10 DPI) and in early remyelination (14 DPI) when compared to sham and non-lesioned controls (Figure 3.5). NFIA levels returned to normal when remyelination was completed at 21 DPI. However, NFIA may also mark reactive astrocytes [228], and more definitive lineage tracing would be required to claim that new astrocyte differentiation was taking place.

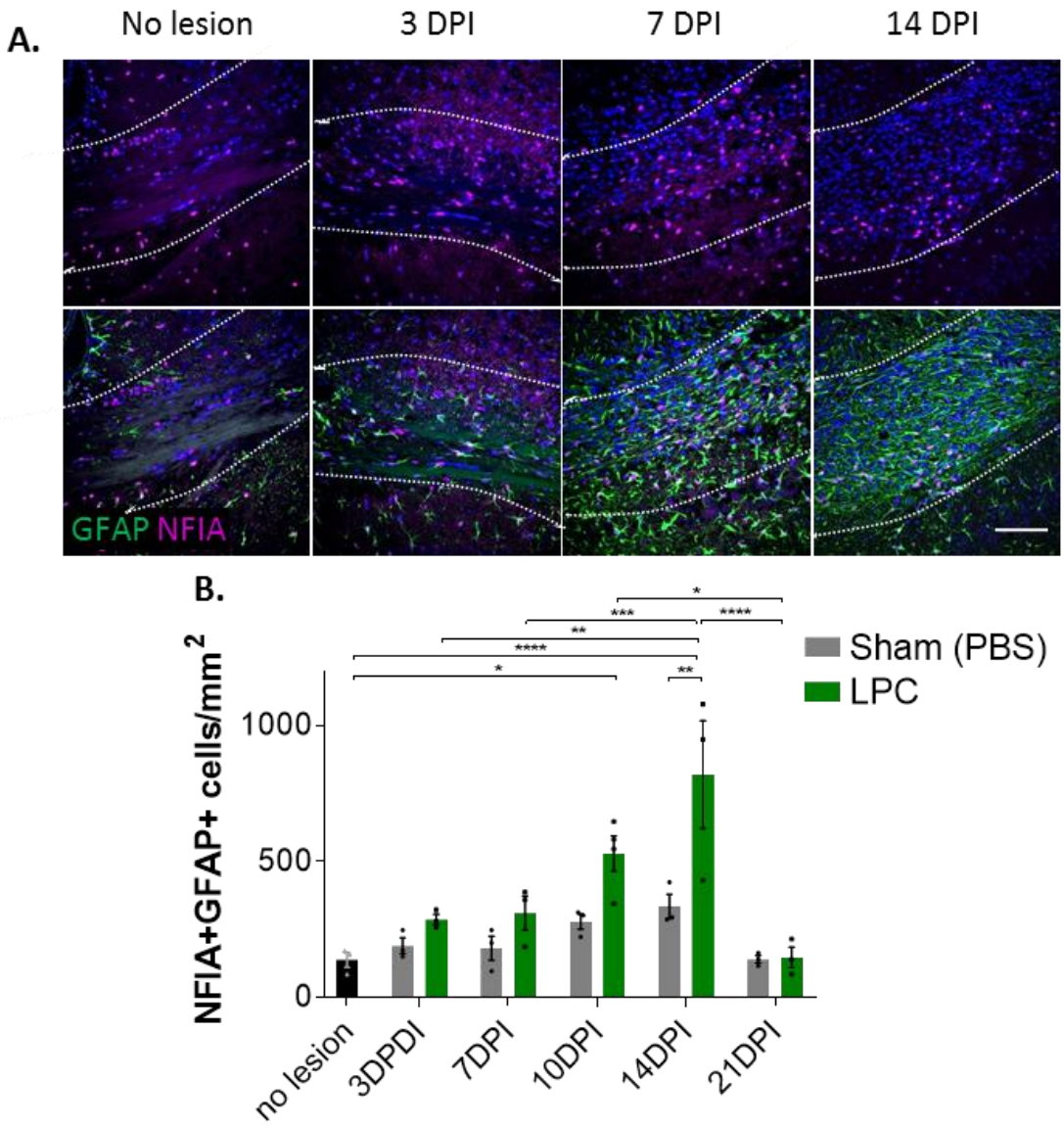

Figure 3.5. Reactive astrocytes express the progenitor marker NFIA during oligodendrocyte differentiation and onset of remyelination. A. Representative images of GFAP+ astrocytes (green) co-stained with NFIA (magenta). Cell nuclei are stained with Hoechst (Blue). Scale bar; 100 µm. Scale bar; 25 µm. **B.** Quantification of NFIA+GFAP+ astrocytes in Sham animals (injected with PBS) and lesion animals (injected with LPC). Significance was determined using one-way ANOVA with multiple comparisons and Tukey posthoc test. Error bars indicate s.e.m. of the number (n) of animals. n=3 animals. **P*<0.05, ***P*<0.01, ****P*<0.001, *****P*<0.0001.

3.2.2. Characterisation of astrocytes after cuprizone-demyelination

3.2.2.1. GFAP+ astrocytes increase during oligodendrocyte differentiation in the cuprizone model

To confirm whether the astrocyte responses observed during remyelination in the LPC-demyelination model could be observed in a distinct remyelination model, I used another model of toxic induced-demyelination, the cuprizone model. Cuprizone is a copper chelator, which affects the cytochrome oxidase activity required for mitochondrial oxidative phosphorylation, which in turn impairs mature oligodendrocyte metabolism leading to apoptosis and demyelination [229, 230]. In this model, cuprizone is administered in the diet of mice to achieve demyelination. Here, cuprizone was provided in the diet for 6 weeks, where after 3 weeks initial demyelination starts and after 5 weeks extensive demyelination and initial oligodendrocyte regenerative responses can be observed (Figure 3.6.A) [231, 232]. Then mice were switched to a normal diet to induce spontaneous remyelination, where early and late remyelination are observed at 7 and 10 weeks, respectively (Figure 3.6. A-B) [232]. The mouse experiments were performed by Prof. Tanja Kuhlmann's lab (University of Muenster, Germany), and I obtained brain sections to assess the astrocyte responses. I first assessed de- and re-myelination in this model using MBP as a marker for myelin. I observed that maximal demyelination was achieved after 5 weeks of cuprizone diet. After 7 weeks of cuprizone, early remyelination was observed followed by nearly complete remyelination at 10 weeks.

I found that astrocyte reactivity (GFAP expression) increased early during the demyelinating phase (3 weeks, figure 3.6), and subsequently peaked when oligodendrocyte differentiation and initial remyelination occur (5 weeks, figure 3.6). GFAP expression then decreased when remyelination is complete (10 weeks, figure 3.6). Similar to what I observed in the LPC-induced demyelination model, in the cuprizone model maximal astrocyte reactivity took place during oligodendrocyte differentiation and onset of remyelination, at 5 weeks (Figure 3.1 and 3.6).

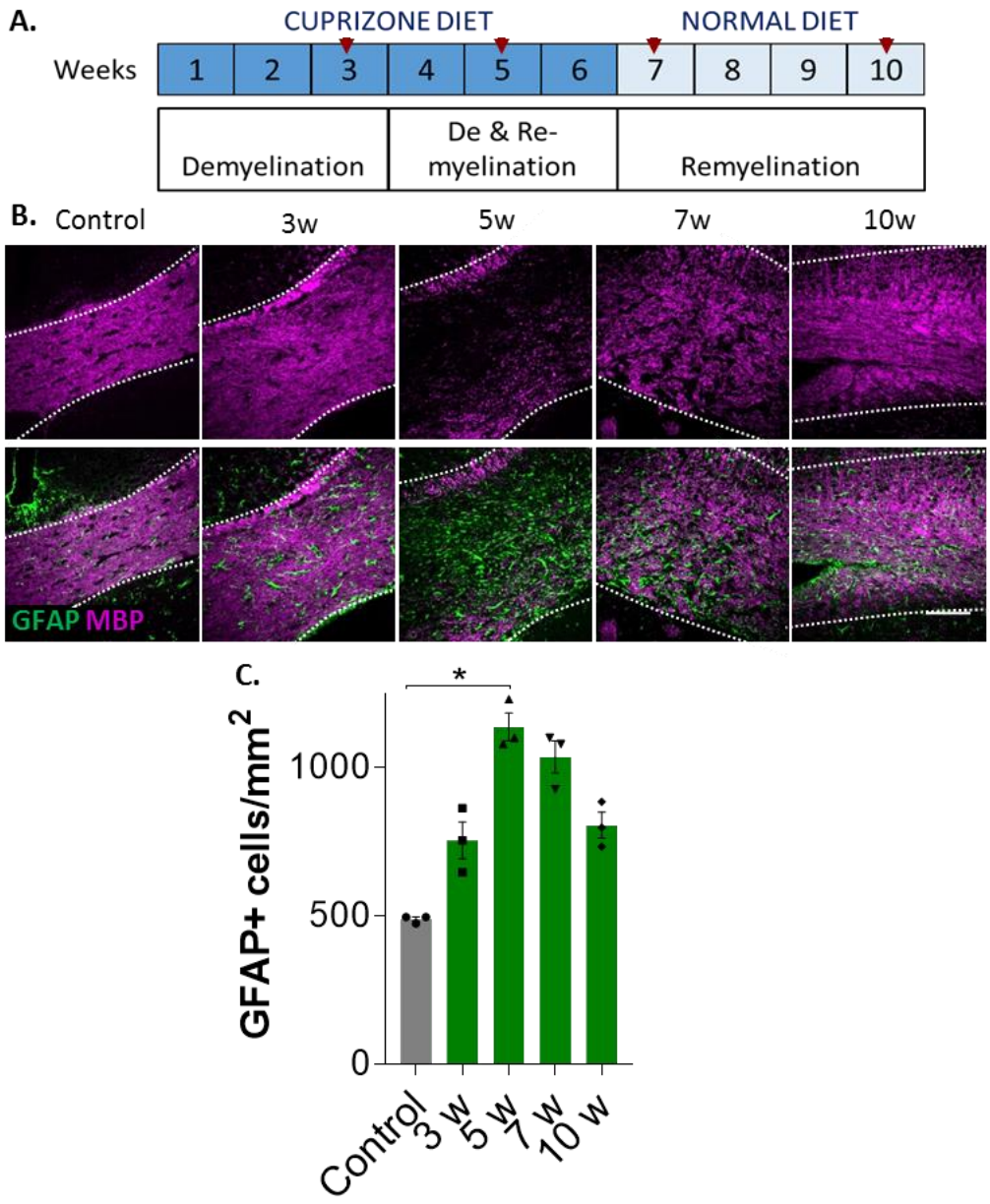

Figure 3.6. Reactive astrocyte numbers peak early in remyelination in the cuprizone model. **B.** Schematic representation of the cuprizone-induced demyelination models, where red arrowheads indicate the time-points used in this study. **B.** Main phases of the cuprizone model are shown by MBP staining (magenta) in the corpus callosum (indicated with dashed lines) where GFAP+ astrocytes are shown in a control animal (no lesion), at 3 weeks (w) (early demyelination phase), 5w (demyelinating/remyelinating phase), 7w (early remyelination phase) and 10w (late remyelination phase). Scale bar; 100 µm. **C.** Quantification of GFAP+

astrocytes. Error bars indicate s.e.m. of the number (n) of animals. n=3 animals. Significance was determined using Kruskal-Wallis with multiple comparisons and Dunn's test correction. *P<0.05.

3.2.2.2. Sox9+ astrocytes decrease during demyelination in the cuprizone model

To assess the total number of astrocytes in the cuprizone model, I used Sox9 as the pan astrocyte marker. Sox9+ cells significantly dropped at 3 weeks of cuprizone administration, compared to non-demyelination controls (Figure 3.7). The numbers of Sox9+ cells were subsequently recovered and did not significantly change after 5 weeks of cuprizone diet (Figure 3.7.B). Moreover, the majority of astrocytes became reactive during demyelination (at 3 weeks) and the onset of remyelination (5 weeks) (measured by the GFAP+ Sox9+/Sox9+ cell ratio; Figure 3.7.C) and this proportion decreased as remyelination proceeded (Figure 3.7.C).

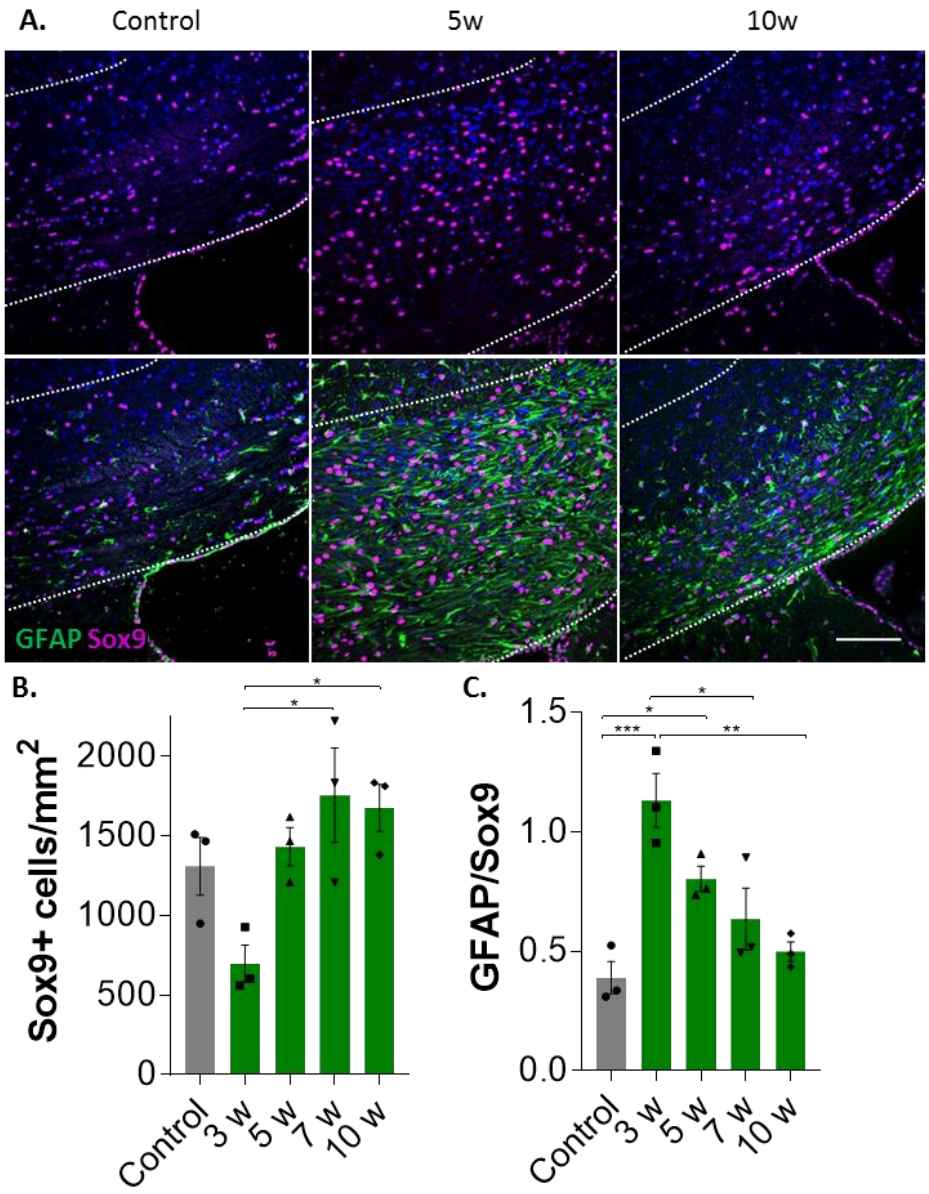

Figure 3.7. Dynamic changes in astrocyte number and reactivity in the cuprizone model. A. Representative images of astrocytes stained with Sox9 (magenta) and GFAP (green). Cell nuclei are stained with Hoechst (Blue). Scale bar; 100 µm. **B.** Quantification of Sox9+ astrocytes. Significance was determined using the Kruskal-Wallis test with multiple comparisons and Dunn's test correction. **C.** Quantification of the GFAP+Sox9+/Sox9+ cell ratio in Sham animals (injected with PBS) and lesion animals (injected with LPC). **B and C.** Significance was determined using one-way ANOVA with multiple comparisons and Tukey

posthoc test. Error bars indicate s.e.m. of the number (n) of animals. n=3 animals. *P<0.05, **P<0.01, ***P<0.001.

3.2.2.3. Vimentin+ and Nestin+ astrocytes increase during remyelination in the cuprizone model

I confirmed astrocyte reactivity by staining for nestin and vimentin (Figure 3.8). A similar pattern was observed with both markers, with a significant increase in GFAP+ cells that were nestin or vimentin positive at 5 weeks, compared to non-lesion controls (Figure 3.8). After this time-point expression of both markers was decreased, and although the vimentin+ GFAP+ cells were not significantly higher compared to control (Figure 3.8.B), they remained significantly increased for nestin+ GFAP+ cells compared to control (Figure 3.8.C).

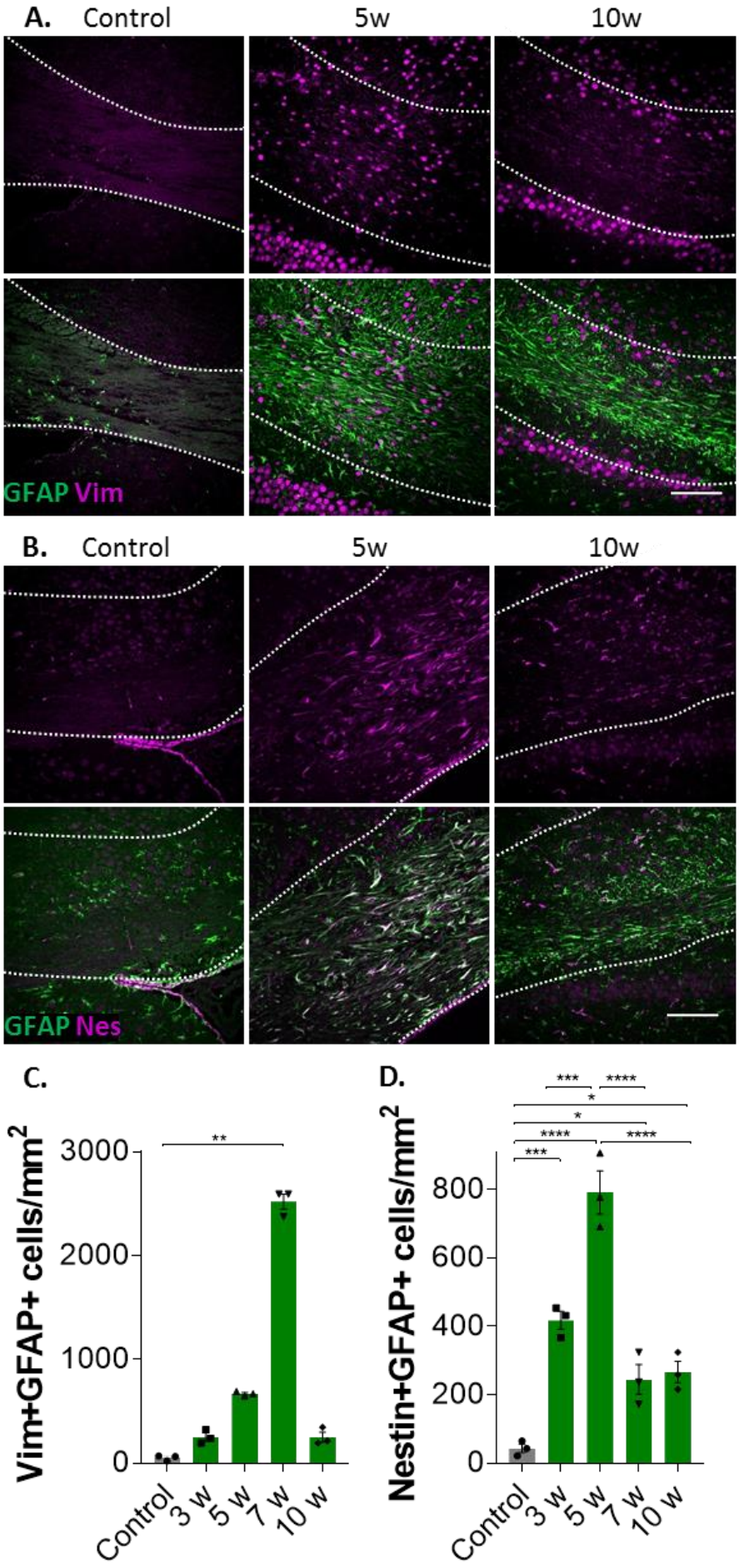
A.
Control
5w
10w
GFAP Vim
B.
Control
5w
10w
GFAP Nes
C.
Vim+GFAP+ cells/mm2
3000
2000
1000
0
**
Control
3 w
5 w
7 w
10 w
D.
Nestin+GFAP+ cells/mm2
800
600
400
200
0
***
****
*
Control
3 w
5 w
7 w
10 w

Figure 3.8. Reactive astrocytes expressing vimentin and nestin peak during oligodendrocyte differentiation and onset of remyelination. A and B. Representative images of GFAP+ astrocytes (green) co-stained with vimentin (A), or nestin (B) (magenta). Scale bar; 100 µm. **C.** Quantification of Vim+GFAP+ astrocytes. Significance was determined by using the Kruskal-Wallis test with multiple comparisons and Dunn's test correction. **D.** Quantification of Nestin+GFAP+ astrocytes. Significance was determined using one-way ANOVA with multiple comparisons and Tukey posthoc test. Error bars indicate s.e.m. of the number (n) of animals. n=3 animals. **P*<0.05, ***P*<0.01, ****P*<0.001, *****P*<0.0001. **Vim;** Vimentin.

3.2.2.4. GFAP+ astrocyte proliferate during demyelination and early remyelination in the cuprizone model

I next investigated astrocyte proliferation in the cuprizone model using the proliferation marker Ki67. GFAP+ Ki67+ astrocytes significantly increased during the demyelinating phase (3 weeks) and during oligodendrocyte differentiation and onset of remyelination phase (5 weeks). This coincided with the increase in the number of GFAP+ astrocytes. GFAP+ Ki67+ cells decreased after early remyelination (7 weeks) and maintained during late remyelination (10 weeks).

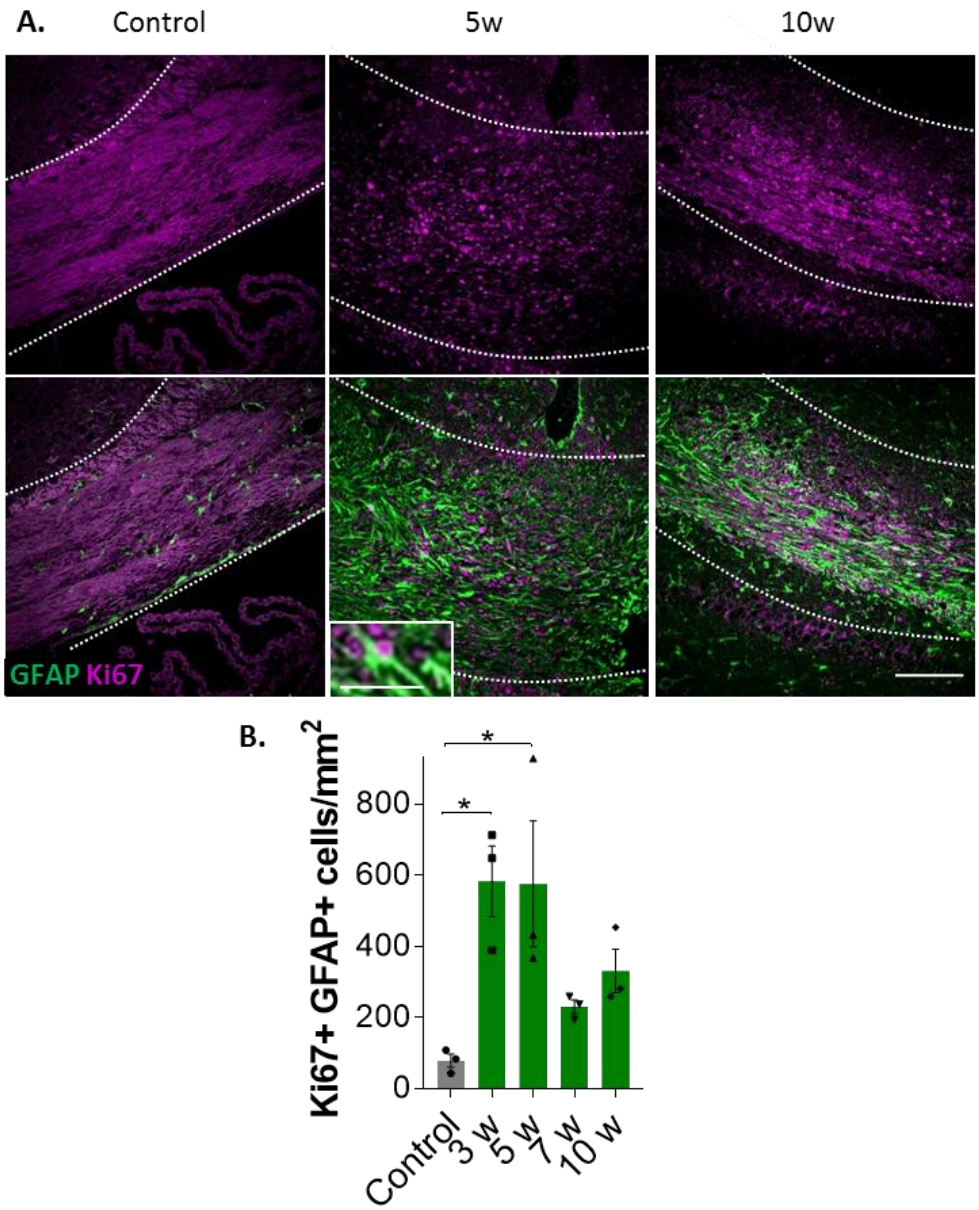

Figure 3.9. Reactive astrocyte proliferation peaks during oligodendrocyte differentiation and early remyelination phases in the cuprizone model. A. Representative images of proliferative astrocytes stained with Ki67 (magenta) and GFAP (green). Scale bar; 100 µm. White box shows magnified view of proliferative reactive astrocyte (Ki67+GFAP+). Scale bar; 25 µm. **B.** Quantification of Ki67+GFAP+ astrocytes. Significance was determined using one-way ANOVA with multiple comparisons and Tukey posthoc test. Error bars indicate s.e.m. of the number (n) of animals. n=3 animals. *P<0.05.

3.3. Discussion

In this chapter, I found that astrocytes undergo significant changes in activation and number during remyelination. These changes were similar in two distinct models of demyelination, a focal lesion model using the myelin toxin LPC, and a widespread demyelination model using the cuprizone diet. After demyelination in both models, immunofluorescent analysis of GFAP showed that astrocyte morphology was hypertrophic, a feature characteristic of a reactive state [163, 233]. Astrocyte morphology was normalised when remyelination was complete, presenting a morphology similar to that in undemyelinated conditions (Figure 3.1 and 3.6). Furthermore, in both models of remyelination, there was a significant increase in the number of GFAP+ astrocytes during the phases of oligodendrocyte differentiation and the onset of remyelination, which returned to normal levels when remyelination was completed. I also found that in both models, the majority of astrocytes became reactive just after demyelination, indicating early activation of astrocytes (Figure 3.2.C and 3.8.C).

In concordance with my results, GFAP+ astrocytes have been shown to accumulate in LPC-demyelinated lesions of the spinal cord [234], and with lesion progression in the EAE model [196]. GFAP is the major component of the astrocyte cytoskeleton and is important for controlling cell division, migration and signal transduction [160]. GFAP upregulation is required to regulate astrocyte function in the cuprizone model, and its overexpression reduces oligodendrocyte apoptosis, demyelination and axonal damage even during chronic demyelination from long-

term cuprizone administration [175]. In agreement with this, depletion of GFAP+ astrocytes was shown to impair remyelination after injury [72, 235]. In my study, an increase in GFAP expression in astrocytes was observed preceding oligodendrocyte precursor differentiation and early remyelination in both models, suggesting that astrocytes may have essential functions that regulate these processes. However, after various CNS insults, an increase in GFAP expression has also been correlated with pathogenesis. For instance, in active and chronic MS plaques, GFAP is found to be highly expressed in astrocytes [236, 237]. Therefore, studying astrocyte functions in the context of efficient remyelination is crucial to understand their contributions during this process to then be able to assess what mechanisms fail in pathology.

Astrocyte activation was confirmed by staining for vimentin and nestin (Figure 3.3 and 3.9), with a similar pattern in expression observed for both markers. However, a more gradual increase was observed in the LPC model, peaking at 14 DPI. In the cuprizone, a moderate increase was observed compared to control, peaking at 5 weeks on the cuprizone diet. Increased vimentin expression has been previously observed in the cuprizone model at 5 weeks, being less pronounced at other time-points [72]. Both of these markers are highly increased in astrocytes during the peak clinical stage of EAE, which subsequently decrease during recovery phases [238].

The small differences I observed in astrocyte responses between the two models could be due to differential severity of each model, with the LPC model being

acute demyelination in a small focal region. In contrast, the cuprizone model incurs a more globalised and continuous demyelination [239]. Differences in vimentin and nestin expression have been observed in comparing an acute stroke model to a more severe LPS model, even though a similar pattern of GFAP activation was observed [161]. Surprisingly, I found vimentin staining to be nuclear in astrocytes. In another report using cuprizone as a model of demyelination, some vimentin+ astrocytes were also observed with a rounded shape [240]. Vimentin filaments bind to the nuclear lamina regulating nuclear shape, maintaining stiffness and providing support [241]. Condensed vimentin filaments around the nucleus could explain this round shape observed in both studies.

To assess the total variation of astrocyte number, I used Sox9, a pan-astrocytic marker that has been defined to be specific for detecting all astrocytes in the adult mouse brain, outside of neurogenic niches [120]. I detected a decrease in the total number of astrocytes during active demyelination in both models compared to non-demyelinated conditions (Figure 3.2 and 3.7), which could reflect the death of astrocytes as a response to injury. Astrocyte numbers were then rapidly recovered to reach basal levels. Given that a recent study showed that LPC could be toxic to astrocytes at a concentration of 100 µM, LPC could have induced the death of astrocytes in my study [242]. However, the same effect of decreased astrocyte numbers was observed in the cuprizone model, indicating it could occur independent of LPC, and raises the question of whether astrocyte death may be an early protective effect in remyelination. Other models of injury have reported astrocyte death after

insult [164, 243], for instance, as a response to spinal cord injury, in which the death of astrocytes was mediated by pro-inflammatory microglia and was observed to be protective [164]. In this model and the LPC model, pro-inflammatory microglia are observed at the time-point in which the drop of astrocytes occurs [244], which may contribute to the astrocyte death and would require further study.

Importantly, although Sox9 has been accepted as a pan-astrocytic marker in the adult brain, it should be taken into account that other NSCs expressing this marker may be migrating into the lesion to repopulate the area. Hence, the numbers of Sox9+ cells could be accounting for progenitor cells within the lesion and not only astrocytes. This would emphasize the need of investigating better markers specific for astrocytes that could be applied for their quantification. Aldh1l1 would be the best marker currently defined [143], however it lacks of good antibodies that can be used in mouse tissue and reporter lines have to be used to this end.

To understand the increase in astrocyte numbers observed in both models I assessed astrocyte proliferation. Astrocyte proliferation took place early during active demyelination and initial remyelination in both the LPC and cuprizone models. This could explain the increase in GFAP+ astrocytes and recovery of Sox9+ cells after the initial decrease. Proliferation after demyelination or another CNS insult is a characteristic feature of astrocytes [72, 240, 245]. A study in which live imaging was performed in a traumatic brain injury model showed that astrocytes had minimal migration after lesioning, but rather proliferated to repopulate injured areas [245].

Interestingly, the levels of reactivity and proliferation of reactive astrocytes in the cuprizone model did not return to basal levels. This was also observed in a previous study in the cuprizone model whereby GFAP+ astrocytes and GFAP+Ki67+ astrocytes decreased upon return to a normal diet, but not back to the levels of non-demyelinated controls [72]. However, this could be explained by a slower recovery in this model due to widespread demyelination, in comparison to a small acute lesion. Nonetheless, overall, similar changes in astrocyte numbers, reactivity and proliferation were observed in both models used. This could due to both models inducing acute demyelinating models, where mainly oligodendrocyte damage causes demyelination and spontaneous remyelination can efficiently take place. Even thought the cuprizone model would has widespread damage over different brain areas, the area assessed in the present study (the corpus callosum) was consistent in both models and this could explain a similar trend of recovery. Moreover, similar patterns of activation have been previously observed in microglia in these two models of demyelination [243]. Given that astrocytes and microglia communicate to drive remyelination that could also explain the similar results observed in the present study.

To explore whether the increase in reactive astrocytes was a result of increased astrocyte differentiation, I used NFIA as a marker for astrocyte progenitors. I observed that NFIA expression showed a gradual increase during remyelination, peaking at 14 DPI LPC compared to non-lesioned controls. I noted that this pattern was similar to that observed for vimentin and nestin in the LPC model, which could

raise the question as to whether GFAP+NFIA+ cells are reactive astrocytes instead of astrocytes recently derived from progenitors. Supporting these findings, a recent study showed that in a model of stroke, astrocytes had increased levels of NFIA expression in damaged grey and white matter [228]. Inhibiting NFIA in astrocytes prevented white matter repair in this model [228]. Moreover, NFIA was required to produce new reactive astrocytes [228]. NFIA is located on the GFAP promoter before the phase of astrocyte differentiation in development, and its inhibition decreases GFAP expression and prevents formation of long processes [160]. It could be that reactive astrocytes express NFIA, and its expression is required for a change in their activation after demyelination. After insult, reactive astrocytes are plastic cells that express progenitor markers and characteristics of neural stem cells [246]. Some of the basic and most commonly used pan-markers for astrocytes are also expressed by radial glia and neural stem cells during development: Aldh1l1, GLAST, and Glt-1[246]. Unlike GFAP, vimentin and nestin are predominantly expressed in the brain during development by radial glia, but this shifts when astrocytes are mature [160]. Often after injury, reports are not clear as to whether the expression of these markers corresponds to astrocytes or progenitor cells [238]. Hence, in the present study, I suggest that NFIA is expressed due to a state of reactivity in astrocytes. To confirm the origin of NFIA+ cells, lineage tracing of NFIA+ cells would be required.

In conclusion, in this chapter, I observed that astrocytes present changes in activation during remyelination. GFAP was observed to be an early marker of activation, and the peak in GFAP+ astrocytes coincided with the timing of

oligodendrocyte differentiation and early remyelination. This suggests that astrocyte activation coincides with oligodendrocyte lineage cell responses and raises the question as to how they might support these processes after demyelination. I then aimed to address this question by performing RNA sequencing of astrocytes isolated at key early time-points during remyelination, discussed in the next chapter.

4. CHAPTER: CHARACTERISATION OF ASTROCYTE TRANSCRIPTOME DURING REMYELINATION

4.1. Introduction

Different methods have been applied to investigate gene expression changes in astrocytes to have a better understanding of their roles in the context of pathology. RNA sequencing is the gold-standard technique currently used to investigate gene expression in an unbiased manner. By these means, astrocytes have been investigated in the context of neurodegeneration, where astrocytes lose homeostatic functions and upregulate inflammatory functions indicated by complement upregulation, engagement of pathways associated with innate immunity and synapse dysfunction, and downregulation of cholesterol synthesis [169, 247-249].

Different techniques are currently applied to isolate specific cells to extract the mRNA and then assess gene expression. These techniques can sort cells using antibodies against cell surface-specific markers, coated beads or enzymes that would dissociate the tissue, which includes fluorescent activated cell sorting (FACS), magnetic-activated cell sorting (MACS) or immunopanning [250, 251]. More recently, methods have been developed to tag the ribosome of specific cells and hence isolate the actively-translating mRNAs, which includes BAC-TRAP and RiboTag [250]. An advantage of these ribosome tagging techniques over other soring approaches is less artefact induced by manipulation from long cell purification processes such as cell panning, fixation, and cell isolation or the addition of enzymes to dissociate cells from specific tissues [251]. In BAC-TRAP and RiboTag methodology, the application of

Cycloheximide just after tissue dissection stops translation [252], and then the mRNA readout corresponds to the moment soon after the animal is terminated.

Furthermore, these techniques enable purifying cell-type-specific ribosomes and the associated translating mRNA, and hence can avoid contamination of mRNA from other cells, for instance, due to phagocytosis [253]. Ribosome tagging methodologies allows us to look at the translatome compared to other sorting techniques like immunopanning, FACS and MACS, which give information on the transcriptome. Hence, TRAP and RiboTag have a more accurate readout of gene expression at a specific time, as not all mRNAs are translated due to elements that bind mRNAs to block translation [254].

A limitation of BAC-TRAP is that transgenic lines for each cell line needs to be developed, in which EGFP-tagging of the ribosomal subunit RPL10 is under the control of a specific promoter [220]. For this reason, new techniques aiming at isolating the ribosome and the translating mRNAs like RiboTag have been developed [255]. The advantage of RiboTag versus BAC-TRAP is that one can use cell-type-specific Cre-LoxP recombinase lines that are crossed to the RiboTag lines, where the RPL22 ribosome subunit is tagged with hemagglutinin (HA) [250, 255]. Moreover, ribosome expression and their ability of translation is heterogenic, where RPL22 ribosome expression is more consistent than RLP10 [256]. Nonetheless, mRNA sequencing should be considered for hypothesis generation, as neither of these methodologies control for transcription efficiency and thus lacks information on the cell proteome, so validation at the protein level is always required.

4.2. Results

4.2.1. Astrocyte mRNA isolated using TRAP for RNA-sequencing

To characterise astrocyte functions at the molecular level during remyelination, I purified the translating mRNAs from astrocytes at key time-points in the focal remyelination model (3, 7 and 10 DPI LPC), by using TRAP methodology. To do so, I performed LPC-induced demyelination of the corpus callosum of an *Aldh1l1*-eGFP/Rpl10a reporter line (ASRIBO line) (Figure 4.1. A), in which astrocytes specifically express a molecule of enhanced GFP (eGFP) on the L10a large ribosomal subunit. Hence, this technique enables purifying only the mRNAs that are actively being translated to protein by using magnetic beads that have been coated with anti-eGFP antibodies (Figure 4.1. B). This methodology successfully enabled me to obtain an enrichment of astrocytic genes (*Aldh1l1, Gfap*) (represented in figure 4.1. C by an increased log2 fold change), over genes enriched in other cell types like neurons (*Eno*), and oligodendrocytes (*Mbp*), when comparing to an input sample, which is collected before the immunoprecipitation step and has mRNA from all cell types. To perform RNA sequencing, I determined the RNA integrity (RIN) score within a scale of 1 (degraded RNA) to 10 (highest RNA integrity), and found my samples to have an average RIN of 7.31±0.52 (Figure 4.1. D).

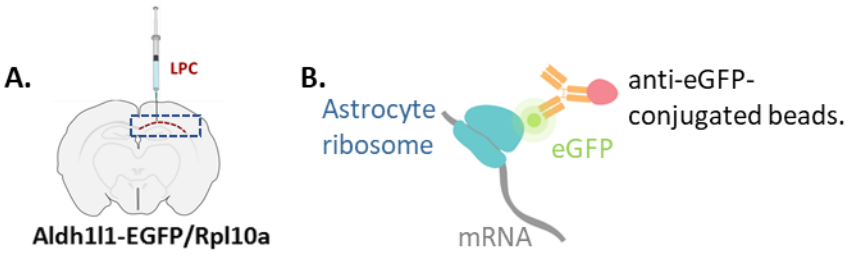

C.

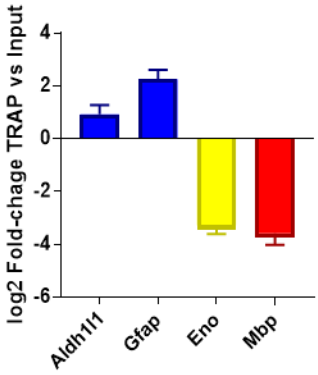

D.

		RIN
no lesion (CT)	1	7.9
	2	7.6
	3	7.5
3DPI PBS	1	7.9
	2	7.4
	3	7
3DPI LPC	1	7
	2	8.1
	3	7
7DPI LPC	1	7.1
	2	7.3
	3	7.2
10DPI LPC	1	7
	2	7.4
	3	6

Figure 4.1. Enrichment of astrocyte genes after TRAP and RNA integrity score for RNA sequencing. A. Schematic representation of the corpus callosum section dissected (blue box) for TRAP after LPC-induced demyelination in the *Aldh1l1*-EGFP/Rpl10a mice. **B.** Representation of the ribosome purification of Aldh1l1+ astrocytes by using a magnetic bead coated with anti-eGFP antibodies. **C.** Astrocytic gene (*Aldh1l1, Gfap*) enrichment in TRAP-isolated samples, compared to genes associated with neurons (*Eno*) and oligodendrocytes (*Mbp*). **D.** RIN score values of samples used for RNA sequencing.

4.2.2. Cluster analysis reveals 6 main cluster of genes during remyelination

Cambridge Genomics performed RNA-sequencing for ultra-low input RNA-sequencing. Bioinformatics was performed by Dr Owen Dando (Prof Hardingham's Lab, University of Edinburgh), where alignment to the mouse genome was performed with STAR RNA-seq aligner, quality control by FastQC and gene expression analysis by DESeq2 package for R (see methods section 2.11). To assess whether there were differences in the global expression of genes in astrocytes after demyelination, I performed an unbiased cluster analysis of the top 5000 most highly expressed genes in the control (no demyelination) using Graphia Professional software (KAJEKA), and compared their expression in astrocytes during remyelination (at 3, 7, and 10 DPI LPC). This type of analysis creates a graph structured according to the correlation of gene expression, in which nodes represent genes, and edges (lines) join nodes according to their similarity in gene expression [257]. In other words, genes that have similar patterns of expression are clustered together, which allows visualisation of gene expression on a global scale. By using this tool and collapsing nodes by MCL cluster (inflation 2.0) (see methods section 2.13), I observed that genes were split across 6 main clusters whose expression was differentially regulated during remyelination (figure 4.2.A). Cluster 1 included 1719 genes mostly upregulated in control and recovered at 7 DPI. Genes included in cluster 1 were associated with neuronal functions like synaptic regulation, energy functions like glycolysis and gluconeogenesis, and growth factor and cytokine receptor expression. Cluster 2

included 1673 genes whose expression peaked at 3 and 10 DPI. Genes included in cluster 2 indicated functions associated with oxidative stress and development.

Interestingly, clusters 3 (520 genes), 4 (541 genes) and 5 (332 genes) represented genes that were most highly upregulated during remyelination, in which the genes were most highly expressed at 3, 7 and 10 DPI, respectively. Cluster 3 represented genes associated with oxidative stress, apoptosis and migration. Cluster 4 contained genes associated with metabolic processes, cholesterol biosynthesis and intracellular processes (changes in structure and function taking place inside the cell, including intracellular organelles). Cluster 5 presented genes associated with regulation of cell cycle and nuclear functions. Lastly, cluster 6 consisted of the smaller cluster with 215 genes whose expression was more pronounced in the control and at 10 DPI (figure 4.2.B), and consisted of genes associated with mRNA metabolic functions, organelle and intracellular changes.

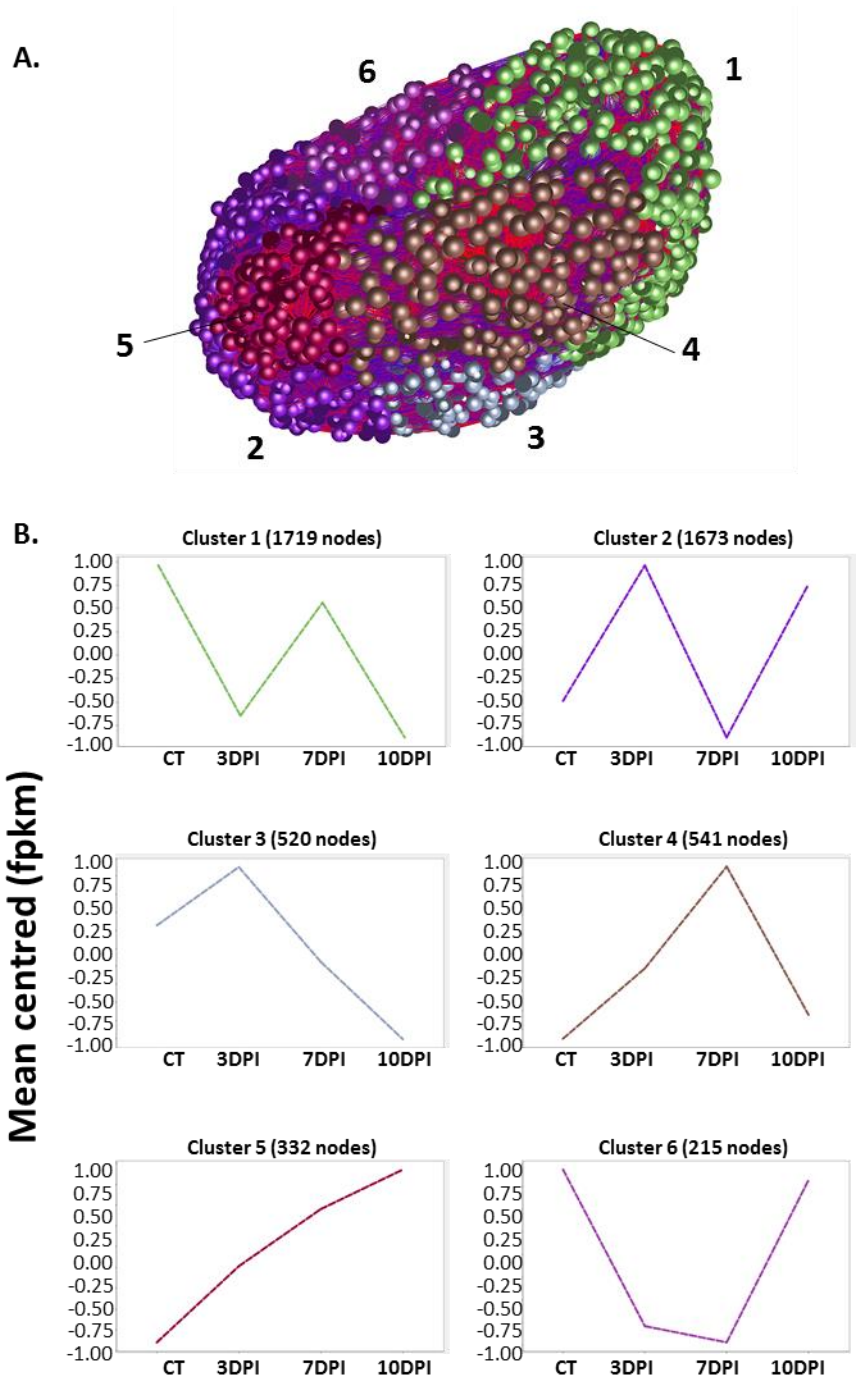

Figure 4.2. Cluster analysis shows global regulation of genes and functional relationship of top 5000 expressed genes in control. Cluster analysis performed using Graphia Professional (KAJEKA) in 3D layout, showing difference in gene expression patterns in astrocytes during remyelination versus the top 5000 highly expressed genes in control, using 0.8 Pearson

correlation threshold and MCL cluster (inflation value 2.0). **A.** Each node (sphere) represents a gene, connected by edges (lines) according to similarity in the pattern of individual gene expression. A total of 6 clusters containing ≥4 nodes are represented. **B.** The graph presenting the change in expression profile for the different clusters is represented, where X are the different time-points, including CT (non-lesion), 3, 7, and 10 DPI and Y is the mean centred FPKM.

4.2.3. Top significantly changed genes of astrocytes during remyelination

I then explored in greater detail the genes that were significantly upregulated and downregulated relative to control during remyelination (at 3, 7 and 10 DPI). I observed that different genes were significantly upregulated and downregulated at each time-point (using a cut-off of 1.3-fold and adjusted *p*-value ≤0.05) (Figure 4.3). Using this threshold, 673 genes were found to be significantly upregulated, and 1380 downregulated at 3DPI, 374 were significantly upregulated and 626 downregulated at 7DPI, and 833 genes were significantly upregulated and 916 downregulated at 10DPI (Figure 3.A-C). The top 25 significantly upregulated genes at each time point included *Timp1*, *S1pr3*, *Lgals1* and *Lgals3* at 3 DPI, *Hmgcs2* at 7 DPI, and *Lgals3* and *S100a11* at 10 DPI, all of which have been reported to be implicated in remyelination (Figure 4.3.D-F) [258-263]. The top 25 significantly downregulated genes at each time point included genes like *Sema3a* at 3DPI, which has been associated with impairment of remyelination (Figure 4.3.D-F) [20, 264].

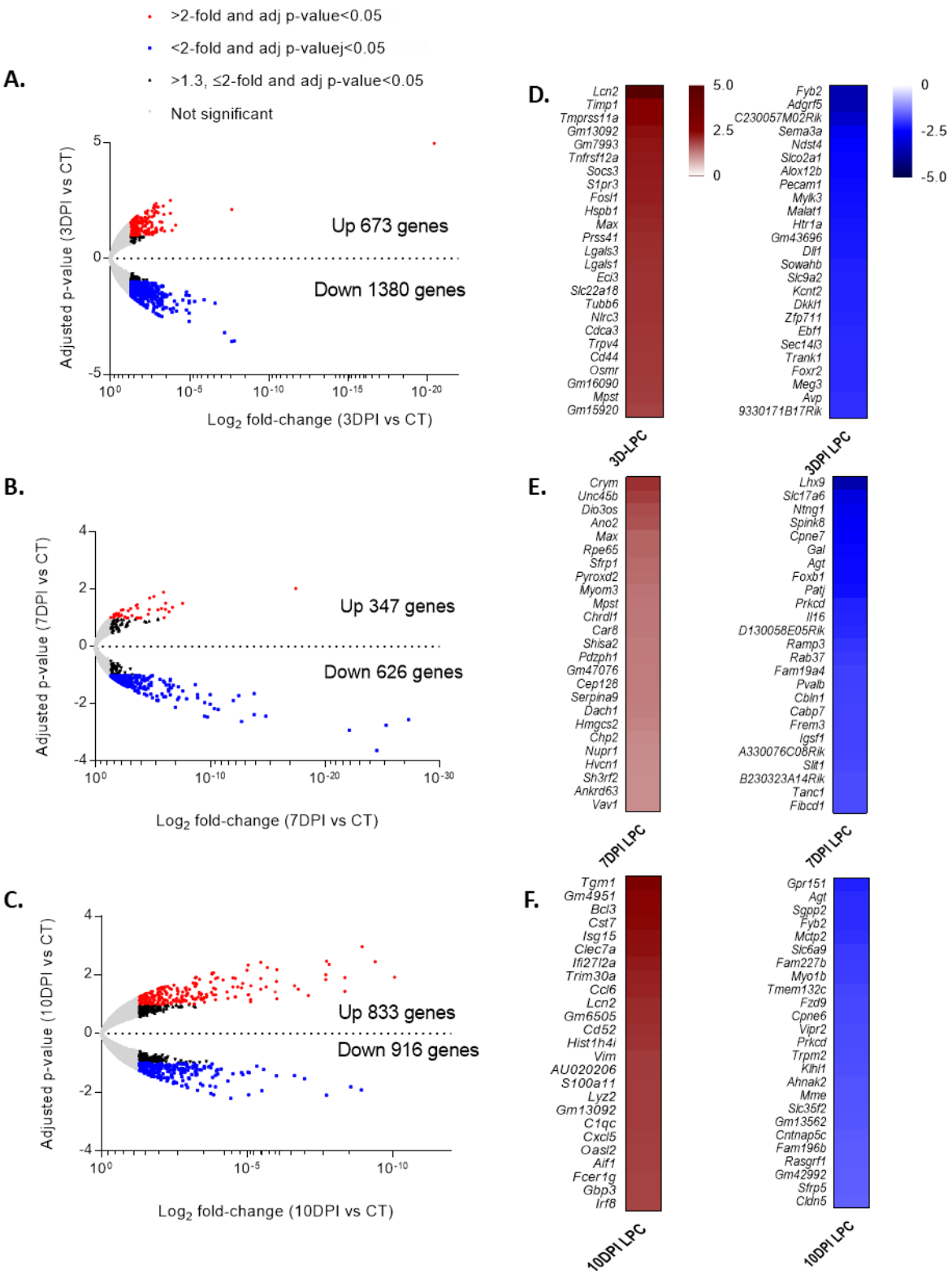
A.
>2-fold and adj p-value<0.05
<2-fold and adj p-valuej<0.05
>1.3, ≤2-fold and adj p-value<0.05
Not significant
Up 673 genes
Down 1380 genes
Adjusted p-value (3DPI vs CT)
Log2 fold-change (3DPI vs CT)
B.
Up 347 genes
Down 626 genes
Adjusted p-value (7DPI vs CT)
Log2 fold-change (7DPI vs CT)
C.
Up 833 genes
Down 916 genes
Adjusted p-value (10DPI vs CT)
Log2 fold-change (10DPI vs CT)
D.
Lcn2
Timp1
Tmprss11a
Gm13092
Gm7993
Tnfrsf12a
Socs3
S1pr3
Fosl1
Hspb1
Max
Prss41
Lgals3
Lgals1
Eci3
Slc22a18
Tubb6
Nlrc3
Cdca3
Trpv4
Cd44
Osmr
Gm16090
Mpst
Gm15920
5.0
2.5
0
3D-LPC
Fyb2
Adgrf5
C230057M02Rik
Sema3a
Ndst4
Slco2a1
Alox12b
Pecam1
Mylk3
Malat1
Htr1a
Gm43696
Dlf1
Sowahb
Slc9a2
Kcnt2
Dkkl1
Zfp711
Ebf1
Sec14l3
Trank1
Foxr2
Meg3
Avp
9330171B17Rik
0
-2.5
-5.0
3DPI LPC
E.
Crym
Unc45b
Dio3os
Ano2
Max
Rpe65
Sfrp1
Pyroxd2
Myom3
Mpst
Chrdl1
Car8
Shisa2
Pdzph1
Gm47076
Cep128
Serpina9
Dach1
Hmgcs2
Chp2
Nupr1
Hvcn1
Sh3rf2
Ankrd63
Vav1
7DPI LPC
Lhx9
Slc17a6
Ntng1
Spink8
Cpne7
Gal
Agt
Foxb1
Patj
Prkcd
Il16
D130058E05Rik
Ramp3
Rab37
Fam19a4
Pvalb
Cbln1
Cabp7
Frem3
Igsf1
A330076C08Rik
Slit1
B230323A14Rik
Tanc1
Fibcd1
7DPI LPC
F.
Tgm1
Gm4951
Bcl3
Cst7
Isg15
Clec7a
Ifi27l2a
Trim30a
Ccl6
Lcn2
Gm6505
Cd52
Hist1h4i
Vim
AU020206
S100a11
Lyz2
Gm13092
C1qc
Cxcl5
Oasl2
Aif1
Fcer1g
Gbp3
Irf8
10DPI LPC
Gpr151
Agt
Sgpp2
Fyb2
Mctp2
Slc6a9
Fam227b
Myo1b
Tmem132c
Fzd9
Cpne6
Vipr2
Prkcd
Trpm2
Klhl1
Ahnak2
Mme
Slc35f2
Gm13562
Cntnap5c
Fam196b
Rasgrf1
Gm42992
Sfrp5
Cldn5
10DPI LPC

Figure 4.3. Significantly upregulated and downregulated genes in astrocytes during remyelination. A-B. Volcano plots constructed using the adjusted P-values plotted against the Log2 fold-change (log10 scale) of 3 DPI (A), 7 DPI (B), and 10 DPI (C) groups compared to the control. The cut-off used to represent the significantly up, and downregulated genes consisted of a 1.3-fold change and adjusted p-value of <0.05. **D-F.** Heat map showing the top 25 significantly up and downregulated genes at 3 DPI (D), 7 DPI (E), and 10 DPI (F) groups compared to the control.

4.2.3.1. Changes in GO terms of significantly upregulated genes during remyelination vs control

The above results show that astrocytes have different gene expression at distinct phases of remyelination. To determine whether this was associated with differing functions I performed pathway analysis to explore gene ontology and pathway networks using the top 200 significantly upregulated genes at each time point. I used ClueGO (Cytoscape), where grouping was based on highest significance, using GO-term fusion (see methods section 2.12). Astrocytes presented different profiles at the different time-points investigated. At 3 DPI, upregulated genes were associated with functions indicative of repair (wound healing involved in inflammatory response, and regulation of establishment of endothelial barrier) and apoptosis (regulation of extrinsic apoptotic signalling pathway via death domain receptor) (Figure 4.4.A); the latter is consistent with the reduced astrocyte numbers observed at 3 DPI (Figure 3.2). At 7 DPI, astrocytes upregulated genes associated with pathways supportive of remyelination like cholesterol processes (cholesterol

metabolism, and cholesterol homeostasis), and increase in glial and neural cells (stem cell differentiation, glial cell migration, and regulation of neural precursor cell proliferation) (Figure 4.4.B). At 10 DPI, astrocytes had a transcriptional profile indicative of inflammatory responses (innate immune response) and repair (wound healing in inflammatory response) (Figure 4.4.C).

A.

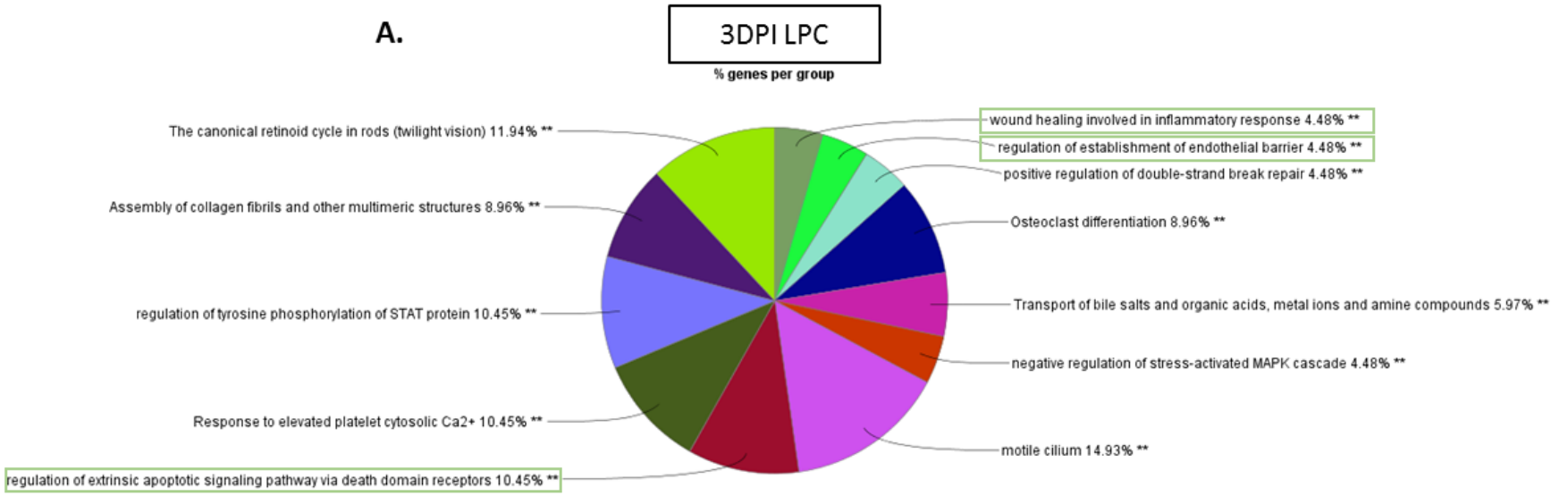
3DPI LPC
% genes per group
The canonical retinoid cycle in rods (twilight vision) 11.94% **
Assembly of collagen fibrils and other multimeric structures 8.96% **
regulation of tyrosine phosphorylation of STAT protein 10.45% **
Response to elevated platelet cytosolic Ca2+ 10.45% **
regulation of extrinsic apoptotic signaling pathway via death domain receptors 10.45% **
wound healing involved in inflammatory response 4.48% **
regulation of establishment of endothelial barrier 4.48% **
positive regulation of double-strand break repair 4.48% **
Osteoclast differentiation 8.96% **
Transport of bile salts and organic acids, metal ions and amine compounds 5.97% **
negative regulation of stress-activated MAPK cascade 4.48% **
motile cilium 14.93% **

B.

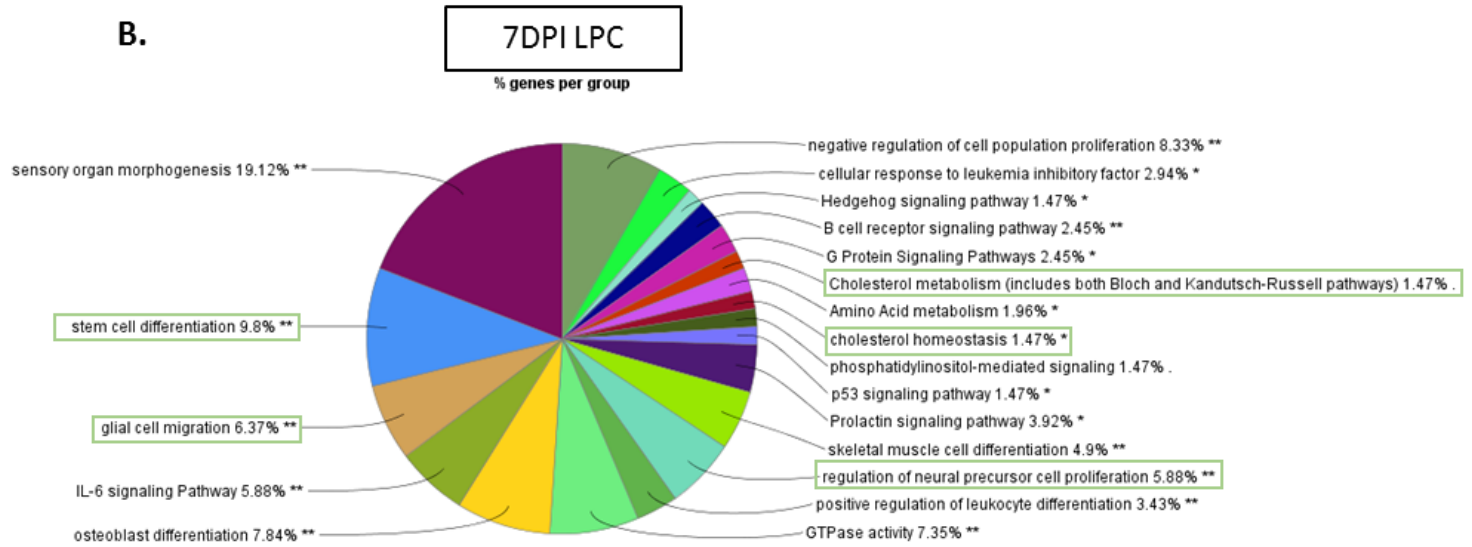
7DPI LPC
% genes per group
sensory organ morphogenesis 19.12% **
stem cell differentiation 9.8% **
glial cell migration 6.37% **
IL-6 signaling Pathway 5.88% **
osteoblast differentiation 7.84% **
negative regulation of cell population proliferation 8.33% **
cellular response to leukemia inhibitory factor 2.94% *
Hedgehog signaling pathway 1.47% *
B cell receptor signaling pathway 2.45% **
G Protein Signaling Pathways 2.45% *
Cholesterol metabolism (includes both Bloch and Kandutsch-Russell pathways) 1.47% .
Amino Acid metabolism 1.96% *
cholesterol homeostasis 1.47% *
phosphatidylinositol-mediated signaling 1.47% .
p53 signaling pathway 1.47% *
Prolactin signaling pathway 3.92% *
skeletal muscle cell differentiation 4.9% **
regulation of neural precursor cell proliferation 5.88% **
positive regulation of leukocyte differentiation 3.43% **
GTPase activity 7.35% **

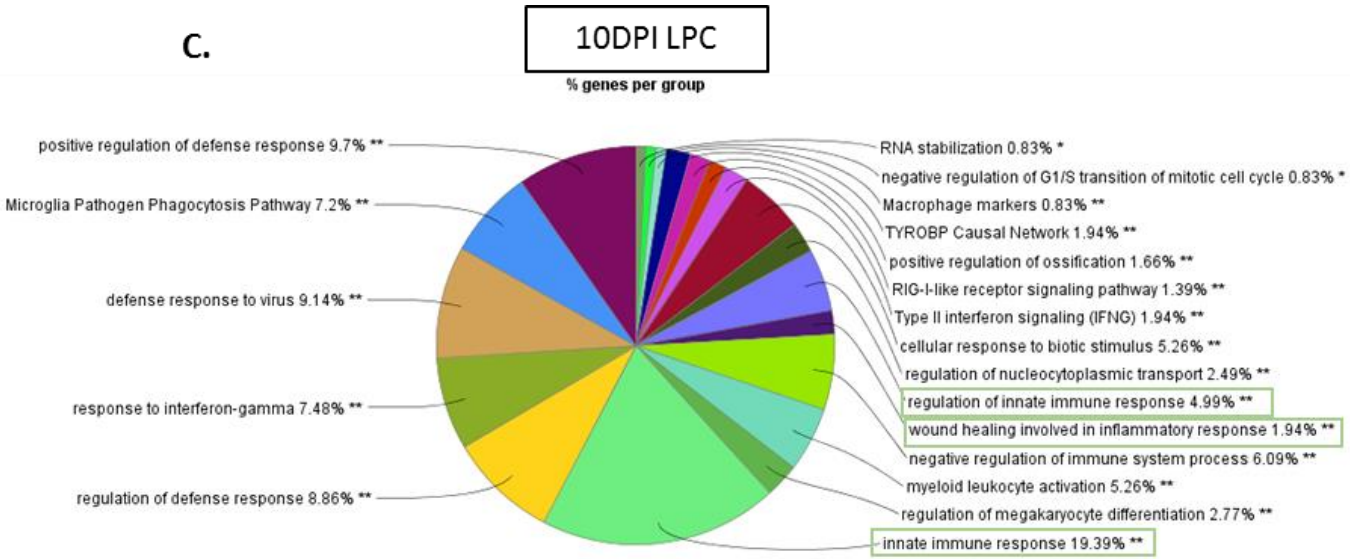

Figure 4.4. Astrocytes present different pathway profiles at 3, 7 and 10 days after LPC-induced demyelination. Pie chart constructed with clueGO (Cytoscape) showing the enriched pathways of the most significantly upregulated genes (2-fold change and adjusted p-value of 0.05) at 3DPI LPC (A), 7DPI LPC (B), and 10DPI LPC (C). GO terms are grouped using functional grouping (% of genes in each GO group) and based on highest significance. Each term is defined with a minimum of 3 genes.

4.2.4. Astrocyte gene expression indicates a change in their phenotype during remyelination

These results show that astrocytes present supportive functions for repair at all the time-points explored, with an inflammatory molecular signature at 10 DPI. Previous work classified astrocytes into phenotypes based on damaging properties (termed A1) and reparative function (termed A2). These were determined using injection of LPS, which was associated with upregulation of inflammatory genes, and an ischemic stroke model (middle cerebral artery occlusion (MCAO)), which upregulated neurotrophic and antioxidant genes [161]. I thus investigated the expression of these A1- and A2-associated genes in astrocytes at 3 DPI, 7 DPI or 10 DPI in comparison to control (using a cut-off of ≥0.5fpkm). The criteria for genes analysed were 1) the top 50 upregulated genes uniquely expressed in MCAO or the LPS model, or 2) genes that were increased more than 4-fold in the MCAO or the LPS model.

I observed a trend at 3 DPI in the upregulation of genes associated with the A2 phenotype (*p*-value = 0.0523 when using the top 50 gens in the MCAO, and *p*-value = 0.0026 when using genes upregulated ≥4FC in the MCAO) (Figure 4.6). A2 genes were found within the most significantly upregulated genes at 3 DPI (Figure 4.6.C). When this analysis was performed using genes for A1 phenotype at 3 DPI, no significance was observed (Figure 4.5). At 10 DPI, astrocytes showed significant expression of A1-associated genes (*p*-value = 0.0495 when using the top 50 gens in the LPS model, and *p*-value = 0.0966 when using genes upregulated ≥4 fold-changes

(FC) in the LPS model) (Figure 4.7), and no significance was observed when assessing A2-associated genes (Figure 4.8). A1 genes were found within the most significantly upregulated genes at 10 DPI (Figure 4.7.C). No A1 or A2 phenotype was observed at 7 DPI using these sets of genes.

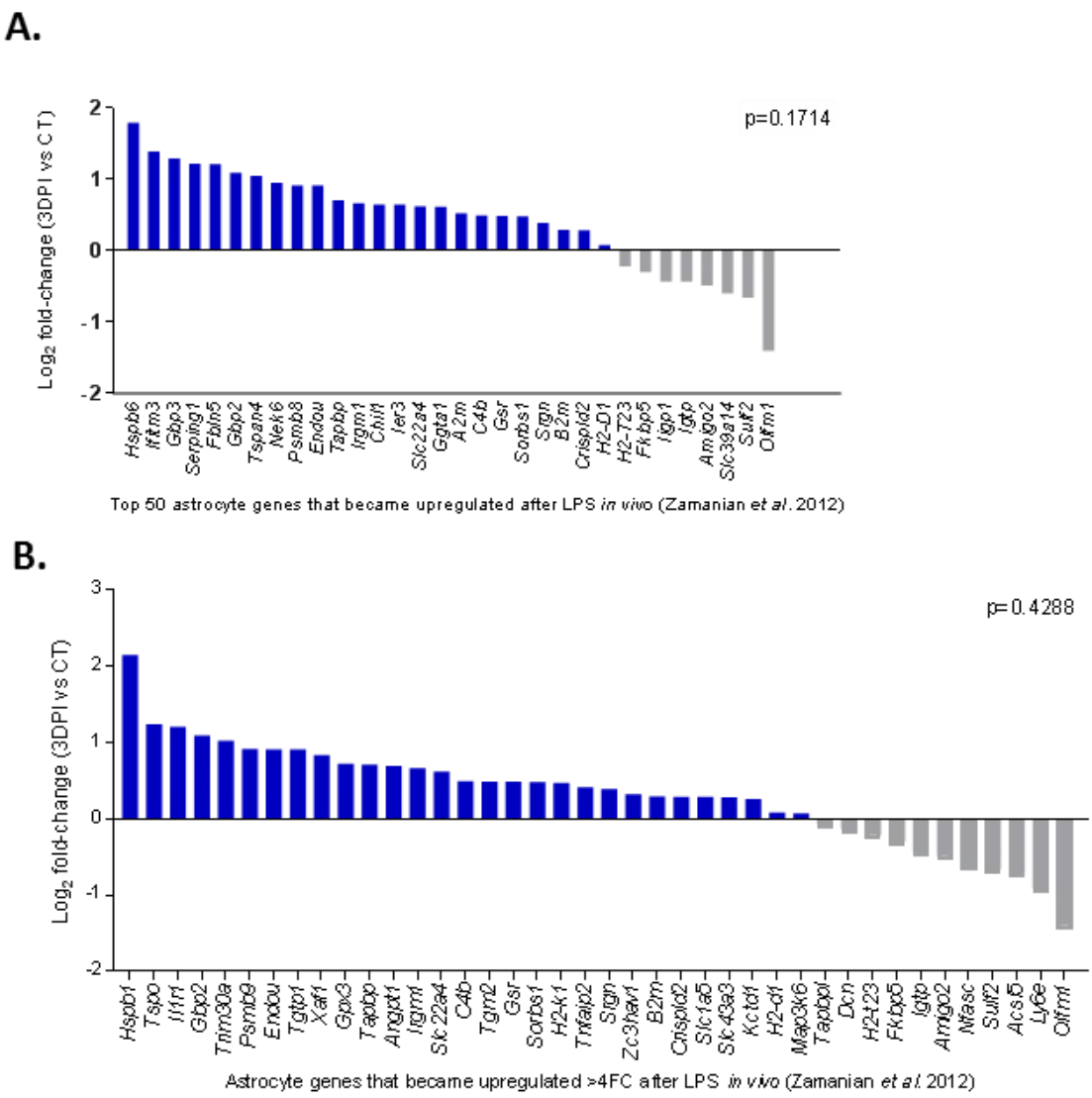

Figure 4.5. Astrocytes do not present a pro-inflammatory phenotype at 3 days post-LPC demyelination. Differential gene expression analysis between the 3 DPI LPC group compared to the control using the top 50 genes that are only upregulated after LPS (A) or the genes

that were > 4-fold increased after LPS (B) in Zamanian *et al.* 2012 [161]. Genes expressing >0.5 FPKM in the 3 DPI LPC and control group were included in the analysis. The represented *p*-value was calculated using a paired t-test between the average FPKM of the 3 DPI LPC vs control.

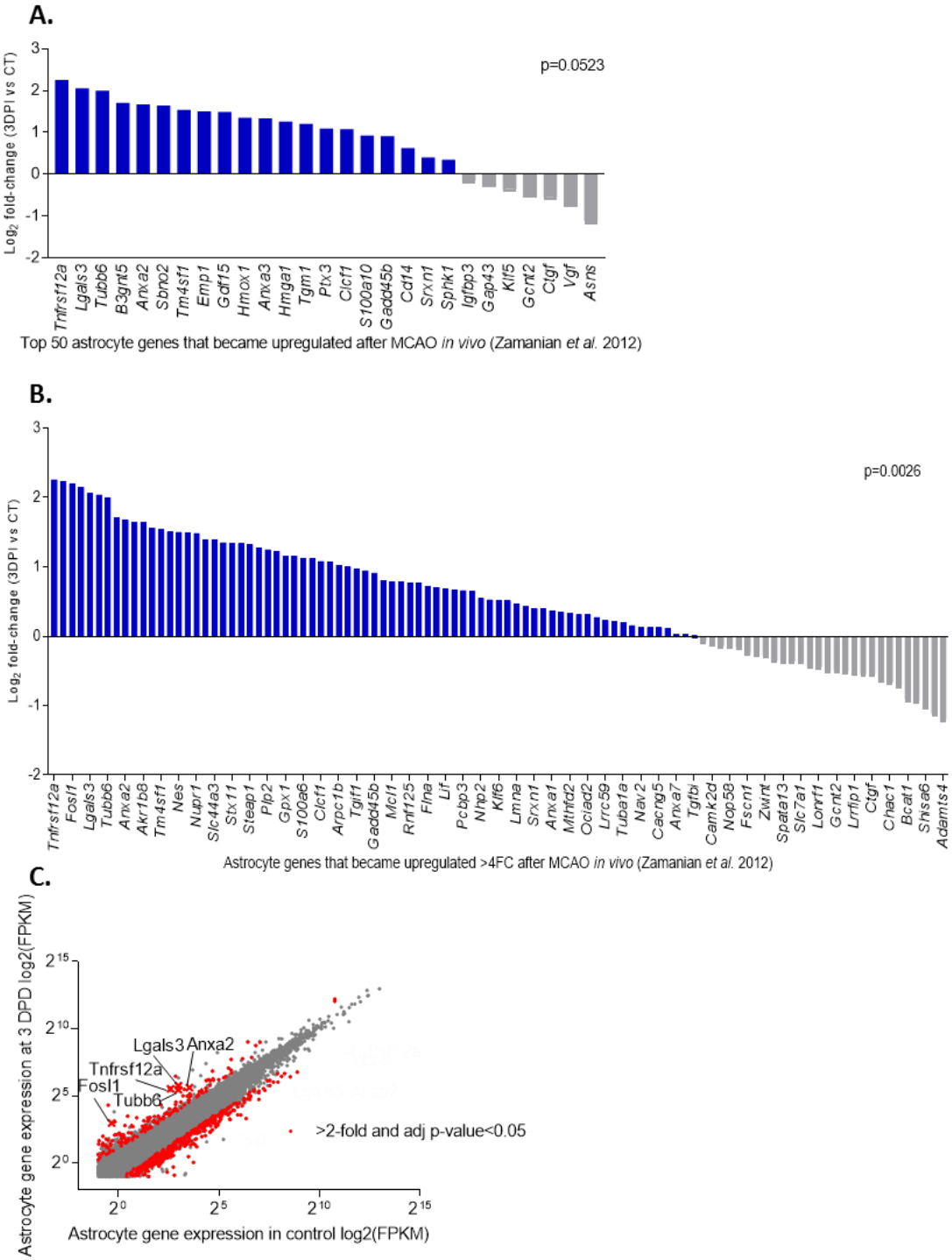

Figure 4.6. Astrocytes present an A2 phenotype at 3 days post-LPC demyelination. Differential gene expression analysis between the 3 DPI LPC group compared to the control using the top 50 genes only upregulated after MCAO (A) or the genes that were > 4-fold

increased after MCAO (B) in Zamanian *et al* 2012 [161]. Genes expressed at >0.5 FPKM in the 3 DPI LPC and control group were included in the analysis. The represented *p*-value was calculated using a paired t-test between the average FPKM of the 3 DPI LPC vs control. **C.** Expression of genes (FPKM) in astrocytes after 3 DPI LPC is plotted against the expression of genes in control astrocytes. Genes expressed >0.5FPKM and significantly changed (*p*-value <0.05) by 2-fold are represented in red, and the top 5 from the 50 most upregulated genes after MCAO in Zamainan *et* al. 2012 [161] are indicated on the plot.

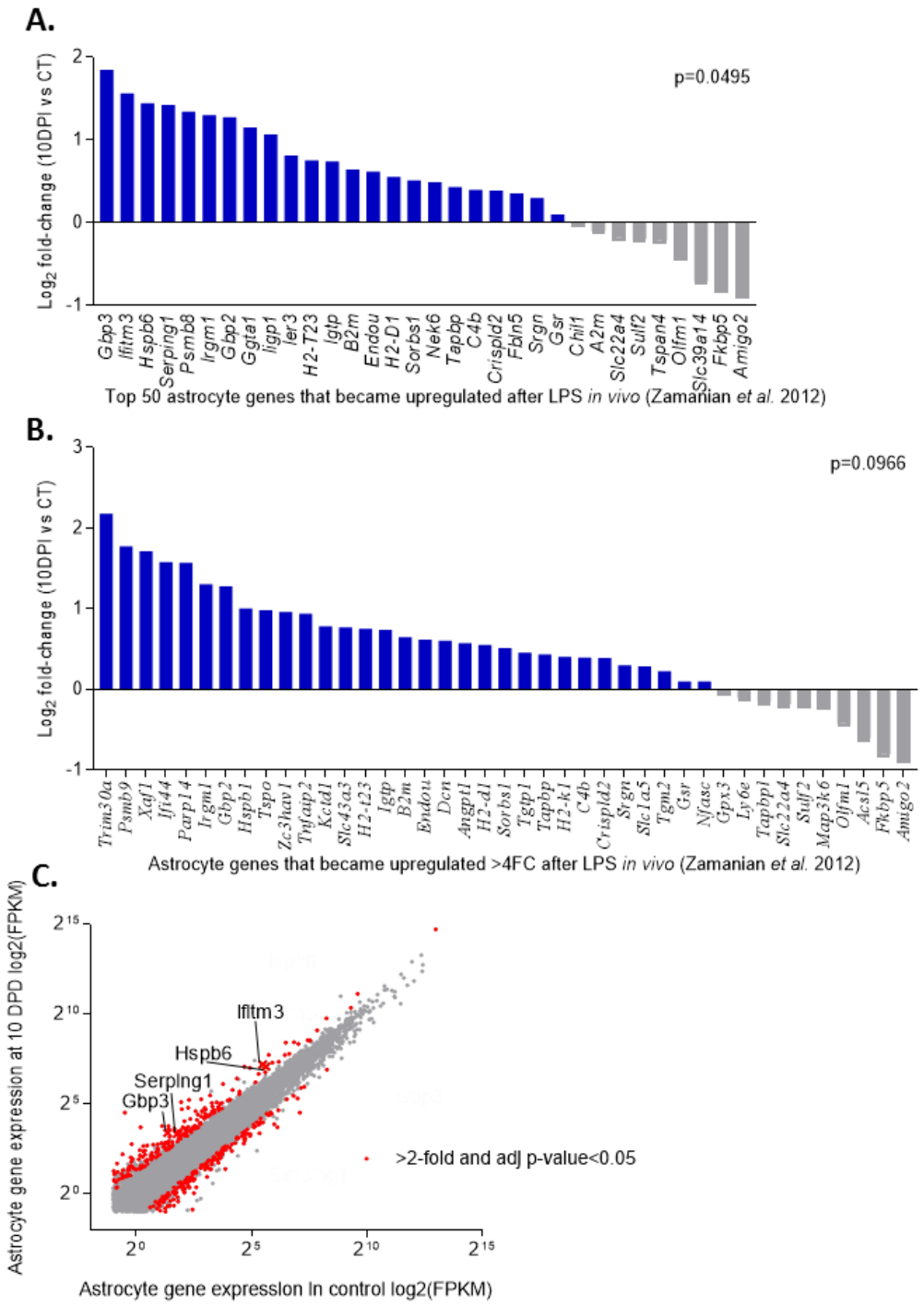

Figure 4.7. Astrocytes present an A1 phenotype at 10 days post-LPC demyelination. Differential gene expression analysis between the 10 DPI LPC group compared to the control using the top 50 genes only upregulated after LPS (A) or the genes that were > 4-fold increased after LPS (B) in Zamanian *et al.* 2012 [161]. Genes expressed >0.5 FPKM in the 10

DPI LPC and control group were included in the analysis. The represented *p*-value was calculated using a paired t-test between the average FPKM of the 10 DPI LPC vs control. **C.** Expression of genes (FPKM) in astrocytes after 10 DPI LPC is plotted against the expression of genes in control astrocytes. Genes expressed >0.5FPKM. Genes significantly changed (*p*-value <0.05) by 2-fold are represented in red, and the top 5 from the 50 most upregulated genes after LPS in Zamainan *et* al. 2012 [161] are indicated on the plot.

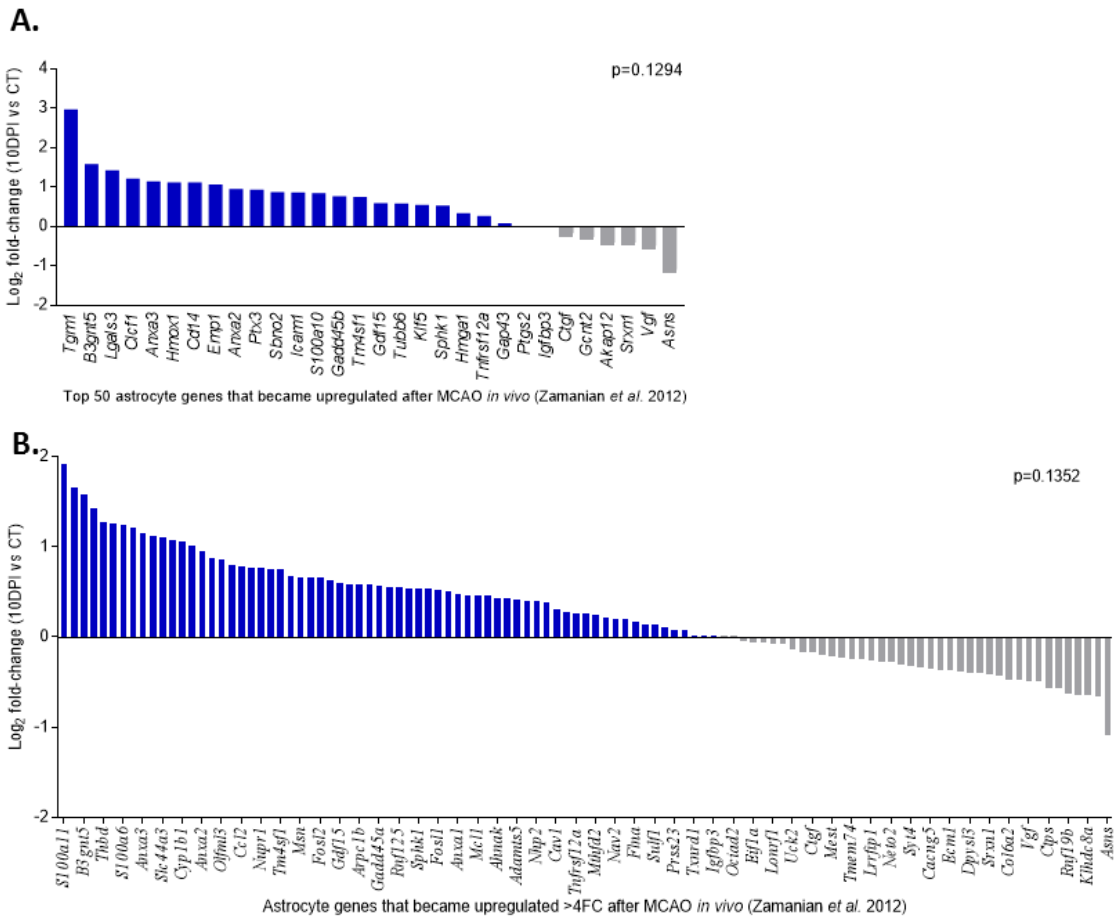

Figure 4.8. Astrocytes do not present an A2 phenotype at 10 days post-LPC demyelination. Differential gene expression analysis between the 10 DPI LPC group compared to the control using the top 50 genes only upregulated after MCAO (A) or the genes that were > 4-fold increased after MCAO (B) in Zamanian *et al.* 2012 [161]. Genes expressed >0.5 FPKM in the

10 DPI LPC and control group were4 included in the analysis. The represented *p*-value was calculated using a paired t-test between the average FPKM of the 10 DPI LPC vs control.

4.2.5. Nrf2 signalling is increased in astrocytes early after LPC-demyelination

To explore astrocyte functions in further detail, IPA analysis was performed. At 3 DPI, Nrf2-mediated oxidative stress response (*p*-value=1.18E-08) was a top upregulated pathway (Figure 4.9). The Nrf2 pathway is of relevance due to its neuroprotective role after degeneration and demyelination [92, 218]. Nrf2 is a transcription factor mediating antioxidant responses by promoting the transcription of antioxidant and detoxification regulators (Figure 4.9.A) [265]. Furthermore, it is involved in other cellular mechanisms like autophagy, stem cell quiescence and intermediary metabolism [265].Nrf2 is bound to Kelch-like ECH-associated protein 1 (Keap1), which is a redox-sensitive E3 ubiquitin ligase substrate adaptor and acts as its negative regulator [265]. In physiological situations, Keap1 targets Nrf2 for ubiquitin degradation [266]. In response to insult, Nrf2 is oxidised and inactivates Keap1, and then translocates to the nucleus and promotes transcription of antioxidant and detoxification enzymes, including the heme oxidase 1 (Hmox1), catalase (cat), NAD(P)H dehydrogenase (quinone) (Nqo1), cystine/glutamate antiporter xCT (Slc7a11), sulfiredoxin 1 (Srxn1), glutamate-cysteine ligase catalytic subunit (Gclc), and oxidative stress-induced growth inhibitor 1 (Osgin1) (Figure 4.9.A) [266]. By comparing the fold change in expression of these Nrf2-target genes

between the control and the different time-points (3, 7 and 10 DPI), I found that Nrf2 signalling was significantly enriched at 3 DPI LPC compared to the control, whereas this was no longer significant at other time points (Figure 4.9.C-D). To validate this finding, Nrf2 activation was assessed at the protein level by co-staining GFAP+ astrocytes with Hmox1. Compared to undemyelinated control and sham-control, a significant increase in GFAP+ Hmox1+ cells was observed at 3 DPI, which subsequently decreased at 7 DPI and was maintained at this level at 10 DPI (Figure 4.9. E-F). Interestingly, when Nrf2 targets were searched within the different clusters from the cluster analysis above (Figure 4.2), genes like *Hmox2 and Srxn1* were found in cluster 3, and *Nqo1* in cluster 2.

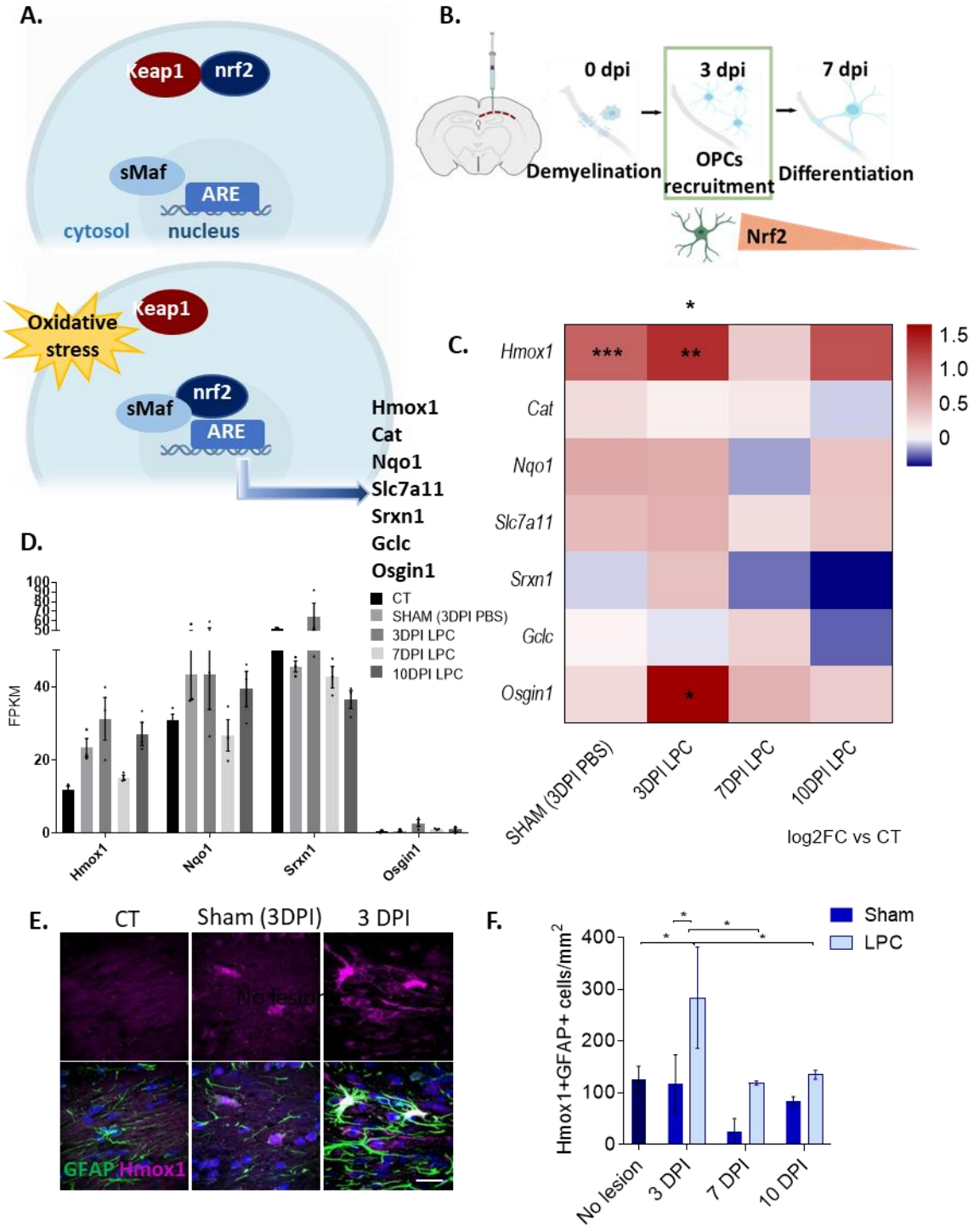

Figure 4.9. Astrocytes significantly upregulate genes of the Nrf2 pathway at 3 days post-LPC-induced demyelination. A. Schematic representation of the Nrf2-pathway, wherein homeostasis Nrf2 is bound to Keap1, and after insult (e.g. oxidative stress) Nrf2 is cleaved

from Keap1 and translocates to the nucleus promoting the transcription of antioxidant genes. **B**. The Nrf2 pathway was found to be upregulated at 3DPI LPC in astrocytes **C.** Heatmap of Nrf2-target genes expressed by astrocytes. Significance between groups was measured using a paired t-test between the control versus the remyelinating time-points. Asterisks in genes represent significance in a sample compared to the control by DESeq2 analysis (*p<0.05, **p<0.01, *** p<0.001). **D.** Plot showing the FPKM values of Nrf2-target genes. **E.** Representative images of GFAP+ astrocytes (green) co-stained with Nrf2-target Hmox1 (magenta) within the lesioned side in the corpus callosum. Scale bar; 25µm. **F.** Quantification of Hmox1+GFAP+ astrocytes at the different time-points investigated. Significance was determined by using a two-way ANOVA (condition (LPC vs sham) and time) with Tukey´s multiple comparisons test. Error bars indicate s.e.m. of the number (n) of animals. n=3 animals.*P<0.05.

4.2.6. Cholesterol biosynthesis signalling is increased in astrocytes during oligodendrocyte differentiation

At 7 DPI, IPA analysis showed upregulation of the cholesterol biosynthesis pathway (p-value=1.18E-08). Cholesterol is the major lipid component of myelin [267]. Whereas oligodendrocytes mainly produce it in development, it is primarily produced by astrocytes during adulthood [136, 268, 269]. Cholesterol biosynthesis is indispensable for oligodendrocyte differentiation and myelin formation [270, 271]. Astrocytes contribute to cholesterol production, which is then transferred to oligodendrocytes during myelination [136]. Cholesterol synthesis in the brain starts by the transformation of acetyl-CoA by the HMG-CoA-synthase-1 (Hmgcs1) to 3-

hydroxy-3-methylglutaryl-CoA (HMG-CoA), which is then transformed into mevalonate by the rate-limiting enzyme HMG-CoA-reductase (Hmgcr) [170, 268, 269]. Downstream, farnesyl pyrophosphate synthase (Fdps) promotes lanosterol synthesis [272]. In astrocytes, final conversion of cholesterol occurs via the Bloch pathway in which desmosterol is transformed by lanosterol-converting enzymes 24-dehydrocholesterol reductase (Dhcr24) (Figure 4.10.A)[269]. Here, I observed that the cholesterol biosynthesis signalling pathway was significantly upregulated at 7 DPI in astrocytes compared to control, as observed by the increase in expression of enzymes within this cascade selectively at this time point (Figure 4.10.B-C). Furthermore, I compared the expression of the astrocyte data set in the present study with the one obtained in a chronic EAE model by Itoh and colleagues (2018) [169]. In this study, the mRNA of GFAP+ astrocytes was isolated by RiboTag purification, and they observed that in the chronic phase of this EAE model (where continuous neurodegeneration and lack of recovery is observed), there was a marked decrease in expression of the cholesterol pathway genes compared to the expression observed in astrocytes during remyelination in the present study (Figure 4.10.B)[169]. I then validated the activation of this pathway at the protein level by co-staining GFAP+ astrocytes for enzymes involved in the cholesterol biosynthesis pathway: Hmgcs1 and Fdps. I observed a significant increase of GFAP co-localization with Hmgcs1+ or Fdps (measured by particles) at 7 DPI LPC, but not less so in the other time-points examined (Figure 4.11). Furthermore, targets of cholesterol biosynthesis were explored within the cluster analysis, *Hmgcs1, Mvk, Mvd,* were found within cluster 4 and *Sqle* and *Acat2* in cluster1.

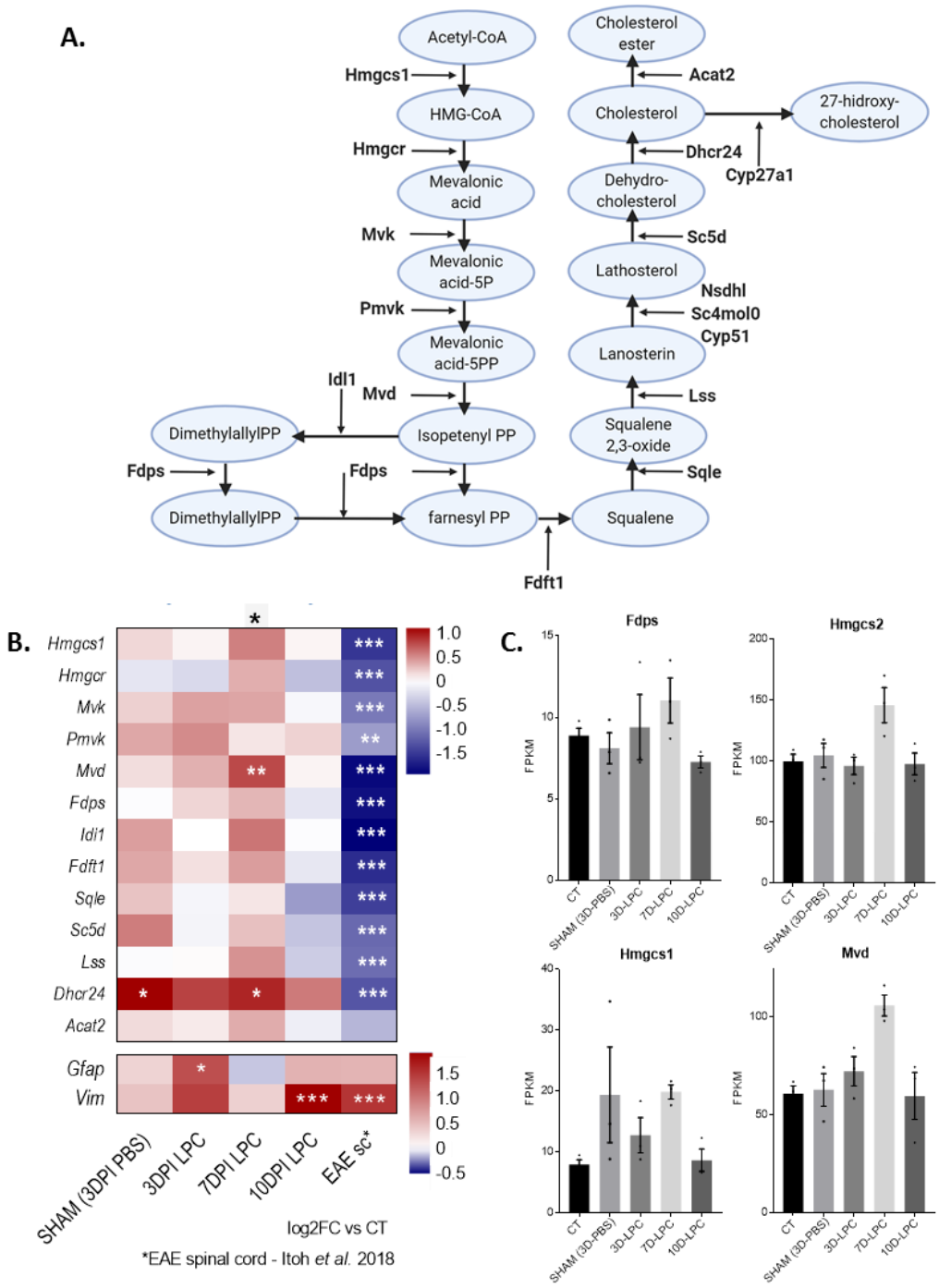

Figure 4.10. Astrocytes significantly upregulate genes of the cholesterol biosynthesis pathway at 7 days post-LPC-induced demyelination. A. Schematic representation of the cholesterol biosynthesis pathway, in bold are represented the enzymes converting the cholesterol intermediate (in blue cycle). **B.** Heatmap of cholesterol pathway genes expressed

by astrocytes. *Gfap* and *Vim* are pan-reactive genes included as a control. Significance between groups was measured using a paired t-test of the FPKM values between the control versus the different conditions (PBS and LPC). Asterisks in genes represent significance in a sample compared to the control by DESeq2 analysis (*p<0.05, **p<0.01, *** p<0.001). Data set from this study is compared to astrocytes from spinal cord (sc) astrocytes in EAE, from Itoh *et al* 2018 **C.** Plots showing the FPKM values of samples genes in the cholesterol biosynthesis pathway.

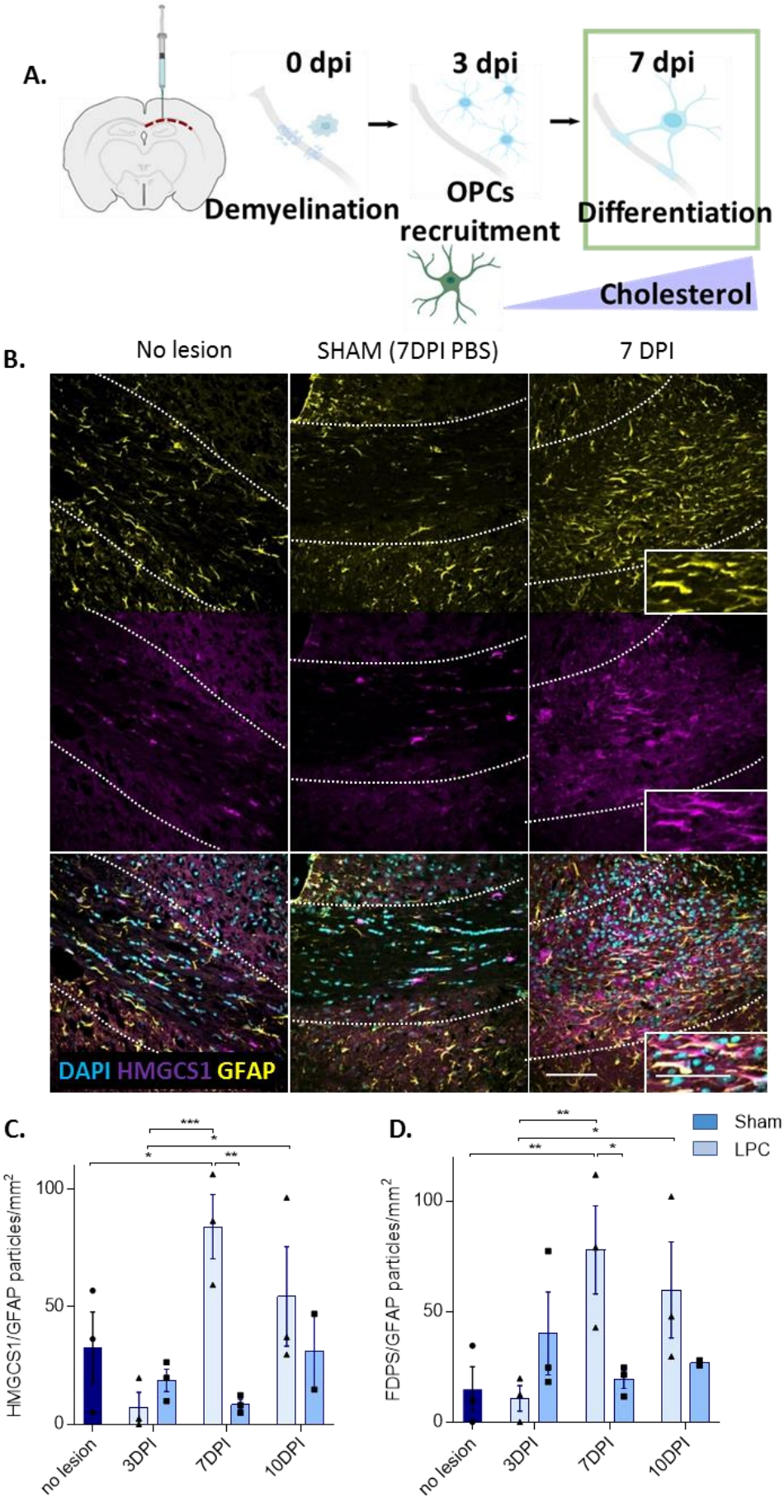
A.
0 dpi
3 dpi
7 dpi
Demyelination
OPCs recruitment
Differentiation
Cholesterol
B.
No lesion
SHAM (7DPI PBS)
7 DPI
DAPI HMGCS1 GFAP
C.
HMGCS1/GFAP particles/mm2
100
50
0
no lesion
3DPI
7DPI
10DPI
D.
Sham (PBS)
LPC
FDPS/GFAP particles/mm2
100
50
0
no lesion
3DPI
7DPI
10DPI

Figure 4.11. Components of the cholesterol biosynthesis pathway are significantly upregulated in astrocytes at 7 days post-LPC-induced demyelination. A. The cholesterol biosynthesis pathway was found to be upregulated at 7DPI LPC in astrocytes. **B.** Representative images of GFAP+ astrocytes (yellow) co-stained with Hmgcs1 (magenta). Scale bar; 100 µm. White box shows a magnification of a Hmgcs1+ GFAP+ astrocyte, Scale bar; 50µm. **C-D.** Quantification of Hmgcs1+ GFAP+ astrocytes (C) and Fdps+ GFAP+ astrocytes (D) at the different time-points investigated. Each particle represents a cell per mm^2. Significance was determined by using a two-way ANOVA (condition (LPC vs sham) and time) with Tukey´s multiple comparisons test. Error bars indicate s.e.m. of the number (n) of animals. n=3 animals. *P<0.05.

4.3. Discussion

The role of astrocytes after demyelination has been controversial. In chronic situations such as in MS, they seem to adopt detrimental functions that exacerbate damage preventing repair [212, 213]. Studying astrocytes in a model where efficient remyelination takes place spontaneously is ideal to have a better understanding of their regenerative functions. In this chapter of the present study, the gene expression of astrocytes has been characterised at key time-points during remyelination. To do so, TRAP-seq has been performed, which indicated that astrocytes dynamically change their functions during remyelination, presenting a neuroprotective phenotype early after demyelination (3 DPI) characterised by the upregulation of the Nrf2 pathway, and moving towards a pro-inflammatory profile at the onset of remyelination (10 DPI). At the time of oligodendrocyte differentiation (7 DPI), enrichment in the cholesterol biosynthesis pathway was observed, suggested to contribute to remyelination. These results would suggest that after an acute demyelinating insult, astrocytes adopt supportive and protective roles to assist remyelination.

To investigate the overall gene regulation in astrocytes in remyelination, cluster analysis was performed looking at the 5000 most enriched genes in the control and observing how they changed in remyelination (Figure 4.2). By doing this analysis, I observed that 6 different clusters were present, from which cluster 3, 4 and 5 included genes that were mostly upregulated at 3, 7 and 10 DPI, respectively (Figure 4.2.B). When looking closely at the most significantly changed genes at these time-

points, different genes were observed to be significantly upregulated or downregulated (Figure 4.3). At 3 DPI, *Timp1*, *S1pr3*, *Lgals1* and *Lgals3* were within the top 25 most significantly upregulated genes. *Timp1* is a gene that encodes for the extracellular protein TIMP-1, which is required for growth factor activation and is a negative regulator of matrix metalloproteinases (MMPs), which together regulate the extracellular matrix (ECM) and BBB integrity [258]. TIMP1 expression in astrocytes confers neuroprotective functions [273], and studies have shown that astrocytic TIMP-1 is important for remyelination in EAE and myelination in development [227, 259, 260].

Lgals1 and *Lgals3*, which encode for the lectins, galactosidase-binding, soluble (galectin)-1 and-3, were also significantly upregulated at 3 DPI, and *Lgals3* was found to be still significantly upregulated at 10 DPI. Galectins have been studied due to their positive effects after demyelination. Lack of galectin-3 impairs spontaneous remyelination in the cuprizone model [261]. Furthermore, galectin-1 treatment after LPC-induced demyelination prevents myelin degeneration and polarises microglia to a pro-regenerative phenotype [262]. Nonetheless, after stab-wound injury, galectin-1 and -3 are upregulated in a subset of reactive astrocytes and their expression is important for regulating astrocyte proliferation and reactivity (assessed by GFAP levels), where all dividing astrocytes express galectin-3 [274]. This could suggest that galectins are important regulators of astrocyte proliferation and increase astrocyte activation state in response to demyelination. However, galectin expression could be required to prevent further damage and promote repair, as its upregulation was

maintained at the onset of remyelination. *S1pr3*, which encodes for the sphingosine1-phosphate (S1P) receptor subtype 3 ($S1P_3$), was also significantly upregulated in astrocytes at 3 DPI, but not at the other time-points. $S1P_3$ is primarily expressed by astrocytes in inflammation and is important for astrocyte proliferation, migration, and production of neurotrophic factors and neuroprotective chemokines [275-277]. $S1P_3$ expression in astrocytes has been observed in MS in actively demyelinating lesions, chronic inactive plaques and their borders [277]. The S1P modulator fingolimod (FTY720), currently applied for RRMS [278], induces neurotrophic mediators and decreases production of toxic factors by astrocytes, which ameliorates EAE pathogenesis [279, 280]. Importantly, in the present study, the expression of $S1P_3$ was transiently expressed at 3 DPI, which would be opposite to what occurs in the context of MS. This could suggest that a controlled regulation of astrocyte functions is required to prevent damage and induce repair. At 7 DPI, *Hmgcs2* was significantly upregulated, which is the rate-limiting enzyme of the fatty acid β-oxidation pathway in mitochondria [281], and β-oxidation of fatty acids in astrocytes is required for myelin maintenance [263]. Furthermore, *Cxcl5* and *S100a11* were significantly enriched at 10 DPI. CXCL5 is a cytokine with chemotactic properties. After myelin phagocytosis in different human demyelinating CNS diseases, astrocytes release CXCL5 which has been suggested to recruit immune cells [192]. CXCL5 is produced by reactive spinal cord astrocytes after the application of IL1β where a neuroprotective phenotype is described due to the upregulation of genes important for axon regeneration [282]. In contrast to the upregulation of these beneficial factors, *Sema3a,* which has chemorepellent properties for OPCs after

demyelination, was downregulated at 3DPI [20]. The upregulation and downregulation of these factors suggest that astrocytes may have protective and regenerative functions rather than detrimental roles during remyelination.

To further assess the specific functions of astrocytes in remyelination, GO terms were investigated. This analysis suggested that astrocytes have specific functions at the different time-points studied (Figure 4.4). Firstly, at 3 DPI, GO terms indicated astrocyte death due to apoptosis which is consistent with my findings of a reduction in the total number of astrocytes (Sox9+ cells) at this time (Figure 3.2). Furthermore, astrocytes upregulated genes that indicated wound healing and reestablishment of the endothelial barrier. Astrocyte end-feet surround the endothelial cells that form the BBB and are essential for its formation and maintenance, and to control the entrance of cells and nutrients [283, 284]. LPC-induced demyelination compromises BBB integrity, which can exacerbate damage due to the infiltration of peripheral immune cells and lack of clearance of toxic products [171, 285]. Astrocytes have the ability to rapidly restore their end-feet on the BBB after ablation [286]. After stab wound injury, astrocyte activation has been suggested to mediate BBB recovery [287]. In the present study, early astrocyte functions could support BBB repair to prevent further damage and prepare the environment for remyelination. Next, GO terms revealed that at 7 DPI astrocytes upregulated genes suggestive of precursor cell proliferation, stem cell differentiation, and glial migration, which could indicate the positive impact of astrocytes on other cells like neurons, oligodendrocyte precursors and microglia at

the time of oligodendrocyte differentiation and onset of remyelination. As discussed in earlier sections, astrocytes can secrete factors that induce oligodendrocyte differentiation (reviewed in Molina-González *et al.* 2019). Astrocytes can also mediate the attraction of other cells like microglia so that remyelination can take place [72]. Lastly, GO term analysis at 10 DPI revealed functions suggestive of an immune response and inflammation. As described in previous chapters, astrocytes can adopt immune functions after demyelination, where they play crucial roles in mediating peripheral immune cell extravasation through the BBB and their activation, and also attract innate immune cells to the demyelinating areas.

After characterising astrocyte transcriptomes and observing that they were adopting regenerative and inflammatory profiles, I questioned whether this was reflected in the A1 and A2 phenotypes previously described. In an attempt to simplify astrocyte phenotypes, Zamanian *et al.* (2012) described the astrocytic gene expression pattern in a stroke model as a neuroprotective phenotype. In contrast, a neuroinflammatory model from LPS injection represented an inflammatory and detrimental phenotype [161]. Supporting the repair functions observed at 3 DPI in the GO terms, astrocytes presented a phenotype that closely resembled a neuroprotective phenotype (A2) described by Zamanian and colleagues (2012). GO terms at 10 DPI demonstrated that later, astrocytes presented a gene expression profile indicative of an A1 phenotype. However, not all A2 or A1-associated genes were regulated in the same way at both 3 and 10 DPI. Indeed, this simplification of A1 and A2 astrocyte phenotypes has failed to be represented in other models of

injury, where often mixed phenotypes are present [196, 249]. Whereas A1 astrocytes were first described as upregulating genes for inflammatory cytokines and immune function, and production of neurotoxic factors that induce neuronal death [162], other studies have shown opposite effects in which prevention of inflammatory astrocyte activation worsens pathology [288]. Indeed, in the present study, remyelination happens successfully even though there is the apparition of an inflammatory astrocyte phenotype at the onset of remyelination. A limitation that could be argued in the study of Zamanian and colleagues (2012) is that the gene expression that is associated with astrocyte phenotypes in these two different models was only studied at a specific and early time-point after insult (1 day after the insult). In both models, this pattern of gene expression could have shifted at later times, as astrocytes may play different roles according to the state of the injury. In other words, the gene expression from the MCAO model could have initially represented a neuroprotective phenotype due to the need for resolving the oxidative stress produced by dying cells, and the need for neurotrophic factors to promote the proliferation of other cells; however, this scenario could be changed at a later time-point due to the infiltration of immune cells that could alter astrocyte phenotype [289, 290].

An interesting feature of the A2 phenotype is the upregulation of genes suggestive of functions in response to oxidative stress like *Hmox1* and *Srxn1* which form part of the Nrf2 pathway (Figure 4.5), a cascade that was found to be significantly upregulated at 3 DPI in the present

study. Interestingly, when Nrf2 targets were searched within the different clusters from the cluster analysis above (Figure 4.2), genes like *Hmox2 and Srxn1* were found in cluster 3, and *Nqo1* in cluster 2. Oxidative stress is a common hallmark in the pathogenesis of different neurodegenerative disorders in which the death of cells and the continuous inflammation caused by microglia/macrophages leads into the accumulation of reactive oxygen and nitrogen species (ROS and RNS) [201]. The increase in oxidative stress induces the activation of Nrf2 signalling [291]. Nrf2 is a member of the Cap'n'Colar (CNC)/basic-leucine zipper subfamily of redox-sensitive transcription factors [265]. CNC has a subunit, the Nrf2-ECH homology 1 (Neh1), which is essential for the binging to its negative partner Keap1. Neh1 also enables Nrf2 to form a heterodimer with the small musculoaponeurotic fibrosarcoma (sMaf) protein, which allows binding to the antioxidant response element promoter region (ARE) [265] [292]. Hence, this promotes the transcription of Phase II detoxification (NADPH, Nqo1, Glutathione peroxidase, ferritin, Hmox1) and antioxidant enzymes which neutralise ROS and RNS, clear xenobiotic (external substances, which are generally toxic) species and reduce inflammation [200]. Astrocytes have been suggested as a main cell which activates Nrf2 after insult, and activation of this pathway has been thought to have neuroprotective functions[201]. For instance, specific overexpression of Nrf2 in GFAP+ astrocytes in a mouse model of amyotrophic lateral sclerosis (ALS), an early-onset form of motor neuron disease, led to delayed disease onset and extended survival [201], demonstrating that Nrf2 is efficient at decreasing neural degeneration. In another study, demyelination after 3 weeks of cuprizone diet, which induces demyelination and gliosis, was assessed in mice in

which GFAP+ astrocytes were deficient for Keap1, leading to hyperactivation of the Nrf2 cascade [92]. Continuous Nrf2 activation in astrocytes prevented demyelination by reducing oligodendrocyte loss, axonal damage and microglia activation [92]. However, Nrf2 hyperactivation effects were not shown during remyelination, nor was demyelination assessed at the ultrastructural level. Importantly, a mechanism of action of DMF is thought to be through the activation of Nrf2, where astrocytes have been described as the primary cells expressing Nrf2 in patients with MS and psoriasis [88]. In the present study, early activation of Nrf2 signalling at 3 DPI could suggest that astrocytes have protective functions to initiate repair, by resolving oxidative damage and reducing inflammation caused by the demyelinating insults.

At 7 DPI, GO terms indicated upregulation of cholesterol metabolism and homeostatic functions. Moreover, IPA analysis found this pathway to be significantly engaged at 7 DPI. Interestingly, and supporting these results, components of the cholesterol pathway were distributed within the clusters 1 and 4, characterised by a peak at 7 DPI. Astrocytes are the primary producers of different lipid species such as cholesterols in the adult brain due to lipid molecules being unable to cross the BBB [170, 269, 293]. Cholesterol is an essential and significant component of myelin [293-295]. Astrocytes actively transfer cholesterols to neurons through the cholesterol transporter, apolipoprotein E (APOE). Although it has never been directly addressed, studies suggest that astrocytic lipid production is essential for myelination [136]. Cholesterol biosynthesis is also decreased in models where deficient remyelination fails, such as in EAE and ageing [169, 248]. Promoting

cholesterol transfer has been shown to promote remyelination in aged mice [296] and dampen EAE clinical course [169]. Moreover, dietary cholesterol in different models of demyelination promotes remyelination [171]. In the present study, cholesterol upregulation was observed at the time of oligodendrocyte differentiation and remyelination, which suggests that astrocytic cholesterol production, might lead to transfer to the oligodendrocyte for myelin membrane formation.

The different functions observed at the different time-points could be regulated by distinct types of astrocytes which are more abundant at each of the time-points. In this study, the different astrocyte populations could be described mainly as antioxidant (protective) at 3 DPI, a metabolically supportive population at 7 DPI and inflammatory at 10 DPI. Wheeler *et al.* (2020) recently discovered that in EAE there was the presence of different astrocyte clusters, from which the most expanded astrocyte population was characterised by an increase in inflammatory pathways and decreased Nrf2 signalling [297]. Future scRNA-sequencing could define whether the different astrocyte phenotype observed in the present study really represent different populations, and this could be compared with the populations observed in the EAE model, other injury models and MS tissue.

In summary, in the present chapter, I conducted a transcriptomic analysis of astrocytes during remyelination which suggested that astrocytes play different roles at the different time-points of the regenerative process. Initially, astrocytes may mediate neuroprotective functions through the upregulation of Nrf2 signalling. During oligodendrocyte differentiation, astrocytes may upregulate the cholesterol

cascade to feed oligodendrocytes so that they can form new myelin sheaths. Lastly, at 10 DPI, astrocytes upregulate inflammatory functions possibly to attract other cells like microglia and macrophages so that they can release factors that can further influence oligodendrocyte beneficial responses. Importantly, I observed that upregulation of these functions was time-regulated. Results shows that the Nrf2 pathway is downregulated when cholesterol biosynthesis signalling is activated. Previous studies have shown that Nrf2 could be a negative regulator of lipid metabolism in the liver [298-302]. In the next section, I tested the role of Nrf2 activation in astrocytes and its potential role in regulating cholesterol biosynthesis during remyelination.

5. CHAPTER: SUSTAINED NRF2 ACTIVATION IN ASTROCYTES IMPAIRS REMYELINATION

5.1. Introduction

In the previous chapter, I observed that during remyelination, astrocytes activate Nrf2 signalling early and transiently after demyelination, and following its downregulation, the cholesterol biosynthesis pathway is activated.

Previous studies carried out in the liver have shown a link between Nrf2 and metabolism of fatty acids, where cholesterol synthesis is negatively regulated by the Nrf2 cascade [298-300, 302-306]. A proposed mechanism is that Nrf2 could affect cholesterol synthesis by decreasing acetyl-CoA production, the initial and fundamental factor for cholesterol synthesis [298, 304]. Proteomics of wild-type and Nrf2 null mouse livers revealed that 7 of the 10 most significantly changed pathways in the knockouts corresponded to lipid homeostasis, which were increased in the Nrf2 null mice. In this study, one of the proteins that was most significantly increased in the Nrf2 null mice was ATP-citrate synthase, which has a crucial role in the formation of Acetyl CoA [307] in the presence of ATP and Coenzyme A [298].

Other studies have explored the effect of Nrf2-signalling on lipid production in the liver, by treating mice with the synthetic oleanolic triterpenoid 1-[2-cyano-3,12-dioxooleana-,9(11)-dien-28-oyl] imidazole (CDDO-Im), a potent Nrf2 inducer, and similar results have been observed [303, 304]. CDDO-Im prevents fatty acid synthesis in an Nrf2-dependent manner *in vitro* [308]. CDDO-Im-treatment *in vivo* decreases expression of genes in the liver encoding enzymes required for acetyl-CoA

production: acetyl-CoA carboxylase 1 (encoded by *Acaca*) and 2 (*Acacb*), fatty acid synthase (*Fasn*), and sterol regulatory element-binding protein-1c (*Srebp1c*), a transcription factor that promotes expression of *Fasn* and *Acaca/b* [304].

Nrf2 is a master regulator of antioxidant defence, wherein the brain it confers neuroprotective effects after demyelination [92], yet its roles during remyelination are unexplored. Lipidosin, an acyl-CoA synthetase, the precursor enzyme in the β-oxidation pathway to form acetyl-CoA in the mitochondria [307], is increased in astrocytes during the remyelinating phase in the cuprizone model, and it has been suggested to be involved in fatty acid metabolism [309]. Nonetheless, the link between these two pathways has never been investigated in the brain, and understanding their interplay is crucial due to the critical functions they mediate after demyelination. Given that I observed that during efficient remyelination, Nrf2 activation in astrocytes is downregulated when cholesterol synthesis is upregulated, in this chapter, I investigated the effects of sustained Nrf2 pathway activation on cholesterol synthesis and remyelination.

5.2. Results

5.2.1. Nrf2 is overexpressed in the GFAP-Nrf2 mice

To investigate the effects of *Nrf2*-overexpression in astrocytes during remyelination, I used a model, the GFAP-Nrf*2* mice, which overexpress *Nrf2* under the control of the *Gfap* promoter [218] (Figure 5.1.A). I confirmed that in these mice, GFAP+ astrocytes had increased Nrf2 activation under basal conditions (non-lesion) when compared to wild-type (WT) mice, as indicated by expression of Nrf2 downstream target Nqo1. (Figure 5.1.B).

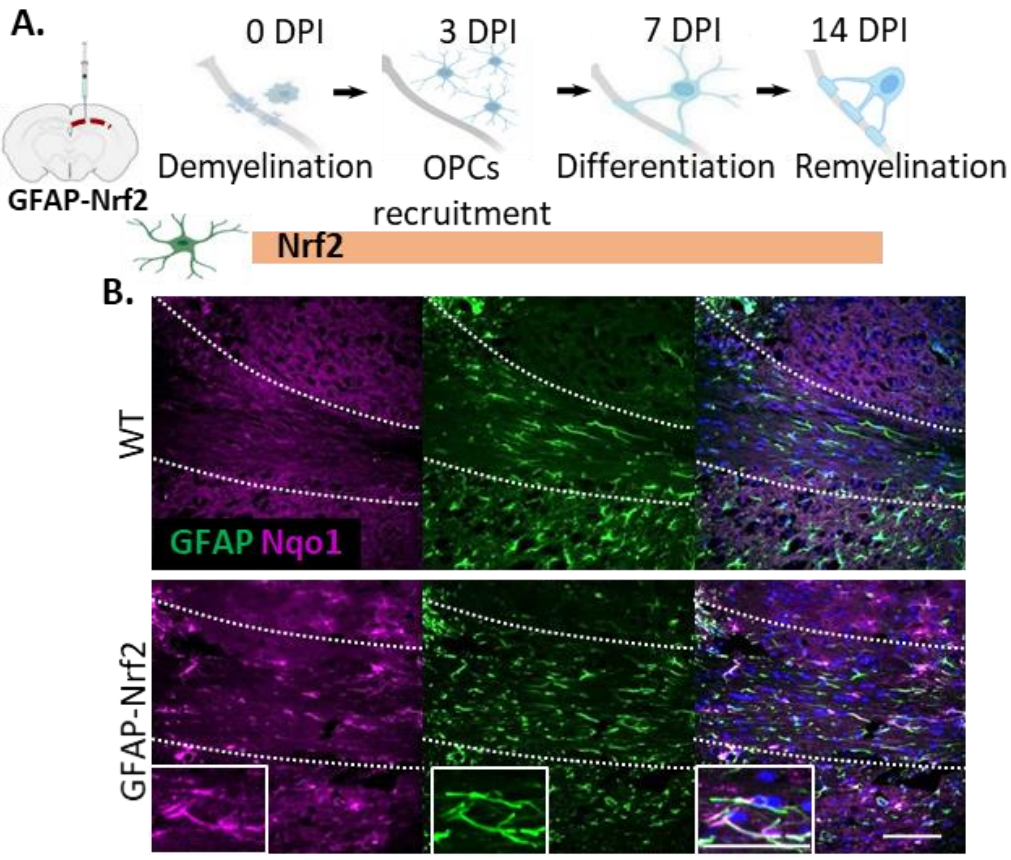

Figure 5.1. Nrf2 activation in reactive astrocytes in the GFAP-Nrf2 model. A. Schematic representation of the experimental timeline in the GFAP-Nrf2 line in which Nrf2 signalling is sustained during remyelination. **B.** Representative images of a non-lesion WT animal and a GFAP-Nrf2 animal, where GFAP+ astrocytes are co-stained with the Nrf2 target Nqo1, confirming Nrf2 activation. Scale bar; 100μm. White box shows a magnification of an Nqo1+ GFAP+ astrocyte. Scale bar; 50μm.

5.2.2. GFAP+ astrocyte decrease during oligodendrocyte differentiation in the GFAP-Nrf2 mice

I next characterised astrocyte responses to investigate whether Nrf2 activation affected astrocytes. To do so, I investigated GFAP levels at the peak of astrocyte reactivity in the wildtype mouse (WT), being 7 and 14 DPI. I observed a decrease in the number of reactive astrocytes (GFAP+) at 7 DPI within the lesion core in GFAP-Nrf2 mice when compared to WT mice (Figure 5.2.A-B). Reactive astrocytes were, however, recovered in number at 14 DPI, to similar levels as observed in WT (Figure 5.2.A-B). Therefore, the GFAP-Nrf2 mice show a delay in astrocyte reactivity.

I also noted that astrocyte hypertrophy seemed more pronounced in the GFAP-Nrf2 mice, particularly at 14 DPI, where astrocytes presented a dysmorphic shape (Figure 5.2.A). Nonetheless, to understand the consequences of this change in shape on astrocyte function, further markers for reactivity (eg. Vimentin, nestin and NFIA) or astrocyte progenitors (delta isoform of GFAP (GFAPδ) [310], should be used and gene expression analysis should be performed.

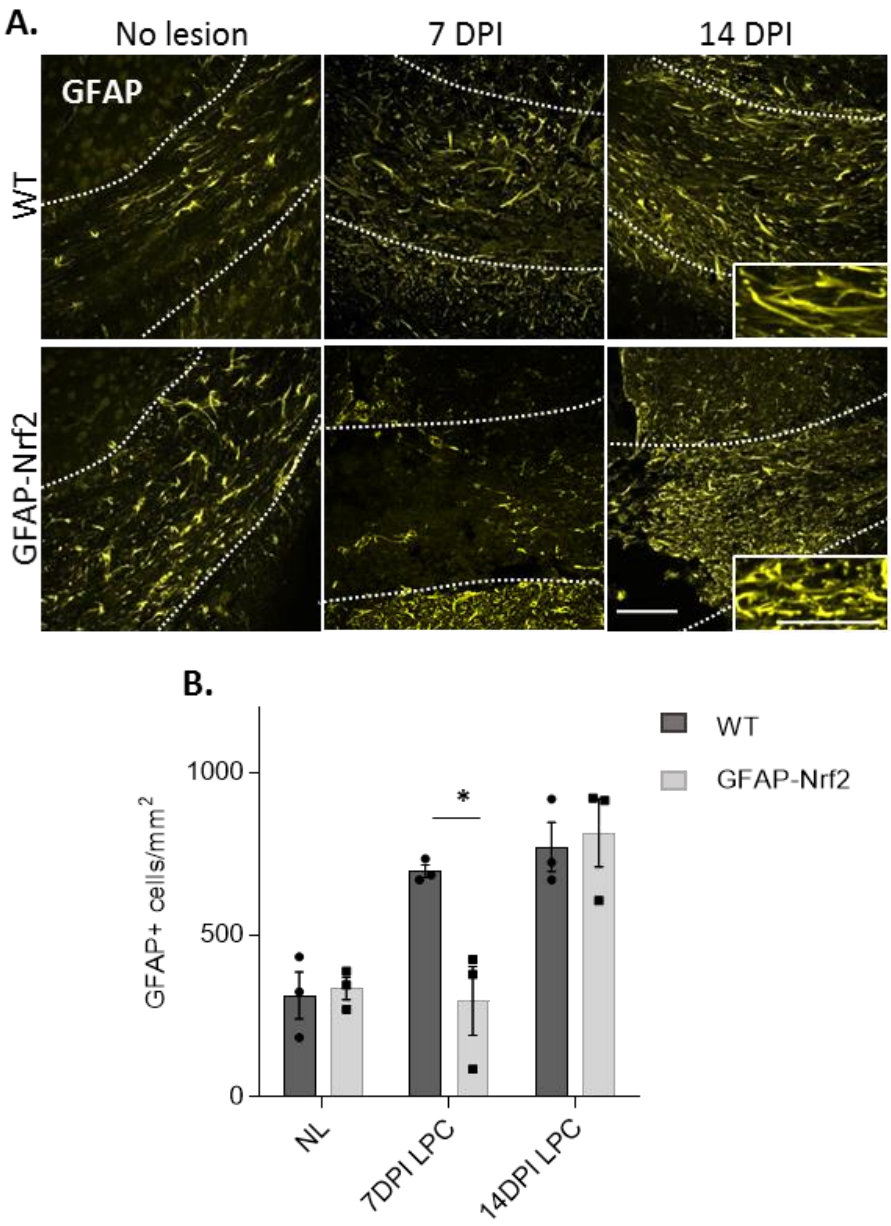

Figure 5.2. Sustained Nrf2 activation in reactive astrocytes leads to decreased numbers after demyelination. A. Representative images of GFAP+ astrocytes in WT and GFAP-Nrf2 mice at different time-points during remyelination. Scale bar; 100 µm. White box shows a magnification of GFAP+ astrocytes. Scale bar; 50µm. **B.** Quantification of GFAP+ astrocytes. Significance was determined by the Kolmogorov-Smirnoff test against non-lesion controls, and at 14 DPI an unpaired t-test with Welch's correction was performed at 7 DPI between

WT and GFAP-Nrf2. Error bars indicate s.e.m. of the number (n) of animals. n= 3 mice per group per time point.

5.2.3. Sox9+ astrocyte decrease during oligodendrocyte differentiation in the GFAP-Nrf2 mice

As a reduction in reactive astrocyte numbers was observed in the GFAP-Nrf2 compared to the WT mice, I next explored whether the total numbers of astrocytes (Sox9+) were changed (Figure 5.3). I observed a trend towards a decrease in astrocyte numbers at 7 DPI compared to the WT group (Figure 5.3.A-B), yet this did not reach significance. The decrease in the total number of astrocytes was similar to the decrease in the number of reactive astrocytes. The total astrocyte number was however similar at 14 DPI between both genotypes, although power calculations indicated that an increase in the sample size would be required to avoid Type I (false negative) and Type II (false positive) errors.

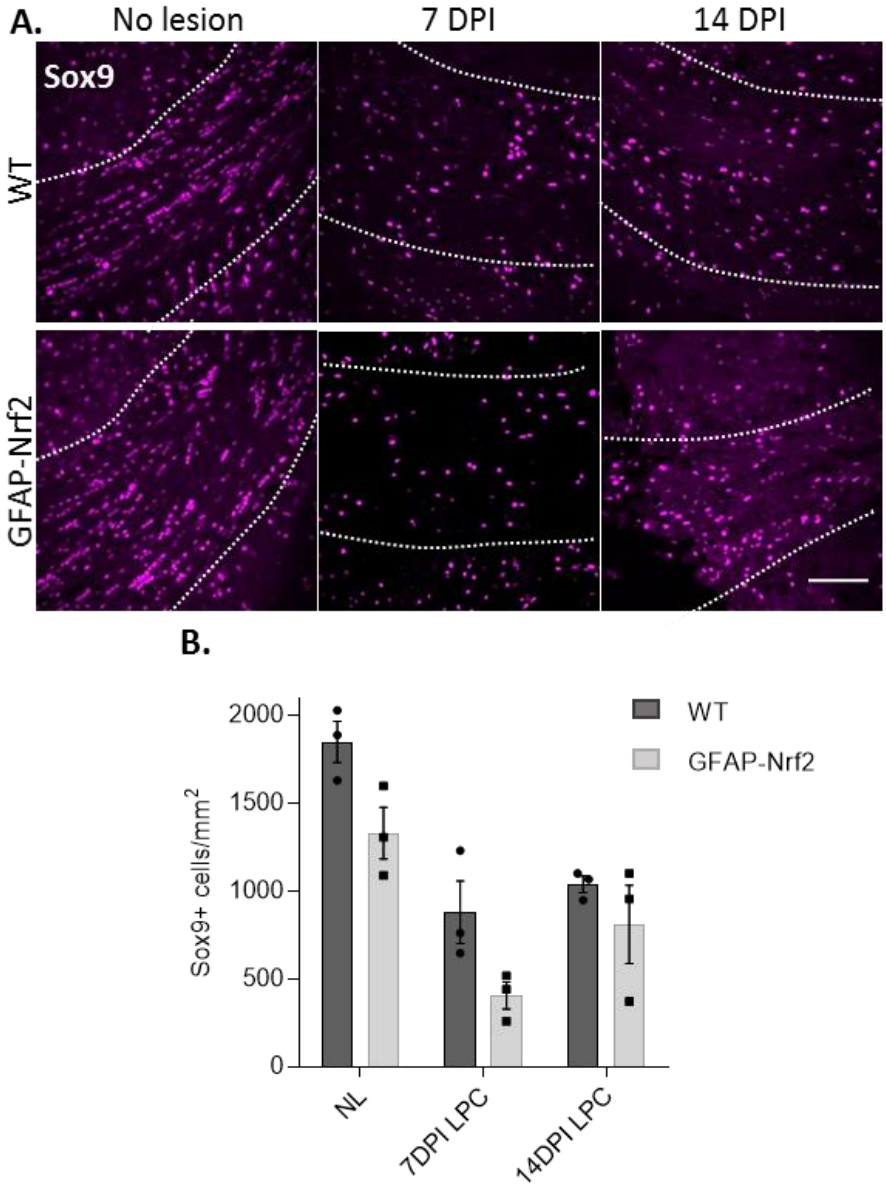

Figure 5.3. Sustained *Nrf2*-overexpression in reactive astrocytes leads to decreased numbers of reactive astrocytes after demyelination. A. Representative images of Sox9+ astrocytes in WT and GFAP-Nrf2 mice at different time-points during remyelination. Scale bar; 50µm. **B.** Quantification of Sox9+ astrocytes. Significance was determined by an unpaired t-test with Welch's correction, comparing 7 and 14 DPI GFAP-Nrf2 to WT. Error bars indicate s.e.m. of the number (n) of animals. n= 3 mice per genotype per time point.

5.2.4. Hmgcs1 and Fdps are decreased in reactive astrocytes during oligodendrocyte differentiation in the GFAP-Nrf2 mice

I next explored whether cholesterol biosynthesis was altered in astrocytes in GFAP-Nrf2 mice, by looking at two enzymes of the cholesterol synthesis pathway, Hmgcs1 and Fdps at 7 DPI, time at which an increase in cholesterol synthesis peaks in WT (Figure 3.20). To do so, I used ImarisSurfaces and analysed the number of Hmgcs1 or Fdps surfaces, in which each surface was adjusted to be the size of a cell (named particle) (see methods section 2.6). I observed that Hmgcs1 and Fpds were decreased in GFAP+ astrocytes when compared to the expression in WT animals (Figure 5.4). These findings could indicate an impairment of the cholesterol biosynthesis pathway in astrocytes when Nrf2-signalling was sustained. Nonetheless, a reduction in reactive astrocyte numbers could have also contributed to the decreased expression of these enzymes in astrocytes within the lesion.

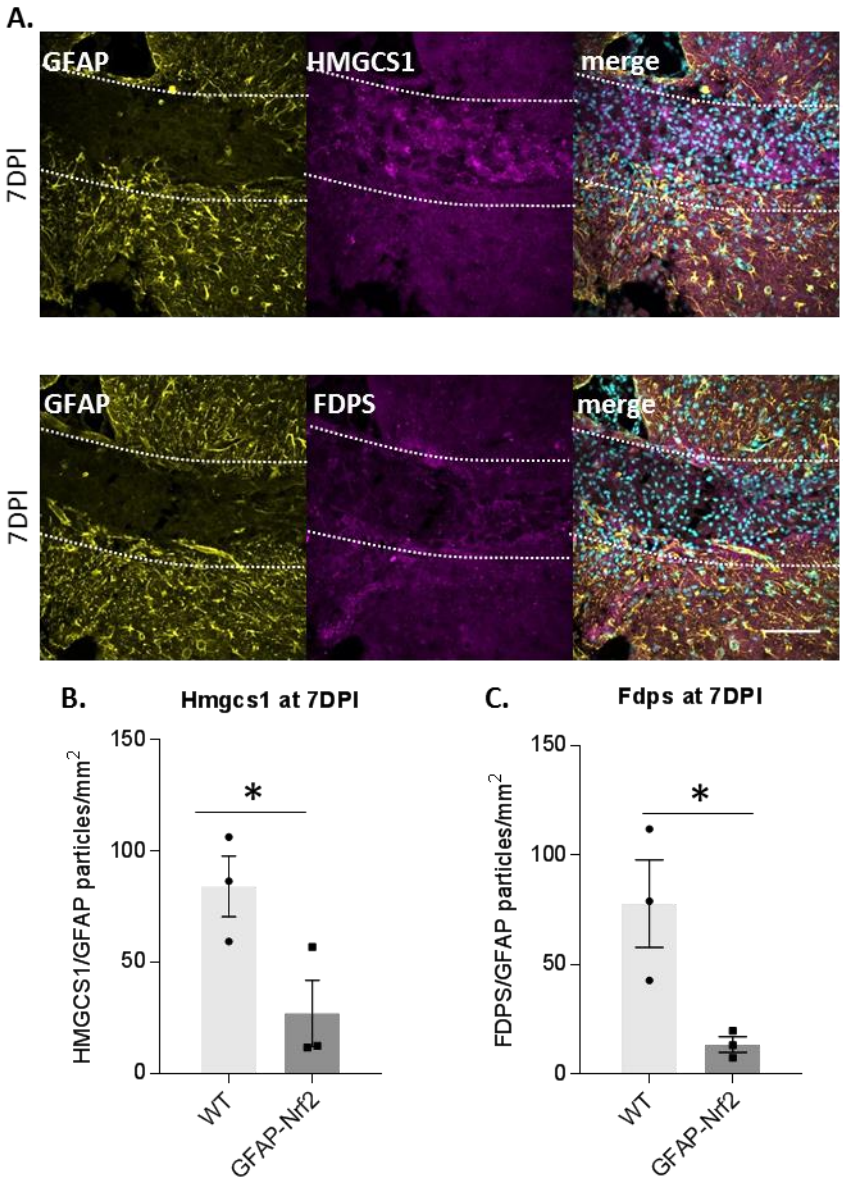

Figure 5.4. Sustained *Nrf2*-overexpression in reactive astrocytes leads to reduced levels of Hmgcs1 and Fdps in astrocytes. A. Representative images of GFAP+ astrocytes (yellow), co-stained with Hmgcs1 or Fdps (magenta). Scale bar; 100µm. **B.** Quantification of Hmgcs1+GFAP+ astrocytes (B) or Fdps+GFAP+ astrocytes (C). Each particle represents a cell per mm^2. Significance was determined using unpaired t-test with Welch's correction. Error bars indicate s.e.m. of the number (n) of animals. n= 3

5.2.5. Oligodendrocyte lineage cells are decreased in the GFAP-Nrf2 mice

I next assessed whether the effect of sustained *Nrf2*-overexpression in astrocytes and associated disruptions to the cholesterol biosynthesis pathway could have an effect on oligodendrocyte differentiation, a critical step in successful remyelination. To do so, I used the pan-oligodendrocyte lineage-cell marker oligodendrocyte transcription factor-2 (Olig2+) and labelled mature oligodendrocytes using the marker anti-adenomatous polyposis coli (APC) (CC1+). I counted the numbers of positive cells at 7 DPI (the time at which oligodendrocyte differentiation is initiated) and 14 DPI (the time at which initial remyelination takes place). I observed a trend decrease in total oligodendrocyte lineage cell numbers (Olig2+) in the GFAP-Nrf2 mice compared to the WT at 7 and 14 DPI (Figure 5.5.A-B). Similarly, when the number of mature oligodendrocytes was assessed (CC1+Olig2+), a trend decrease was observed at these two time-points (Figure 5.5.C). However, when the percentage of total oligodendrocyte lineage cells (Olig2+) which were mature oligodendrocytes (CC1+Olig2+) was analysed, a similar proportion was observed in both genotypes, which could suggest that although there was a reduction in the number of oligodendrocyte lineage cells in Gfap-Nrf2 mice, the cells that were present were able to differentiate into mature oligodendrocytes (Figure 5.5.D). This suggests that GFAP-Nrf2 mice show a reduction in total numbers of oligodendrocyte lineage cells, but differentiation was not impaired, suggesting a reduction in proliferation/migration of OPCs to the lesion and/or induction of apoptosis due to elevated Nrf2 levels. Future, experiments assessing OPCs

proliferation by co-staining with Ki67 would be required to confirm this. Moreover, assessing oligodendrocyte-lineage cell apoptosis by flow cytometry and Annexin-V expression, a marker for cell death, could also be performed. Nonetheless, an increase in 'n' numbers would be required to reach the statistical power as variability between the samples was observed.

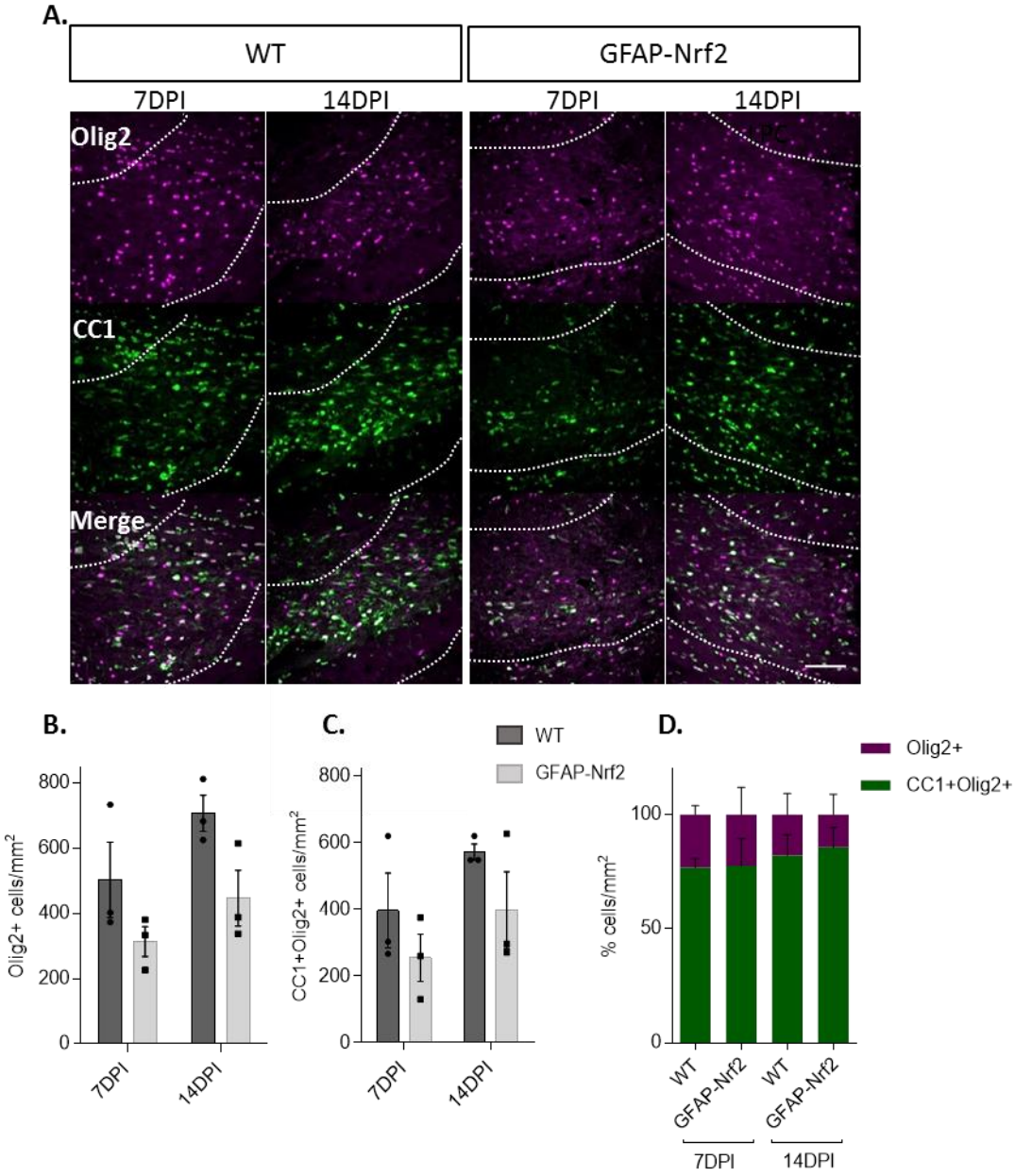

Figure 5.5. Sustained *Nrf2*-overexpression in reactive astrocytes does not affect oligodendrocyte differentiation. A. Representative images of co-staining for the pan-oligodendrocyte lineage cell marker, Olig2 (magenta), and the mature oligodendrocyte marker, CC1 (green) at 7 and 14 DPI in the WT and GFAP-Nrf2 mice. Scale bar; 100 µm. **B-C.** Quantification of Olig2+ cells (B) and CC1+ cells (C) per mm^2 at 7 and 14 DPI in WT and GFAP-Nrf2 mice. Significance was determined by using an unpaired t-test with Welch's correction

comparing WT and GFAP-Nrf2 at 7 and 14 DPI. **D.** Percentage of Olig2+ cells which are CC1+ (green) and negative (magenta) in the WT and GFAP-Nrf2 mice at 7 and 14 DPI. Error bars indicate s.e.m. of the number (n) of animals. n= 3 mice per genotype per time point.

5.2.6. Total number of cells are decreased early after LPC-demyelination in the GFAP-NRf2 mice

I next assessed whether the total number of cells that were not astrocytes were different between the WT and the GFAP-NRf2 mice during remyelination. To do so, I subtracted the total number of astrocytes (Sox9+) from the total number of cells (Hoechst+). There was a trend decrease in the total number of cells that were not astrocytes (Hoechst + Sox9-) at 3 DPI (Figure 5.6.A-B), although this did not reach significance. No significant differences were observed at the other time-points investigated (Figure 5.6.A-B). Nonetheless, an increase in 'n' numbers would be required to avoid Type I and Type II errors. This decrease in the total number of cells that were not astrocytes at this early time-point could reflect a decrease in microglia infiltration, as this is when microglia are expected to migrate to the lesion site [244]. Nonetheless, further characterisation with microglial markers would be required to confirm these findings.

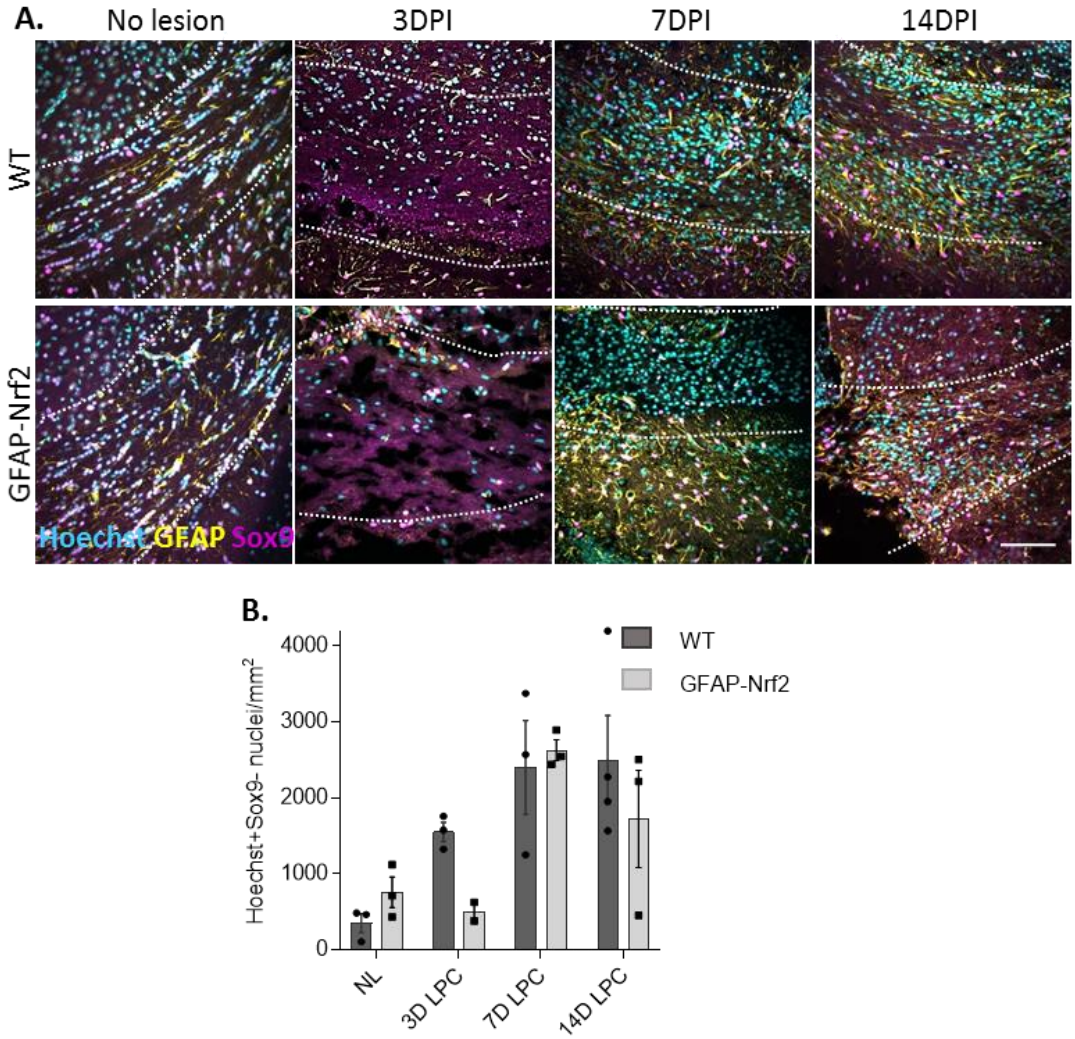

Figure 5.6. Sustained *Nrf2*-overexpression in reactive astrocytes leads to a trend decrease in the total number of cells. A. Representative image of Hoechst staining (cyan), GFAP+ astrocytes (yellow) and Sox9+ cells (magenta). Scale bar; 100 µm. **B.** Quantification of Hoechst+ cells that were negative for Sox9 and GFAP. Significance was determined using an unpaired t-test with Welch's correction comparing WT and GFAP-Nrf2 at 7 and 14 DPI. Error bars indicate s.e.m. of the number (n) of animals. n= 2-3 mice per genotype per time point.

5.2.7. Nrf2 and cholesterol biosynthesis associated genes are dysregulated in astrocyte in ageing

Due to the potential link between the Nrf2 and the cholesterol biosynthesis pathways, I next aimed to explore whether the Nrf2 and cholesterol pathways are altered in astrocytes in ageing, where there is decreased remyelination efficiency [296, 311, 312]. To explore these pathways in aged mice, I performed TRAP to isolate the mRNA of astrocytes and quantify the expression of target genes by qPCR. Nrf2-signalling was reported to be increased in ageing in a region and cell-dependent manner [202]. Hence, I first assessed the basal levels of Nrf2 signalling in astrocytes in aged animals (9-12 months of age) compared to young mice (2-3 months) under basal conditions (non-demyelinated animals), by assessing mRNA expression of *Hmox1* and *Cat.* I found that the log2 fold-change in expression of these two genes in astrocytes was increased in aged mice versus young mice by around 0.7 (Figure 5.7.A). I then performed demyelination and looked at mRNA expression of these two genes at 7 DPI in aged animals, when Nrf2-signalling is normally shut down in young mice. No difference in mRNA expression levels was observed between lesion and control (non-demyelinated) in aged animals (Figure 5.7.B), suggesting that Nrf2 levels were sustained after demyelination. I then investigated expression of cholesterol biosynthesis-associated genes *Hmgcs1* an *Fdps* at 7 DPI in aged mice, and compared expression to that at 7 DPI in younger animals, and found a decrease in expression (log2 fold-change) in aged mice (Figure 5.7.C). These findings could indicate that in ageing, the *Nrf2* activation levels in astrocytes are increased, sustained following demyelination, and associated with dysregulated cholesterol biosynthesis. These

results reinforce the concept of a crosstalk between the Nrf2 and cholesterol biosynthesis pathways and the importance in their correct regulation in astrocytes to ensure that remyelination can take place.

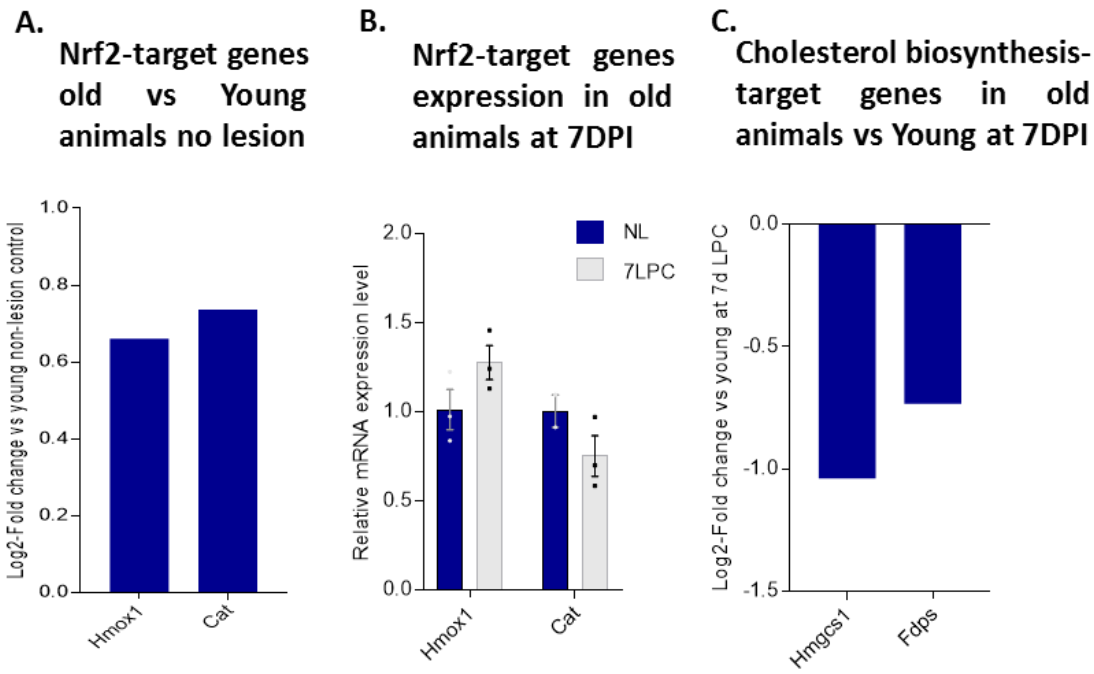

Figure 5.7. Dysregulation of Nrf2 and cholesterol biosynthesis associated genes in astrocytes in ageing. A. Log2-Fold-change in expression of the Nrf2 target genes *Hmox1* and *Cat* in non-lesioned old mice (9-12 months old) compared to young mice (2-3 months old). **B.** *Hmox1* and *Cat* relative mRNA expression at 7 DPI in old mice. **C.** Log2-Fold-change in expression of the cholesterol biosynthesis associated genes *Hmgcs1* and *Fdps* at 7 DPI in old mice compared to young mice. n= 3 mice per group.

5.2.8. Remyelination is reduced in the GFAP-Nrf2 mice

The data from the GFAP-Nrf2 model suggested a reduction of the cholesterol synthesis pathway, and there was a decrease in overall oligodendrocyte lineage cell numbers. I next explored consequences for remyelination. When LPC-induced demyelination was performed in these mice, I observed a trend in decreased remyelination at 14 DPI in the GFAP-Nrf2 mice compared to WT, as indicated by a decrease in MBP staining (Figure 5.8.A-B). As 'n' numbers were low, further experiments would be needed. Calculation of sample size for statistical power showed that 'n' numbers at 7 and 14 DPI should be increased to avoid Type I and Type II errors.

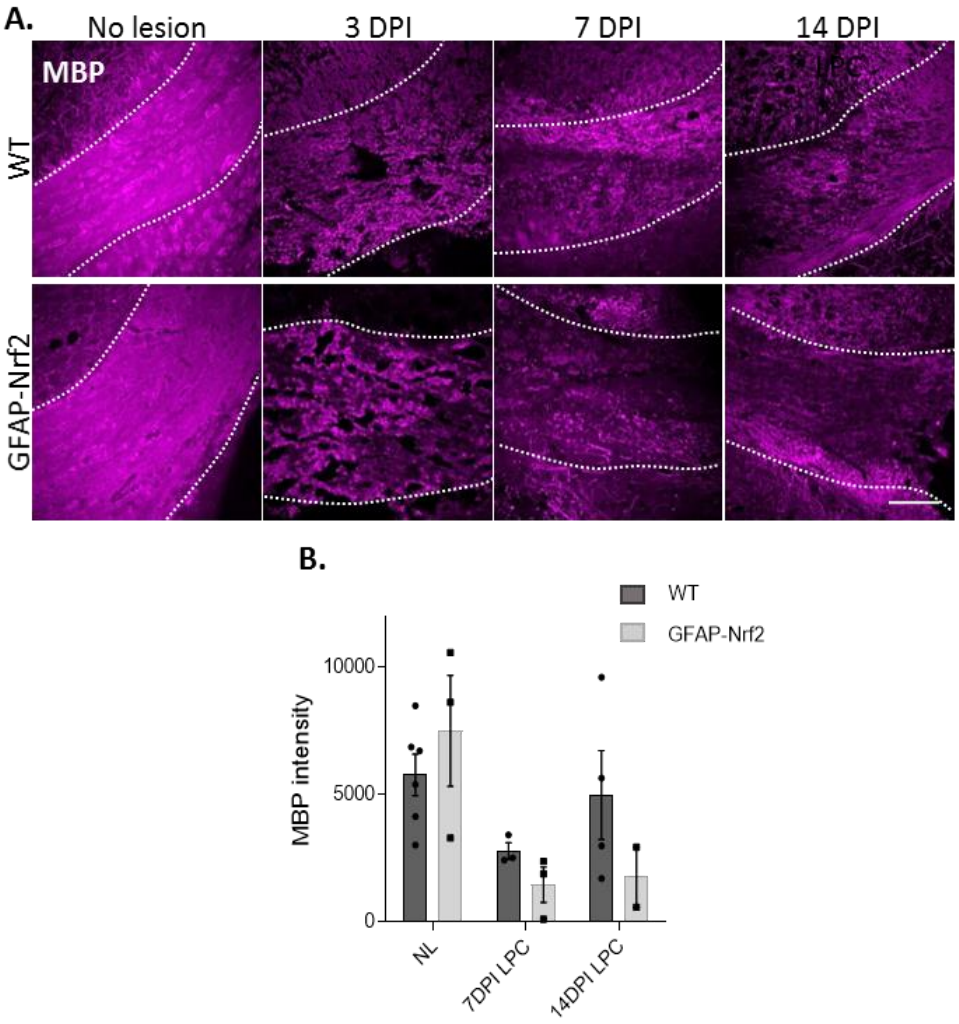

Figure 5.8. Sustained *Nrf2*-overexpression in reactive astrocytes leads to impaired remyelination. A. Representative images of MBP staining (magenta) in the corpus callosum (indicated with dashed lines) at the main time-points explored in the WT and GFAP-Nrf2 mice. **B.** Quantification of MBP staining intensity in the WT vs the GFAP-Nrf2 mice. Significance was determined by the Kolmogorov-Smirnoff test compared to non-lesion controls, and an unpaired t-test with Welch's correction was performed at 7 DPI between WT and GFAP-Nrf2. No statistical quantification was performed at 3 and 14 DPI due insufficient "n" numbers. Error bars indicate s.e.m. of the number (n) of animals. n= 2-6 mice per group per time point.

5.3. Discussion

In this chapter, the effects of sustained Nrf2 activation in astrocytes on astrocyte behaviour, the cholesterol biosynthesis pathway, and oligodendrocyte-lineage cell responses during remyelination were investigated. Although some findings are preliminary as an increase in 'n' numbers would be required, my data thus far suggests that when Nrf2 activation is maintained in reactive astrocytes following demyelination, oligodendrocyte lineage cell responses and remyelination are impaired (Figure 3.21). This may be due to a reduction in cholesterol biosynthesis activation in astrocytes (Figure 5.4). Accordingly, I observed that in aged animals, which are known to remyelinate poorly, basal Nrf2 pathway activation is high and maintained following demyelination, and this is associated with decreased expression of cholesterol synthesis-associated genes compared to young mice at 7 DPI (Figure 5.7). Sustained *Nrf2* activation in astrocytes seemed not to impair differentiation of oligodendrocytes, although overall oligodendrocyte lineage cell numbers were decreased (Figure 5.5), which was then associated with reduced remyelination.

Furthermore, given the importance of cholesterol in myelin membrane formation, dysregulated cholesterol biosynthesis in astrocytes could have impaired the capacity of oligodendrocytes to form myelin. Moreover, sustained Nrf2 activation in astrocytes affected the total number of cells present in the lesion early after demyelination (Figure 5.6). This decrease in numbers could reflection a decrease in OPCs present that would then differentiate to myelin-forming oligodendrocytes,

and/or microglia that would clear myelin debris, which in turn could also be a reason for impaired remyelination.

In the present study, RNA sequencing suggested an early and transient engagement of the Nrf2 pathway in astrocytes after demyelination, which was then confirmed at the protein level (Figure 4.9). Similar observations were previously made in the cuprizone model, in which early activation of Nrf2 is present in astrocytes, peaking at 3 days of cuprizone diet [92]. After insult, there is high generation of oxidative stress and cytotoxic molecules, which induce cell death [201, 313]. Neurons and oligodendrocyte are more vulnerable to oxidative stress compared to astrocytes and microglia, which may be explained by the difference in expression of intrinsic players regulating antioxidant responses [291]. Nrf2 signalling is an intrinsic mechanism that mediates cellular defence, by the upregulation of antioxidant and cytoprotective genes that are involved in detoxification, antioxidant function, redox balance and metabolism regulation [265].Treatment-induced-Nrf2 activation in astrocytes *in vitro* promotes cell defence functions and protects them against cytotoxic stimuli like hydrogen peroxide (H_2O_2) and platelet-activating factor (PAF) [313]. In addition, specific Nrf2 expression in astrocytes protects neurons from H_2O_2 toxicity and glutamate toxicity in a mixed culture system [314], indicating that Nrf2 activation in astrocytes is protective for neighbouring cells.

Early induction of Nrf2 after demyelination is required to control inflammation, as a lack of this signal early in demyelinating models aggravates inflammation, and thus demyelination. For instance, Nrf2-deficient mice have higher numbers of

apoptotic cells after 1 and 3 weeks of cuprizone treatment, and reduced numbers of oligodendrocytes and astrocytes, likely due to cell death [315]. Moreover, after 3 weeks of cuprizone diet, there was more severe demyelination, increased axonal damage and higher numbers of microglia when compared to WT animals [315]. Similarly, Nrf2 induction in astrocytes, by *Gfap*-specific deletion of *Keap1*, prevents oligodendrocyte and myelin loss and decreases microglia activation after 3 weeks of cuprizone administration [92]. In EAE, mice lacking Nrf2 present an early onset of clinical symptoms and worse clinical scores than WT mice [316]. At 14 days of EAE induction, which is the onset of pathology, Nrf2 null mice exhibited severe demyelination, higher peripheral immune cell infiltration and microglial activation compared to WT mice with EAE [316]. However, in this study, the normality of myelin was not evaluated before EAE induction in the transgenic mice. These findings, alongside my results, indicate that early and transient activation of Nrf2 signalling is required after demyelination to control and prevent further damage.

Fumarate esters (FAE), consisting of monomethyl fumarate (MMF) and DMF, have been shown to have immunomodulatory effects, decrease inflammatory cell infiltration and confer neuroprotection [90, 317, 318]. Moreover, a principal mechanism by which FAE are thought to act is by preventing oxidative stress and promoting cytoprotection via Nrf2 signalling activation [87, 319, 320]. Interestingly, in tissue obtained from brain autopsies of MS patients that had been treated with DMF, Nrf2 activation is mainly observed in astrocytes [88]. DMF promotes neuronal recovery after experimental demyelination. This was assessed by treating mice with

DMF for 7 days after cuprizone-induced demyelination and upon return to normal diet, isolating brain slices from these mice, and performing electrophysiological analysis [320]. Nonetheless, DMF is only effective in RRMS forms, potentially due to its neuroprotective effects [203, 318]. Accordingly, rats treated with DMF early after EAE do not show any recovery in EAE clinical score after treatment [321]. In this study, DMF was only provided three days after EAE induction, suggesting that earlier intervention could have been required to confer neuroprotection.

Moreover, treatment with DMF and MMF does not prevent demyelination and axonal damage within 6 weeks of cuprizone demyelination, nor does it confer any protective effect on oligodendrocytes [322]. DMF also does not improve white matter pathology outcomes after ischemic insult [323]. Future studies would be required to assess the direct effects of DMF on remyelination, by investigating the effect on oligodendrocytes or investigating myelin at the ultrastructural level.

The studies investigating the neuroprotective effects of Nrf2 have only been performed during demyelination, and DMF, which acts in part via activating Nrf2 in astrocytes, has not been shown to improve white matter pathology. Moreover, the specific effects of *Nrf2* overexpression in astrocytes during remyelination have never been explored. In the present study, a reduction in remyelination was observed at 14 DPI in lesioned mice with sustained Nrf2 expression in astrocytes compared to WT animals, a time at which early remyelination is expected in this model (Figure 3.21.C). Similarly, overexpression of Nrf2 in astrocytes did not recover white matter integrity of the corpus callosum in an ischemic mouse model [324].

In addition, I observed a reduction in the overall number of cells within demyelinated lesions, including astrocytes and oligodendrocytes (Figure 4.11, 23 & 25). Although Nrf2 activation (induced genetically or with drugs) confers neuroprotective effects, Nrf2 expression is already present in cells within MS lesions. High levels of Nrf2 are expressed by degenerating oligodendrocytes and astrocytes in actively demyelinating lesions of RRMS patients [203]. Similarly, in another study, Nrf2 signalling was found to be highly upregulated in astrocytes in chronic inactive MS lesions (which have reduced remyelination potential) and to a lesser extent in active lesions [297, 325]. Nrf2 activation can mediate activation of the integrated stress response (ISR) [326], which if transiently activated is associated with a pro-survival response and restoration of homeostasis. In contrast, a prolonged ISR activation promotes cell death [327]. This could have taken place in my model, in which continued overexpression of Nrf2 could have induced a negative feedback loop, further increasing ISR mechanisms resulting in cell death, which could then explain the reduced numbers of cells found within the lesions of GFAP-Nrf2 mice.

I found that at 3 DPI, there was a decrease in the total number of cells that were not astrocytes (Figure 5.6). *Nrf2* overexpression reduces microglia numbers and activation during the demyelinating stage of different demyelination models [92, 315, 316]. In the LPC-induced demyelination model, pro-inflammatory microglia numbers peak at 3 DPI [244, 328]. My findings could thus indicate a reduction of the numbers of microglia early after demyelination. Moreover, microglia are required to phagocytose myelin debris after demyelination [72, 262, 296, 329], and their

reduction could be a further explanation as to why remyelination is impaired consequently to *Nrf2* overexpression in astrocytes. This could be explored by co-staining with the transmembrane protein-119 (TMEM119), which specifically labels microglia, and the activating-macrophage lineage marker cluster of differentiation-68 (CD68), which labels phagocytic macrophages, and explore whether upon astrocytic Nrf2-overexpression, these cells contain fragments of myelin, detected by damaged MBP (dMBP) staining.

I also found that *Nrf2* overexpression in astrocytes following demyelination was associated with a dysmorphic morphology in reactive astrocytes, characterised by blunt processes, which were not as elongated as during normal hypertrophy (Figure 4.11). This feature, along with reduced astrocyte numbers, is also observed in astrocytopathies (leukodystrophies caused by astrocyte pathology) like vanishing white matter disease (VWM) [146]. Interestingly, VWM is also characterised by a reduction in the number of oligodendrocytes, thinner and reduced myelin sheaths [146]. These are striking results, where a similar pathology as VWM is observed upon *Nrf2* overexpression in astrocytes after demyelination. To further confirm the similarity in pathology, staining with delta isoform of GFAP (GFAPδ), which is highly expressed in VWM astrocytes, could be performed which indicates a defect in final maturation of astrocytes, which in turn affects oligodendrocyte responses [310].

Furthermore, impaired remyelination consequent to overexpression of Nrf2 in astrocytes could be mediated, at least in part, due to a decrease in cholesterol synthesis (Figure 5.4, 26). As I have previously described, Nrf2 negatively regulates

cholesterol synthesis in the liver [298-300, 302-306]. The present data have shown that proteins and genes associated with cholesterol synthesis are downregulated in two different models in which remyelination is impaired, and which are characterised by increased Nrf2 levels (ageing and transgenically sustained Nrf2 expression). Cholesterol is required to drive myelination and remyelination [272], and inhibiting cholesterol production in astrocytes during developmental myelination leads to hypomyelination [136]. The data from this last chapter indicates that in the brain, a similar mechanism of Nrf2-cholesterol crosstalk may be taking place as observed in the liver. Upon *Nrf2* overexpression in astrocytes, I found cholesterol synthesis associated proteins to be lower in expression, oligodendrocyte lineage cells dysregulated, and remyelination to be impaired.

6. CHAPTER: THESIS DISCUSSION

This thesis describes how astrocytes change to mediate repair in a model of efficient remyelination, the LPC-demyelination model. RNA sequencing revealed that astrocytes are dynamic and change their molecular profile throughout this process. To characterise astrocytes in two models of remyelination (LPC and cuprizone) different markers have been applied. Nonetheless, better markers could be applied in future studies for a more accurate characterisation. Aldh1l1 is the most specific marker for astrocytes in the adult brain but there is a lack of good antibodies for immunohistochemical characterisation. Comparing different RNA sequencing datasets could be performed in future studies to find highly expressed markers that are definitive for astrocytes. Bioinformatic analysis of single cell and bulk RNA sequencing could help to define different astrocyte subpopulations, which could be validated through lineage tracing of subpopulation specific promoter activity to confirm that these markers are stable and specific in adulthood. This also would provide information on astrocyte functions in these different subpopulations. For instance, in the present study it was observed that astrocytes mainly present antioxidant, metabolic and inflammatory profiles at the different time-points investigated which could have represented a change in function or a change in the dominance of different astrocyte populations. Investigating this further in diseases such as MS could reveal that some subpopulations are mainly prevalent in disease which would reveal specific target for therapeutic intervention.

Current approved treatments for MS only modulate the inflammatory component, and there are no therapies available that repair the lesions, leaving the disease with no cure. The present study focused on the Nrf2 and cholesterol signalling in astrocytes and their crosstalk to mediate remyelination. New therapies for MS could combine drugs that are aimed at targeting these pathways such as DMF for Nrf2 and Biotin for cholesterol synthesis [102]. Drugs could be directed to astrocytes via nanocapsules targeting receptors specific for astrocytic markers, for example the newly discovered astrocyte cell surface antigen (ACSA)-2 [330]. Nonetheless, specificity of this marker in WM has never been investigated and would need to be validated. Current drugs may have off-target effects throughout the body if given orally or via infusions, highlighting the need to design better ways to deliver MS drugs. For instance, drugs aimed at increasing cholesterol metabolism should be targeted to the CNS and animal studies should check cholesterol production in the liver. One promising drug delivery strategy is intranasal delivery, due to the direct transport to the CNS [331]. Moreover, this could address the issue of systematically-administered drugs poorly reaching the CNS, for example DMF reaches the CNS at very low levels and the different statin types have different capacity to cross the BBB [332, 333].

6.1. Conclusion

The work of this thesis describes astrocyte responses at the cellular and molecular level during remyelination. I found that after demyelination, astrocytes undergo a series of significant changes in number, proliferation and activation. Astrocytic expression of reactive markers (GFAP, Nestin, Vimentin and NFIA) was found to be temporally regulated during remyelination. Interestingly, GFAP+ astrocyte numbers increased early and peaked at the time of oligodendrocyte differentiation and early remyelination in two different models of toxin-induced demyelination, the LPC and cuprizone models. This increase in astrocyte reactivity during oligodendrocyte regenerative responses led to the next question as to how they might support these processes after demyelination. To address this question, I performed RNA sequencing of TRAP isolated astrocytic mRNA at key time-points during remyelination which consisted of the phase of OPC proliferation (3 DPI), oligodendrocyte differentiation (7 DPI), and the onset of remyelination (10 DPI). Gene expression and pathway analysis suggested a dynamic change of astrocyte functions during remyelination. Gene expression indicated that astrocytes presented a change from a neuroprotective profile at 3 DPI, to a pro-inflammatory profile at 10 DPI. This neuroprotective phenotype was characterised by an early and transient activation of Nrf2-signalling. Upon the downregulation of the Nrf2 pathway, astrocytes upregulated the cholesterol biosynthesis pathway at the time of oligodendrocyte differentiation (7 DPI), a pathway suggested to be important for myelination and remyelination. Due to previous data from liver studies indicating

that Nrf2 is a negative regulator of cholesterol synthesis, I next aimed to investigate this crosstalk in the context of remyelination. I used a mouse model in which Nrf2 is overexpressed in reactive astrocytes (GFAP+). Although the results obtained are still preliminary, they indicated that Nrf2-overexpression in astrocytes during remyelination decreased expression of genes and proteins involved in cholesterol synthesis. Remyelination was impaired in association with reduced numbers of oligodendrocyte lineage cells, although oligodendrocyte differentiation was not impaired, which could indicate that cholesterol is important for final maturation to myelin-producing oligodendrocytes. The link between Nrf2 signalling and cholesterol biosynthesis was also observed in aged mice, in which increased basal levels of Nrf2 pathway activation were observed in comparison to young animals. After demyelination of aged mice, decreased expression of enzymes involved in cholesterol synthesis was documented at 7 DPI compared to young mice. In addition, Nrf2 overexpression in astrocytes reduced the total number of cells in the lesion early after demyelination. This could indicate that Nrf2 is a master regulator of astrocytic functions during remyelination, and its dysregulation causes impairment in their cholesterol synthesis, responses from other cells, and in turn, remyelination (Figure 6.1).

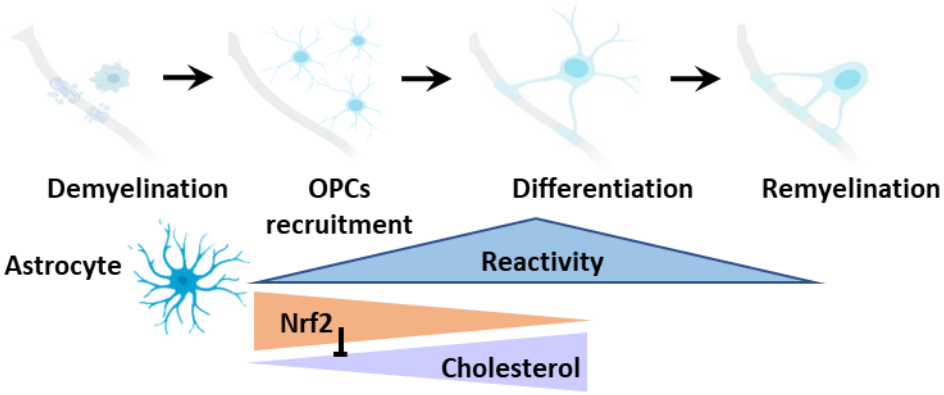

Figure 6.1. Nrf2 activation may interplay with cholesterol biosynthesis required for remyelination. Schematic representation of astrocyte responses during remyelination. Astrocytes increase in reactivity (as determined by increased GFAP, vimentin, nestin and NFIA levels) at the onset of oligodendrocyte differentiation and remyelination in the LPC and cuprizone models. Early after demyelination, astrocytes increase *Nrf2* expression, which is downregulated during oligodendrocyte differentiation and at the onset of remyelination, when cholesterol biosynthesis is activated. *Nrf2* may control cholesterol biosynthesis as sustained *Nrf2* activation in astrocytes dysregulated expression of cholesterol biosynthesis-associated genes/proteins and consequently impaired oligodendrocyte lineage cell responses and remyelination.

6.2. Limitation of thesis

The present study describes the cellular and molecular changes in astrocytes during remyelination and defines a mechanism by which their regenerative functions may be regulated. Nonetheless, there are experimental limitations that could be overcome in future studies.

During activation, astrocytes express markers also associated with progenitors and neural stem cells (NSCs) [246]. Hence, although different markers were used in conjunction with astrocytic markers, their expression could be associated with other cells in the lesion. Sox9 was used as a pan-astrocytic marker. However, NSCs can also express Sox9 in neurogenic areas, and after lesioning some of the Sox9+ nuclei could have represented NSCs migrating to the lesion. In an attempt to overcome this limitation, I used the ASRIBO line, in which only astrocytes express green fluorescent protein due to expression of the astrocyte-specific gene *Aldh1l1*. Nonetheless, fluorescence in this line was not sufficiently strong for quantification, and anti-GFP antibodies could have been used to amplify this signal. Future experiments could be done to address this and confirm that the markers used in this study were primarily associated with astrocytes after demyelination.

In the RNA sequencing experiments, qPCR validation is not shown as variability was found within the groups, and further repetitions were required. This could have been of importance, especially to validate the expression of the genes explicitly upregulated from demyelination rather than from injection alone (sham controls). However, I overcame this by using protein validation by immunofluorescence.

Further ‘n’ numbers would be required for the experiments described in the last chapter to achieve statistical power. Moreover, although I used an Nrf2-target gene product as validation of overexpression of *Nrf2* in the GFAP-Nrf2 mice, *Nrf2* overexpression itself was not confirmed nor was pathway activation after lesioning measured.

In the present study, I assessed the expression of two enzymes essential for cholesterol synthesis as a proxy for this pathway. To further validate cholesterol production by astrocytes, other approaches could be applied. Different mass spectrometry variances have been used to detect and quantify lipids in the serum and liver [301, 334]. Mass spectrometry characterises, identifies and quantifies molecules according to their molecular weight and fragmentation profile, which identifies ionic properties [335]. To obtain cholesterol esters and its intermediates from astrocytes, they would need first to be isolated from the lesion using FACS or MACS; however, the risk would be obtaining enough protein from the isolated cells within the lesion, and would likely require pooling several animals to obtain a single quantification.

In the last chapter, my preliminary data suggests that GFAP-Nrf2 mice show a failure in remyelination. Further analysis at the ultrastructural level is underway and is required to confirm this finding, and detect any other abnormality in myelin integrity. Moreover, the experiments performed in aged animals would require further characterisation and validation at the protein level to support the qPCR data.

6.3. Future directions

In the first results chapter, I showed a different temporal pattern of expression of reactive markers by astrocytes during remyelination. Briefly, GFAP and vimentin were increased, starting from 7 DPI, whereas NFIA and Nestin showed a gradual increase in expression peaking at 14 DPI. Moreover, not all GFAP+ astrocytes were positive for the other reactive markers used, representing heterogeneity of astrocytes in the lesion. Future studies could investigate whether different types of astrocytes exist after demyelination and if these have different functions, or whether this difference in expression of markers reflects different maturation states. Single-cell (sc) RNA-sequencing analysis could be performed to study this. Importantly, the data could be compared with the GFAP-Nrf2 model and see whether the different populations are changed or explore whether there is a maturation effect. This could then be compared to subpopulations in MS tissue and see whether there are changes. Jäkel and colleagues recently performed scRNA-sequencing from white matter of MS patients and from control (healthy) patients [71]. In this study, although the focus was characterising oligodendrocyte populations, they discovered two different astrocyte clusters in white matter that were differently distributed between MS and controls [71]. Following up on this study, I could further explore the reactive markers used in the present study, and investigate their expression in different MS lesions to compare whether in pathology there is a higher expression of those markers in different astrocyte subpopulations, and in which lesions they are most highly expressed. In addition, it could be interesting to explore in this data set

whether there is a defect in the Nrf2 and cholesterol synthesis pathways in different astrocyte populations found in MS lesions.

Following up on the Nrf2 and cholesterol signalling interplay, it would be interesting to stimulate cholesterol signalling in the *Nrf2*-overexpressing mice to explore whether this can rescue effects on remyelination. To do so, cholesterol biosynthesis could be stimulated with a cholesterol efflux enhancer CS-6253, previously used in the EAE model, to which enhanced cholesterol synthesis in astrocytes [169]. Then cholesterol biosynthesis pathway activation could be confirmed at 7 DPI as I have done, and remyelination could be assessed at 14 DPI by MBP staining and at the ultrastructural level. This would determine whether the impairment in remyelination caused by *Nrf2*-overexpression can be overcome by stimulating cholesterol synthesis. Alternatively, if stimulating cholesterol synthesis is not sufficient to promote remyelination, *Nrf2*-overexpression could be inhibited by retinoic acid treatment. Nrf2 protein has seven Nrf2-ECH homology (Neh) domains, Neh1-7, which enable regulating different functions [265]. The Neh7 domain binds to the retinoid X receptor α to repress its transcriptional activation [336]. Thus treatment with retinoic acid (all-*trans* retinoic acid (ATRA)) to inhibit Nrf2 signalling could be used to explore whether the defects observed in GFAP-Nrf2 mice can be rescued [337, 338].

In the present study, I observed that a reduction in the total number of cells that were not astrocytes occurred early after demyelination at 3 DPI. For future studies, it would be interesting to explore whether these cells reduced in the lesion were

microglia. Astrocytes respond to microglia after demyelination. Oxidative stress is a hallmark of MS [339], and microglia are the main inducers of oxidative stress pathways during demyelination [340]. In the LPC model, pro-inflammatory microglia, characterised by the expression of inducible nitric oxide synthetase (iNOS) which produces reactive nitrogen species (RNS), are most abundant at 3 DPI [244, 328]. Astrocytes may overcome the oxidative stress produced by microglia at this time through the activation of the Nrf2 cascade [202]. Overexpression of Nrf2-signalling activation after demyelination may inhibit microglia migration and activation after demyelination. A reduced number of microglia in the lesion could lead to impaired myelin debris clearance [72], and the production of regenerative factors for remyelination [328]. This could explain why the lesions characterised by higher *Nrf2* expression in astrocytes are generally the ones with less remyelinating capacity in MS lesions [88]. Investigating this could enable finding new therapeutic targets that balance Nrf2-pathway activation in astrocytes so that the downstream cascade of regenerative events can successfully take place to promote remyelination.

ABBREVIATIONS

A1: Pro-inflammatory astrocytes

A2: Pro-repair astrocytes

Acaca: Acetyl-CoA carboxylase 1 gene

Acacb: Acetyl-CoA carboxylase 2 gene

Acat2: Acetyl-CoA Acetyltransferase 2 gene

Aldh1l1: Aldehyde dehydrogenase 1 family membrane L1

ALS: Amyotrophic lateral sclerosis

ANGPL4: Angiopoietin-like 4

APC: Antigen-presenting cells

ApoE: Apolipoprotein E

Aqp4: Aquaporin 4

ASRIBO: Tg(Aldh1l1-EGFP/Rpl10a)JD130

ATP: Adenosine triphosphate

ATRA: All-*trans* retinoic acid

B4GALT6: Beta-1,4-Galactosyltransferase 6

BBB: Block blood-brain barrier

BMP: Bone morphogenic protein

C1q: Complement complex-1q

C3: Complement complex-3

CC: Corpus callosum

CC1: Anti-adenomatous polyposis coli (APC)

CI: Confidence interval

CCL: C-C motif chemokine ligand

CD: Cluster of differentiation

CDDO-Im: Oleanolic triterpenoid 1-[2-cyano-3,12-dioxooleana-,9(11)-dien-28-oyl] imidazole

Chd7: Chromodomain Helicase DNA Binding Protein 7

CHX: Cycloheximide

CIH3L1: Chitinase 3 like 1

CIS: Clinically isolated syndrome

CNS: Central nervous system

CNTF: Ciliary neurotrophic factor

CO_2: Carbon dioxide

CSF: Cerebrospinal fluid

Cx: Connexin

CXCL: Chemokine (C-X-C motif) ligand

CXCR: C-X-C chemokine receptor type

DHPC: 1,2-diheptanoyl-*sn*-glycero-3-phosphocholine

Dhcr24: 24-dehydrocholesterol reductase

dMBP: Damage MBP

DMF: Dimethyl fumarate

DPI: Days post-injection

DTT: DL-Dithiothreitol

EAE: Experimental autoimmune encephalomyelitis

eGFP: Enhanced green fluorescent protein

ErbB1: Epithermal growth factor receptor

ET-1: Endothelin-1

FABP-7: Fatty acid-binding protein 7

FACS: Fluorescent activated cell sorting

FAE: Fumarate esters

Fasn: Fatty acid synthase

FC: Fold-change

FDA: Food and drug administration

Fpn: Ferroportin

Fdps: Farnesyl diphosphate synthase

FGF: Fibroblast growth factor

FPKM: Fragments per kilobase of transcript per million mapped reads

Gclc: Glutamate-cysteine ligase catalytic subunit

GFAP: Glial fibrillary acidic protein

GFP: Green fluorescent protein

GLAST: Glutamate aspartate transporter-1

GLT-1: Glutamate transporter soluble carrier family 1, member 2

GM-CSF: Granulocyte-macrophage colony-stimulating factor

GO: Gene ontology

CCL: C-C motif chemokine ligand

CXCL: Chemokine (C-X-C motif) ligand

H_2O_2: Hydrogen peroxide

HA: Hemagglutinin

HIER: Heat inactivated antigen retrieval

HLA: Human leukocyte antigen

HMG-CoA: 3-hydroxy-3-methylglutaryl-coenzyme A

Hmgcr: Hydroxymethylglutaryl-CoA reductase

Hmgcs: Hydroxymethylglutaryl-CoA synthase

Hmox: Hemeoxygenase

IGF: Insulin growth factor

IL: Interleukin

iNOS: Inducible nitric oxide synthetase

iPSC: Induced pluripotent stem cells

IPA: Ingenuity pathway analysis

iTreg: inducible regulatory T-cell

ISR: Integrated stress response

KCl: Potassium chloride

Keap1: Kelch-like ECH-associated protein 1

KOR: Kappa opioid receptor

LacCer: Lactosylceramide

LINGO-1: Leucine-rich repeat and immunoglobulin-like domain-containing nogo receptor-interaction protein 1

Lgasl: Galectin gene

LPC: Lysolecithin

LPS: Lipopolysaccharide

M1: Pro-inflammatory microglia/macrophages

M2: Pro-repair microglia/macrophages

MACS: Magnetic-activated cell sorting

MAG: Myelin associated glycoprotein

Mash1: Achaete-scute complex homolog 1

MBP: Myelin basic protein

MCAO: Middle cerebral artery occlusion

MCL: Markov clustering algorithm

$MgCl_2$: Magnesium Chloride

MHCII: Major histocompatibility class II

MMF: Monomethyl fumarate

MOG: Myelin oligodendrocyte glycoprotein

MS: Multiple sclerosis

Mvd: Mevalonate diphosphate decarboxylase

Mvk: Mevalonate kinase gene

Myrf: Myelin regulatory factor

MyT1: Myelin transcription factor 1

Na+: Sodium

NaOH: Sodium hydroxide

NAWM: Normal appearing white matter

Neh: Nrf2-ECH homology domain

Nes: Nestin

NF-H: Neurofilament

NFIA: Nuclear factor IA

NF-κB: Nuclear factor kappa-light-chain enhancer of activated B cells

NG2: Chondroitin sulfate proteoglycan

Nkx: Homeodomain factor

NMO: Neuromyelitis Optica

NMOSD: NMO spectrum disorder

NP40: Nonidet P-40

NPC: Niemann-Pick type C

NPC1: NPC intracellular cholesterol transported-1

Nqo1: NAD(P)H quinone dehydrogenase1

NSC: Neural stem cells

mRNA: Messenger ribonucleic acid

Nrf2: Nuclear factor (erythroid-derived 2)-like 2

OCT: Optical cutting temperature compound

Olig: Oligodendrocyte transcription factor

OPCs: Oligodendrocytes precursor cells

Osgin1: Oxidative stress-induced growth inhibitor 1

P2YR1: P2Y purinoceptor 1

PAF: Platelet-activating factor

PBS: Phosphate buffered saline

PCR: Polymerase chain reaction

PFA: Paraformaldehyde

PLP: Proteolipid protein

PMS: Progressive multiple sclerosis

PPMS: Primary progressive multiple sclerosis

PTP: Permeability transition pore

qPCR: Quantitative polymerase chain reaction

RNA: Ribonucleic acid

RIN: RNA integrity number

ROS: Reactive oxygen species

RNS: Reactive nitrogen species

RRMS: Relapse remitting multiple sclerosis

RXR-γ: Retinoid X receptor-γ

scRNA-seq: Single-cell RNA-sequencing

s.e.m: Standard error of the mean

S100: S100 Calcium Binding Protein

Sema: Semaphorin

Shh: Sonic hedgehog

Slc7a11: Cystine/glutamate antiporter xCT

sMaf: Small musculoaponeurotic fibrosarcoma

Sox: Sry-type HMG box

S1pr3: Sphingosine-1-phosphate receptor 3

Sp7: Osterix 7

SPMS: Secondary progressive multiple sclerosis

Sqle: Squalene monooxygenase gene

Srebp1c: Sterol regulatory element-binding protein-1c

Srxn1: Sulfiredoxin 1

STAT3: Signal transducer and activator of transcription 3

TBE: Tris-borate-EDTA

TG2: Transglutaminase-2

TGF: Transforming grow factor

Th1: Pro-inflammatory T-helper type 1

Th2: anti-inflammatory T-helper type 2

TMEM119: Transmembrane protein-119

TIMP-1: Tissue inhibitor metalloproteinase-1

TNF-α: Tumour necrosis factor-α

TRAP: Translational ribosome affinity purification

T-reg: T-regulatory cells

VCAM-1: Vascular cell adhesion molecule-1

VEGF: Vascular endothelial growth factor

VEGFR: Vascular endothelial growth factor receptor

Vim: Vimentin

VZ: Ventricular zone

W: Week

WT: Wild-type

Zbtb20: Zinc finger- and BTB domain-containing protein 20

µm: Micrometre

REFERENCES

1. Salzer, J.L., *Schwann cell myelination.* Cold Spring Harb Perspect Biol, 2015. **7**(8): p. a020529.

2. Simons, M. and K.-A. Nave, *Oligodendrocytes: Myelination and Axonal Support.* Cold Spring Harbor Perspectives in Biology, 2016. **8**(1).

3. Almeida, R.G.a.L., D.A., *On myelinated axons plasticity and neuronal circuit formation and function.* Journal of Neuroscience, 2017. **37**(42): p. 12.

4. Stadelmann, C., et al., *Myelin in the central nervous system: Structure, function, and pathology.* Physiol Rev, 2019. **99**: p. 51.

5. Lee, Y.D., et al., *Oligodendroglial metabolically support axons and contribute to neurodegeneration.* Nature, 2012. **487**: p. 8.

6. Fünfschilling, U., et al., *Glycolytic oligodendrocytes maintain myelin and long-term axonal integrity.* Nature, 2012. **485**(7399): p. 18.

7. Bercury, K.K. and W.B. Macklin, *Dynamics and Mechanisms of CNS Myelination.* Developmental Cell, 2015. **32**: p. 12.

8. Freeman, M.R. and D.H. Rowitch, *Evolving Concepts of Gliogenesis: A Look Way Back and Ahead to the Next 25 Years.* Neuron, 2013. **80**: p. 11.

9. van Tilborg, E., et al., *Origin and dynamics of oligodendrocytes in the developing brain: Implications for perinatal white matter injury.* Glia, 2018. **66**: p. 18.

10. Miron, V.E., T. Kuhlmann, and J. Antel, *Cells of the oligodendroglial lineage, myelination, and remyelination.* Biochim Biophys Acta, 2011. **1812**: p. 10.

11. Sock, E. and M. Wegner, *Transcriptional control of myelination and remyelination.* Glia, 2019. **67**(11): p. 13.

12. Fulton, D., P.M. Paez, and A.T. Campagnoni, *The multiple roles of myelin protein genes during the development of the oligodendrocyte.* ASN Neuro, 210. **2**(1): p. 13.

13. Foran, D.R. and A.C. Peterson, *Myelin Acquisition in the Central Nervous System of the Mouse Revealed by an MBP-Lac Z Transgene.* Journal of Neuroscience, 1992. **12**(12): p. 8.

14. Miller, D.J., et al., *Prolonged myelination in human neocortical evolution.* PNAS, 2012. **109**(41): p. 6.

15. Swire, M. and C. Ffrench-Constant, *Seeing Is Believing: Myelin Dynamics in the Adult CNS.* Neuron, 2018. **16**: p. 3.

16. Love, S., *Demyelinating diseases.* J Clin Pathol, 2005. **59**: p. 9.

17. Franklin, R.J. and C. Ffrench-Constant, *Regenerating CNS myelin — from mechanisms to experimental medicines.* Nat Rev Neurosci, 2017. **18**: p. 17.

18. Duncan, I.D., et al., *Extensive remyelination of the CNS leads to functional recovery.* PNAS, 2009. **106**(16): p. 5.

19. Gensert, J.M. and J.E. Goldman, *Endogenous Progenitors Remyelinate Demyelinated Axons in the Adult CNS.* Neuron, 1997. **19**: p. 7.

20. Boyd, A., Zhang, H., and Williams, A., *Insufficient OPC migration into demyelinated lesions is a cause of poor remyelination in MS and mouse models.* Acta Neuropathol, 2013. **125**: p. 19.

21. Duncan, I.D., et al., *The adult oligodendrocyte can participate in remyelination.* PNAS, 2018. **115**(50): p. E11807–E11816.

22. Yeung, M.S.Y., et al., *Dynamics of oligodendrocyte generation in multiple sclerosis.* Nature, 2019. **566**(7745): p. 538-542.

23. Fancy , S.P., et al., *Myelin Regeneration: A Recapitulation of Development?* Annu Rev Neurosci, 2011. **34**: p. 25.

24. Kalinick, T., *Multiple Sclerosis Relapses: Epidemiology, Outcomes and Management. A Systematic Review.* Neuro epidemiology, 2015. **44**: p. 16.

25. Faissner, S., et al., *Progressive multiple sclerosis: from pathophysiology to therapeutic strategies.* Nat Rev Drug Discov, 2019. **18**(12): p. 18.

26. Inojosa, H., et al., *A focus on secondary progressive multiple sclerosis (SPMS): challenges in diagnosis and definition.* Journal of Neurology, 2019: p. 12.

27. Kuhlmann, T., Ludwin, S., Prat, A., Antel, J., Brück, W. and Lassmann, H., *An updated histological classification system for multiple sclerosis lesions.* Acta Neuropathol, 2017. **133**: p. 11.

28. Dillenburg, A., et al., *Activin receptors regulate the oligodendrocyte lineage in health and disease.* Acta Neuropathol, 2018. **135**(6): p. 887-906.

29. Collaborators, G.M.S., *Global, regional, and national burden of multiple sclerosis 1990–2016: a systematic analysis for the Global Burden of Disease Study 2016.* Lancet Neurol, 2019. **18**: p. 17.

30. Kearns, P.K.A., et al., *Regional variation in the incidence rate and sex ratio of multiple sclerosis in Scotland 2010–2017: findings from the Scottish Multiple Sclerosis Register.* Journal of Neurology, 2019. **266**(10): p. 2376-2386.

31. Dombrowski, Y., et al., *Regulatory T cells promote myelin regeneration in the central nervous system.* Nat Neurosci, 2017. **20**(5): p. 674-680.

32. Avila, M., et al., *The Role of Sex Hormones in Multiple Sclerosis.* Eur Neurol, 2018. **80**: p. 93-99.

33. Confavreux, C., et al., *RATE OF PREGNANCY-RELATED RELAPSE IN MULTIPLE SCLEROSIS.* N Engl J Med, 1998. **339**(5): p. 285-91.

34. Marin-Husstegea, M., et al., *Oligodendrocyte Progenitor Proliferation and Maturation Is Differentially Regulated by Male and Female Sex Steroid Hormones.* Dev Neurosci, 2004. **26**: p. 245–254.

35. Sicotte, N.L., et al., *Treatment of Multiple Sclerosis with the Pregnancy Hormone Estriol.* Ann Neurol, 2002. **52**(4): p. 421-8.

36. Greenberg, D.L., et al., *Differences in brain volumes among males and female hormone-therapy users and nonusers.* Psychiatry Research: Neuroimaging 2006. **147**: p. 127-134.

37. Voskuhl, R.R., et al., *Estriol combined with glatiramer acetate for women with relapsing-remitting multiple sclerosis: a randomised, placebo-controlled, phase 2 trial.* Lancet Neurol, 2016. **15**: p. 36-46.

38. Parnell, G.P. and D.R. Booth, *The Multiple Sclerosis (MS) Genetic Risk Factors indicate both Acquired and innate immune Cell Subsets Contribute to MS Pathogenesis and identify novel Therapeutic Opportunities.* Front Immunol, 2017. **8**(425): p. 1-6.

39. Kular, L. and e. al., *DNA methylation as a mediator of HLA-DRB1*15:01 and a protective variant in multiple sclerosis.* Nat Commun, 2018. **9**(1): p. 1-15.

40. Gourraud, P.A., et al., *The genetics of multiple sclerosis: an up-to-date review.* Immnol Rev, 2012. **248**: p. 87-103.

41. Gale, C.R. and C.N. Martyin, *Migrant studies in multiple sclerosis.* Prog Neurobiol, 1995. **47**: p. 425-448.

42. Belbasi, L., et al., *Environmental risk factors and multiple sclerosis: an umbrella review of systematic reviews and meta-analyses.* Lancet Neurol, 2015. **14**: p. 263-273.

43. O'Gorman, C., R. Lucas, and B. Taylor, *Environmental Risk Factors for Multiple Sclerosis: A Review with a Focus on Molecular Mechanisms.* Int J Mol Sci, 2012. **13**: p. 11718-11752.

44. Brown, R.A., S. Narayanan, and D.L. Arnold, *Imaging of repeated episodes of demyelination and remyelination in multiple sclerosis.* Neuroimage Clin, 2014. **6**: p. 20-5.

45. Chen, J.T., et al., *Magnetization transfer ratio evolution with demyelination and remyelination in multiple sclerosis lesions.* Ann Neurol, 2008. **63**(2): p. 254-62.

46. Moore, C.S., et al., *How factors secreted from astrocytes impact myelin repair.* J Neurosci Res, 2011. **89**(1): p. 13-21.

47. Schwartzbach, C.J., et al., *Lesion remyelinating activity of GSK239512 versus placebo in patients with relapsing-remitting multiple sclerosis: a randomised, single-blind, phase II study.* J Neurol, 2017. **264**(2): p. 304-315.

48. Peters, A. and C. Sethares, *Oligodendrocytes, their progenitors and other neuroglial cells in the aging primate cerebral cortex.* Cereb Cortex, 2004. **14**(9): p. 995-1007.

49. Tripathi, R.B., et al., *Remarkable Stability of Myelinating Oligodendrocytes in Mice.* Cell Rep, 2017. **21**(2): p. 316-323.

50. Franklin, R.J., *Why does remyelination fail in multiple sclerosis?* Nat Neurosci Rev, 2002. **5**: p. 705-714.

51. Schulz, K., A. Kroner, and S. David, *Iron efflux from astrocytes plays a role in remyelination.* J Neurosci, 2012. **32**(14): p. 4841-7.

52. Giera, S. and e. al., *Microglial transglutaminase-2 drives myelination and myelin repair via GPR56/ ADGRG1 in oligodendrocyte precursor cells.* Elife, 2018. **7**: p. pii: e33385.

53. Zhang, S. and e. al., *Sox2 Is Essential for Oligodendroglial Proliferation and Differentiation during Postnatal Brain Myelination and CNS Remyelination.* J Neurosci, 2018. **38**(7): p. 1802-1820.

54. Chari, D.M. and W.F. Blakemore, *New insights into remyelination failure in multiple sclerosis: implications for glial cell transplantation.* Mult Scler, 2012. **8**: p. 271-277.

55. Lucchinetti, C.F., et al., *Distinct Patterns of Multiple Sclerosis Pathology Indicates Heterogeneity in Pathogenesis.* Brain Pathol, 1996. **6**: p. 259-274.

56. Spassky, N. and e. al., *Directional Guidance of Oligodendroglial Migration by Class 3 Semaphorins and Netrin-1.* J Neurosci, 2002. **22**(14): p. 5992-6004.

57. Williams, A. and e. al., *Semaphorin 3A and 3F: key players in myelin repair in multiple sclerosis?* Brain, 2007. **130**: p. 2554-2565.

58. Chang, A. and e. al., *Premyelinating oligodendrocytes in chronic lesions of multiple sclerosis.* N Engl J Med, 2002. **346**(3): p. 165-174.

59. Lee, X. and e. al., *NGF Regulates the Expression ofAxonal LINGO-1 to Inhibit Oligodendrocyte Differentiation and Myelination.* J Neurosci, 2007. **27**(1): p. 220-225.

60. Mi, S. and e. al., *LINGO-1 negatively regulates myelination by oligodendrocytes.* Nat Neurosci, 2005. **8**(6): p. 745-751.

61. Wang, C. and e. al., *Lingo-1 Inhibited by RNA Interference Promotes Functional Recovery of Experimental Autoimmune Encephalomyelitis.* The Anatomical Record, 2014. **297**: p. 2356–2363.

62. Gresle, M.M. and e. al., *Blocking LINGO-1 in vivo reduces degeneration and enhances regeneration of the optic nerve.* Multiple Sclerosis Journal - Experimental, Translational and Clinical, 2016. **2**: p. 1-13.

63. Shao, Z. and e. al., *LINGO-1 Regulates Oligodendrocyte Differentiation through the Cytoplasmic Gelsolin Signaling Pathway.* J Neurosci, 2017. **37**(12): p. 3127–3137.

64. Li, X. and e. al., *LINGO-1-Fc-Transduced Neural Stem Cells Are Effective Therapy for Chronic Stage Experimental Autoimmune Encephalomyelitis.* Mol Neurobiol, 2017. **54**: p. 4365–4378.

65. Rosenberg, S. and J.R. Chan, *Modulating myelination: knowing when to say Wnt.* Genes Dev, 2009. **23**: p. 1487–1493.

66. Fancy , S.P. and e. al., *Dysregulation of the Wnt pathway inhibits timely myelination and remyelination in the mammalian CNS.* Genes Dev, 2009. **23**: p. 1571–1585.

67. Back, S.A., et al., *Hyaluronan accumulates in demyelinated lesions and inhibits oligodendrocyte progenitor maturation.* Nat Med, 2005. **11**(9): p. 966-72.

68. See, J.M. and J.B. Grinspan, *Sending Mixed Signals: Bone Morphogenetic Protein in Myelination and Demyelination.* J Neuropathol Exp Neurol, 2009. **68**(6): p. .595-604.

69. Wang, S. and e. al., *Notch Receptor Activation Inhibits Oligodendrocyte Differentiation.* Neuron, 1998. **21**: p. 63-75.

70. Falcão, A.M. and e. al., *Disease-specific oligodendrocyte lineage cells arise in multiple sclerosis.* Nat Med, 2018. **24**: p. 1837-1844.

71. Jakel, S. and L. Dimou, *Glial Cells and Their Function in the Adult Brain: A Journey through the History of Their Ablation.* Front Cell Neurosci, 2017. **11**: p. 24.

72. Skripuletz, T., et al., *Astrocytes regulate myelin clearance through recruitment of microglia during cuprizone-induced demyelination.* Brain, 2013. **136**(1): p. 147-167.

73. Lampron, A. and e. al., *Inefficient clearance of myelin debris by microglia impairs remyelinating processes.* J Exp Med, 2015. **212**(4): p. 481-495.

74. Cantuti-Castelvetri, L. and e. al., *Defective cholesterol clearance limits remyelination in the aged central nervous system.* Science, 2018. **359**: p. 1-5.

75. Safaiyan, S. and e. al., *Age-related myelin degradation burdens the clearance function of microglia during aging.* Nat Neurosci, 2016. **19**(8): p. 995-998.

76. Kotter, M.R. and e. al., *Myelin Impairs CNS Remyelination by Inhibiting Oligodendrocyte Precursor Cell Differentiation.* J Neurosci, 2006. **26**(1): p. 328 –332.

77. Franklin, R.J. and C. ffrench-Constant, *Remyelination in the CNS: from biology to therapy.* Nat Rev Neurosci, 2008. **9**: p. 839-855.

78. Sim, F.J., et al., *The Age-Related Decrease in CNS Remyelination Efficiency Is Attributable to an Impairment of Both Oligodendrocyte Progenitor Recruitment and Differentiation.* J Neurosci, 2002. **22**(77): p. 2451–2459.

79. Shen, S. and e. al., *Age-dependent epigenetic control of differentiation inhibitors is critical for remyelination efficiency.* Nat Neurosci, 2008. **11**(9): p. 1024-1034.

80. Montalban, X. and e. al., *Ocrelizumab versus Placebo in Primary Progressive Multiple Sclerosis.* The New England Journal of Medicine, 2017. **376**(3): p. 209-220.

81. Hooijmans, C. and e. al., *Remyelination promoting therapies in multiple sclerosis animal models: a systematic review and metaanalysis.* Scientific Reports, 2019. **9**(822): p. 1-17.

82. Dhib-Jalbut, S., *Mechanisms of action of interferons and glatiramer acetate in multiple sclerosis.* Neurology, 2002. **58**(8).

83. Guarnera, C., P. Bramanti, and E. Mazzon, *Comparison of efficacy and safety of oral agents for the treatment of relapsing-remitting multiple sclerosis.* Drug Des Devel Ther, 2017. **11**: p. 2193-2207.

84. Hauser, S.L., et al., *Ocrelizumab versus Interferon Beta-1a in Relapsing Multiple Sclerosis.* N Engl J Med, 2017. **376**(3): p. 221-234.

85. Massey, J., et al., *B cell depletion therapy resulting in sustained remission of severe autoimmune complications following Alemtuzumab treatment of Multiple Sclerosis.* Multiple Sclerosis and Related Disorders 2019. **35**: p. 100-103.

86. Granqvist, M., et al., *Comparative effectiveness of dimethyl fumarate as the initial and secondary treatment for MS.* Mult Scler, 2019: p. 1352458519866600.

87. Scannevin, R.H., et al., *Fumarates promote cytoprotection of central nervous system cells against oxidative stress via the nuclear factor (erythroid-derived 2)-like 2 pathway.* J Pharmacol Exp Ther, 2012. **341**(1): p. 274-84.

88. Metz, I., et al., *Glial cells express nuclear nrf2 after fumarate treatment for multiple sclerosis and psoriasis.* Neurol Neuroimmunol Neuroinflamm, 2015. **2**(3): p. e99.

89. Galloway, D.A., J.B. Williams, and C.S. Moore, *Effects of fumarates on inflammatory human astrocyte responses and oligodendrocyte differentiation.* Ann Clin Transl Neurol, 2017. **4**(6): p. 381-391.

90. McGuire, V.A., et al., *Dimethyl fumarate blocks pro-inflammatory cytokine production via inhibition of TLR induced M1 and K63 ubiquitin chain formation.* Sci Rep, 2016. **6**: p. 31159.

91. Ciolac, D. and e. al., *Selective Brain Network and Cellular Responses Upon Dimethyl Fumarate Immunomodulation in Multiple Sclerosis.* Frontiers in Immunology, 2019. **10**(1179): p. 1-12.

92. Draheim, T., et al., *Activation of the astrocytic Nrf2/ARE system ameliorates the formation of demyelinating lesions in a multiple sclerosis animal model.* Glia, 2016. **64**(12): p. 2219-2230.

93. Huang, J.K., et al., *Retinoid X receptor gamma signaling accelerates CNS remyelination.* Nat Neurosci, 2011. **14**(1): p. 45-53.

94. Chandraratna, R., R.J. Noelle, and E.C. Nowak, *Treatment with retinoid X receptor agonist IRX4204 ameliorates experimental autoimmune encephalomyelitis.* Am J Transl Res, 2016. **8**(2): p. 1016-1026.

95. Cole, K.L.H., J.J. Early, and L.D. A., *Drug discovery for remyelination and treatment of MS.* Glia, 2017. **65**: p. 1565-1589.

96. Kremer, D., P. Kury, and R. Dutta, *Promoting remyelination in multiple sclerosis: current drugs and future prospects.* Mult Scler, 2015. **21**(5): p. 541-9.

97. Kremer, D., et al., *Current advancements in promoting remyelination in multiple sclerosis.* Mult Scler, 2019. **25**(1): p. 7-14.

98. Bordet, T., et al., *Olesoxime (TRO19622): A Novel Mitochondrial-Targeted Neuroprotective Compound.* Pharmaceuticals (Basel), 2010. **3**(2): p. 345-368.

99. Chitnis, T., *The role of testosterone in MS risk and course.* Mult Scler, 2018. **24**(1): p. 36-41.

100. Stangel, M., et al., *Achievements and obstacles of remyelinating therapies in multiple sclerosis.* Nat Rev Neurol, 2017. **13**: p. 742-754.

101. Waslo, C., et al., *Lipoic Acid and Other Antioxidants as Therapies for Multiple Sclerosis.* Curr Treat Options Neurol, 2019. **21**(6): p. 26.

102. Tourbah, A., et al., *MD1003 (high-dose biotin) for the treatment of progressive multiple sclerosis: A randomised, double-blind, placebo-controlled study.* Mult Scler, 2016. **22**(13): p. 1719-1731.

103. LaGanke, C., et al., *Safety/tolerability of the anti-semaphorin 4D Antibody VX15/2503 in a randomized phase 1 trial.* Neurol Neuroimmunol Neuroinflamm, 2017. **4**(4): p. e367.

104. Fox, R.J., et al., *Phase 2 Trial of Ibudilast in Progressive Multiple Sclerosis.* N Engl J Med, 2018. **379**(9): p. 846-855.

105. Liu, B., A.G. Teschemacher, and S. Kasparov, *Neuroprotective potential of astroglia.* J Neurosci Res, 2017. **95**(11): p. 2126-2139.

106. Matyash, V. and H. Kettenmann, *Heterogeneity in astrocyte morphology and physiology.* Brain Res Rev, 2010. **63**(1-2): p. 2-10.

107. Tsai, H.H., et al., *Regional astrocyte allocation regulates CNS synaptogenesis and repair.* Science, 2012. **337**(6092): p. 358-62.

108. Araque, A., et al., *Gliotransmitters travel in time and space.* Neuron, 2014. **81**(4): p. 728-39.

109. Perea, G., M. Navarrete, and A. Araque, *Tripartite synapses: astrocytes process and control synaptic information.* Trends Neurosci, 2009. **32**(8): p. 421-31.

110. Abbott, N.J., L. Ronnback, and E. Hansson, *Astrocyte-endothelial interactions at the blood-brain barrier.* Nat Rev Neurosci, 2006. **7**(1): p. 41-53.

111. Suzuki, A., et al., *Astrocyte-neuron lactate transport is required for long-term memory formation.* Cell, 2011. **144**(5): p. 810-23.

112. Howarth, C., *The contribution of astrocytes to the regulation of cerebral blood flow.* Front Neurosci, 2014. **8**: p. 103.

113. MacVicar, B.A. and E.A. Newman, *Astrocyte regulation of blood flow in the brain.* Cold Spring Harb Perspect Biol, 2015. **7**(5).

114. Olsen, M.L., et al., *New Insights on Astrocyte Ion Channels: Critical for Homeostasis and Neuron-Glia Signaling.* J Neurosci, 2015. **35**(41): p. 13827-35.

115. Colombo, E. and C. Farina, *Astrocytes: Key Regulators of Neuroinflammation.* Trends Immunol, 2016. **37**(9): p. 608-620.

116. Liddelow, S.A. and B.A. Barres, *Reactive Astrocytes: Production, Function, and Therapeutic Potential.* Immunity, 2017. **46**(6): p. 957-967.

117. Kamphuis, W. and e. al., *GFAP Isoforms in Adult Mouse Brain with a Focus on Neurogenic Astrocytes and Reactive Astrogliosis in Mouse Models of Alzheimer Disease.* PLoS One, 2012. **7**(8): p. 1-24.

118. Molofsky, A.V., et al., *Astrocytes and disease: a neurodevelopmental perspective.* Genes Dev, 2012. **26**(9): p. 891-907.

119. Cahoy, J.D., et al., *A transcriptome database for astrocytes, neurons, and oligodendrocytes: a new resource for understanding brain development and function.* J Neurosci, 2008. **28**(1): p. 264-78.

120. Sun, W., et al., *SOX9 Is an Astrocyte-Specific Nuclear Marker in the Adult Brain Outside the Neurogenic Regions.* J Neurosci, 2017. **37**(17): p. 4493-4507.

121. Reemst, K., et al., *The Indispensable Roles of Microglia and Astrocytes during Brain Development.* Front Hum Neurosci, 2016. **10**: p. 566.

122. Deneen, B., et al., *The Transcription Factor NFIA Controls the Onset of Gliogenesis in the Developing Spinal Cord.* Neuron, 2006. **52**(6): p. 953-968.

123. Kang, P., et al., *Sox9 and NFIA coordinate a transcriptional regulatory cascade during the initiation of gliogenesis.* Neuron, 2012. **74**(1): p. 79-94.

124. Nagao, M., et al., *Zbtb20 promotes astrocytogenesis during neocortical development.* Nat Commun, 2016. **7**: p. 11102.

125. Molofsky, A.V. and B. Deneen, *Astrocyte development: A Guide for the Perplexed.* Glia, 2015. **63**(8): p. 1320-1329.

126. Zeisel, A., et al., *Molecular Architecture of the Mouse Nervous System.* Cell, 2018. **174**(4): p. 999-1014 e22.

127. Ben Haim, L. and D.H. Rowitch, *Functional diversity of astrocytes in neural circuit regulation.* Nat Rev Neurosci, 2017. **18**(1): p. 31-41.

128. Arranz, A.M. and B. De Strooper, *The role of astroglia in Alzheimer's disease: pathophysiology and clinical implications.* Lancet Neurol, 2019. **18**(4): p. 406-414.

129. Lundgaard, I., et al., *White matter astrocytes in health and disease.* Neuroscience, 2014. **276**: p. 161-73.

130. Meyer-Franke, A., S. Shen, and B.A. Barres, *Astrocytes Induce Oligodendrocyte Processes to Align with and Adhere to Axons.* Molecular and Cellular Neuroscience, 1999. **14**: p. 385-397.

131. Liedtke, W. and e. al., *GFAP Is Necessary for the Integrity of CNS White Matter Architecture and Long-Term Maintenance of Myelination.* Neuron, 1996. **17**: p. 607-615.

132. Jiang, P., et al., *Human iPSC-Derived Immature Astroglia Promote Oligodendrogenesis by Increasing TIMP-1 Secretion.* Cell Reports, 2016. **15**(6): p. 1303-1315.

133. Nash, B., et al., *Functional Duality of Astrocytes in Myelination.* Journal of Neuroscience, 2011. **31**(37): p. 13028-13038.

134. Modi, K.K., M. Sendtner, and K. Pahan, *Up-regulation of ciliary neurotrophic factor in astrocytes by aspirin: implications for remyelination in multiple sclerosis.* J Biol Chem, 2013. **288**(25): p. 18533-45.

135. Stankoff, B. and e. al., *Ciliary Neurotrophic Factor (CNTF) Enhances Myelin Formation: A Novel Role for CNTF and CNTF-Related Molecules.* The Journal of Neuroscience, 2002. **22**(21): p. 9221-9227.

136. Camargo, N., et al., *Oligodendroglial myelination requires astrocyte-derived lipids.* PLoS Biol, 2017. **15**(5): p. e1002605.

137. Padovani-Claudio, D.A., et al., *Alterations in the oligodendrocyte lineage, myelin, and white matter in adult mice lacking the chemokine receptor CXCR2.* Glia, 2006. **54**(5): p. 471-83.

138. Serwanski, D.R., P. Jukkola, and A. Nishiyama, *Heterogeneity of astrocyte and NG2 cell insertion at the node of ranvier.* J Comp Neurol, 2017. **525**(3): p. 535-552.

139. Dutta, D.J., et al., *Regulation of myelin structure and conduction velocity by perinodal astrocytes.* Proc Natl Acad Sci U S A, 2018. **115**(46): p. 11832-11837.

140. Rash, J.E., *Molecular disruptions of the panglial syncytium block potassium siphoning and axonal saltatory conduction: pertinence to neuromyelitis optica and other demyelinating diseases of the central nervous system.* Neuroscience, 2010. **168**(4): p. 982-1008.

141. Niu, J., et al., *Connexin-based channels contribute to metabolic pathways in the oligodendroglial lineage.* J Cell Sci, 2016. **129**(9): p. 1902-14.

142. Orthmann-Murphy, J.L., C.K. Abrams, and S.S. Scherer, *Gap junctions couple astrocytes and oligodendrocytes.* J Mol Neurosci, 2008. **35**(1): p. 101-16.

143. Tress, O. and e. al., *Panglial Gap Junctional Communication is Essential for Maintenance ofMyelin in the CNS.* The Journal of Neuroscience, 2012. **32**(22): p. 7499-7518.

144. Biancheri, R., et al., *Expanded spectrum of Pelizaeus–Merzbacher-like disease: literature revision and description of a novel GJC2 mutation in an unusually severe form.* European Journal of Human Genetics, 2012. **21**(1): p. 34-39.

145. Orthmann-Murphy, J.L., et al., *Loss-of-function GJA12/Connexin47 mutations cause Pelizaeus-Merzbacher-like disease.* Mol Cell Neurosci, 2007. **34**(4): p. 629-41.

146. van der Knaap, M.S. and M. Bugiani, *Leukodystrophies: a proposed classification system based on pathological changes and pathogenetic mechanisms.* Acta Neuropathol, 2017. **134**(3): p. 351-382.

147. Lanciotti, A., et al., *Astrocytes: Emerging Stars in Leukodystrophy Pathogenesis.* Transl Neurosci, 2013. **4**(2).

148. Olivera-Bravo, S., et al., *Astrocyte Dysfunction in Developmental Neurometabolic Diseases.* Adv Exp Med Biol, 2016. **949**: p. 227-243.

149. Bu, B., et al., *Deregulation of cdk5, Hyperphosphorylation, and Cytoskeletal Pathology in the Niemann–Pick Type C Murine Model.* The Journal of Neuroscience, 2002. **22**(15): p. 6515-6525.

150. Zhang, M. and e. al., *Astrocyte-Only Npc1 Reduces Neuronal Cholesterol and Triples Life Span of Npc1−/−Mice.* J Neurosci Res, 2008. **86**(13): p. 2848-2856.

151. Jitrapakdee, S., et al., *Structure, mechanism and regulation of pyruvate carboxylase.* Biochem J, 2008. **413**(3): p. 369-87.

152. Coci, E.G., et al., *Pyruvate carboxylase deficiency type A and type C: Characterization of five novel pathogenic variants in PC and analysis of the genotype-phenotype correlation.* Hum Mutat, 2019. **40**(6): p. 816-827.

153. Marin-Valencia, I., C.R. Roe, and J.M. Pascual, *Pyruvate carboxylase deficiency: Mechanisms, mimics and anaplerosis.* Molecular Genetics and Metabolism, 2010. **101**(1): p. 9-17.

154. Nobuta, H., et al., *STAT3-mediated astrogliosis protects myelin development in neonatal brain injury.* Ann Neurol, 2012. **72**(5): p. 750-65.

155. Yoon, H., et al., *Astrocyte heterogeneity across the brain and spinal cord occurs developmentally, in adulthood and in response to demyelination.* PLoS One, 2017. **12**(7): p. e0180697.

156. Fasciani, I., et al., *Directional coupling of oligodendrocyte connexin-47 and astrocyte connexin-43 gap junctions.* Glia, 2018. **66**(11): p. 2340-2352.

157. Dooves, S., et al., *Cell Replacement Therapy Improves Pathological Hallmarks in a Mouse Model of Leukodystrophy Vanishing White Matter.* Stem Cell Reports, 2019. **12**(3): p. 441-450.

158. Varela-Echevarría, A., Vargas-Barroso, V., Lozano-Flores, C. and Larriva-Sahd, J., *Is There Evidence for Myelin Modeling by Astrocytes in the Normal Adult Brain?* Frontiers in Neuroanatomy, 2017. **11**(75): p. 23.

159. Sofroniew, M.V., *Molecular dissection of reactive astrogliosis and glial scar formation.* Trends Neurosci, 2009. **32**(12): p. 638-47.

160. Middeldorp, J. and E.M. Hol, *GFAP in health and disease.* Prog Neurobiol, 2011. **93**(3): p. 421-43.

161. Zamanian, J.L., et al., *Genomic Analysis of Reactive Astrogliosis.* Journal of Neuroscience, 2012. **32**(18): p. 6391-6410.

162. Liddelow, S.A., et al., *Neurotoxic reactive astrocytes are induced by activated microglia.* Nature, 2017. **541**(7638): p. 481-487.

163. Shinozaki, Y., et al., *Transformation of Astrocytes to a Neuroprotective Phenotype by Microglia via P2Y1 Receptor Downregulation.* Cell Rep, 2017. **19**(6): p. 1151-1164.

164. Fan, H., et al., *Reactive astrocytes undergo M1 microglia/macrohpages-induced necroptosis in spinal cord injury.* Mol Neurodegener, 2016. **11**: p. 14.

165. Quintas, C., et al., *Microglia P2Y(6) receptors mediate nitric oxide release and astrocyte apoptosis.* J Neuroinflammation, 2014. **11**: p. 141.

166. Franklin, R.J., A.J. Crang, and W.F. Blakemore, *Transplanted type-1 astrocytes facilitate repair of demyelinating lesions by host oligodendrocytes in adult rat spinal cord.* J Neurocytol, 1991. **20**(5): p. 420-30.

167. Albrecht, P.J., et al., *Astrocytes produce CNTF during the remyelination phase of viral-induced spinal cord demyelination to stimulate FGF-2 production.* Neurobiology of Disease, 2003. **13**(2): p. 89-101.

168. Selvaraju, R., et al., *Osteopontin is upregulated during in vivo demyelination and remyelination and enhances myelin formation in vitro.* Mol Cell Neurosci, 2004. **25**(4): p. 707-21.

169. Itoh, N., et al., *Cell-specific and region-specific transcriptomics in the multiple sclerosis model: Focus on astrocytes.* Proceedings of the National Academy of Sciences, 2018. **115**(2): p. E302-E309.

170. Zhang, J. and Q. Liu, *Cholesterol metabolism and homeostasis in the brain.* Protein Cell, 2015. **6**(4): p. 254-64.

171. Berghoff, S.A., et al., *Dietary cholesterol promotes repair of demyelinated lesions in the adult brain.* Nat Commun, 2017. **8**: p. 14241.

172. Kamizato, K., et al., *The role of fatty acid binding protein 7 in spinal cord astrocytes in a mouse model of experimental autoimmune encephalomyelitis.* Neuroscience, 2019. **409**: p. 120-129.

173. Robinson, S. and R.H. Miller, *Contact with central nervous system myelin inhibits oligodendrocyte progenitor maturation.* Dev Biol, 1999. **216**(1): p. 359-68.

174. Kotter, M.R., et al., *Myelin impairs CNS remyelination by inhibiting oligodendrocyte precursor cell differentiation.* J Neurosci, 2006. **26**(1): p. 328-32.

175. Kramann, N., et al., *Glial fibrillary acidic protein expression alters astrocytic chemokine release and protects mice from cuprizone-induced demyelination.* Glia, 2019. **67**(7): p. 1308-1319.

176. Madadi, S., et al., *Astrocyte ablation induced by La-aminoadipate (L-AAA) potentiates remyelination in a cuprizone demyelinating mouse model.* Metab Brain Dis, 2019. **34**(2): p. 593-603.

177. Kamermans, A., et al., *Reduced Angiopoietin-Like 4 Expression in Multiple Sclerosis Lesions Facilitates Lipid Uptake by Phagocytes via Modulation of Lipoprotein-Lipase Activity.* Front Immunol, 2019. **10**: p. 950.

178. Blakemore, W.F., J.M. Gilson, and A.J. Crang, *The presence of astrocytes in areas of demyelination influences remyelination following transplantation of oligodendrocyte progenitors.* Experimental Neurology, 2003. **184**(2): p. 955-963.

179. Hammond, T.R., et al., *Astrocyte-derived endothelin-1 inhibits remyelination through notch activation.* Neuron, 2014. **81**(3): p. 588-602.

180. Rothhammer, V., et al., *Microglial control of astrocytes in response to microbial metabolites.* Nature, 2018. **557**(7707): p. 724-728.

181. Li, J., et al., *Tumor necrosis factor alpha mediates lipopolysaccharide-induced microglial toxicity to developing oligodendrocytes when astrocytes are present.* J Neurosci, 2008. **28**(20): p. 5321-30.

182. Wetzels, S., et al., *Methylglyoxal-Derived Advanced Glycation Endproducts Accumulate in Multiple Sclerosis Lesions.* Frontiers in Immunology, 2019. **10**.

183. Mayo, L., et al., *Regulation of astrocyte activation by glycolipids drives chronic CNS inflammation.* Nature Medicine, 2014. **20**(10): p. 1147-1156.

184. Eilam, R., et al., *Astrocyte disruption of neurovascular communication is linked to cortical damage in an animal model of multiple sclerosis.* Glia, 2018. **66**(5): p. 1098-1117.

185. Kim, R.Y., et al., *Astrocyte CCL2 sustains immune cell infiltration in chronic experimental autoimmune encephalomyelitis.* Journal of Neuroimmunology, 2014. **274**(1-2): p. 53-61.

186. Kang, Z., et al., *Astrocyte-Restricted Ablation of Interleukin-17-Induced Act1-Mediated Signaling Ameliorates Autoimmune Encephalomyelitis.* Immunity, 2010. **32**(3): p. 414-425.

187. Waisman, A. and L. Johann, *Antigen-presenting cell diversity for T cell reactivation in central nervous system autoimmunity.* J Mol Med (Berl), 2018. **96**(12): p. 1279-1292.

188. Gimenez, M.A., J.E. Sim, and J.H. Russell, *TNFR1-dependent VCAM-1 expression by astrocytes exposes the CNS to destructive inflammation.* J Neuroimmunol, 2004. **151**(1-2): p. 116-25.

189. Ulivieri, C., et al., *A T Cell Suppressive Circuitry Mediated by CD39 and Regulated by ShcC/Rai Is Induced in Astrocytes by Encephalitogenic T Cells.* Front Immunol, 2019. **10**: p. 1041.

190. Brambilla, R., et al., *Astrocytes play a key role in EAE pathophysiology by orchestrating in the CNS the inflammatory response of resident and peripheral immune cells and by suppressing remyelination.* Glia, 2014. **62**(3): p. 452-67.

191. Claycomb, K.I., et al., *Astrocyte regulation of CNS inflammation and remyelination.* Brain Sci, 2013. **3**(3): p. 1109-27.

192. Ponath, G., et al., *Myelin phagocytosis by astrocytes after myelin damage promotes lesion pathology.* Brain, 2017. **140**(2): p. 399-413.

193. Galloway, D.A., et al., *Phagocytosis in the Brain: Homeostasis and Disease.* Front Immunol, 2019. **10**: p. 790.

194. Ponath, G., C. Park, and D. Pitt, *The Role of Astrocytes in Multiple Sclerosis.* Frontiers in Immunology, 2018. **9**.

195. Anderson, M.A., et al., *Astrocyte scar formation aids central nervous system axon regeneration.* Nature, 2016. **532**(7598): p. 195-200.

196. Haindl, M.T., et al., *The formation of a glial scar does not prohibit remyelination in an animal model of multiple sclerosis.* Glia, 2019. **67**(3): p. 467-481.

197. Toft-Hansen, H., L. Fuchtbauer, and T. Owens, *Inhibition of reactive astrocytosis in established experimental autoimmune encephalomyelitis favors infiltration by myeloid cells over T cells and enhances severity of disease.* Glia, 2011. **59**(1): p. 166-76.

198. Bannerman, P., et al., *Astrogliosis in EAE spinal cord: Derivation from radial glia, and relationships to oligodendroglia.* Glia, 2007. **55**(1): p. 57-64.

199. Waller, R., et al., *Gene expression profiling of the astrocyte transcriptome in multiple sclerosis normal appearing white matter reveals a neuroprotective role.* J Neuroimmunol, 2016. **299**: p. 139-146.

200. Ahmed, S.M., et al., *Nrf2 signaling pathway: Pivotal roles in inflammation.* Biochim Biophys Acta Mol Basis Dis, 2017. **1863**(2): p. 585-597.

201. Vargas, M.R. and J.A. Johnson, *The Nrf2-ARE cytoprotective pathway in astrocytes.* Expert Rev Mol Med, 2009. **11**: p. e17.

202. Liddell, J.R., *Are Astrocytes the Predominant Cell Type for Activation of Nrf2 in Aging and Neurodegeneration?* Antioxidants (Basel), 2017. **6**(3).

203. Licht-Mayer, S., et al., *Cell type-specific Nrf2 expression in multiple sclerosis lesions.* Acta Neuropathol, 2015. **130**(2): p. 263-77.

204. Kleopa, K.A., I. Sargiannidou, and K. Markoullis, *Connexin pathology in chronic multiple sclerosis and experimental autoimmune encephalomyelitis.* Clinical and Experimental Neuroimmunology, 2013. **4**: p. 45-58.

205. Masaki, K., et al., *Connexin 43 astrocytopathy linked to rapidly progressive multiple sclerosis and neuromyelitis optica.* PLoS One, 2013. **8**(8): p. e72919.

206. Stoffels, J.M.J., et al., *Fibronectin aggregation in multiple sclerosis lesions impairs remyelination.* Brain, 2013. **136**(1): p. 116-131.

207. Harlow, D.E. and W.B. Macklin, *Inhibitors of myelination: ECM changes, CSPGs and PTPs.* Exp Neurol, 2014. **251**: p. 39-46.

208. Sloane, J.A., et al., *Hyaluronan blocks oligodendrocyte progenitor maturation and remyelination through TLR2.* Proc Natl Acad Sci U S A, 2010. **107**(25): p. 11555-60.

209. Bugiani, M., et al., *Hyaluronan accumulation and arrested oligodendrocyte progenitor maturation in vanishing white matter disease.* Brain, 2013. **136**(Pt 1): p. 209-22.

210. Gomes, W.A., M.F. Mehler, and J.A. Kessler, *Transgenic overexpression of BMP4 increases astroglial and decreases oligodendroglial lineage commitment.* Developmental Biology, 2003. **255**(1): p. 164-177.

211. Sabo, J.K., et al., *Remyelination is altered by bone morphogenic protein signaling in demyelinated lesions.* J Neurosci, 2011. **31**(12): p. 4504-10.

212. Harnisch, K., et al., *Myelination in Multiple Sclerosis Lesions Is Associated with Regulation of Bone Morphogenetic Protein 4 and Its Antagonist Noggin.* Int J Mol Sci, 2019. **20**(1).

213. Nataf, S., M. Barritault, and L. Pays, *A Unique TGFB1-Driven Genomic Program Links Astrocytosis, Low-Grade Inflammation and Partial Demyelination in Spinal Cord Periplaques from Progressive Multiple Sclerosis Patients.* International Journal of Molecular Sciences, 2017. **18**(10).

214. Elkjaer, M.L., et al., *Molecular signature of different lesion types in the brain white matter of patients with progressive multiple sclerosis.* Acta Neuropathol Commun, 2019. **7**(1): p. 205.

215. Canto, E., et al., *Chitinase 3-like 1 plasma levels are increased in patients with progressive forms of multiple sclerosis.* Mult Scler, 2012. **18**(7): p. 983-90.

216. Kassubek, R., et al., *GFAP in early multiple sclerosis: A biomarker for inflammation.* Neurosci Lett, 2017. **657**: p. 166-170.

217. Mane-Martinez, M.A., et al., *Glial and neuronal markers in cerebrospinal fluid in different types of multiple sclerosis.* J Neuroimmunol, 2016. **299**: p. 112-117.

218. Vargas, M.R., et al., *Nrf2 activation in astrocytes protects against neurodegeneration in mouse models of familial amyotrophic lateral sclerosis.* J Neurosci, 2008. **28**(50): p. 13574-81.

219. Franklin, K.B.J., *The mouse brain in stereotaxic coordinates*, ed. G. Paxinos. 1997, San Diego London: San DiegoLondon : Academic Press.

220. Heiman, M., et al., *Cell type-specific mRNA purification by translating ribosome affinity purification (TRAP).* Nat Protoc, 2014. **9**(6): p. 1282-91.

221. Cunningham, F., et al., *Ensembl 2019.* Nucleic Acids Res, 2019. **47**(D1): p. D745-d751.

222. Dobin, A., et al., *STAR: ultrafast universal RNA-seq aligner.* Bioinformatics, 2013. **29**(1): p. 15-21.

223. Liao, Y., G.K. Smyth, and W. Shi, *featureCounts: an efficient general purpose program for assigning sequence reads to genomic features.* Bioinformatics, 2014. **30**(7): p. 923-30.

224. Love, M.I., W. Huber, and S. Anders, *Moderated estimation of fold change and dispersion for RNA-seq data with DESeq2.* Genome Biol, 2014. **15**(12): p. 550.

225. Theocharidis, A., et al., *Network visualization and analysis of gene expression data using BioLayout Express(3D).* Nat Protoc, 2009. **4**(10): p. 1535-50.

226. Pekny, M. and M. Pekna, *Astrocyte Reactivity and Reactive Astrogliosis: Costs and Benefits.* Physiological Reviews, 2014. **94**(4): p. 1077-1098.

227. Crocker, S.J., et al., *Persistent macrophage/microglial activation and myelin disruption after experimental autoimmune encephalomyelitis in tissue inhibitor of metalloproteinase-1-deficient mice.* Am J Pathol, 2006. **169**(6): p. 2104-16.

228. Laug, D., et al., *Nuclear factor I-A regulates diverse reactive astrocyte responses after CNS injury.* J Clin Invest, 2019. **129**(10): p. 4408-4418.

229. Gudi, V., et al., *Glial response during cuprizone-induced de- and remyelination in the CNS: lessons learned.* Frontiers in Cellular Neuroscience, 2014. **8**.

230. Matsushima, G.K. and P. Morell, *The neurotoxicant, cuprizone, as a model to study demyelination and remyelination in the central nervous system.* Brain Pathol, 2001. **11**(1): p. 107-16.

231. Hesse, A., et al., *In toxic demyelination oligodendroglial cell death occurs early and is FAS independent.* Neurobiol Dis, 2010. **37**(2): p. 362-9.

232. Albrecht, S., et al., *Recovery from Toxic-Induced Demyelination Does Not Require the NG2 Proteoglycan.* PLoS One, 2016. **11**(10): p. e0163841.

233. Morizawa, Y.M., et al., *Reactive astrocytes function as phagocytes after brain ischemia via ABCA1-mediated pathway.* Nat Commun, 2017. **8**(1): p. 28.

234. Monteiro de Castro, G., et al., *Astrocyte Activation via Stat3 Signaling Determines the Balance of Oligodendrocyte versus Schwann Cell Remyelination.* The American Journal of Pathology, 2015. **185**(9): p. 2431-2440.

235. Liedtke, W., et al., *GFAP is necessary for the integrity of CNS white matter architecture and long-term maintenance of myelination.* Neuron, 1996. **17**(4): p. 607-15.

236. Black, J.A., J. Newcombe, and S.G. Waxman, *Astrocytes within multiple sclerosis lesions upregulate sodium channel Nav1.5.* Brain, 2010. **133**(Pt 3): p. 835-46.

237. Holley, J.E., et al., *Astrocyte characterization in the multiple sclerosis glial scar.* Neuropathol Appl Neurobiol, 2003. **29**(5): p. 434-44.

238. Shin, T.K., Y.D. Lee, and K.B. Sim, *Embryonic intermediate filaments, nestin and vimentin, expression in the spinal cords of rats with experimental autoimmune encephalomyelitis.* J Vet Sci, 2003. **4**(1): p. 9-13.

239. Kipp, M., et al., *The cuprizone animal model: new insights into an old story.* Acta Neuropathol, 2009. **118**(6): p. 723-36.

240. Hibbits, N., et al., *Astrogliosis during acute and chronic cuprizone demyelination and implications for remyelination.* ASN Neuro, 2012. **4**(6): p. 393-408.

241. Patteson, A.E., et al., *Vimentin protects cells against nuclear rupture and DNA damage during migration.* J Cell Biol, 2019. **218**(12): p. 4079-4092.

242. Plemel, J.R., et al., *Mechanisms of lysophosphatidylcholine-induced demyelination: A primary lipid disrupting myelinopathy.* Glia, 2018. **66**(2): p. 327-347.

243. Miller, A.P., et al., *Acute death of astrocytes in blast-exposed rat organotypic hippocampal slice cultures.* PLoS One, 2017. **12**(3): p. e0173167.

244. Lloyd, A.F., et al., *Central nervous system regeneration is driven by microglia necroptosis and repopulation.* Nat Neurosci, 2019. **22**(7): p. 1046-1052.

245. Bardehle, S., et al., *Live imaging of astrocyte responses to acute injury reveals selective juxtavascular proliferation.* Nat Neurosci, 2013. **16**(5): p. 580-6.

246. Götz, M., et al., *Reactive astrocytes as neural stem or progenitor cells: In vivo lineage, In vitro potential, and Genome-wide expression analysis.* Glia, 2015. **63**(8): p. 1452-1468.

247. Clarke, L.E., et al., *Normal aging induces A1-like astrocyte reactivity.* Proc Natl Acad Sci U S A, 2018. **115**(8): p. E1896-E1905.

248. Boisvert, M.M., et al., *The Aging Astrocyte Transcriptome from Multiple Regions of the Mouse Brain.* Cell Rep, 2018. **22**(1): p. 269-285.

249. Diaz-Castro, B., et al., *Astrocyte molecular signatures in Huntington's disease.* Sci Transl Med, 2019. **11**(514).

250. Jung, J. and H. Jung, *Methods to analyze cell type-specific gene expression profiles from heterogeneous cell populations.* Animal Cells and Systems, 2016. **20**(3): p. 113-117.

251. Hu, P., et al., *Single Cell Isolation and Analysis.* Front Cell Dev Biol, 2016. **4**: p. 116.

252. Schneider-Poetsch, T., et al., *Inhibition of eukaryotic translation elongation by cycloheximide and lactimidomycin.* Nat Chem Biol, 2010. **6**(3): p. 209-217.

253. Haimon, Z., et al., *Re-evaluating microglia expression profiles using RiboTag and cell isolation strategies.* Nat Immunol, 2018. **19**(6): p. 636-644.

254. Cooper, G.M., *The cell: A Molecular Approach*. 2nd ed. Translation of mRNA. 2000, Sunderland: Sinauer Associates.

255. Sanz, E., et al., *RiboTag: Ribosomal Tagging Strategy to Analyze Cell-Type-Specific mRNA Expression In Vivo.* Curr Protoc Neurosci, 2019. **88**(1): p. e77.

256. Shi, Z., et al., *Heterogeneous Ribosomes Preferentially Translate Distinct Subpools of mRNAs Genome-wide.* Mol Cell, 2017. **67**(1): p. 71-83 e7.

257. Freeman, T.C., et al., *Construction, visualisation, and clustering of transcription networks from microarray expression data.* PLoS Comput Biol, 2007. **3**(10): p. 2032-42.

258. Gardner, J. and A. Ghorpade, *Tissue inhibitor of metalloproteinase (TIMP)-1: the TIMPed balance of matrix metalloproteinases in the central nervous system.* J Neurosci Res, 2003. **74**(6): p. 801-6.

259. Thorne, M., C.S. Moore, and G.S. Robertson, *Lack of TIMP-1 increases severity of experimental autoimmune encephalomyelitis: Effects of darbepoetin alfa on TIMP-1 null and wild-type mice.* J Neuroimmunol, 2009. **211**(1-2): p. 92-100.

260. Moore, C.S., et al., *Astrocytic tissue inhibitor of metalloproteinase-1 (TIMP-1) promotes oligodendrocyte differentiation and enhances CNS myelination.* J Neurosci, 2011. **31**(16): p. 6247-54.

261. Hoyos, H.C., et al., *Galectin-3 controls the response of microglial cells to limit cuprizone-induced demyelination.* Neurobiol Dis, 2014. **62**: p. 441-55.

262. Rinaldi, M., et al., *Galectin-1 circumvents lysolecithin-induced demyelination through the modulation of microglial polarization/phagocytosis and oligodendroglial differentiation.* Neurobiol Dis, 2016. **96**: p. 127-143.

263. Morita, M., et al., *Very long chain fatty acid beta-oxidation in astrocytes: contribution of the ABCD1-dependent and -independent pathways.* Biol Pharm Bull, 2012. **35**(11): p. 1972-9.

264. Williams, A., et al., *Semaphorin 3A and 3F: key players in myelin repair in multiple sclerosis?* Brain, 2007. **130**(Pt 10): p. 2554-65.

265. Tonelli, C., I.I.C. Chio, and D.A. Tuveson, *Transcriptional Regulation by Nrf2.* Antioxid Redox Signal, 2018. **29**(17): p. 1727-1745.

266. Baxter, P.S. and G.E. Hardingham, *Adaptive regulation of the brain's antioxidant defences by neurons and astrocytes.* Free Radic Biol Med, 2016. **100**: p. 147-152.

267. Morell, P., et al., *Gene expression in brain during cuprizone-induced demyelination and remyelination.* Mol Cell Neurosci, 1998. **12**(4-5): p. 220-7.

268. Vance, J.E., *Dysregulation of cholesterol balance in the brain: contribution to neurodegenerative diseases.* Dis Model Mech, 2012. **5**(6): p. 746-55.

269. Petrov, A.M., M.R. Kasimov, and A.L. Zefirov, *Brain Cholesterol Metabolism and Its Defects: Linkage to Neurodegenerative Diseases and Synaptic Dysfunction.* Acta Naturae, 2016. **8**(1): p. 58-73.

270. Saher, G., et al., *High cholesterol level is essential for myelin membrane growth.* Nat Neurosci, 2005. **8**(4): p. 468-75.

271. Gonzalez Cardona, J., et al., *Quetiapine has an additive effect to triiodothyronine in inducing differentiation of oligodendrocyte precursor cells through induction of cholesterol biosynthesis.* PLoS One, 2019. **14**(9): p. e0221747.

272. Hubler, Z., et al., *Accumulation of 8,9-unsaturated sterols drives oligodendrocyte formation and remyelination.* Nature, 2018. **560**(7718): p. 372-376.

273. Suryadevara, R., et al., *Regulation of tissue inhibitor of metalloproteinase-1 by astrocytes: links to HIV-1 dementia.* Glia, 2003. **44**(1): p. 47-56.

274. Sirko, S., et al., *Astrocyte reactivity after brain injury-: The role of galectins 1 and 3.* Glia, 2015. **63**(12): p. 2340-61.

275. Miron, V.E., et al., *Fingolimod (FTY720) enhances remyelination following demyelination of organotypic cerebellar slices.* Am J Pathol, 2010. **176**(6): p. 2682-94.

276. Fischer, M.T., et al., *Disease-specific molecular events in cortical multiple sclerosis lesions.* Brain, 2013. **136**(Pt 6): p. 1799-815.

277. Fischer, I., et al., *Sphingosine kinase 1 and sphingosine 1-phosphate receptor 3 are functionally upregulated on astrocytes under pro-inflammatory conditions.* PLoS One, 2011. **6**(8): p. e23905.

278. Baer, A., W. Colon-Moran, and N. Bhattarai, *Characterization of the effects of immunomodulatory drug fingolimod (FTY720) on human T cell receptor signaling pathways.* Sci Rep, 2018. **8**(1): p. 10910.

279. Hoffmann, F.S., et al., *Fingolimod induces neuroprotective factors in human astrocytes.* J Neuroinflammation, 2015. **12**: p. 184.

280. Rothhammer, V., et al., *Sphingosine 1-phosphate receptor modulation suppresses pathogenic astrocyte activation and chronic progressive CNS inflammation.* Proc Natl Acad Sci U S A, 2017. **114**(8): p. 2012-2017.

281. Grabacka, M., et al., *Regulation of Ketone Body Metabolism and the Role of PPARalpha.* Int J Mol Sci, 2016. **17**(12).

282. Teh, D.B.L., et al., *Transcriptome Analysis Reveals Neuroprotective aspects of Human Reactive Astrocytes induced by Interleukin 1β.* Scientific Reports, 2017. **7**(1).

283. Ezan, P., et al., *Deletion of astroglial connexins weakens the blood-brain barrier.* J Cereb Blood Flow Metab, 2012. **32**(8): p. 1457-67.

284. Quintana, F.J., *Astrocytes to the rescue! Glia limitans astrocytic endfeet control CNS inflammation.* J Clin Invest, 2017. **127**(8): p. 2897-2899.

285. Muramatsu, R., et al., *Prostacyclin prevents pericyte loss and demyelination induced by lysophosphatidylcholine in the central nervous system.* J Biol Chem, 2015. **290**(18): p. 11515-25.

286. Kubotera, H., et al., *Astrocytic endfeet re-cover blood vessels after removal by laser ablation.* Sci Rep, 2019. **9**(1): p. 1263.

287. Ikeshima-Kataoka, H. and M. Yasui, *Correlation between astrocyte activity and recovery from blood-brain barrier breakdown caused by brain injury.* Neuroreport, 2016. **27**(12): p. 894-900.

288. Hartmann, K., et al., *Complement 3+-astrocytes are highly abundant in prion diseases, but their abolishment led to an accelerated disease course and early dysregulation of microglia.* Acta Neuropathologica Communications, 2019. **7**(1).

289. Roy-O'Reilly, M. and L.D. McCullough, *Astrocytes fuel the fire of lymphocyte toxicity after stroke.* Proc Natl Acad Sci U S A, 2017. **114**(3): p. 425-427.

290. Garg, S.K., R. Banerjee, and J. Kipnis, *Neuroprotective immunity: T cell-derived glutamate endows astrocytes with a neuroprotective phenotype.* J Immunol, 2008. **180**(6): p. 3866-73.

291. Lassmann, H. and J. van Horssen, *Oxidative stress and its impact on neurons and glia in multiple sclerosis lesions.* Biochim Biophys Acta, 2016. **1862**(3): p. 506-10.

292. Katsuoka, F. and M. Yamamoto, *Small Maf proteins (MafF, MafG, MafK): History, structure and function.* Gene, 2016. **586**(2): p. 197-205.

293. Anchisi, L., et al., *Cholesterol homeostasis: a key to prevent or slow down neurodegeneration.* Front Physiol, 2012. **3**: p. 486.

294. Schmitt, S., L.C. Castelvetri, and M. Simons, *Metabolism and functions of lipids in myelin.* Biochim Biophys Acta, 2015. **1851**(8): p. 999-1005.

295. Saher, G. and S.K. Stumpf, *Cholesterol in myelin biogenesis and hypomyelinating disorders.* Biochim Biophys Acta, 2015. **1851**(8): p. 1083-94.

296. Cantuti-Castelvetri, L., et al., *Defective cholesterol clearance limits remyelination in the aged central nervous system.* Science, 2018. **359**(6376): p. 684-688.

297. Wheeler, M.A., et al., *MAFG-driven astrocytes promote CNS inflammation.* Nature, 2020. **578**(7796): p. 593-599.

298. Kitteringham, N.R., et al., *Proteomic analysis of Nrf2 deficient transgenic mice reveals cellular defence and lipid metabolism as primary Nrf2-dependent pathways in the liver.* J Proteomics, 2010. **73**(8): p. 1612-31.

299. Tanaka, Y., et al., *NF-E2-related factor 2 inhibits lipid accumulation and oxidative stress in mice fed a high-fat diet.* J Pharmacol Exp Ther, 2008. **325**(2): p. 655-64.

300. Zhang, Y.K., et al., *Enhanced expression of Nrf2 in mice attenuates the fatty liver produced by a methionine- and choline-deficient diet.* Toxicol Appl Pharmacol, 2010. **245**(3): p. 326-34.

301. Huang, J., et al., *Transcription factor Nrf2 regulates SHP and lipogenic gene expression in hepatic lipid metabolism.* Am J Physiol Gastrointest Liver Physiol, 2010. **299**(6): p. G1211-21.

302. Dodson, M., R. Castro-Portuguez, and D.D. Zhang, *NRF2 plays a critical role in mitigating lipid peroxidation and ferroptosis.* Redox Biol, 2019: p. 101107.

303. Yates, M.S., et al., *Genetic versus chemoprotective activation of Nrf2 signaling: overlapping yet distinct gene expression profiles between Keap1 knockout and triterpenoid-treated mice.* Carcinogenesis, 2009. **30**(6): p. 1024-31.

304. Shin, S., et al., *Role of Nrf2 in prevention of high-fat diet-induced obesity by synthetic triterpenoid CDDO-imidazolide.* Eur J Pharmacol, 2009. **620**(1-3): p. 138-44.

305. Sugimoto, H., et al., *Deletion of nuclear factor-E2-related factor-2 leads to rapid onset and progression of nutritional steatohepatitis in mice.* Am J Physiol Gastrointest Liver Physiol, 2010. **298**(2): p. G283-94.

306. Zhao, X.J., et al., *Polydatin prevents fructose-induced liver inflammation and lipid deposition through increasing miR-200a to regulate Keap1/Nrf2 pathway.* Redox Biol, 2018. **18**: p. 124-137.

307. Wood, E.J., *Medical biochemistry (4th ed.): Bhagavan, N. V.* Biochemistry and Molecular Biology Education, 2002. **30**(5): p. 270-271.

308. Shin, S., et al., *NRF2 modulates aryl hydrocarbon receptor signaling: influence on adipogenesis.* Mol Cell Biol, 2007. **27**(20): p. 7188-97.

309. Song, S.Y., et al., *Expression of an acyl-CoA synthetase, lipidosin, in astrocytes of the murine brain and its up-regulation during remyelination following cuprizone-induced demyelination.* J Neurosci Res, 2007. **85**(16): p. 3586-97.

310. Bugiani, M., et al., *Defective glial maturation in vanishing white matter disease.* J Neuropathol Exp Neurol, 2011. **70**(1): p. 69-82.

311. Sim, F.J., et al., *The age-related decrease in CNS remyelination efficiency is attributable to an impairment of both oligodendrocyte progenitor recruitment and differentiation.* J Neurosci, 2002. **22**(7): p. 2451-9.

312. Neumann, B., et al., *Remyelination and ageing: Reversing the ravages of time.* Multiple Sclerosis Journal, 2019. **25**(14): p. 1835-1841.

313. Lee, J.M., et al., *Identification of the NF-E2-related factor-2-dependent genes conferring protection against oxidative stress in primary cortical astrocytes using oligonucleotide microarray analysis.* J Biol Chem, 2003. **278**(14): p. 12029-38.

314. Kraft, A.D., D.A. Johnson, and J.A. Johnson, *Nuclear factor E2-related factor 2-dependent antioxidant response element activation by tert-butylhydroquinone and sulforaphane occurring preferentially in astrocytes conditions neurons against oxidative insult.* J Neurosci, 2004. **24**(5): p. 1101-12.

315. Nellessen, A., et al., *Nrf2 deficiency increases oligodendrocyte loss, demyelination, neuroinflammation and axonal damage in an MS animal model.* Metab Brain Dis, 2019.

316. Johnson, D.A., et al., *The absence of the pro-antioxidant transcription factor Nrf2 exacerbates experimental autoimmune encephalomyelitis.* Toxicol Sci, 2010. **114**(2): p. 237-46.

317. Schilling, S., et al., *Fumaric acid esters are effective in chronic experimental autoimmune encephalomyelitis and suppress macrophage infiltration.* Clin Exp Immunol, 2006. **145**(1): p. 101-7.

318. Piroli, G.G., Manuel, A.M., Patel, T., Walla, M.D., Shi, L., Lanci, S.A., Wang, J., Galloway, A., Ortinski, P.I., Smith, D.S., and Frizzell, N., *Identification of Novel Protein Targets of Dimethyl Fumarate Modification in Neurons and Astrocytes Reveals Actions Independent of Nrf2 Stabilization.* Molecular & Cellular Proteomics, 2019. **18**: p. 15.

319. Linker, R.A., et al., *Fumaric acid esters exert neuroprotective effects in neuroinflammation via activation of the Nrf2 antioxidant pathway.* Brain, 2011. **134**(Pt 3): p. 678-92.

320. Cerina, M., et al., *Protective potential of dimethyl fumarate in a mouse model of thalamocortical demyelination.* Brain Struct Funct, 2018. **223**(7): p. 3091-3106.

321. Kasarello, K., et al., *Effect of dimethyl fumarate on heme oxygenase-1 expression in experimental allergic encephalomyelitis in rats.* Folia Neuropathol, 2017. **55**(4): p. 325-332.

322. Moharregh-Khiabani, D., et al., *Effects of fumaric acids on cuprizone induced central nervous system de- and remyelination in the mouse.* PLoS One, 2010. **5**(7): p. e11769.

323. Fowler, J.H., et al., *Dimethyl fumarate improves white matter function following severe hypoperfusion: Involvement of microglia/macrophages and inflammatory mediators.* J Cereb Blood Flow Metab, 2018. **38**(8): p. 1354-1370.

324. Sigfridsson, E., et al., *Astrocyte-specific overexpression of Nrf2 protects against optic tract damage and behavioural alterations in a mouse model of cerebral hypoperfusion.* Sci Rep, 2018. **8**(1): p. 12552.

325. van Horssen, J., et al., *Nrf2 and DJ1 are consistently upregulated in inflammatory multiple sclerosis lesions.* Free Radic Biol Med, 2010. **49**(8): p. 1283-9.

326. Teske, N., et al., *Chemical hypoxia-induced integrated stress response activation in oligodendrocytes is mediated by the transcription factor nuclear factor (erythroid-derived 2)-like 2 (NRF2).* J Neurochem, 2018. **144**(3): p. 285-301.

327. Pakos-Zebrucka, K., et al., *The integrated stress response.* EMBO Rep, 2016. **17**(10): p. 1374-1395.

328. Miron, V.E., et al., *M2 microglia and macrophages drive oligodendrocyte differentiation during CNS remyelination.* Nat Neurosci, 2013. **16**(9): p. 1211-1218.

329. Lampron, A., et al., *Inefficient clearance of myelin debris by microglia impairs remyelinating processes.* J Exp Med, 2015. **212**(4): p. 481-95.

330. Batiuk, M.Y., et al., *An immunoaffinity-based method for isolating ultrapure adult astrocytes based on ATP1B2 targeting by the ACSA-2 antibody.* J Biol Chem, 2017. **292**(21): p. 8874-8891.

331. Miyake, M.M. and B.S. Bleier, *The blood-brain barrier and nasal drug delivery to the central nervous system.* Am J Rhinol Allergy, 2015. **29**(2): p. 124-7.

332. Kumar, P., et al., *Stearic acid based, systematically designed oral lipid nanoparticles for enhanced brain delivery of dimethyl fumarate.* Nanomedicine (Lond), 2017. **12**(23): p. 2607-2621.

333. Shepardson, N.E., G.M. Shankar, and D.J. Selkoe, *Cholesterol level and statin use in Alzheimer disease: II. Review of human trials and recommendations.* Arch Neurol, 2011. **68**(11): p. 1385-92.

334. Honda, A., et al., *Highly sensitive quantification of key regulatory oxysterols in biological samples by LC-ESI-MS/MS.* J Lipid Res, 2009. **50**(2): p. 350-7.

335. Vogeser, M. and K.G. Parhofer, *Liquid chromatography tandem-mass spectrometry (LC-MS/MS)--technique and applications in endocrinology.* Exp Clin Endocrinol Diabetes, 2007. **115**(9): p. 559-70.

336. Wang, H., et al., *RXRalpha inhibits the NRF2-ARE signaling pathway through a direct interaction with the Neh7 domain of NRF2.* Cancer Res, 2013. **73**(10): p. 3097-108.

337. Valenzuela, M., et al., *Retinoic acid synergizes ATO-mediated cytotoxicity by precluding Nrf2 activity in AML cells.* Br J Cancer, 2014. **111**(5): p. 874-82.

338. Zhu, J., et al., *An overview of chemical inhibitors of the Nrf2-ARE signaling pathway and their potential applications in cancer therapy.* Free Radic Biol Med, 2016. **99**: p. 544-556.

339. Mao, P. and P.H. Reddy, *Is multiple sclerosis a mitochondrial disease?* Biochim Biophys Acta, 2010. **1802**(1): p. 66-79.

340. Dunham, J., et al., *Severe oxidative stress in an acute inflammatory demyelinating model in the rhesus monkey.* PLoS One, 2017. **12**(11): p. e0188013.

PUBLICATIONS

- Rojo, R., *et al. Deletion of a Csf1r enhancer selectively impacts CSF1R expression and development of tissue macrophage populations.* Nat Commun, 2019. **10,** 3215 doi:10.1038/s41467-019-11053-8.

- Molina-Gonzalez, I. and V.E. Miron, *Astrocytes in myelination and remyelination.* Neurosci Lett, 2019. **713**: p. 134532 doi.org/10.1016/j.neulet.2019.134532

nature COMMUNICATIONS

ARTICLE

https://doi.org/10.1038/s41467-019-11053-8 OPEN

Deletion of a *Csf1r* enhancer selectively impacts CSF1R expression and development of tissue macrophage populations

Rocío Rojo[1,2], Anna Raper[1], Derya D. Ozdemir[1], Lucas Lefevre[1], Kathleen Grabert[1,3], Evi Wollscheid-Lengeling[1], Barry Bradford[1], Melanie Caruso[1], Iveta Gazova[1], Alejandra Sánchez[1], Zofia M. Lisowski[1], Joana Alves[1], Irene Molina-Gonzalez[4], Hayk Davtyan[5], Rebecca J. Lodge[6], James D. Glover[1], Robert Wallace[7], David A.D. Munro[8], Eyal David[9], Ido Amit[9], Véronique E. Miron[4], Josef Priller[8], Stephen J. Jenkins[6], Giles E. Hardingham[8,10], Mathew Blurton-Jones[5], Neil A. Mabbott[1], Kim M. Summers[11], Peter Hohenstein[1,12], David A. Hume[11,14] & Clare Pridans[6,13,14]

The proliferation, differentiation and survival of mononuclear phagocytes depend on signals from the receptor for macrophage colony-stimulating factor, CSF1R. The mammalian *Csf1r* locus contains a highly conserved super-enhancer, the *fms*-intronic regulatory element (FIRE). Here we show that genomic deletion of FIRE in mice selectively impacts CSF1R expression and tissue macrophage development in specific tissues. Deletion of FIRE ablates macrophage development from murine embryonic stem cells. *Csf1r*$^{\Delta FIRE/\Delta FIRE}$ mice lack macrophages in the embryo, brain microglia and resident macrophages in the skin, kidney, heart and peritoneum. The homeostasis of other macrophage populations and monocytes is unaffected, but monocytes and their progenitors in bone marrow lack surface CSF1R. Finally, *Csf1r*$^{\Delta FIRE/\Delta FIRE}$ mice are healthy and fertile without the growth, neurological or developmental abnormalities reported in *Csf1r*$^{-/-}$ rodents. *Csf1r*$^{\Delta FIRE/\Delta FIRE}$ mice thus provide a model to explore the homeostatic, physiological and immunological functions of tissue-specific macrophage populations in adult animals.

[1] The Roslin Institute & Royal (Dick) School of Veterinary Studies, University of Edinburgh, Easter Bush, Midlothian EH25 9RG, UK. [2] Tecnologico de Monterrey, Escuela de Medicina y Ciencias de la Salud, Av. Ignacio Morones Prieto 3000 Pte, Col. Los Doctores, C.P. 64710 Monterrey, N.L., Mexico. [3] Department of Environmental Medicine, Toxicology Unit, Karolinska Institutet, Box 210SE-171 77 Stockholm, Sweden. [4] The MRC University of Edinburgh Centre for Reproductive Health, The Queen's Medical Research Institute, Edinburgh BioQuarter, 47 Little France Crescent, Edinburgh EH16 4TJ, UK. [5] Department of Neurobiology and Behavior, University of California Irvine, 3014 Gross Hall 845 Health Sciences Rd, Irvine, CA 92697-1705, USA. [6] University of Edinburgh Centre for Inflammation Research, The Queen's Medical Research Institute, Edinburgh BioQuarter, 47 Little France Crescent, Edinburgh EH16 4TJ, UK. [7] The Department of Orthopedic Surgery, University of Edinburgh, Chancellor's Building, Edinburgh BioQuarter, 49 Little France Crescent, Edinburgh EH16 4SB, UK. [8] UK Dementia Research Institute, The University of Edinburgh, Chancellor's Building, Edinburgh BioQuarter, 49 Little France Crescent, Edinburgh EH16 4SB, UK. [9] Department of Immunology, Weizmann Institute of Science, 234 Herzl St., Rehovot 7610001, Israel. [10] Centre for Discovery Brain Sciences, University of Edinburgh, Hugh Robson Building, 15 George Square, Edinburgh EH8 9XD, UK. [11] Mater Research Institute-University of Queensland, Translational Research Institute, Woolloongabba, QLD 4102, Australia. [12] Leiden University Medical Center, P.O. Box 96002300 RC Leiden, The Netherlands. [13] Simons Initiative for the Developing Brain, Centre for Discovery Brain Sciences, University of Edinburgh, Hugh Robson Building, George Square, Edinburgh EH8 9XD, UK. [14] These authors jointly supervised this work: David A. Hume, Clare Pridans. Correspondence and requests for materials should be addressed to D.A.H. (email: David.Hume@uq.edu.au) or to C.P. (email: clare.pridans@ed.ac.uk)

The proliferation, differentiation, and survival of vertebrate macrophages is controlled by signals from the macrophage colony-stimulating factor (CSF1) receptor (CSF1R), encoded by the *c-fms* protooncogene[1], now known as *Csf1r*. The function of the receptor and its two ligands, CSF1 and interleukin 34 (IL34), in macrophage differentiation is conserved in all amniotes (i.e. reptiles, birds, and humans)[2,3]. Deletion of the *Csf1r* locus in the mouse or rat germ line produces a global deficiency in most tissue macrophage populations[4,5]. Mutant animals are osteopetrotic (associated with loss of osteoclasts) and exhibit severe postnatal growth retardation and multiple pleiotropic impacts on development. Tissue macrophages remain dependent upon CSF1R in adult mice and can be depleted by treatment with an inhibitory anti-CSF1R antibody[6] or treatment with orally available inhibitors of CSF1R kinase activity[7]. In humans, dominant-negative mutations in the tyrosine kinase domain are associated with an adult-onset neurodegenerative disease[8].

The expression of *Csf1r* mRNA is restricted to myeloid cells. During embryonic development, *Csf1r* mRNA is expressed in the earliest macrophages identifiable in the yolk sac and transcription of this gene in pluripotent bone marrow (BM) progenitors is the hallmark of commitment to the monocyte–macrophage lineage. Accordingly, the molecular basis for myeloid-restricted transcription regulation of *Csf1r* has been studied in considerable detail (reviewed in ref. [9]). The second intron, downstream of the first coding exon, contains a conserved 337bp sequence known as the *fms*-intronic regulatory element (FIRE), identified as a super-enhancer in genome-wide analysis of chromatin in mouse macrophages. The mouse FIRE sequence contains binding sites for numerous macrophage-expressed transcription factors[9]. The combination of a 3.5 kb *Csf1r* promoter and intron 2, containing FIRE, is sufficient to direct reproducible transgenic reporter gene expression in progenitors, monocytes, granulocytes, classical dendritic cells, and tissue macrophages that also express *Csf1r* mRNA[10,11]. Removal of FIRE from the reporter construct abolishes expression[10]. The same *Csf1r* construct was used to drive conditional Cre-recombinase in lineage-trace studies that dissected the role of the yolk sac in macrophage development[12]. In mammals, the FIRE sequence is more highly conserved than any of the exons of the *Csf1r* gene[13]. A FIRE sequence is present in the same relative intronic location of the *Csf1r* locus in all reptile and bird species, and a core element required for enhancer activity[14] is perfectly conserved[13]. The chicken *CSF1R* promoter and FIRE sequences are also sufficient to direct macrophage-specific expression in chicken transgenic lines and to highlight the appearance of the earliest phagocyte populations in the yolk sac[15].

There have been relatively few studies of the function of macrophage-specific enhancers in their genomic context. A highly conserved upstream regulatory element that is present in the *Spi1* locus (which encodes the macrophage-specific transcription factor PU.1) is required for regulated expression in myeloid cells. Deletion of this element in the germline produces a failure of myeloid differentiation and development of acute myeloid leukemia[16]. Deletion of a super-enhancer within the locus of the orphan nuclear receptor transcription factor (*Nr4a1*) reveals its functional specificity, as only the LY6C^{lo} monocytes are lost, whilst the sensitivity of other monocyte and macrophage subsets to pro-inflammatory stimuli is preserved[17].

We aimed to determine the function of FIRE by deleting it from the mouse germ line. If FIRE is essential for *Csf1r* transcription, genomic deletion should partly or completely phenocopy the loss of tissue macrophages observed in *Csf1r*$^{-/-}$ mice. Here we report that deletion of FIRE has an organ-specific effect on *Csf1r* expression and macrophage differentiation. Despite the lack of brain microglia and resident macrophages in skin, heart, kidney, and peritoneum, *Csf1r*$^{\Delta FIRE/\Delta FIRE}$ mice are healthy and fertile. Aside from highlighting the likely function of other regulatory elements in the *Csf1r* locus, these mice provide a model to explore tissue-specific macrophage transcriptional regulation and function.

Results

In vitro validation of CRISPRs targeting the FIRE sequence. Guide RNAs (gRNAs) designed to delete FIRE (Fig. 1a) were first validated in the RAW 264.7 macrophage cell line and in E14 mouse embryonic stem cells (ESC). The macrophage cell line expresses *Csf1r* mRNA and was used in all of the transfection studies that previously led to the characterization of the role of FIRE[14]. Both cell types were co-transfected with pairs of Cas9-2A-EGFP constructs each expressing single gRNAs (US1+DS1 or DS2), and pools of EGFP^{+} cells were screened via PCR to detect the deletion of FIRE mediated by the CRISPR/Cas9 system. Both pairs of gRNAs produced deletions in E14 ESC and RAW 264.7 cells (Supplementary Fig. 1a). The deletion of FIRE and the absence of mismatches in the remaining *Csf1r* sequence in E14 ESC were confirmed by Sanger sequencing (Supplementary Fig. 1b). In RAW 264.7 macrophage cells, individual *Csf1r*$^{\Delta FIRE/\Delta FIRE}$ clones carried slightly different deletions of the FIRE sequence (Supplementary Fig. 1c). RAW 264.7 cells are not CSF1R-dependent and most of the cellular CSF1R protein is retained in the Golgi apparatus. We therefore analyzed cell-associated CSF1R by flow cytometry in permeabilized cells. The deletion of FIRE completely ablates detectable intracellular CSF1R (Fig. 1b). There is no impact of the FIRE mutation on cell morphology (Fig. 1c) or phagocytic capacity of cells (Fig. 1d). Neither the frequency nor the median fluorescence intensity (MFI) of the macrophage surface marker F4/80 distinguishes between *Csf1r*$^{+/+}$ and *Csf1r*$^{\Delta FIRE/\Delta FIRE}$ clones (Fig. 1e). We conclude that FIRE is required specifically for the expression of CSF1R in the RAW 264.7 macrophage cell line.

E14 mouse ESC can be cultured in the absence of feeders and form embryoid bodies (EB)[18] with the potential to generate cells belonging to all the primary embryonic germ layers (i.e. endoderm, mesoderm, and ectoderm). Macrophage differentiation from EB was induced by supplementing culture medium with murine IL3 (mIL3) and recombinant human CSF1 (rhCSF1). *Csf1r*$^{\Delta FIRE/\Delta FIRE}$ mouse ESC generated using the gRNA pair US1+DS2 are able to produce EB that are indistinguishable from the controls (Fig. 1f, Day 0). By day 7, they give rise to cells that attach to culture plates, indicating that the deletion of FIRE does not affect responsiveness to IL3. By 2 weeks post-differentiation, a lawn of ESC-derived macrophages are produced from the *Csf1r*$^{+/+}$ EB, whereas the number of macrophages from *Csf1r*$^{\Delta FIRE/\Delta FIRE}$ clones was ≈200-fold lower (Fig. 1f). Overall, these in vitro results indicate that FIRE is required for expression of *Csf1r* and/or macrophage differentiation in EB.

Generation of *Csf1r*$^{\Delta FIRE/\Delta FIRE}$ mice. To produce *Csf1r*$^{\Delta FIRE/\Delta FIRE}$ mice, vectors encoding the FIRE gRNAs US1 and DS2 and Cas9 were microinjected into C57BL/6J/CBA F1 mouse oocytes. One male founder with the expected 418 bp deletion was crossed with *Csf1r*$^{+/+}$ C57BL/6J females and the progeny were interbred. The frequencies of *Csf1r*$^{+/+}$, *Csf1r*$^{+/\Delta FIRE}$ and *Csf1r*$^{\Delta FIRE/\Delta FIRE}$ mice at weaning are 26%, 55%, and 19%, respectively ($n = 501$). Unlike *Csf1r*$^{-/-}$ mice or the *Csf1*$^{op/op}$ mouse[4] there is no postnatal growth retardation, failure of tooth eruption or evidence of osteopetrosis in *Csf1r*$^{\Delta FIRE/\Delta FIRE}$ mice (Fig. 2a–c). The proximal growth plates of control and *Csf1r*$^{\Delta FIRE/\Delta FIRE}$ mice are indistinguishable and normal numbers of osteoclasts are present (Fig. 2d, e). Brain abnormalities

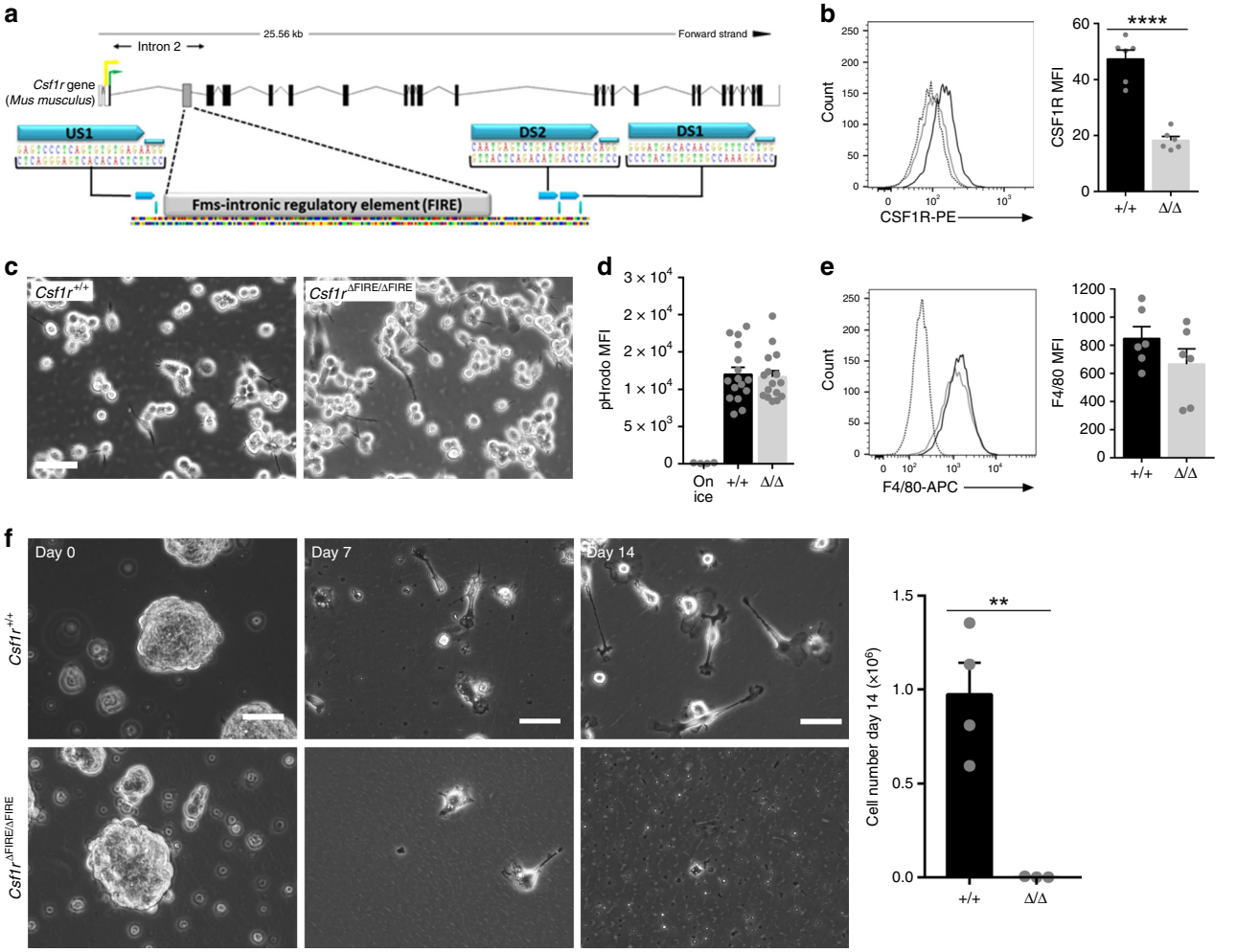

Fig. 1 FIRE deletion reduced CSF1R expression and prevented macrophage differentiation. **a** Schematic of *Csf1r* gene and location of gRNAs (US1, DS1, DS2), targeting FIRE. Protospacer adjacent motifs (PAM) are located to the right of each gRNA. Black boxes = coding exons, white boxes = untranslated regions, lines connecting exons = intronic sequences, yellow and green arrows = trophoblast/osteoclast promoter and macrophage transcription start sites, respectively. **b** Flow cytometry analysis of total CSF1R in fixed and permeabilized RAW 264.7 cell clones. Histograms are representative of three clones per genotype, from two repeat experiments in duplicate. MFI median fluorescence intensity, black line = +/+, gray line = Δ/Δ, dotted line = isotype control. $P \leq 0.0001$ (****). **c** CRISPR-treated $Csf1r^{+/+}$ and $Csf1r^{\Delta FIRE/\Delta FIRE}$ RAW 264.7 cells cultured in vitro. Scale bar = 50 µm. **d** A phagocytosis assay was performed with RAW 264.7 cells and pHrodo® Red *E. coli* BioParticles® followed by flow cytometry analysis. $n = 4$ clones per genotype from two repeat experiments. MFI median fluorescence intensity. **e** Flow cytometry analysis of surface F4/80 in RAW 264.7 cell clones. Histograms are representative of three clones per genotype from two repeat experiments in duplicate. **f** $Csf1r^{+/+}$ and $Csf1r^{\Delta FIRE/\Delta FIRE}$ E14 ESC clones were differentiated into macrophages with mIL3 and rhCSF1. Scale bars = 200 µm (Day 0, embryoid bodies) and 50 µm (Days 7 and 14). $n = 3$ clones per genotype, $P = 0.005$ (**). All source data are provided within a Source Data excel file. Graphs show mean + SEM and *P* values were determined by two-tailed *t*-tests

in $Csf1r^{-/-}$ mice include reduced brain size, severely enlarged ventricles, hollow olfactory bulbs, deficient myelination and failure of commissure closing in the corpus callosum[19]. The $Csf1r^{\Delta FIRE/\Delta FIRE}$ brains are not macroscopically distinguishable from controls and Luxol fast blue staining reveals no differences in myelination (Fig. 2f, g).

$Csf1^{op/op}$, $Csf1r^{-/-}$ mice and adult mice treated with anti-CSF1R antibody lack lamina propria and Peyer's patch macrophages in the small intestine. These mice also show associated changes in villus architecture, increased goblet cell numbers detected with periodic acid-schiff (PAS) staining, reduced proliferation in the crypts and defects in differentiation of Paneth cells[6,20,21]. *Csf1r* mRNA is not expressed in intestinal epithelial cells and the impacts of anti-CSF1R treatment are attributable to the loss of macrophages surrounding the crypts[21]. There are no detectable alterations in intestinal epithelia that distinguish between $Csf1r^{+/+}$ and $Csf1r^{\Delta FIRE/\Delta FIRE}$ mice (Fig. 2h and Supplementary Fig. 2).

The development of normal sexual maturity is compromised in both male and female $Csf1^{op/op}$ mice[22,23] and in $Csf1r^{-/-}$ rats[5]. By contrast, the $Csf1r^{\Delta FIRE/\Delta FIRE}$ mice reach sexual maturity and are fertile.

The impact of FIRE deletion in blood and BM. Two subsets of blood monocytes can be distinguished based upon the expression of LY6C. The differentiation of the $LY6C^{lo}$ subset depends upon CSF1R signaling[6,24]. $Csf1r^{\Delta FIRE/\Delta FIRE}$ mice have normal cell populations in peripheral blood (Fig. 3a) and F4/80, LY6C, and CD11b expression is unchanged compared to littermates (Fig. 3b–d). However, the expression of CSF1R detected with anti-CD115 antibody is abolished (Fig. 3c). Furthermore, the binding of labeled CSF1 ($pCSF1\text{-}Fc^{AF647}$)[11] is undetectable in the mutant mice, whereas in littermates it provides a sensitive marker

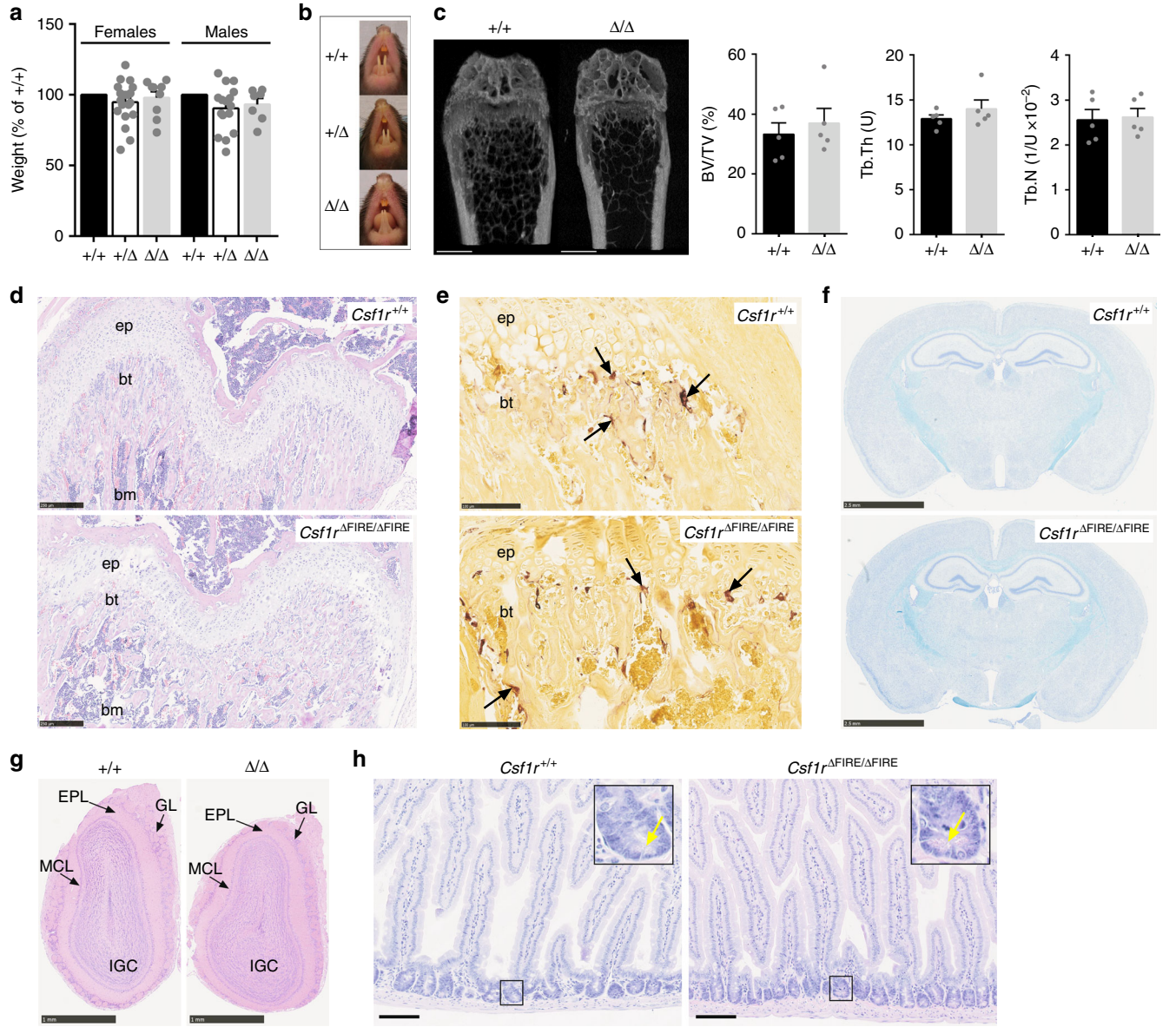

Fig. 2 FIRE-deficient mice displayed none of the gross phenotypes found in *Csf1r*$^{-/-}$-mice. **a** Mice were weighed between 2 and 11 weeks of age. $n = 7$, 20, 9 (females) and 5, 16, 7 (males) for +/+, +/Δ, and Δ/Δ, respectively. **b** Representative images of tooth eruption in adult mice. **c** Femurs from 4-week-old male and female mice were scanned by Micro-CT. Scale bars = 1 mm. $n = 5$ mice per genotype. BV/TV bone volume over total volume (bone density), Tb. Th trabecular thickness, Tb.N trabecular number. **d** Hematoxylin and eosin (H&E) staining of sections of bone. Images are representative of six mice per genotype; ep epiphyseal plate, bt bony trabeculae, bm bone marrow. Scale bar = 250 µm. **e** Femurs from the same cohort of mice above were stained for tartrate-resistant acid phosphatase (TRAP). Arrows point to TRAP^{+} osteoclasts. Scale bar = 100 µm. **f** Luxol Fast Blue staining of paraffin-embedded formalin-fixed adult brains. Images are representative of three mice per genotype. Scale bar = 2.5 mm. **g** H&E staining of olfactory bulbs from adult mice. Images are representative of six mice per genotype. EPL external plexiform layer, GL glomerular layer, IGC internal granular cell layer of the olfactory bulbs, MCL mitral cell layer. Scale bar = 1 mm. **h** H&E staining of sections of duodenum from adult mice. Yellow arrows point to Paneth cells. Images are representative of six mice per genotype. Scale bar = 100 µm. All source data are provided within a Source Data excel file. Graphs show mean + SEM

for F4/80^{+} blood monocytes (Fig. 3d). Notably, the level of both CSF1R and CSF1 binding is reduced by around 50% in the heterozygotes (Fig. 3c, d), which is consistent with a lack of dosage compensation at the mRNA level also reported in *Csf1r*-deficient mice and rats[4,5].

Unlike *Csf1r* and *Csf1* mutant mice[4], *Csf1r*$^{\Delta FIRE/\Delta FIRE}$ mice are not osteoclast-deficient and osteopetrotic. Total BM cellularity remains unchanged by the FIRE mutation (Supplementary Fig. 3a). Aside from progenitors, BM contains multiple specialized macrophage populations that regulate bone homeostasis and hematopoietic differentiation (reviewed in ref. [25]). BM cell populations were analyzed by flow cytometry as described in Supplementary Fig. 3b. Two populations of F4/80^{+} cells are detected in control mice that differed in the level of CSF1R. The proportion of F4/80^{+} cells is unchanged in *Csf1r*$^{\Delta FIRE/\Delta FIRE}$ mice, but CSF1R expression and CSF1 binding is abolished in both F4/80^{+} populations (Supplementary Fig. 3c and d). As in the blood, the level of CSF1R is reduced around 50% in heterozygotes. BM contains a population of monocyte–dendritic cell progenitors (MDP) that express KIT, FLT3, and CSF1R, and committed proliferative LY6C^{+} progenitors derived from the MDP that lack both KIT and FLT3[26]. Although CSF1R expression is lost in *Csf1r*$^{\Delta FIRE/\Delta FIRE}$ BM, there is no

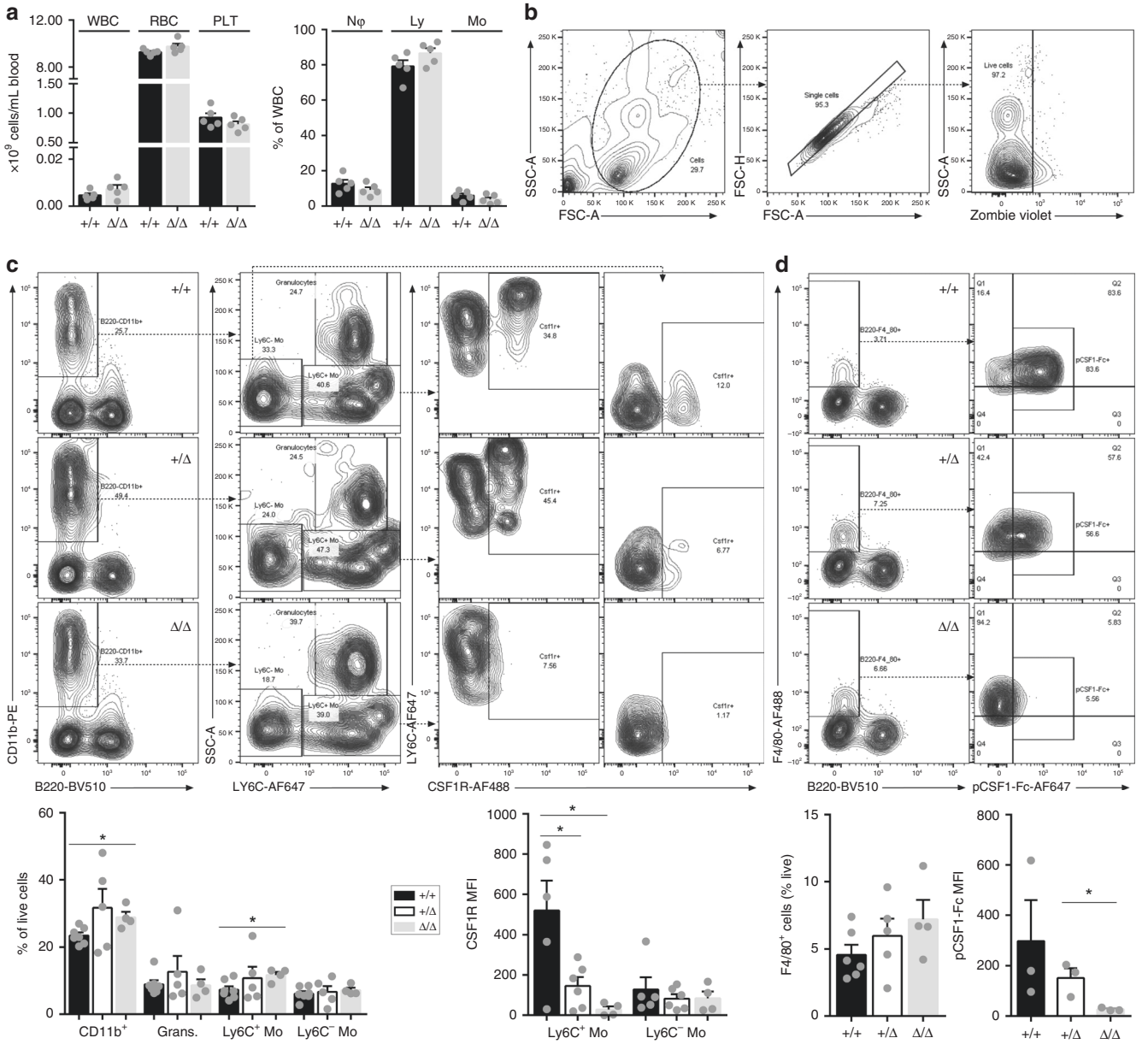

Fig. 3 FIRE deletion reduced functional CSF1R expression in blood. **a** Cell populations in whole blood of 11–13-week-old *Csf1r*$^{\Delta FIRE/\Delta FIRE}$ mice (Δ/Δ) and controls (+/+) were quantified using an automated hematology analyzer. $n = 5$ mice per genotype. WBC white blood cells, RBC red blood cells, PLT platelets, Nφ neutrophils, Ly lymphocytes, Mo monocytes. **b** Whole EDTA-blood from 11 to 13-week-old mice was analyzed by flow cytometry. Plots show the representative gating strategy to identify live single cells for subsequent analysis. **c** Myeloid cells were identified as CD11b^{+}B220^{-} (Panel 1) then separated by LY6C and SSC to identify granulocytes (LY6C^{+}SSC^{hi}, panel 2). The LY6C^{+} and LY6C^{lo} monocyte populations were then analyzed for CSF1R expression (Panels 3 and 4, respectively). $n = 7$+/+, 5+/Δ, and 4 Δ/Δ from four experiments. For % of live cells $P = 0.012$ (*CD11b^{+}) and 0.019 (*LY6C^{+} Mo). For median fluorescence intensity (MFI) of CSF1R $P = 0.027$ (*+/+ vs. +/Δ), and 0.022 (*+/+ vs. Δ/Δ). Grans. granulocytes, Mo monocyte. **d** F4/80^{+}B220^{-} myeloid cells were analyzed for binding of CSF1 (pCSF1-Fc^{AF647})[11]. $n = 3$ mice per genotype from four experiments. $P = 0.033$ (*). All source data are provided within a Source Data excel file. Graphs show mean + SEM and *P* values were determined by two-tailed *t*-tests

reduction in the number of cells expressing LY6C, KIT, or FLT3 (Supplementary Fig. 3e). In view of the apparent loss of CSF1R protein, we examined whether BM from mutant mice is responsive to CSF1. BM-derived macrophages (BMDM) are generated from *Csf1r*$^{\Delta FIRE/\Delta FIRE}$ BM, but with greatly reduced yield compared to controls (Supplementary Fig. 3f). The macrophages derived from *Csf1r*$^{\Delta FIRE/\Delta FIRE}$ BM still express F4/80 and CD11b but have lower levels of surface CSF1R detected with pCSF1-Fc^{AF647} relative to controls (Supplementary Fig. 3g). Hence, the production/survival of these few BMDM relies on some mechanism that compensates for the absence of FIRE.

Macrophage populations in *Csf1r*$^{\Delta FIRE/\Delta FIRE}$ mice. We performed flow cytometry and/or immunohistochemistry analyses on major organs as shown in Fig. 4, Supplementary Figs. 4 and 5. Liver macrophages (Kupffer cells, KC) are CSF1R-dependent[4,6], CSF1-responsive[27], and the main site of clearance of labeled CSF1[11]. The number, location, or morphology of KC and the liver-to-body weight ratio of *Csf1r*$^{\Delta FIRE/\Delta FIRE}$ mice are similar to littermate controls (Supplementary Fig. 4a, b). Flow cytometry analysis confirmed the unchanged numbers of KC and dendritic cell subsets (cDC2 as defined previously[11]) (Fig. 4a) and retention of KC-specific markers such as TIM4 (Supplementary Fig. 4c).

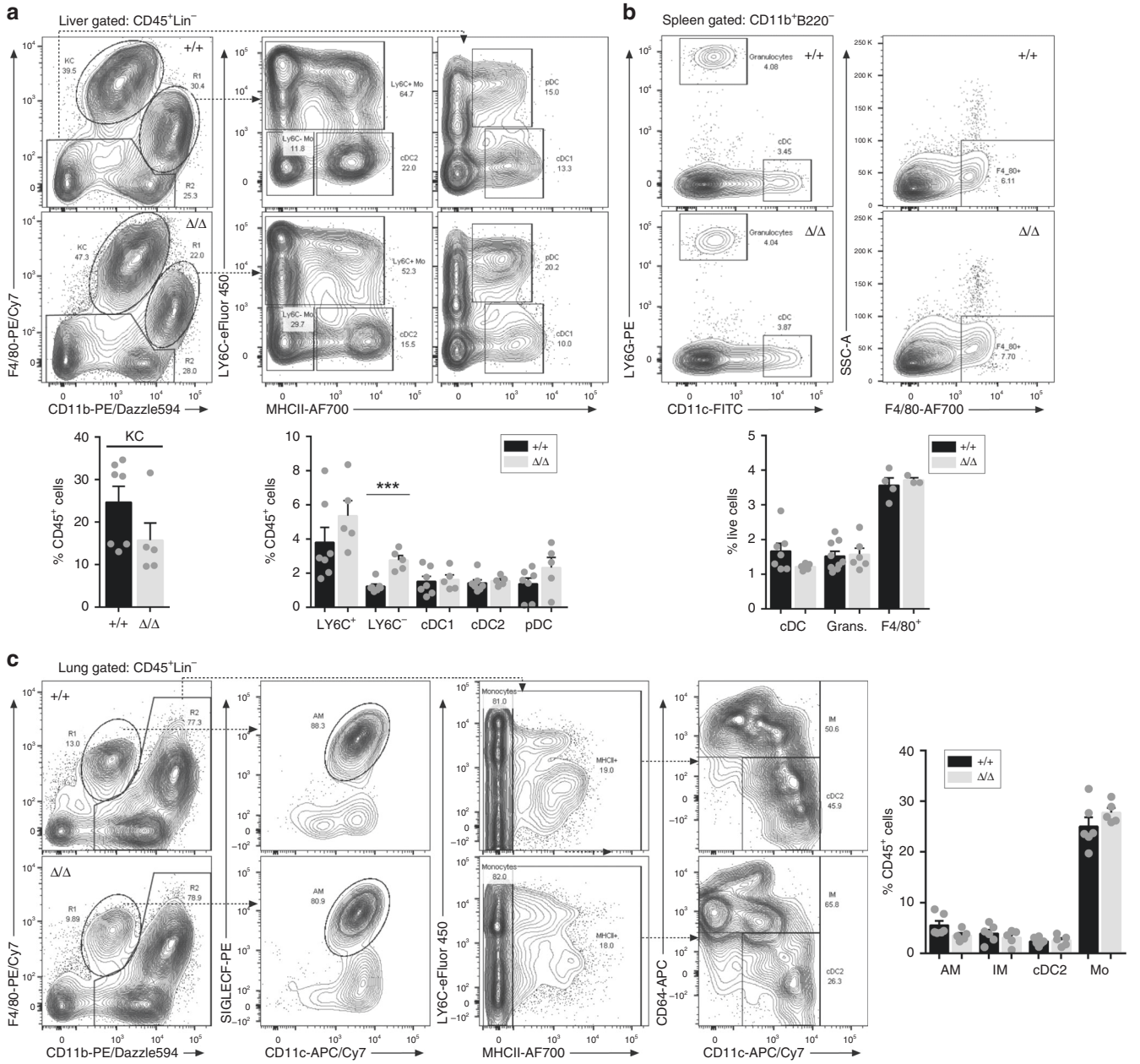

Fig. 4 Macrophage populations in liver, spleen, and lungs are unaffected in FIRE-deficient mice. **a** Leukocyte populations were analyzed from enzymatically digested livers from mice aged between 8 and 10 weeks. Flow cytometry profiles show representative *Csf1r*$^{+/+}$ (+/+) and *Csf1r*$^{\Delta FIRE/\Delta FIRE}$ (Δ/Δ) mice using the gating strategy described by Hawley et al.[11]. Kupffer cells (KC) were identified as CD45$^+$, lineage$^-$ (Lin-; CD3$^-$CD19$^-$LY6G$^-$) and F4/80^{hi}CD11b^{lo} (Panel 1). F4/80^{lo}/CD11b^{hi} and F4/80$^-$/CD11b$^-$ populations were further separated on the basis of LY6C and MHCII expression (Panels 2 and 3). Mo monocyte, cDC conventional dendritic cell, pDC plasmacytoid dendritic cell. $n = 7$+/+ and 5 Δ/Δ from 3 repeat experiments. $P = 0.0002$ (***). **b** Leukocyte populations were analyzed from enzymatically digested spleens from mice aged between 8 and 10 weeks. The flow cytometry profiles show representative *Csf1r*$^{+/+}$ (+/+) and *Csf1r*$^{\Delta FIRE/\Delta FIRE}$ (Δ/Δ) mice. Conventional dendritic cells (cDC) were identified as CD11b$^+$B220$^-$CD11c$^+$LY6G$^-$ and granulocytes as CD11b$^+$B220$^-$CD11c$^-$LY6G$^+$ (Panel 1). Red pulp macrophages were identified as CD11b$^+$B220$^-$F4/80$^+$SSC^{lo} (Panel 2). $n = 3$–9 mice per genotype from 4 repeat experiments. **c** Single cell suspensions of digested lungs were analyzed by flow cytometry as described above for the liver using the same cohort of mice. Alveolar macrophages (AM) were defined as F480$^+$CD11b^{lo} (Panel 1) and CD11c$^+$SIGLECF$^+$ (Panel 2). The CD11b$^+$F4/80$^{-/+}$ cells were further analyzed to define the monocytes (Mo, MHCII$^-$LY6C$^{-/+}$, Panel 3), interstitial macrophages (IM, MHCII$^+$CD11c$^{-/+}$CD64$^+$) and conventional dendritic cells subset 2 (cDC2, MHCII$^+$CD11c$^+$CD64$^-$) in Panel 4. All source data are provided within a Source Data excel file. Graphs show mean + SEM and *P* values were determined by two-tailed *t*-tests

However, there is a significant increase in LY6C^{lo} monocyte-like cells (CD11b$^+$F4/80^{lo}). The full gating strategy for liver flow cytometry data is shown in Supplementary Fig. 4d.

The marginal zone is completely absent in the spleen of *Csf1*$^{op/op}$ mice[28] and in *Csf1r*$^{-/-}$ rats[5]. In *Csf1r*$^{\Delta FIRE/\Delta FIRE}$ mice the overall architecture and relative area of the marginal zone is indistinguishable from the controls (Supplementary Fig. 4e and f). As in the liver, there is no change in the spleen-to-body weight ratio or the relative abundance of myeloid populations defined by staining for F4/80$^+$ or other markers (Supplementary Fig. 4g, h and Fig. 4b). The full gating strategy for spleen flow cytometry data is shown in Supplementary Fig. 4i.

Lung macrophage populations are primarily controlled by CSF2 (also known as GM-CSF, encoded by *Csf2*), rather than CSF1[29], but lung macrophages do express *Csf1r* and bind CSF1[11]. The *Csf1r*-EGFP macrophage-reporter transgene is highly expressed in both alveolar (AM) and interstitial macrophage populations in the lung[10], which have distinct developmental origins and renewal mechanisms during adulthood[30]. Furthermore, expression of *Csf1r*-EGFP in AM is dependent upon the inclusion of FIRE in the transgene[10]. Macrophages of the lung are partly depleted in $Csf1^{op/op}$ mice[31] and double mutant $Csf1^{op/op}$ and $Csf2^{-/-}$ mice develop severe alveolar proteinosis[29]. AM can be identified based upon expression of SIGLECF[30]. Interstitial myeloid populations have been classified as macrophage and conventional dendritic cell subpopulations, based upon expression of CD64, CD11b, CD11c, and MHCII[11]. To assess the impact of the FIRE deletion on these populations, lungs were digested and analyzed by flow cytometry as previously described[11]. The full gating strategy is shown in Supplementary Fig. 5a. We also measured *Csf1r* mRNA in the lung of wild-type and $Csf1r^{\Delta FIRE/\Delta FIRE}$ mice (Supplementary Fig. 5b). FIRE deletion has no effect on AM or any of the interstitial myeloid populations of the lung (Fig. 4c). A marginal reduction in *Csf1r* mRNA is likely attributable to the loss of expression in monocytes in both blood and BM (Fig. 3c, d and Supplementary Fig. 3c, d). F4/80 is barely detectable in either of the major lung macrophage populations and is primarily associated with monocytes[30]. Accordingly, the levels of total *Adgre1* (encoding F4/80) and *Itgam* (CD11b) mRNA in the lung are unaffected by the deletion of FIRE. We conclude that FIRE is not required for expression of *Csf1r* mRNA in lung macrophages nor for their development or monocyte trafficking in the lung.

The large macrophage population of the intestine is constantly renewed from recruited blood monocytes[32]. The Peyer's patch and surrounding mucosa contain several specialized mononuclear phagocyte populations, distinguished by mRNA or protein expression of the surface markers F4/80 (ADGRE1), CD4, SIGLEC1, SIRPA, MERTK, TIM4, CX3CR1, and ITGAX (CD11c)[33], including a recently described long-lived population[34,35]. All of these populations depend upon continuous CSF1R signaling[6,21]. Monocytes enter the lamina propria constantly and respond to the local environment with progressive changes in surface phenotype and gene expression in a so-called monocyte waterfall[32]. Supplementary Fig. 6 shows the comparison of these populations in the $Csf1r^{+/+}$ and $Csf1r^{\Delta FIRE/\Delta FIRE}$ mice. There is no detectable difference in distribution of monocyte-like, DC-like, or macrophage populations in either small or large intestine.

Macrophages are so abundant in the intestine that the level of macrophage-specific transcripts can be reproducibly detected by analysis of total mRNA. To complement the analysis of isolated cells, we isolated mRNA from Peyer's patches and surrounding mucosa in the ileum of $Csf1r^{+/+}$ and $Csf1r^{\Delta FIRE/\Delta FIRE}$ mice and profiled gene expression using microarrays. There is no significant difference in *Csf1r* expression between $Csf1r^{+/+}$ and $Csf1r^{\Delta FIRE/\Delta FIRE}$ mice nor in the level of mRNA encoding any of the markers of intestinal macrophage subpopulations mentioned above, including *Itgam* (CD11b) and *Ly6c1*, which are rapidly down-regulated following extravasation into the intestine[32] (Supplementary Data 1). These findings demonstrate that FIRE is not required by intestinal macrophages for expression of *Csf1r* and that the loss of CSF1R in monocytes has no impact on intestinal macrophage homeostasis. In addition, the expression of transcripts that mark cell types controlled indirectly by signals from CSF1R-dependent macrophages, including markers of Paneth cells (*Lyz1*), microfold cells (*Spib, Ccl9, Tnfrsf11a*) or goblet cells (*Muc2*)[21], are unaffected (Supplementary Data 1).

Loss of macrophage populations in $Csf1r^{\Delta FIRE/\Delta FIRE}$ mice. The resident macrophages of the peritoneal cavity may be subdivided into two populations, based upon relative size and the level of TIM4 and F4/80 antigen they express[36]. Both populations of peritoneal macrophages (PM) are absent from $Csf1^{op/op}$ and $Csf1r^{-/-}$ mice[4,28] and from mice treated with anti-CSF1R antibody[6]. The major $TIM4^{+}F4/80^{hi}CD11b^{hi}$ large PM population is almost entirely lost in $Csf1r^{\Delta FIRE/\Delta FIRE}$ mice (Fig. 5a and Supplementary Fig. 6a). The minor residual PM population consists of the small PM that are $TIM4^{-}F4/80^{lo}$[36]. These cells were shown previously to bind labeled CSF1 preferentially compared to large PM[11]. Both anti-CSF1R (CD115) and CSF1-Fc binding to these residual populations are absent in the $Csf1r^{\Delta FIRE/\Delta FIRE}$ mice (Fig. 5a). In $Csf1r^{\Delta FIRE/+}$ mice the PM populations are retained but as in blood and BM, there is a reduction in the level of surface receptor detected with either labeled CSF1 or anti-CSF1R antibody, which is consistent with the lack of dosage compensation. In summary, in the peritoneum, the $Csf1r^{\Delta FIRE/\Delta FIRE}$ mutation phenocopies the *Csf1r*-deficient mice.

The abundant interstitial $F4/80^{hi}$ macrophage populations of the kidney have recognized roles in renal growth and development[37], homeostasis and immune surveillance[38]. $F4/80^{hi}$ kidney macrophages were almost absent from both $Csf1^{op/op}$ and $Csf1r^{-/-}$ mice[4]. To identify populations of renal mononuclear phagocytes we enzymatically digested kidneys and analyzed $CD45^{+}$ myeloid cells by flow cytometry. The gating strategy is shown in Supplementary Fig. 7b. $Csf1r^{\Delta FIRE/\Delta FIRE}$ mice have fewer total $CD45^{+}$ cells and the $F4/80^{hi}CD11b^{lo}$ resident kidney macrophages (KM)[38] are undetectable (Fig. 5b). In both control and mutant, a subset of the $CD11b^{hi}$ cells are $F4/80^{lo}MHCII^{-}$ monocytes but the majority of cells in the $F4/80^{lo}CD11b^{hi}$ (R1) gate are also $MHCII^{+}/CD64^{+}$. Their surface phenotype is reminiscent of the monocyte-derived small PM discussed above. As in the peritoneum, their abundance is slightly increased by the FIRE mutation (Fig. 5b). Conventional dendritic cells (cDC) in the kidney are difficult to separate from macrophages based upon surface markers. A minor subpopulation of cDC ($F4/80^{-}CD11b^{+}MHCII^{+}$) is detected in both control and $Csf1r^{\Delta FIRE/\Delta FIRE}$ kidneys (R2 gate) (Fig. 5b). Although exogenous CSF1 can promote mouse kidney morphogenesis in vitro and growth of the kidney in vivo[37], there is no change in the kidney-to-body weight ratio in $Csf1r^{\Delta FIRE/\Delta FIRE}$ mice (Supplementary Fig. 7c) and kidneys are histologically normal (Supplementary Fig. 7d).

Macrophages of the heart can also be separated into subpopulations attributed distinct roles in cardiac homeostasis and repair following injury[39–41]. Supplementary Fig. 7e shows the flow cytometry gating strategy for the heart and Fig. 5c summarizes the analysis of digested cardiac macrophage populations from control and $Csf1r^{\Delta FIRE/\Delta FIRE}$ mice. The total cardiac $CD45^{+}$ population is greatly reduced in the $Csf1r^{\Delta FIRE/\Delta FIRE}$ mice due to selective loss (70–80%) of both the $F4/80^{hi}CD64^{+}$ macrophage ($MHCII^{hi}$) and monocyte-like ($MHCII^{lo}$) populations previously described by others[39–41]. Interestingly, a recent study proposed a link between resident macrophages of the kidney and the heart in the generation of an adaptive response to cardiac pressure overload[40]. However, as in the kidney, we detect no change in the heart-to-body weight ratio in $Csf1r^{\Delta FIRE/\Delta FIRE}$ mice (Supplementary Fig. 7f) and the histology is indistinguishable from controls (Supplementary Fig. 7g).

There are two major macrophage populations in the skin, the Langerhans cells of the epidermis and the dermal macrophages. Both are CSF1R-dependent[4,6] but Langerhans cells, like microglia, depend specifically on the alternative CSF1R ligand, IL34[42]. Langerhans cells are absent in epidermal sheets from tails of $Csf1r^{\Delta FIRE/\Delta FIRE}$ mice (Fig. 6a). The loss of this cell population

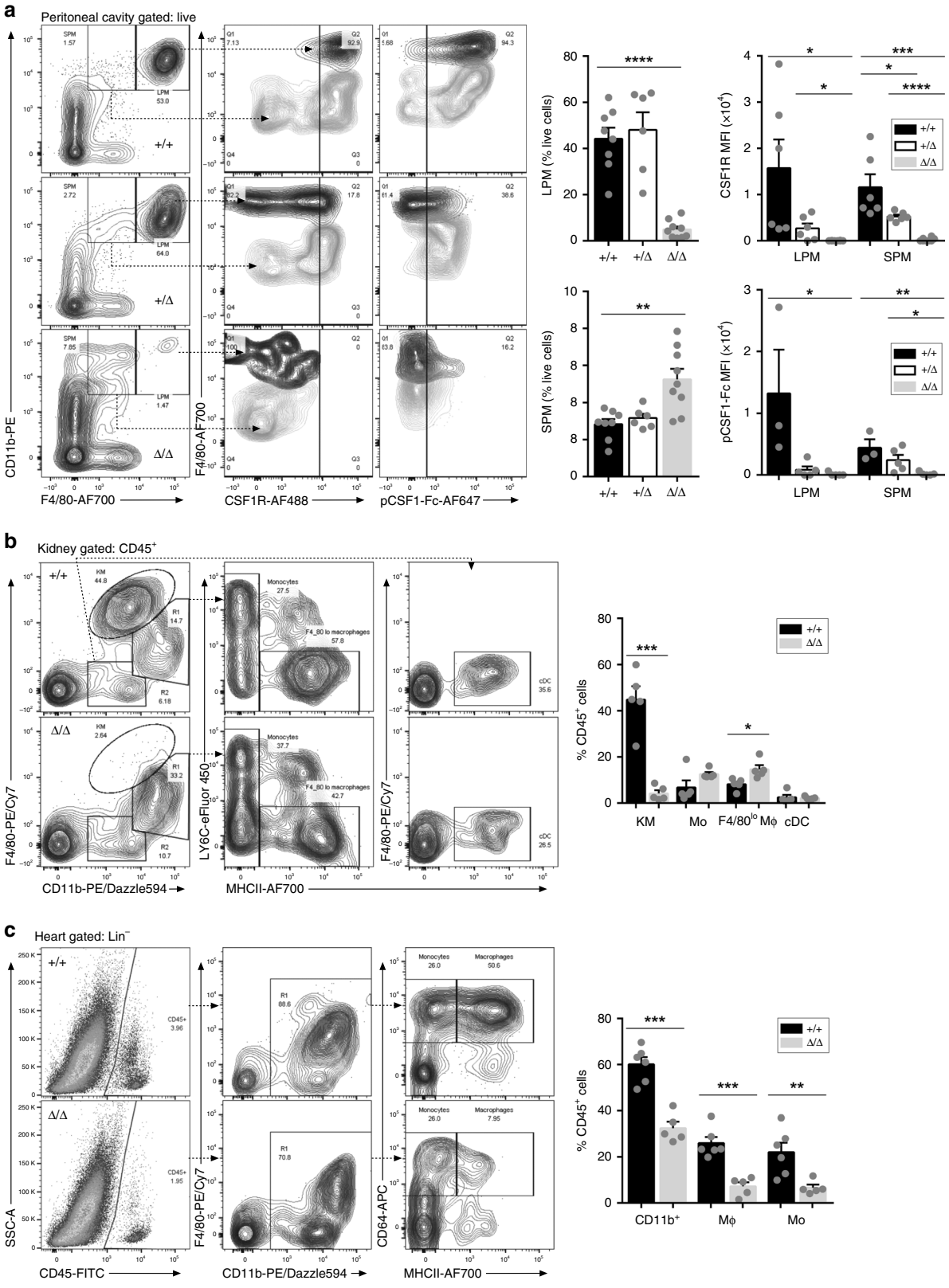

has no effect on the morphology of the epidermis or the dermis (Fig. 6b). Dermal macrophage populations accumulate melanosomes from neighboring melanocytes and, like macrophages of the gut, they turn over rapidly[43]. The stellate melanophagic macrophage populations of the dermis are F4/80^{+} and are not affected by the FIRE mutation (Fig. 6b).

Loss of microglia in *Csf1r*$^{\Delta FIRE/\Delta FIRE}$ mice. Microglia, the tissue-resident macrophage population of the brain, arise very early in mouse embryonic development and depend upon CSF1R signaling[44]. Microglia detected by localization of IBA1 or P2RY12 in littermate controls are absent in the brain of *Csf1r*$^{\Delta FIRE/\Delta FIRE}$ mice (Fig. 7a, b). Disaggregation of the whole

Fig. 5 FIRE deletion results in loss of macrophages in the peritoneal cavity, kidney, and heart. **a** Flow cytometry profiles show peritoneal cells from representative *Csf1r*$^{+/+}$ and *Csf1r*$^{\Delta FIRE/\Delta FIRE}$ mice using the gating strategy described by Bain et al.[36]. Small peritoneal macrophages (SPM) were identified as F4/80^{lo}CD11b^{+} and large peritoneal macrophages (LPM) as F4/80^{hi}CD11b^{+} (Panel 1). These populations were analyzed for CSF1R expression (Panel 2) and binding of pCSF1-Fc (Panel 3). $n = 8$ +/+, 6+/Δ and 9 Δ/Δ mice aged between 10 and 15 weeks, from five experiments. $P = 0.012$–0.048 (*), 0.002–0.006 (**), 0.001 (***) and <0.0001 (****). **b** Leukocyte populations were isolated from enzymatically digested kidneys and gated for CD45 expression. The flow cytometry profiles show analysis of representative *Csf1r*$^{+/+}$ and *Csf1r*$^{\Delta FIRE/\Delta FIRE}$ mice. Kidney macrophages (KM) were identified as F4/80^{hi}CD11b^{lo} (Panel 1), pooled LY6C$^{-/+}$ monocytes (Mo) as F4/80^{lo}MHCII^{-} (Panel 2), putative monocyte-derived macrophages as F4/80^{lo}MHCII^{+} (Panel 2), and conventional dendritic cells (cDC) as F4/80^{-}CD11b^{lo}MHCII^{+} (Panel 3). $n = 5$ mice per genotype aged 8–10 weeks, from three experiments. $P = 0.015$ (*) and 0.0001 (***). **c** Single cell suspensions of enzymatically digested hearts from the same cohort were analyzed by flow cytometry. Cells were gated lineage^{-} (Lin^{-} = CD3/CD19/LY6G). $n = 6$+/+ and 5 Δ/Δ from three experiments. MΦ macrophage, Mo monocyte. $P = 0.009$ (**), 0.0003 (*** MΦ), and 0.0001 (*** CD11b^{+}). All source data are provided within a Source Data excel file. Graphs show mean + SEM and *P* values were determined by two-tailed *t*-tests

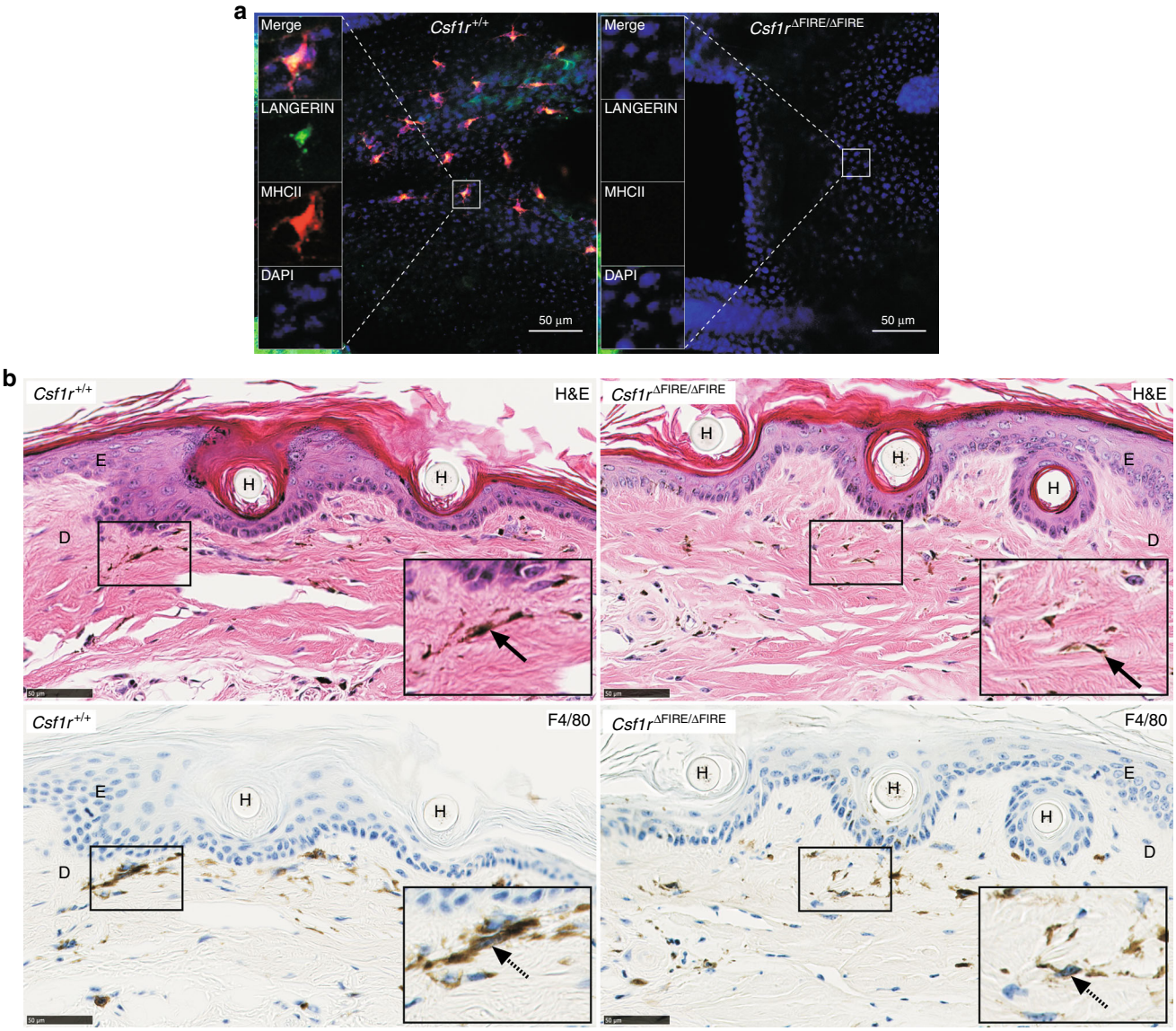

Fig. 6 The deletion of FIRE results in loss of Langerhans cells. **a** Whole-mount epidermal tail sheets were stained with antibodies against LANGERIN (green) and MHCII (red). Nuclei were stained with DAPI (blue). Images are representative of four mice per genotype, aged between 8 and 10 weeks. Scale bars = 50 µm. **b** Decalcified tails from the same cohort of mice above were stained with hematoxylin and eosin (H&E, upper panel) and an antibody against F4/80 (lower panel). E epidermis, D dermis, H hair follicle. Scale bars = 50 µm

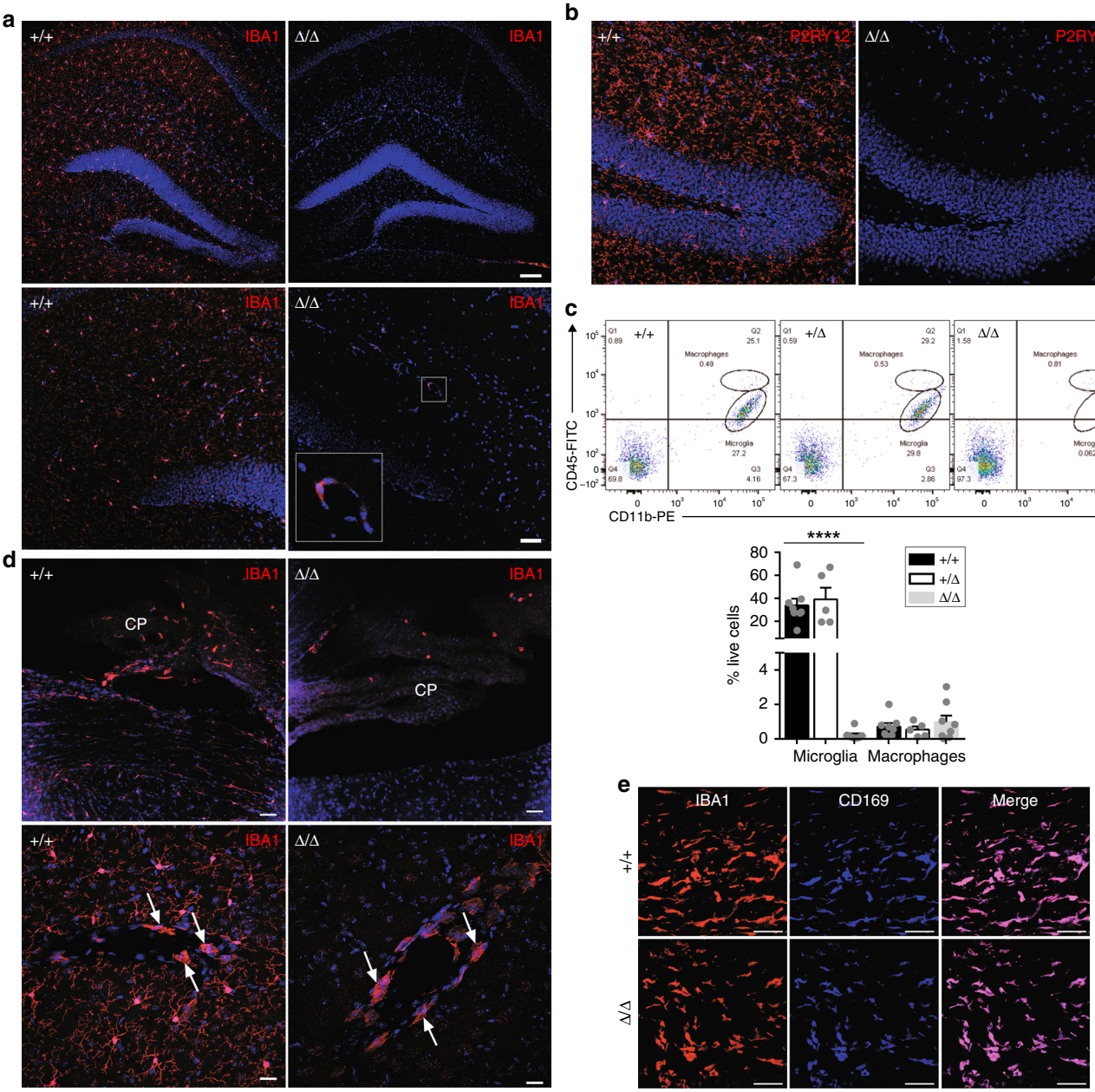

Fig. 7 FIRE deletion results in selective loss of microglia. **a** Cryosections of adult brains were stained with an antibody against IBA1. Boxed area shows an IBA1$^+$ perivascular macrophage in the *Csf1r*$^{\Delta FIRE/\Delta FIRE}$ mouse brain. Scale bars = 100 μm, 50 μm in the upper and lower panels, respectively. Images are representative of four mice per genotype. **b** Cryosections of adult brains were stained with an antibody against P2RY12. Scale bar = 40 μm. **c** Single cell suspensions of myelin-depleted brains from males and females aged 10 weeks to 9 months were analyzed by flow cytometry for CD45 and CD11b expression as per[45]. Microglia = CD45^{low}CD11b$^+$. Macrophages = CD45$^+$CD11b$^+$. $n = 8+/+$, $5+/\Delta$, 8 Δ/Δ from five experiments. $P < 0.0001$ (****) Δ/Δ compared to $+/+$. **d** Cryosections of adult brains stained with an antibody against IBA1 using the same cohort of mice in **a** and **b**. Upper panel shows the choroid plexus (CP) and white arrows point to perivascular macrophages in the lower panel. Images are representative of three mice. Scale bars = 40 and 20 μm in the upper and lower panels, respectively. **e** Dissected meningeal dura mater was stained with antibodies against IBA1 and CD169. Images are representative of two mice per genotype. Scale bars = 50 μm. All source data are provided within a Source Data excel file. Graphs show mean + SEM and *P* values were determined by two-tailed *t*-tests

brain and analysis by flow cytometry[45] confirms the loss of CD45^{low}/CD11b$^+$ microglia which persists up to 9 months of age (Fig. 7c). The full flow cytometry gating strategy is shown in Supplementary Fig. 8a. Heterozygous mutation (haploinsufficiency) of *Csf1r* has been proposed as a model for the human neurodegenerative disease ALSP (adult onset leukoencephalopathy with axonal spheroids and pigmented glia)[46]. However, there is no detectable effect of the heterozygous mutation in mice (*Csf1r*$^{\Delta FIRE/+}$) on microglial numbers. The brain also contains populations of CD45^{hi} classical macrophages associated with the vasculature, meninges, and choroid plexus with a distinct transcriptional profile[47,48]. CD45^{hi} cells are retained in *Csf1r*$^{\Delta FIRE/\Delta FIRE}$ brain digests (Fig. 7c) This was confirmed by immunolocalization of CD169, shown recently to be a marker alongside CD206 and LYVE1 for a perivascular macrophage population in most tissues[49] (Fig. 7d, e). The brain-to-body weight ratios in adult male and female *Csf1r*$^{\Delta FIRE/\Delta FIRE}$ mice remains unchanged (Supplementary Fig. 8b).

Microglia are so abundant in the brain that their gene expression profile is readily detected in total mRNA. The complete loss of microglia in *Csf1r*$^{-/-}$ rat brains was associated with commensurate loss of known microglia-associated transcripts in four brain regions[5]. To confirm the loss of microglia we compared the gene expression profiles of *Csf1r*$^{\Delta FIRE/\Delta FIRE}$ and *Csf1r*$^{+/+}$ hippocampi. The results, including ANOVA analysis of significantly regulated transcripts, are contained within Supplementary Data 2. Overall, 85 genes are significantly downregulated in the *Csf1r*$^{\Delta FIRE/\Delta FIRE}$ mouse hippocampus and 77 genes from this group (including *Csf1r*) have been previously shown to be expressed in human and mouse microglia[45,50,51]. Of the top 35 transcripts found by Elmore and colleagues to be down-regulated in the brains of adult mice treated with a CSF1R kinase inhibitor[52], 26 are also significantly reduced in the hippocampus of *Csf1r*$^{\Delta FIRE/\Delta FIRE}$ mice. The gene set affected by the *Csf1r*$^{\Delta FIRE/\Delta FIRE}$ mutation includes a small set of novel genes that may be implicated in microglial biology. Amongst these, the immune checkpoint protein, VISTA (*Vsir*), was recently localized in both human and mouse and was attributed functions in CNS pathologies[53]. In addition, HVCN1 was previously shown to regulate the production of microglial reactive oxygen species[54]. Consistent with the retention of the, CD45^{hi}CD11b^{+}CD169^{+} brain macrophage population in the *Csf1r*$^{\Delta FIRE/\Delta FIRE}$ mice (Fig. 7b–e), *Ptprc* (encoding CD45 antigen) and myeloid markers, such as *Mrc1(Cd206), Siglec1, Siglecf, Cd163, Csf2ra/b/b2, Fcgr2b, Tnfrfsf11a* (RANK) that have all been associated with these populations[47,48] are not significantly affected by the deletion of FIRE (Supplementary Data 2). The complete loss of detectable *Csf1r* expression implies that the perivascular and brain-associated macrophages, like blood monocytes and the macrophages of the BM, have lost *Csf1r* expression but are nevertheless produced normally.

Microglia have been implicated in oligodendrocyte maturation and synaptic plasticity[55]. The loss or induced depletion of microglia in other models leads to alterations in synaptic pruning, hippocampal neurogenesis, myelination, oligodendrocyte maturation, and astrocyte activation[56]. By contrast to phenotypes reported in *Csf1*$^{op/op}$ and *Csf1r*$^{-/-}$ mice[4], we observe no evidence of auditory or visual abnormalities in the *Csf1r*$^{\Delta FIRE/\Delta FIRE}$ mice. Sensory neuronal deficits have been associated with deficient hippocampal neurogenesis but in the *Csf1r*$^{\Delta FIRE/\Delta FIRE}$ mice there is no loss of expression of markers associated with neuronal progenitor cells (such as doublecortin (*Dcx*), and *Sox2*[57]) (Supplementary Data 2). Nandi et al.[58] claimed that *Csf1r* is expressed in subsets of neuronal progenitors, and noted the relative loss of excitatory neurons, expressing *Cux1* or *Ctip2* (BCll1b) in the *Csf1r*$^{-/-}$ mouse brain. *CUX1* mRNA was also reduced in the brain in a recently described human patient with a homozygous *CSF1R* mutation[59]. Neither transcript is down-regulated in the hippocampus of *Csf1r*$^{\Delta FIRE/\Delta FIRE}$ mice (Supplementary Data 2).

Zhang et al.[60] used expression profiles of isolated cells to identify a set of signatures of brain cell populations that can support deconvolution of whole brain expression data. As shown in Supplementary Fig. 8c, there is no significant effect of the *Csf1r*$^{\Delta FIRE/\Delta FIRE}$ mutation on any cell-type-specific signature (neuron, astrocyte, oligodendrocyte, endothelium) other than microglia. The lack of impact on astrocyte numbers or morphology was confirmed by immunolocalization of the specific markers GFAP and SOX9 in the hippocampus, as well as the striatum, olfactory bulbs, and cerebellum (Supplementary Fig. 8d). Whereas microglia have been implicated as major sources of trophic factors, mRNA expression of *Bdnf, Igf1, Tgfb1,2*, and *3* is not affected by the absence of microglia in *Csf1r*$^{\Delta FIRE/\Delta FIRE}$ mice (Supplementary Data 2). Similarly, macrophages and microglia selectively express very high levels of lysosomal-associated genes (e.g. *Lamp1, Ctsb, Atp6v0e*) and receptors for apoptotic cells (e.g. *Mertk, Axl*) compared to whole brain regions (e.g. see biogps.org) but the loss of microglia has no effect on the expression of any lysosome-associated transcripts in the hippocampus of *Csf1r*$^{\Delta FIRE/\Delta FIRE}$ mice. This conclusion is consistent with the proposal that astrocytes are potentially also engaged with apoptotic cell clearance[61] and might fill this role in the absence of microglia.

Embryonic macrophage development in *Csf1r*$^{\Delta FIRE/\Delta FIRE}$ mice. Many tissue resident macrophages are seeded during embryonic development from the yolk sac and fetal liver progenitors[24,30,41,44,62,63]. *Csf1r*$^{-/-}$ mice lack yolk sac-derived macrophages and microglia but develop fetal monocytes[44]. Treatment of a pregnant mouse with anti-CSF1R resulted in the loss of embryonic macrophages derived from the yolk sac, whereas circulating liver-derived monocytes were unaffected[63]. As shown in Fig. 8a the *Csf1r*$^{\Delta FIRE/\Delta FIRE}$ embryos develop normally but the overall density of IBA1^{+} macrophages throughout the body is greatly reduced. In the critical window in which liver hematopoiesis is established and the blood–brain barrier is closed (embryonic day 12–13), IBA1^{+} ameboid microglia are prevalent in controls but undetectable in *Csf1r*$^{\Delta FIRE/\Delta FIRE}$ embryos (Fig. 8b–d). Numerous macrophages expressing the CSF1R-ECFP and CSF1R-EGFP reporter genes line the ventricular and external surfaces of the developing brain from 9.5 dpc[10,64]. These cells are absent in *Csf1r*$^{\Delta FIRE/\Delta FIRE}$ embryos (Fig. 8b, c). Only occasional monocyte-like cells associated with blood vessels are seen in the brain parenchyma (Fig. 8b). By contrast, IBA1^{+} monocytes/macrophages are detected in the meninges and choroid plexus in both control and mutant embryos (Fig. 8c, d), consistent with our findings in the adult brain (Fig. 7). There is also a reduction in the IBA1^{+} macrophages in the fetal liver at the same stages of development (Fig. 8e). We conclude that the *Csf1r*$^{\Delta FIRE/\Delta FIRE}$ mice recapitulate the phenotype of *Csf1r*$^{-/-}$ mice in early hematopoiesis, producing a selective deficiency of yolk sac-derived cells. The major macrophage populations that are retained in the adult *Csf1r*$^{\Delta FIRE/\Delta FIRE}$ mice (liver, lung, spleen, intestine, dermis, etc.) are established late in gestation and postnatally from monocytes derived from progenitors in the fetal liver[24,30,44,62,63]. This conclusion is consistent with analysis of expression of tissue macrophage-specific genes across an embryonic gene expression time course[65].

The chromatin landscape of *Csf1r*. Chromatin analysis and ChIP-seq data identifies at least four other *Csf1r* enhancers that are active in mouse BMDM. Each is bound by JUN, STAT1, PU.1, and CEBPA, which also bind cooperatively to many other macrophage-associated enhancers (reviewed in ref. [9]). To extend these findings to other macrophage populations, we explored data from a previous study that compared the enhancer profiles of monocytes, microglia, and macrophages isolated from lung, liver, spleen, intestine, and peritoneal cavity[66]. Peaks of H3K4me1 methylation (indicative of poised enhancers) appear throughout the *Csf1r* locus and extend upstream into the neighboring *Pdgfrb* gene (Fig. 9a). This extended H3K4me1 signal is almost undetectable in neutrophils, which express *Csf1r* mRNA and *Csf1r* reporter genes at low levels but do not express surface CSF1R[11]. These additional elements lie outside the 3.5 kb promoter region, and intron containing FIRE, used in production of *Csf1r*-reporter genes (Fig. 9a). The ATAC-seq data revealed heterogeneity amongst monocyte–macrophage populations. FIRE is clearly a major peak of open chromatin detected in microglia and peritoneal macrophages, consistent with the impact of deletion of this

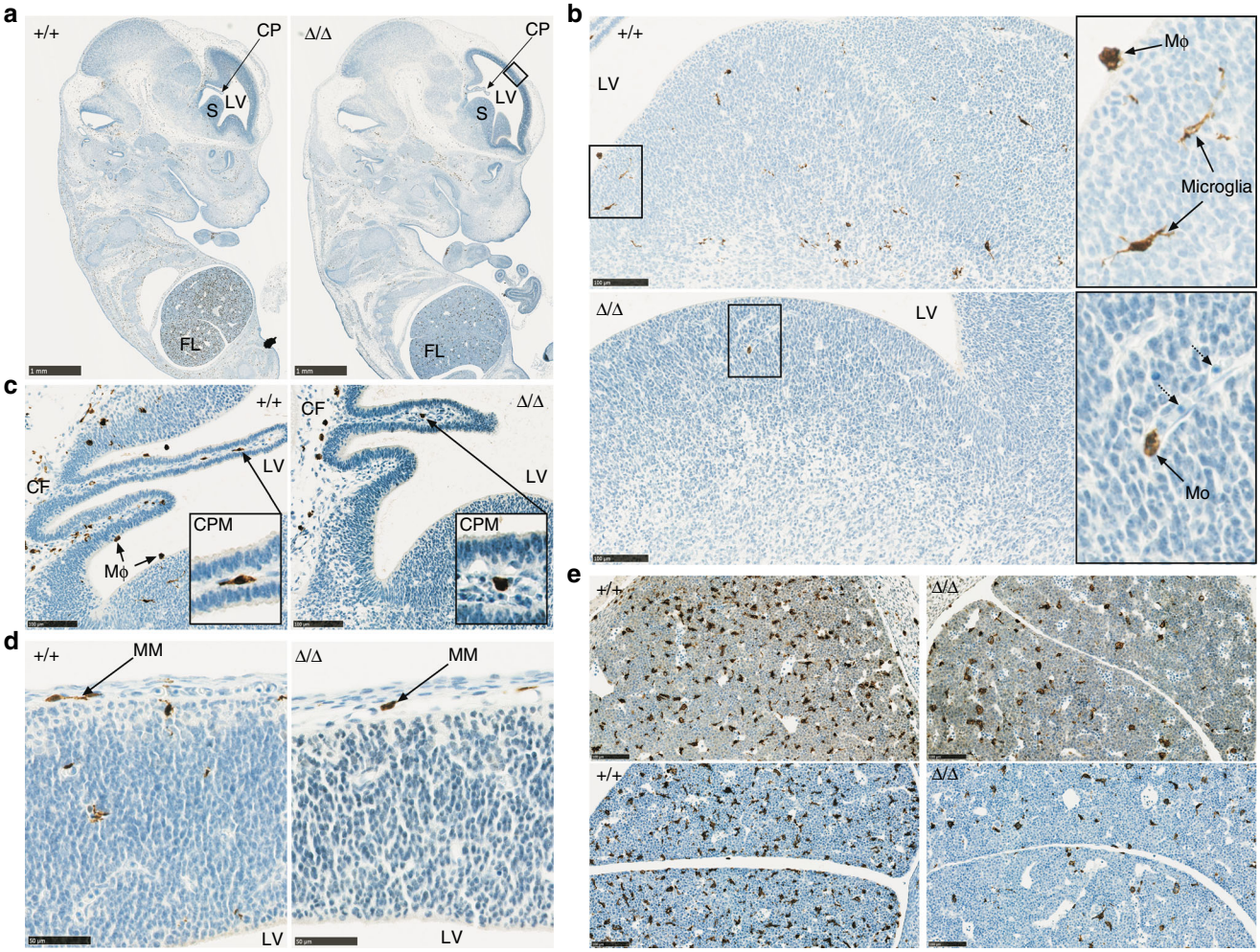

Fig. 8 FIRE deletion results in a reduction of embryonic macrophages. **a** Formalin-fixed paraffin-embedded embryos (E13) were stained with antibodies against IBA1. Images are representative of seven embryos per genotype at E12, E12.5, and E13 and four repeat experiments. CP choroid plexus, LV lateral ventricle, S striatum, FL fetal liver. Black rectangle indicates the area magnified for panel **d**. Scale bar = 1 mm. **b** View of the striatum from E12.5 embryos highlighting IBA1$^+$ microglia and ventricular macrophages (MΦ) in the control embryo and a monocyte (Mo) in the FIRE deficient embryo. Dotted arrows point to immature red blood cells in a blood vessel. Scale bar = 100 μm. **c** Images of the choroid plexus in the lateral ventricle (LV) of E12.5 embryos. CPM choroid plexus macrophage, MΦ ventricular macrophages, CF choroidal fissure. Scale bar = 100 μm. **d** IBA1$^+$ meningeal macrophages (MM) in the forebrain (boxed area in panel **a**) of control and *Csf1r*$^{\Delta FIRE/\Delta FIRE}$ embryos at E12.5. Scale bar = 50 μm. **e** IBA1$^+$ fetal liver monocytes at E12 and E13 in upper and lower panels, respectively. Scale bar = 100 μm

element (Fig. 9b). By contrast, the signal associated with FIRE is barely detectable in isolated lung and intestinal macrophages. Indeed, the promoter-associated ATAC-seq signal is barely detectable, consistent with relatively low expression of *Csf1r* mRNA in these cells[35,67,68] and lack of phenotype observed in these tissues in *Csf1r*$^{\Delta FIRE/\Delta FIRE}$ mice[21]. The ATAC-seq data in Fig. 9b reveals multiple additional elements in cells that clear the majority of CSF1 from the circulation (notably in KC and splenic macrophages), that likely contribute to the redundancy of FIRE and to the high level of *Csf1r* expression in these cell types[11]. One of these elements includes the distal promoter element (DPE). Located 5′ of the macrophage transcription start site, the DPE also has tissue-specific functions[64]. It includes a separate transcription start site cluster used by osteoclasts[69]. Expression of an amplified *Csf1r*-ECFP (MacBlue) reporter transgene, in which the DPE was deleted from the promoter, was undetectable in most tissue macrophages[64]. The exceptions that retained reporter gene expression were those populations impacted in the *Csf1r*$^{\Delta FIRE/\Delta FIRE}$ mouse; embryonic macrophages, BM progenitors and monocytes, microglia, Langerhans cells, and peritoneal macrophages. Therefore, we conclude that FIRE and the DPE interact to control expression of *Csf1r* in embryonic macrophages and in some tissue-resident macrophage populations but that both are partly redundant.

Discussion

We show that the regulatory element, FIRE, is not required to support *Csf1r* transcription in all macrophage populations. FIRE is essential for the generation or maintenance of specific CSF1R-dependent tissue macrophages, including those of the embryo, the brain (microglia), skin (Langerhans cells), peritoneum, heart, and kidney but redundant for expression of *Csf1r* mRNA in adult mononuclear phagocyte populations in the intestine and lung. FIRE is not required for the development of CSF1R-dependent macrophages in other locations (i.e. dermis, spleen, liver, and bone). The microglial population of the brain is established early in development from yolk sac-derived progenitors. Apart from a transient postnatal monocyte influx, microglia are maintained by self-renewal in a CSF1R-dependent manner[70]. The loss of IBA1$^+$ cells in *Csf1r*$^{\Delta FIRE/\Delta FIRE}$ embryos (Fig. 8) indicates that

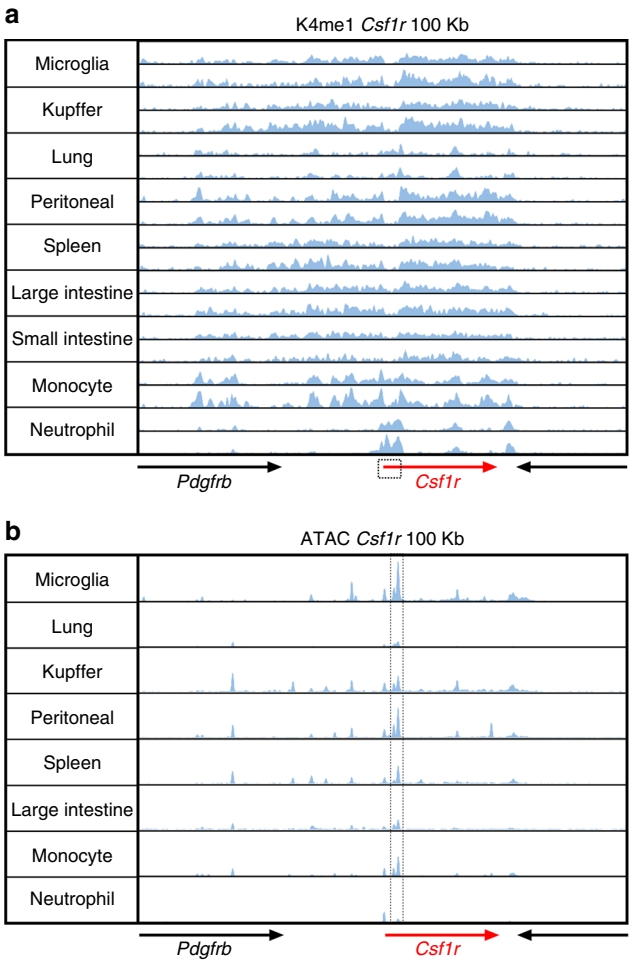

Fig. 9 Chromatin landscape of the mouse *Csf1r* locus. ChIP-seq and ATAC-seq data for the 100 kb window surrounding mouse *Csf1r* for each of the isolated myeloid cell populations shown was extracted from the primary data generated in Lavin et al.[66]. **a** ChIP-seq data showing the location of poised enhancers (H3K4me1). The boxed area indicates the 3.5 kb promoter region used in the production of *Csf1r* reporter genes. **b** ATAC-seq data showing the locations of open chromatin. The dotted lines surround the double peak in the second intron; the more prominent peak is FIRE

microglial development fails early in embryogenesis. This is consistent with the apparent failure of macrophage production from $Csf1r^{\Delta FIRE/\Delta FIRE}$ EB in the E14 ESC model (Fig. 1f).

The relative independence of the large majority of tissue-resident macrophages on the enhancer activity of FIRE begs the question of why this element is so highly conserved across evolution. Enhancer redundancy (i.e. the presence of shadow enhancers), is widespread in eukaryotic developmental systems[71]. Nevertheless, redundancy is often incomplete and the non-overlapping functions presumably explain why multiple enhancers within a locus are conserved across evolution[71]. The core element within FIRE, conserved from reptiles to humans, contains binding sites for AP1 and PU.1 that are essential for enhancer activity[14]. Colocalization of AP1 and PU.1 motifs is a feature of many mouse macrophage-specific constitutive enhancers[72]. The non-redundant role of FIRE in *Csf1r* transcription in only a subset of macrophages may be a consequence of tissue-specific expression of transcription factors that bind selectively to this region of the *Csf1r* locus. Candidate regulators have been identified in many CSF1R-dependent macrophage populations. For example, microglia are uniquely dependent upon specific transcriptional regulators encoded by *Sall1*[73] and *Irf8*[74]. Whilst multiple open chromatin sites are bound by PU.1, CEBPA, and other transcription factors in BMDM, IRF8 bound strongly and exclusively to FIRE (reviewed in ref. [9]). *Irf8* mRNA is co-expressed with *Csf1r* in the earliest committed monocyte progenitors[75] and upregulated in erythro-myeloid progenitors in parallel with *Csf1r* during early embryonic development[67]. Renal macrophages, which are also lost in $Csf1r^{\Delta FIRE/\Delta FIRE}$ mice, along with blood monocytes, share high gene expression of *Irf8* with microglia[67]. RUNX1 is another transcription factor that interacts with FIRE in both mouse and human macrophages and controls CSF1-dependent macrophage growth[76]. Accordingly, *Runx1* mRNA is expressed in the earliest progenitors of CSF1R-positive microglia[44] and is amongst the transcription factors down-regulated in the hippocampus in $Csf1r^{\Delta FIRE/\Delta FIRE}$ mice (Supplementary Data 1).

CSF1R deficiency causes embryonic or perinatal death in most mouse strains and the few surviving *Csf1r* mutant mice have numerous developmental abnormalities[77]. The $Csf1r^{\Delta FIRE/\Delta FIRE}$ mice that are born survive and thrive. Aside from survival, other major differences between the pleiotropic impacts of $Csf1r^{\Delta FIRE/\Delta FIRE}$ and $Csf1r^{-/-}$ mutations[4,77] are clearly related to the selective retention of most *Csf1r*-dependent macrophage populations in mice with the FIRE deletion. The expression profiling of the hippocampus supports the view that trophic and phagocytic functions attributed to microglia can be compensated in part by other cells. Notably, neuronal development, including expression of markers such as *Cux1*, is unaffected by the complete loss of *Csf1r* expression. This observation argues strongly against a functional role for *Csf1r* in neuronal progenitors[58] and instead supports that *Csf1r* is expressed and functional only in microglia[19]. So, we suggest that the reported developmental and homeostatic roles of *Csf1r*-dependent macrophages, including microglia and those of the epidermis, peritoneum, kidney, and heart are at least partly redundant. By extension, the loss of most peripheral macrophages and the associated systemic impacts of that loss must contribute to the severe brain developmental abnormality observed in $Csf1r^{-/-}$ mice[19,78]. Severe postnatal growth retardation is a shared feature of *Csf1* and *Csf1r* mutant mice and rats[4,5] and is a consequence of impacts on the growth hormone (GH)/insulin-like growth factor 1 (IGF1) axis (reviewed in ref. [79]). By contrast to the *Csf1r*-deficient mice, liver macrophages develop normally in $Csf1r^{\Delta FIRE/\Delta FIRE}$ animals (Fig. 4a and Supplementary Fig. 4a) and somatic growth, as well as the male–female sexual dimorphism in body weight gain, is unaffected by the mutation. In *Csf1* mutant rats, there was no postnatal surge in circulating IGF1[79]) and the *Csf1r* mutation in rats reduced expression of both *Ghr* and *Igf1* mRNA in the liver[5]. Circulating IGF1 in turn crosses the blood brain barrier and regulates many aspects of neuronal health (reviewed in ref. [80]).

In overview, our objective in this study was to investigate the role of a conserved enhancer in a key macrophage-expressed gene. We have confirmed the functional importance of FIRE in specific macrophage populations. In the process, we have generated a unique mouse model in which to identify non-redundant functions of specific resident tissue macrophages, especially those of the brain, heart, skin, kidney, and peritoneum, in mice that are otherwise healthy and fertile.

Methods

CRISPR design and plasmid preparation. gRNAs were designed to complement the flanking regions of the FIRE element of intron 2 (from 2646 to 3015 bp downstream of the end of exon 2; NCBI Reference Sequence: NM_001037859.2) using the online tool at http://crispr.mit.edu. Table 1 shows the guides designed, the corresponding protospacer-adjacent motif (PAM) and the complementary

Table 1 CRISPR guide RNAs

Guide	Top BbSI-flanking sequence	Guide sequence	Bottom BbSI-flanking sequence	PAM
US1-top	CACC	5′ GAGTCCCTCAGTGTGTGAGA	-	AGG
US1-bottom	-	3′ TCTCACACACTGAGGGACTC	CAAA	-
DS1-top	CACC	5′ GGGATGACACAACGGTTTCC	-	TGG
DS1-bottom	-	3′ GGAAACCGTTGTGTCATCCC	CAAA	-
DS2-top	CACC	5′ CAATGAGTCTGTACTGGAGC	-	AGG
DS2-bottom	-	3′ GCTCCAGTACAGACTCATTG	CAAA	-

US upstream FIRE, *DS* downstream FIRE, *PAM* protospacer-adjacent motif

BbSI-overhang sequences. Top and bottom oligonucleotides corresponding to each gRNA were aligned, phosphorylated, and cloned into the pSpCas9(BB)-2A-GFP (Px458) plasmid (Addgene), and transformed into competent DH5α *E. coli*. Following verification of gRNAs insertion by Sanger sequencing, plasmids were purified using endotoxin-free MaxiPrep (QIAGEN).

Cell culture. RAW 264.7 macrophages (ATCC® TIB-71™) were cultured on Sterilin-plastic dishes in RPMI 1640 medium (Sigma) supplemented with 10% endotoxin-free FBS (GE Healthcare), 2 mM GlutaMAX (Invitrogen), 25 U/mL of penicillin, and 25 µg/mL of streptomycin (Gibco). Cells were incubated at 37 °C in a 5% CO_2 humidified incubator. E14 (129P2/OlaHsd) mouse ESC (ATCC® CRL-1821™) were cultured on porcine gelatin-coated (Sigma) flasks in GMEM (Invitrogen) supplemented with 10% ESC-tested FBS (Hyclone), 2 mM GlutaMAX (Invitrogen), 1X MEM non-essential amino acids, 1 mM sodium pyruvate, 0.1 mM 2-mercaptoethanol (Gibco), and 100 U/mL leukemia inhibitory factor (LIF, Merck), at 37 °C in a 5% CO_2 humidified incubator.

Generation of CRISPR/Cas9 deletions in vitro. E14 cells were passaged twice and plated at 8×10^4 cells/cm^2 for 24 h prior to transfection. Cells were transfected with a total of 2 µg DNA (i.e. pairs of Cas9-2A-EGFP vectors, each expressing single gRNAs: US1+DS1 or DS2) using the Amaxa P3 Primary cell 4D-Nucleofector X Kit (Lonza) and incubated with supplemented GMEM for 36 h. Cells were then resuspended in Dulbecco's phosphate buffered saline (DPBS, Sigma), diluted in sterile Baxter water (TPS Healthcare/Baxter), supplemented with 2% FBS and kept at 4 °C. The GFP$^+$ cells were collected with a FACS Aria IIIu cell sorter (BD). To generate single cell clones of CRISPR-modified E14 cells, sorted pools of GFP$^+$ cells were plated on 0.1% gelatin-coated 100 mm culture dishes at a density of 18 cells/cm^2 and single colonies picked approximately 2 weeks later. RAW 264.7 cells (5×10^6) were resuspended in 250 µL of culture medium containing 10 µL of DPBS ± 20 µg DNA (as pairs of FIRE-targeting Cas9-2A-EGFP vectors, as specified above) and incubated at RT for 10 min. Electroporation was performed in 0.4 cm electroporation cuvettes (BioRad) using the BioRad Gene Pulser II (BioRad), at 320 V and a capacitance of 950 µF. Cells were cultured for 36 h and GFP$^+$ cells were single-cell sorted into polystyrene flat-bottom 96-well plates, using a FACS Aria IIIu cell sorter (BD).

PCR analysis and sequencing of transfected E14 ESC and RAW 264.7 cells. Isolation of DNA from sorted pools of GFP$^+$ cells (either E14 ESC or RAW 264.7 cells), or from cells cultured in plates other than 96-well plates was performed with the QIAGEN DNeasy Blood and Tissue Kit (QIAGEN), according to the manufacturer's instructions. Genomic DNA from single-cell-derived clones cultured in 96-well plates was isolated by adding a 1:1 mix of DirectPCR Lysis Reagent (Viagen) and nuclease-free water (Invitrogen) supplemented with 20 µg of Proteinase K (QIAGEN), per well. Cells were incubated in a heated orbital shaker at 200 rpm and 55 °C, for 12 h and Proteinase K was inactivated at 85 °C for 45 min. Conventional PCR was performed using 50 ng DNA per reaction, Taq DNA polymerase (Invitrogen) and the primers F-5′: GCTGCCCTGTCACTGTGTA and R-5′: TCGTTTCCCATCCCAGGA, at an annealing temperature of 55 °C. PCR products were run by electrophoresis to obtain a *Csf1r*$^{+/+}$ of 925 bp, or *Csf1r* $^{\Delta FIRE/\Delta FIRE}$ amplicons of either 485 bp (CRISPR pair: US1 and DS1) or 507 bp (CRISPR pair: US1 and DS2). PCR amplicons were separated by standard electrophoresis, purified with the QIAquick PCR purification kit (QIAGEN) and then sequenced using the oligonucleotides listed in Supplementary Table 1.

DNA isolation and genotyping. Mouse ear biopsies were digested overnight at 50 °C, in mouse biopsy buffer containing 100 mM Tris–HCl (Sigma) pH 8.5, 0.2% SDS (Ambion), 200 mM NaCl (Sigma), 5 mM EDTA (Ambion), and 160 µg Proteinase K (QIAGEN). Digested tissues were centrifuged at 12,000×*g* for 15 min at 4 °C and DNA was precipitated through the isopropanol–ethanol method. DNA pellets were dried at RT, resuspended in nuclease-free water and quantified using a Nanodrop™ 1000 (Thermo Fisher Scientific). PCR amplification was performed as described above and products were purified using the QIAquick PCR purification kit (QIAGEN) and sequenced using the oligonucleotides listed in Supplementary Table 1.

Phagocytosis assay. RAW 264.7 cells were cultured in high glucose DMEM (Gibco) supplemented with 10% endotoxin-free FBS (GE Healthcare) and 1 mM GlutaMAX (Life Technologies). Cells were incubated at 37 °C for 2 h in the presence of pHrodo® Red *E. coli* BioParticles® (Thermofisher) at a ratio of 100 µg/10^6 cells. Negative control samples were incubated on ice. Cells were analyzed using the BD LSR Fortessa flow cytometer. Dead cells were identified and excluded based upon DAPI uptake.

Flow cytometry. Cells were analyzed by flow cytometry using standard procedures. Inhibition of non-specific binding was achieved by incubating the cells for 30 min on ice in purified anti-CD16/32 (1 µg/mL, BioLegend, 101302) or hybridoma 2.4G2 supernatant. All antibodies are listed in Supplementary Table 2. Where indicated, cells were fixed and permeabilized prior to staining using the Leucoperm™ kit (BioRad). Blood was processed using the Uti-Lyse reagent (Agilent). Data analysis was performed in FlowJo® v10.0 (Tree Star). Gates were determined with isotype controls or FMO for all experiments.

Differentiation of ESC-derived macrophages. E14 ESCs were harvested and plated at a density of 5×10^6 cells per 50 mm Sterilin-plastic dishes, using culture medium without LIF. After 4 days, cell debris was removed using 70 µm cell strainers. Fresh culture medium containing 50 ng/mL of rhCSF1 (a gift from Chiron, USA) and 10 ng/mL of mouse recombinant interleukin 3 (IL3, Invitrogen) was added. After 7 days the culture medium was replaced to contain 100 ng/mL of rhCSF1 for 10 days, without IL3.

Generation of Csf1r$^{\Delta FIRE/\Delta FIRE}$ mice. Ethical approval was obtained from The Roslin Institute's and The University of Edinburgh's Protocols and Ethics Committees, under the authority of a UK Home Office Project License under the regulations of the Animals (Scientific Procedures) Act 1986. Mice were bred and housed under specific pathogen-free conditions. *Csf1r*$^{\Delta FIRE/\Delta FIRE}$ mice were produced by pronuclear injection of oocytes with the plasmids encoding FIRE-CRISPRs US1 and DS2 (10 µg of each) and *Cas9* mRNA. Both donor and recipient females were B6CBAF1/J (JAX™, stock number 100011). Founders were then crossed to C57BL/6 mice and their offspring interbred.

Micro CT. Micro CT was performed on formalin-fixed, paraffin-embedded decalcified femurs. Specimens were held in 1% agarose in a 20 mL universal tube before mounting in a Skyscan 1172 desktop micro CT (Bruker). The tubes were then scanned through 360° using a step of 0.28° between exposures. A voxel resolution of 6.03 µm was obtained using the following control settings: 54 kV source voltage, 185 µA source current with an exposure time of 1767 ms. A 0.5 mm aluminum filter and two frame averaging were used to optimize the scan. After scanning, the data was reconstructed using Skyscan software NRecon v1.6.9 (Bruker). The reconstruction thresholding window was optimized to encapsulate the target image, with the same values used for all bones. Reconstructed bones were oriented around their vertical axis using DataViewer v1.5.2.4 (Bruker). The trabecular region of bone 200 µm thick starting 100 µm proximal to the primary spongiosa was identified, and volumetric analysis to determine the micro-architecture of this region was performed using CTAn v1.16.4.

Histology and immunohistochemistry. Tissues were fixed in 10% neutral buffered formalin and processed into paraffin using standard procedures. For examination of tissue architecture, sections were stained with hematoxylin and eosin (H&E) or Luxol fast blue. Femurs and tails were decalcified in EDTA. Osteoclasts were detected by staining sections with the tartrate-resistant acid phosphatase (TRAP) kit (Sigma), according to instructions.

Goblet cells were stained by treating sections of small intestine with 1% periodic acid for 7 min and incubating them in Schiff's reagent for 15 min, with washes in water between steps; followed by counterstaining for 15 s with Hematoxylin.

For immunohistochemistry, antigen retrieval was performed with Proteinase K for 5 min at 37 °C prior to staining. Tissue-resident macrophages in spleen and liver sections were detected by staining with the rat anti-mouse F4/80 monoclonal antibody (1:600; AbD Serotec, MCA497G). For staining of adult brains, primary antibodies were applied overnight at 4 °C in a humid chamber. These included

chicken anti-GFAP (1:500; Cambridge Bioscience, 829401) and rabbit anti-SOX9 (1:500; Millipore, AB5535). Following three washes in PBS, fluorescently conjugated secondary antibodies were applied (1:500; Life Technologies) for 2 h at RT, then slides were counterstained with DAPI for 10 min and mounted with Fluoromount G (Cambridge Bioscience). For isolation of epidermal sheets, dissected tail skin was incubated in 2 mg/mL Dispase II (Sigma) at 37 °C for 20 min. Epidermal skin samples were fixed overnight in 4% PFA at 4 °C. After washing with TBS, samples were incubated for 1 h at RT in permeabilization buffer (PB)—TBS containing 0.25% gelatin from cold water fish skin (Sigma), 0.5% Triton X100 (Sigma), and 5% heat-treated goat serum (Sigma). Epidermal samples were then incubated in PB containing rat anti-mouse MHCII (Clone 2G9, 1:100, BD, 553621) and 1:30 goat anti-human Langerin (1:30, Thermo Fisher Scientific, PA5-47250) overnight at 4 °C. Samples were washed five times for 1 h at RT in TBS containing 0.02% Tween 20 (Fisher Scientific) (TBST) followed by incubation overnight at RT with anti-goat and anti-rat Alexa Fluour secondary antibodies (Life Technologies) diluted 1:500 in PB. After washing four times for 1 h in TBST, epidermal sheets were counterstained with DAPI (Sigma) and mounted in Prolong Gold (Life Technologies).

Frozen sections of 4% PFA perfused adult brains were processed and stained with rabbit anti-IBA1 (1:500, Wako, 019-19741), rabbit anti-P2RY12 (Sigma, 1:125, HPA013796), and Alexa Fluor® conjugated secondary antibodies using standard procedures.

Dura mater were removed into ice-cold PBS, fixed for 1 h in 4% PFA, treated for 30 min at 37 °C in PBS containing 20 mM EDTA and then blocked in 3% BSA, 0.3% Triton X100 in PBS for 30 min. Whole mount staining steps were performed in blocking buffer containing rabbit anti-IBA1 overnight (1:1000, Wako, 019-19741), goat anti-rabbit Alexa Fluor® 594 1 h (1:400, Life Technologies, A-11012), Alexa Fluor® 647 anti-mouse CD169 1 h (Clone Siglec-1, 1:200, BioLegend, 142408), with washes in buffer in between incubations. Stained tissues were then mounted onto glass slides with mounting medium and cover-slipped. Slides were imaged via a LSM710 confocal microscope (Zeiss) using Zen software.

Image acquisition and quantification. Whole-slide bright field images were acquired using the NanoZoomer slide scanner. Image analysis was performed with the NDP.view software v2.4.26 (Hamamatsu) and with ImageJ v1.46h. For spleen and liver, 10 regions of interest (ROI) were exported per sample as jpg format from the NDP.view files. Signal was quantified from the whole area corresponding to each ROI (i.e. each jpg file). For analysis of small intestine, individual villi were set as a ROI in the jpg file derived from PAS-staining. Villus perimeter, as well as the area and the number of Goblet cells (PAS^+ cells) were quantified. Measurement of villus length was performed in H&E images where 30 villi were measured per sample, from the mucosal base adjacent to the crypts to the apex, using the "ruler" function of the NDP.view v2.4.26 software. Entire brain tissue sections were imaged using a Zeiss AxioScan SlideScanner and visualized with Zen2 software. Epidermal tail sheets were imaged with a Zeiss LSM 710 confocal microscope and ZEN software. For astrocyte analysis the images were obtained by z-stacks using a Zeiss Axio Scan.Z1 (10× objective) and an Olympus 3i Spinning Disk confocal microscope (30× silicone objective) using SlideBook software. For astrocytes counts, tiff files from max projections were imported to Image J, and the images were converted to 8-bit fluorescence RGB tiff and thresholded. For nuclear counts, watershed segmentation on binary images was used to separate objects and then images were analyzed. Two fields of view were quantified and then the mean was calculated and converted to mm^2. To count the proportion of GFAP-positive cells, the number of $GFAP^+$ cells was divided by the number of $SOX9^+$ nuclei.

Blood analysis. Blood was isolated through cardiac puncture, using syringe and needle coated with 2% EDTA. Blood was collected into 2 mL EDTA tubes (BD Vacutainer®) containing 1.8 mg of EDTA per mL of blood. Total blood cell counts were performed using the ABX Pentra 60 hematology analyzer and differential counts of WBC subsets were performed on blood smears.

BM isolation and cell culture. BM was isolated by flushing femurs with RPMI containing 5 mM EDTA. For flow cytometry analysis, erythrocytes were not lysed to prevent cleavage of CSF1R. For macrophage differentiation, erythrocytes were lysed with RBC lysis buffer (BioLegend) and BM cells were cultured on Sterilin-plastic dishes in the presence of rhCSF1 (at 100 ng/mL, a gift from Chiron) for 7 days. Fresh media containing rhCSF1 was added on Day 4.

Isolation of peritoneal cells. Cells for flow cytometry analysis were isolated from mice by lavage of the peritoneal cavity with PBS. Cells were centrifuged at 400×*g* for 5 min at 4 °C prior to resuspension in PBS containing 2% endotoxin-free FBS (GE Healthcare).

Preparation of organs for flow cytometry. The spleen, liver, lung, heart, and kidneys were prepared for flow cytometry from non-perfused mice. Organs were removed, chopped finely, and digested in RPMI containing 0.625 mg/mL collagenase D (Roche), 0.85 mg/mL collagenase V (Sigma), 1 mg/mL dispase (Life Technologies), and 30 U/mL DNase (Roche) for 22 min (lung) or 45 min (other organs) in a shaking incubator at 37 °C. Organ preparations were passed through 100 µm cell strainers and centrifuged at 300×*g* for 5 min at 4 °C prior to resuspension in PBS containing 2% endotoxin-free FBS. Erythrocytes were then lysed using RBC lysis buffer (BioLegend).

Isolation of intestinal cells. Single cell suspensions of small and large intestines (colon) from non-perfused mice were prepared for flow cytometry. Intestines were opened longitudinally and cut into 2–3 cm segments in ice-cold PBS and intestinal contents removed by gentle shaking. Tissue segments were incubated at 37 °C for 20 min whilst shaking in RPMI containing 3% endotoxin-free FBS (GE Healthcare), 20 mM HEPES (Gibco), 5 mM EDTA (Sigma), 1 mM DTT (Promega), and 100 U/mL polymyxin B (Sigma). Segments were transferred to RPMI containing 2 mM EDTA and 20 mM HEPES and shaken by hand to ensure optimal dissociation of epithelial cells and lamina propria leukocytes. Tissues were minced with scissors and digested at 37 °C for 30 min, whilst shaking in RPMI containing 20 mM HEPES, 0.425 mg/mL Collagenase V (Sigma), 0.625 mg/mL Collagenase D (Roche), 1 mg/mL Dispase (Gibco), and 30 µg/mL DNase (Roche). Cell suspensions were passed through 70 µm then 40 µm cell strainers in RPMI containing 10% endotoxin-free FBS and 100 U/mL polymyxin B. After centrifugation at 400×*g* at 4 °C for 5 min, including a wash step, cells were resuspended in PBS containing 2% FBS for flow cytometry.

Myelin depletion of brains and isolation of cells. Myelin-depleted brain suspensions were prepared from saline perfused mice for flow cytometry. Whole brains were finely minced with scissors in ice-cold Hank's balanced salt solution (HBSS, Sigma, without calcium or magnesium) and centrifuged at 400×*g* for 5 min at 4 °C. Minced brains were then digested in HBSS containing 50 U/mL Collagenase IV (Gibco), 100 µg/mL Nα-Tosyl-L-lysine chloromethyl ketone hydrochloride (Sigma), 5 U/mL DNase I (Roche) and 8.5 U/mL Dispase (Gibco) for 1 h at 37 °C whilst shaking. The digested tissue was homogenized in a glass Dounce tissue grinder for 20 passes and an equal volume of HBSS containing 10% endotoxin-free FBS was then added. After centrifugation at 400×*g* for 5 min at 4 °C, the cell pellet was resuspended in 16 mL 35% Percoll in HBSS, overlaid with 10 mL HBSS and incubated on ice for 5 min. The gradient was centrifuged at 800×*g* for 45 min at 4 °C with no brake. The cell pellets were then resuspended in PBS containing 2% FBS for flow cytometry.

RNA isolation and microarrays. For RNA isolation, tissues from saline perfused mice were snap frozen, and subsequently disrupted in the Precellys24 Homogenizer® (Bertin Instruments). RNA isolation was performed using the RNeasy Plus Mini kit (QIAGEN). Library preparation and hybridization to the Affymetrix Mouse Gene 1.0 ST array was performed by Edinburgh Genomics, University of Edinburgh. CEL files were RMA normalized and annotated in R/Bioconductor. Analysis of differential expression was performed using the Affymetrix Transcription Analysis Console (Thermo Fisher).

Analysis of hippocampi microarray data. These data were interrogated with sets of genes whose expression is highly enriched in specific cell types of the brain (astrocytes, oligodendrocytes, microglia, neurons, brain endothelial cells). These sets were curated from published RNA-seq data (GEO, accession number GSE73721) describing the transcriptome of astrocytes, oligodendrocytes, microglia, neurons, and brain endothelial cells[60]. The inclusion criteria consisted of (a) being expressed at least five-fold higher in the cell type of interest than all other cell types and (b) being expressed at least 50 FPKM to enable robust detection in the mixed cell type environment of a whole hippocampus.

cDNA synthesis and quantitative real-time PCR. Complementary DNA (cDNA) was synthesized from RNA using the SuperScript III. First-Strand Synthesis System and remaining template was removed by incubation with RNase H (Invitrogen). Oligonucleotides were designed in Primer3 v4.0.0 (available at http://bioinfo.ut.ee/primer3/). Real-time qPCR reactions were performed using the Fast SYBR green master mix and the 7500 Fast System (Applied Biosystems). Analysis was performed with 7500 software v2.0.6 (Applied Biosystems, Life Technologies Corporation). For analysis of relative changes in gene expression, data were normalized according to the $2^{-\Delta\Delta CT}$ method. Hypoxanthine guanine phosphoribosyl transferase (*Hprt*) was used as a loading control/housekeeping gene. Oligonucleotide sequences are listed in Supplementary Table 3.

Reporting summary. Further information on research design is available in the Nature Research Reporting Summary linked to this article.

Data availability

The authors declare that all data supporting the findings in this study are available within the article and its Supplementary Information files or from the corresponding authors on reasonable request. The RNA expression datasets are publicly available in the gene expression omnibus (GEO; https://www.ncbi.nlm.nih.gov/gds) via the accession number GSE108207. Published ATAC-seq and ChIP-seq data used in this manuscript is available via GEO accession number GSE63341. The RNA-seq data used to curate cell type specific

genes in the brain is available via GEO accession number GSE73721. The data used to identify microglia-enriched genes versus macrophage genes is available via GEO accession number GSE48579. All other data contained within this manuscript is located in the Source Data excel file.

Received: 29 January 2019 Accepted: 15 June 2019
Published online: 19 July 2019

References

1. Sherr, C. J. et al. The c-fms proto-oncogene product is related to the receptor for the mononuclear phagocyte growth factor, CSF-1. *Cell* **41**, 665–676 (1985).
2. Garceau, V. et al. Pivotal advance: avian colony-stimulating factor 1 (CSF-1), interleukin-34 (IL-34), and CSF-1 receptor genes and gene products. *J. Leukoc. Biol.* **87**, 753–764 (2010).
3. Wang, T. et al. Identification of IL-34 in teleost fish: differential expression of rainbow trout IL-34, MCSF1 and MCSF2, ligands of the MCSF receptor. *Mol. Immunol.* **53**, 398–409 (2013).
4. Dai, X. M. et al. Targeted disruption of the mouse colony-stimulating factor 1 receptor gene results in osteopetrosis, mononuclear phagocyte deficiency, increased primitive progenitor cell frequencies, and reproductive defects. *Blood* **99**, 111–120 (2002).
5. Pridans, C. et al. Pleiotropic impacts of macrophage and microglial deficiency on development in rats with targeted mutation of the Csf1r locus. *J. Immunol.* **201**, 2683–2699 (2018).
6. MacDonald, K. P. et al. An antibody against the colony-stimulating factor 1 receptor depletes the resident subset of monocytes and tissue- and tumor-associated macrophages but does not inhibit inflammation. *Blood* **116**, 3955–3963 (2010).
7. Elmore, M. R. et al. Colony-stimulating factor 1 receptor signaling is necessary for microglia viability, unmasking a microglia progenitor cell in the adult brain. *Neuron* **82**, 380–397 (2014).
8. Rademakers, R. et al. Mutations in the colony stimulating factor 1 receptor (CSF1R) gene cause hereditary diffuse leukoencephalopathy with spheroids. *Nat. Genet.* **44**, 200–205 (2012).
9. Rojo, R., Pridans, C., Langlais, D. & Hume, D. A. Transcriptional mechanisms that control expression of the macrophage colony-stimulating factor receptor locus. *Clin. Sci.* **131**, 2161–2182 (2017).
10. Sasmono, R. T. et al. A macrophage colony-stimulating factor receptor-green fluorescent protein transgene is expressed throughout the mononuclear phagocyte system of the mouse. *Blood* **101**, 1155–1163 (2003).
11. Hawley, C. A. et al. Csf1r-mApple transgene expression and ligand binding in vivo reveal dynamics of CSF1R expression within the mononuclear phagocyte system. *J. Immunol.* **200**, 2209–2223 (2018).
12. Schulz, C. et al. A lineage of myeloid cells independent of Myb and hematopoietic stem cells. *Science* **336**, 86–90 (2012).
13. Hume, D. A., Wollscheid-Lengeling, E., Rojo, R. & Pridans, C. The evolution of the macrophage-specific enhancer (Fms intronic regulatory element) within the CSF1R locus of vertebrates. *Sci. Rep.* **7**, 17115 (2017).
14. Sauter, K. A. et al. The function of the conserved regulatory element within the second intron of the mammalian Csf1r locus. *PLoS One* **8**, e54935 (2013).
15. Balic, A. et al. Visualisation of chicken macrophages using transgenic reporter genes: insights into the development of the avian macrophage lineage. *Development* **141**, 3255–3265 (2014).
16. Rosenbauer, F. et al. Acute myeloid leukemia induced by graded reduction of a lineage-specific transcription factor, PU.1. *Nat. Genet.* **36**, 624–630 (2004).
17. Thomas, G. D. et al. Deleting an Nr4a1 super-enhancer subdomain ablates Ly6C(low) monocytes while preserving macrophage gene function. *Immunity* **45**, 975–987 (2016).
18. Evans, M. J. & Kaufman, M. H. Establishment in culture of pluripotential cells from mouse embryos. *Nature* **292**, 154–156 (1981).
19. Erblich, B., Zhu, L., Etgen, A. M., Dobrenis, K. & Pollard, J. W. Absence of colony stimulation factor-1 receptor results in loss of microglia, disrupted brain development and olfactory deficits. *PLoS One* **6**, e26317 (2011).
20. Akcora, D. et al. The CSF-1 receptor fashions the intestinal stem cell niche. *Stem Cell Res.* **10**, 203–212 (2013).
21. Sehgal, A. et al. The role of CSF1R-dependent macrophages in control of the intestinal stem-cell niche. *Nat. Commun.* **9**, 1272 (2018).
22. Pollard, J. W., Hunt, J. S., Wiktor-Jedrzejczak, W. & Stanley, E. R. A pregnancy defect in the osteopetrotic (op/op) mouse demonstrates the requirement for CSF-1 in female fertility. *Dev. Biol.* **148**, 273–283 (1991).
23. Cohen, P. E., Hardy, M. P. & Pollard, J. W. Colony-stimulating factor-1 plays a major role in the development of reproductive function in male mice. *Mol. Endocrinol.* **11**, 1636–1650 (1997).
24. Yona, S. et al. Fate mapping reveals origins and dynamics of monocytes and tissue macrophages under homeostasis. *Immunity* **38**, 79–91 (2013).
25. Kaur, S. et al. Role of bone marrow macrophages in controlling homeostasis and repair in bone and bone marrow niches. *Semin. Cell Dev. Biol.* **61**, 12–21 (2017).
26. Hettinger, J. et al. Origin of monocytes and macrophages in a committed progenitor. *Nat. Immunol.* **14**, 821–830 (2013).
27. Gow, D. J. et al. Characterisation of a novel Fc conjugate of macrophage colony-stimulating factor. *Mol. Ther.* **22**, 1580–1592 (2014).
28. Witmer-Pack, M. D. et al. Identification of macrophages and dendritic cells in the osteopetrotic (op/op) mouse. *J. Cell Sci.* **104**, 1021–1029 (1993).
29. Lieschke, G. J. et al. Mice lacking both macrophage- and granulocyte-macrophage colony-stimulating factor have macrophages and coexistent osteopetrosis and severe lung disease. *Blood* **84**, 27–35 (1994).
30. Tan, S. Y. & Krasnow, M. A. Developmental origin of lung macrophage diversity. *Development* **143**, 1318–1327 (2016).
31. Shibata, Y., Zsengeller, Z., Otake, K., Palaniyar, N. & Trapnell, B. C. Alveolar macrophage deficiency in osteopetrotic mice deficient in macrophage colony-stimulating factor is spontaneously corrected with age and associated with matrix metalloproteinase expression and emphysema. *Blood* **98**, 2845–2852 (2001).
32. Bain, C. C. et al. Constant replenishment from circulating monocytes maintains the macrophage pool in the intestine of adult mice. *Nat. Immunol.* **15**, 929–937 (2014).
33. Da Silva, C., Wagner, C., Bonnardel, J., Gorvel, J. P. & Lelouard, H. The Peyer's patch mononuclear phagocyte system at steady state and during infection. *Front. Immunol.* **8**, 1254 (2017).
34. Shaw, T. N. et al. Tissue-resident macrophages in the intestine are long lived and defined by Tim-4 and CD4 expression. *J. Exp. Med.* **215**, 1507–1518 (2018).
35. De Schepper, S. et al. Self-maintaining gut macrophages are essential for intestinal homeostasis. *Cell* **175**, 400–415 e413 (2018).
36. Bain, C. C. et al. Long-lived self-renewing bone marrow-derived macrophages displace embryo-derived cells to inhabit adult serous cavities. *Nat. Commun.* **7**, ncomms11852 (2016).
37. Alikhan, M. A. et al. Colony-stimulating factor-1 promotes kidney growth and repair via alteration of macrophage responses. *Am. J. Pathol.* **179**, 1243–1256 (2011).
38. Stamatiades, E. G. et al. Immune monitoring of trans-endothelial transport by kidney-resident macrophages. *Cell* **166**, 991–1003 (2016).
39. Lavine, K. J. et al. Distinct macrophage lineages contribute to disparate patterns of cardiac recovery and remodeling in the neonatal and adult heart. *Proc. Natl Acad. Sci. USA* **111**, 16029–16034 (2014).
40. Fujiu, K. et al. A heart-brain-kidney network controls adaptation to cardiac stress through tissue macrophage activation. *Nat. Med.* **23**, 611–622 (2017).
41. Dick, S. A. et al. Self-renewing resident cardiac macrophages limit adverse remodeling following myocardial infarction. *Nat. Immunol.* **20**, 29–39 (2019).
42. Wang, Y. et al. IL-34 is a tissue-restricted ligand of CSF1R required for the development of Langerhans cells and microglia. *Nat. Immunol.* **13**, 753–760 (2012).
43. Baranska, A. et al. Unveiling skin macrophage dynamics explains both tattoo persistence and strenuous removal. *J. Exp. Med.* **215**, 1115–1133 (2018).
44. Ginhoux, F. et al. Fate mapping analysis reveals that adult microglia derive from primitive macrophages. *Science* **330**, 841–845 (2010).
45. Grabert, K. et al. Microglial brain region-dependent diversity and selective regional sensitivities to aging. *Nat. Neurosci.* **19**, 504–516 (2016).
46. Chitu, V. et al. Phenotypic characterization of a Csf1r haploinsufficient mouse model of adult-onset leukodystrophy with axonal spheroids and pigmented glia (ALSP). *Neurobiol. Dis.* **74C**, 219–228 (2014).
47. Goldmann, T. et al. Origin, fate and dynamics of macrophages at central nervous system interfaces. *Nat. Immunol.* **17**, 797–805 (2016).
48. Van Hove, H. et al. A single-cell atlas of mouse brain macrophages reveals unique transcriptional identities shaped by ontogeny and tissue environment. *Nat. Neurosci.* **22**, 1021–1035 (2019).
49. Chakarov, S. et al. Two distinct interstitial macrophage populations coexist across tissues in specific subtissular niches. *Science* **363**, https://doi.org/10.1126/science.aau0964 (2019).
50. Galatro, T. F. et al. Transcriptomic analysis of purified human cortical microglia reveals age-associated changes. *Nat. Neurosci.* **20**, 1162–1171 (2017).
51. Gosselin, D. et al. An environment-dependent transcriptional network specifies human microglia identity. *Science* **356**, https://doi.org/10.1126/science.aal3222 (2017).
52. Elmore, M. R., Lee, R. J., West, B. L. & Green, K. N. Characterizing newly repopulated microglia in the adult mouse: impacts on animal behavior, cell morphology, and neuroinflammation. *PLoS One* **10**, e0122912 (2015).
53. Borggrewe, M. et al. VISTA expression by microglia decreases during inflammation and is differentially regulated in CNS diseases. *Glia* **66**, 2645–2658 (2018).
54. Kawai, T. et al. Unconventional role of voltage-gated proton channels (VSOP/Hv1) in regulation of microglial ROS production. *J. Neurochem.* **142**, 686–699 (2017).

55. Parkhurst, C. N. et al. Microglia promote learning-dependent synapse formation through brain-derived neurotrophic factor. *Cell* **155**, 1596–1609 (2013).
56. Prinz, M., Erny, D. & Hagemeyer, N. Ontogeny and homeostasis of CNS myeloid cells. *Nat. Immunol.* **18**, 385–392 (2017).
57. Amador-Arjona, A. et al. SOX2 primes the epigenetic landscape in neural precursors enabling proper gene activation during hippocampal neurogenesis. *Proc. Natl Acad. Sci. USA* **112**, E1936–1945 (2015).
58. Nandi, S. et al. The CSF-1 receptor ligands IL-34 and CSF-1 exhibit distinct developmental brain expression patterns and regulate neural progenitor cell maintenance and maturation. *Dev. Biol.* **367**, 100–13 (2012).
59. Oosterhof, N. et al. Homozygous mutations in CSF1R cause a pediatric-onset leukoencephalopathy and can result in congenital absence of microglia. *Am. J. Hum. Genet.* **104**, 936–947 (2019).
60. Zhang, Y. et al. Purification and characterization of progenitor and mature human astrocytes reveals transcriptional and functional differences with mouse. *Neuron* **89**, 37–53 (2016).
61. Cahoy, J. D. et al. A transcriptome database for astrocytes, neurons, and oligodendrocytes: a new resource for understanding brain development and function. *J. Neurosci.* **28**, 264–278 (2008).
62. Hoeffel, G. & Ginhoux, F. Fetal monocytes and the origins of tissue-resident macrophages. *Cell. Immunol.* **330**, 5–15 (2018).
63. Hoeffel, G. et al. C-Myb(+) erythro-myeloid progenitor-derived fetal monocytes give rise to adult tissue-resident macrophages. *Immunity* **42**, 665–678 (2015).
64. Sauter, K. A. et al. The MacBlue binary transgene (csf1r-gal4VP16/UAS-ECFP) provides a novel marker for visualisation of subsets of monocytes, macrophages and dendritic cells and responsiveness to CSF1 administration. *PLoS One* **9**, e105429 (2014).
65. Summers, K. M. & Hume, D. A. Identification of the macrophage-specific promoter signature in FANTOM5 mouse embryo developmental time course data. *J. Leukoc. Biol.* **102**, 1081–1092 (2017).
66. Lavin, Y. et al. Tissue-resident macrophage enhancer landscapes are shaped by the local microenvironment. *Cell* **159**, 1312–1326 (2014).
67. Mass, E. et al. Specification of tissue-resident macrophages during organogenesis. *Science* **353**, https://doi.org/10.1126/science.aaf4238 (2016).
68. Schridde, A. et al. Tissue-specific differentiation of colonic macrophages requires TGFbeta receptor-mediated signaling. *Mucosal Immunol.* **10**, 1387–1399 (2017).
69. Ovchinnikov, D. A., DeBats, C. E., Sester, D. P., Sweet, M. J. & Hume, D. A. A conserved distal segment of the mouse CSF-1 receptor promoter is required for maximal expression of a reporter gene in macrophages and osteoclasts of transgenic mice. *J. Leukoc. Biol.* **87**, 815–822 (2010).
70. Askew, K. et al. Coupled proliferation and apoptosis maintain the rapid turnover of microglia in the adult brain. *Cell Rep.* **18**, 391–405 (2017).
71. Cannavo, E. et al. Shadow enhancers are pervasive features of developmental regulatory networks. *Curr. Biol.* **26**, 38–51 (2016).
72. Ghisletti, S. et al. Identification and characterization of enhancers controlling the inflammatory gene expression program in macrophages. *Immunity* **32**, 317–328 (2010).
73. Buttgereit, A. et al. Sall1 is a transcriptional regulator defining microglia identity and function. *Nat. Immunol.* **17**, 1397–1406 (2016).
74. Hagemeyer, N. et al. Transcriptome-based profiling of yolk sac-derived macrophages reveals a role for Irf8 in macrophage maturation. *EMBO J.* **35**, 1730–1744 (2016).
75. Paul, F. et al. Transcriptional heterogeneity and lineage commitment in myeloid progenitors. *Cell* **164**, 325 (2016).
76. Himes, S. R., Cronau, S., Mulford, C. & Hume, D. A. The Runx1 transcription factor controls CSF-1-dependent and -independent growth and survival of macrophages. *Oncogene* **24**, 5278–5286 (2005).
77. Chitu, V. & Stanley, E. R. Regulation of embryonic and postnatal development by the CSF-1 receptor. *Curr. Top. Dev. Biol.* **123**, 229–275 (2017).
78. Bennett, F. C. et al. A combination of ontogeny and CNS environment establishes microglial identity. *Neuron* **98**, 1170–1183 e1178 (2018).
79. Gow, D. J., Sester, D. P. & Hume, D. A. CSF-1, IGF-1, and the control of postnatal growth and development. *J. Leukoc. Biol.* **88**, 475–481 (2010).
80. Gray, S. M. & Thorner, M. O. Spatiotemporal regulation of insulin-like growth factor-1 and its receptor in the brain: is there a role for growth hormone? *Endocrinology* **158**, 229–232 (2017).

Acknowledgements

This work was supported by the medical research council (MRC) UK grant MR/M019969/1. R.R. was supported by a doctoral scholarship (application number: 314413, file number: 218819) granted by CONACyT Nuevo Leon—I2T2, Mexico. J.A. was supported by Wellcome Trust grant 201531/Z/16/Z. D.A.H. and K.M.S. are supported by The Mater Foundation. P.H. was supported by the biotechnology and biological sciences research council (BBSRC) grant BB/P013732/1. D.D.O. was supported by MRC grant MR/M010341/1. C.P. is supported by the Simons Foundation Autism Research Initiative. Flow cytometry data was generated with support from the Queen's Medical Research Institute (QMRI) and Roslin Institute Flow Cytometry and cell sorting facility, University of Edinburgh. Histology data was generated with support from Easter Bush Pathology and Shared University Research Facilities at the University of Edinburgh. We thank the assistance provided by animal technicians at the University of Edinburgh, particularly Christine Marshall.

Author contributions

D.A.H. and C.P. conceived the study. P.H. and D.D.O. supervised the CRISPR/Cas9 work. R.R., D.A.H. and C.P. wrote the manuscript. K.G., E.W., V.E.M., D.A.D.M, J.P., N.A.M. and K.M.S. edited the manuscript. R.R., A.R., D.D.O., L.L., K.G., E.W., M.C., I.G., A.S., Z.M.L., J.A., B.B., I.M., H.D., R.J.L., D.A.D.M., J.D.G., R.W., S.J.J., M.B. and C.P. performed experiments. E.D. and I.A. provided ChIP-seq and ATAC-seq data. R.R., G.E.H., K.M.S., D.A.H. and C.P. analyzed data.

Additional information

Supplementary Information accompanies this paper at https://doi.org/10.1038/s41467-019-11053-8.

Competing interests: The authors declare no competing interests.

Reprints and permission information is available online at http://npg.nature.com/reprintsandpermissions/

Peer review information: *Nature Communications* thanks the anonymous reviewer(s) for their contribution to the peer review of this work. Peer reviewer reports are available.

Publisher's note: Springer Nature remains neutral with regard to jurisdictional claims in published maps and institutional affiliations.

Open Access This article is licensed under a Creative Commons Attribution 4.0 International License, which permits use, sharing, adaptation, distribution and reproduction in any medium or format, as long as you give appropriate credit to the original author(s) and the source, provide a link to the Creative Commons license, and indicate if changes were made. The images or other third party material in this article are included in the article's Creative Commons license, unless indicated otherwise in a credit line to the material. If material is not included in the article's Creative Commons license and your intended use is not permitted by statutory regulation or exceeds the permitted use, you will need to obtain permission directly from the copyright holder. To view a copy of this license, visit http://creativecommons.org/licenses/by/4.0/.

© The Author(s) 2019

Neuroscience Letters 713 (2019) 134532

Contents lists available at ScienceDirect

Neuroscience Letters

journal homepage: www.elsevier.com/locate/neulet

Review article

Astrocytes in myelination and remyelination

Irene Molina-Gonzalez, Veronique E. Miron*

Medical Research Council Centre for Reproductive Health, The Queen's Medical Research Institute, The University of Edinburgh, Edinburgh, United Kingdom

ARTICLE INFO

Keywords:
Astrocyte
Myelination
Remyelination
Oligodendrocyte
Multiple sclerosis
Microglia

ABSTRACT

Astrocytes are known to play critical roles in central nervous system development, homeostasis, and response to injury. In addition to well-defined functions in synaptic signalling and blood-brain barrier control, astrocytes are now emerging as important contributors to white matter health. Here, we review the roles of astrocytes in myelin formation and regeneration (remyelination), focusing on both direct interactions with oligodendrocyte lineage cells, and indirect influences via crosstalk with central nervous system resident macrophages, microglia.

1. Introduction

In the central nervous system (CNS), the ensheathment of axons with myelin membrane by oligodendrocytes provides insulation for efficient electrical impulse conduction and trophic/ metabolic support [1,2]. Lack of myelination (as seen in leukodystrophies) or destruction of myelin, termed demyelination (as seen in multiple sclerosis (MS), Alzheimer's disease, and motor neuron disease) contributes to axonal dysfunction and/or loss and, consequently, clinical impairments. However, myelin can be regenerated in a process termed remyelination, which restores axonal health and function [3,4]. Lineage tracing and human neuropathological tissue analysis have demonstrated that differentiation of oligodendrocyte precursor cells (OPCs) into new myelinating oligodendrocytes leads to remyelination [5,6]. In addition, recent studies suggest a potential contribution of existing mature oligodendrocytes to this process [7–9].

Both myelination and remyelination are guided in part by interaction of oligodendrocyte lineage cells with other cell types: microglia and astrocytes. Microglia are required for normal developmental myelination (in the brain), and support remyelination via phagocytosis of myelin debris and secretion of regenerative factors that drive OPC recruitment/proliferation and differentiation [10]. Much less is known regarding the contribution of the astrocyte to these processes, however, despite being the most abundant glial cell type in the CNS and its known interactions with microglia. A specific type of astrocyte is found in the white matter (termed 'fibrous'), distinct from protoplasmic astrocytes in the grey matter, Müller glia in the retina, and Bergmann glia in the cerebellum [11]. As astrocytes are considered to adapt their functions to the requirements of cells in their surroundings [12], as demonstrated by well-defined roles in regulation of synaptogenesis/ synaptic signalling [13–15], the blood-brain barrier (BBB) [16], cerebral blood flow [17,18], energy supply and metabolism [19], ion and pH homeostasis [20], and antioxidant responses and inflammation [21], it is likely that they also play significant roles in the development, homeostasis, and regeneration of white matter. Here, we review the evidence for the function of astrocytes in developmental myelination and remyelination.

2. Astrocytes in development

The investigation of astrocytes in development has in the past been challenging due to the lack of specific markers [22]. Glial fibrillary acidic protein (GFAP) has been the most widely used, however it should be noted that it only labels 30% of all astrocytes, with a very low expression in grey matter [23]. In addition, other cells such as neuronal progenitors can also express GFAP [24]. Other markers such as S100 calcium-binding protein B (S100B), aquaporin-4 (AQP4), glutamate transporter-1 (GLT-1) and glutamate aspartate transporter-1 (GLAST-1) have been used to investigate astrocytes, yet some of these can also be expressed by OPCs and ependymal cells [25]. Nonetheless, the recently identified aldehyde dehydrogenase 1 family member L1 (Aldh1l1) and Sox9 are considered to be more specific pan-astrocytic markers, the latter outside neurogenic regions [26,27].

2.1. Astrocyte origins

Astrocytes are derived from neuroepithelium, together with oligodendrocytes and neurons. Neural precursor cells in the ventricular zone

* Corresponding author at: 47 Little France Crescent, The Queen's Medical Research Institute, The University of Edinburgh, Edinburgh, EH16 4TJ, United Kingdom.
E-mail address: vmiron@ed.ac.uk (V.E. Miron).

https://doi.org/10.1016/j.neulet.2019.134532
Received 15 June 2019; Received in revised form 13 September 2019; Accepted 1 October 2019
Available online 04 October 2019
0304-3940/ © 2019 Elsevier B.V. All rights reserved.

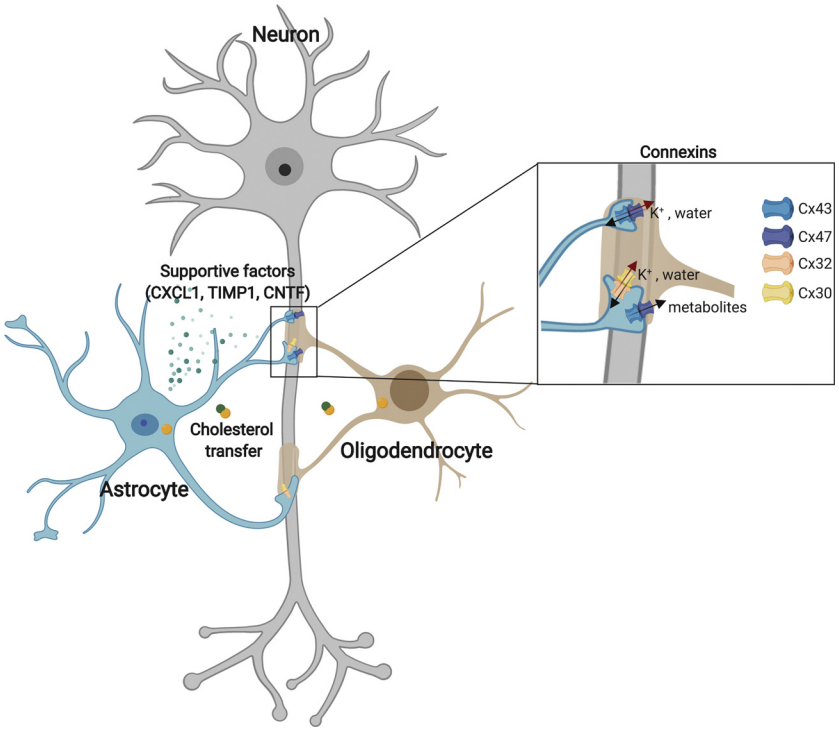

Fig. 1. Astrocytes regulate developmental myelination. Astrocytes support developmental myelination by expression of supportive factors such as C-X-C motif ligand 1, CXCL1, tissue inhibitor of metalloproteinase 1 (TIMP1), and ciliary neurotrophic factor (CNTF), transfer of cholesterol, and channels with oligodendrocytes via connexins (Cx) which allow flow of ions (K +), water and metabolites.

(VZ) differentiate into radial glia which give rise to neurons and macroglia. Neurogenesis and gliogenesis take place within a tightly regulated time-window. The switch from neurogenesis to gliogenesis is controlled by upregulation of nuclear factor I A (NFIA) and Sox9 [28–30]. Astrogenesis in the mouse brain initiates at embryonic day (E) 12.5 in the spinal cord and E16-18 in the brain [28,31], and astrocyte fate is defined by the upregulation of the transcription factor Zinc finger- and BTB domain-containing protein 20 (Zbtb20). These cells migrate throughout the CNS with support from radial glia then mature, involving changes in gene expression, morphology, connectivity and electrophysiological characteristics that in turn define their function [22,28]. Recent studies have revealed heterogeneity in the astrocyte population, with different subtypes of astrocytes seen throughout the brain [32]. These arise from distinct progenitors with specific molecular identities and localization within the neuroepithelium [33,34].

2.2. Astrocytes in developmental myelination

White matter astrocytes have small cell bodies and an elongated morphology that aligns with myelinated axons [35]. These astrocytes express higher levels of GFAP compared to protoplasmic astrocytes [36]. Further regional specialisation is present within the white matter, with spinal cord and brain astrocytes showing differential marker expression during development and in adulthood [37]. Although the functions of astrocytes in the white matter are still being defined, there is evidence that they play important roles during developmental myelination.

The capacity of astrocytes to support myelination may depend on their reactivity. Astrocytes which are activated (by treatment with ciliary neurotrophic factor; CNTF) promote *in vitro* myelination of dissociated rat spinal cord cultures, whereas quiescent astrocytes (treated with tenascin-C) inhibit myelination [38]. Astrocytes communicate with oligodendrocytes via secretion of factors that promote the onset of myelination. For instance, culturing rat optic nerve oligodendrocyte lineage cells with astrocytes promotes oligodendrocyte differentiation and extension of processes along axons, which is not observed in the absence of astrocytes [39]. Additionally, conditioned media generated from human induced pluripotent stem cell (iPSC)-derived immature astrocytes increases OPC differentiation into mature oligodendrocytes, in part via expression of tissue inhibitor metalloproteinase-1 (TIMP-1) [40]. Astrocytes also secrete CNTF, which supports *in vitro* oligodendrocyte differentiation [41] and survival [42]. Furthermore, astrocytic release of chemokine (C-X-C motif) ligand 1 (CXCL1) acts on C-X-C chemokine receptor type 2 (CXCR2) on oligodendrocyte lineage cells to promote differentiation and myelination *in vivo* [43]. Lastly, astrocytes contribute to biosynthesis and supply of lipids to oligodendrocytes during developmental myelination [44]; although postulated to occur via horizontal transfer, the mechanisms underpinning lipid transfer during myelination are still unclear.

Astrocytes directly provide oligodendrocytes with nutrients and substrates to support the metabolically-demanding process of myelin sheath formation and maintenance, via gap junctions [45]. Oligodendrocytes and astrocytes can form two different types of heterodimeric connections involved in ion/water homeostasis and energy supply, through connexin 30 (Cx30) and connexin 43 (Cx43) in astrocytes, binding to connexin 32 (Cx32) and connexin 47 (Cx47) in oligodendrocytes, respectively [45–47]. Mice lacking both Cx47 and Cx30 fail to couple oligodendrocytes to astrocytes, leading to decreased survival, reduced number of oligodendrocytes, vacuolated and thinner myelin, and severe astro- and micro-gliosis [48].

The importance of the communication between astrocytes and oligodendrocytes is further demonstrated by the disruption of this interaction leading to myelin disorders. For instance, Pelizaeus-Merzbacher-like disease is an autosomal recessive hypomyelinating condition caused by a mutation in the gene encoding Cx47, GJC2 [49], and mutations in Cx47 prevent formation of functional channels [50]. Additionally, leukodystrophies can arise from mutations in genes predominantly expressed by astrocytes, such as *GFAP*, leading to Alexander's disease [51] and NPC-1 (intracellular cholesterol transported-1), causing failure in cholesterol storage and metabolism leading to Niemann-Pick type C disease [52–54]. Another example is where hypomyelination is caused by deficiency of pyruvate carboxylase, an enzyme which in the CNS is mainly found in the mitochondria of astrocytes and controls glucogenesis, lipogenesis and insulin secretion [55–57]. Astrocytes also regulate the outcome of white matter development after perinatal insult. Transplantation of human iPSC-derived

immature astrocytes into a model of neonatal hypoxic-ischemic injury rescues hypomyelination and promotes behavioural recovery [40], and conditional ablation of STAT3 signalling in reactive astrocytes aggravates white matter injury in a model of infection-induced myelin pathology [59].

In summary, astrocytes have a vital role in communicating with oligodendrocyte lineage cells during developmental myelination, and disruption of this communication underpins myelin pathology in several neurodevelopmental disorders (Fig. 1). There are still open questions that need to be answered to fully understand the role of astrocytes in myelination, relating to potentially distinct roles of astrocytes in different white matter tracts [37], the importance of the direction of ion/ water flow through gap junctions between astrocytes and oligodendrocytes [59], and whether manipulation or transplant of astrocytes can restore healthy myelination in the context of developmental disease [60].

3. Astrocytes in remyelination

Astrocytes are also important for myelin health in the adult brain. Varela-Echevarria and colleagues (2017) observed that astrocyte processes are in contact with myelinated fibres. When opposed to areas of disrupted myelin in normal adult animals (e.g. myelin collapse or loss of myelin), these show accumulation of lysosomes containing lipid droplets or membrane-like debris [61], suggesting a role for oligodendrocyte-astrocyte contacts in myelin turnover and maintenance. In addition, reduction of exocytosis in astrocytes is associated with paranodal loop detachment, increased nodal gap length, and thinning of myelin in the optic nerve, pointing to the importance of astrocytes in maintaining myelin in homeostasis [62]. An example of this function is illustrated by the demyelination incurred from damage to astrocytes, observed in Neuromyelitis Optica (NMO) where auto-antibodies target acquaporin4 (AQP4)– expressed in astrocyte end-feet at the BBB– causing astrocyte cytotoxicity, BBB disruption, inflammation, peripheral immune cell recruitment, and demyelination [63–66]. One of the first studies to suggest a role for astrocytes in remyelination came from their transplantation into focally demyelinated spinal cord lesions, which revealed that astrocytes encourage remyelination mediated by oligodendrocytes over that by Schwann cells [67]. Subsequent studies have suggested both beneficial and deleterious functions of astrocytes following white matter injury (Fig. 2).

3.1. Pro-remyelination functions of astrocytes

In the cuprizone toxin diet model, in which widespread demyelination occurs, ablation of GFAP-expressing astrocytes impairs remyelination [68], and overexpression of GFAP reduces neuronal damage and demyelination [69]. Astrocytes may support remyelination by secreting regenerative factors, as they express CNTF [70] and osteopontin [71] during remyelination following viral- or cuprizone-induced demyelination, respectively, and these factors support oligodendrocyte lineage cell responses *in vitro* [41,42,71]. Astrocytes may also regulate remyelination through cholesterol metabolism. Dietary cholesterol promotes remyelination [72], suggested to function in part by influencing astrocyte phenotype or by encouraging their secretion of the pro-remyelination factor fibroblast growth factor 2 (FGF2) [72]. In adulthood, astrocytes are the main producers of cholesterol in the CNS. Downregulation of cholesterol biosynthesis genes in astrocytes has been observed in the context of chronic demyelination: in the autoimmune-mediated demyelination model experimental autoimmune encephalomyelitis (EAE) and in the optic chiasm in MS [73]. Cholesterol transport occurs via apolipoprotein E (ApoE) [74]; increasing cholesterol efflux to extracellular ApoE in EAE increases cholesterol synthesis gene expression and, consequently, decreases EAE severity [73]. Importantly, the upstream molecular signals that control these pro-remyelination functions of astrocytes remain unknown.

3.2. Damaging functions of astrocytes

Astrocytes have also been suggested to impair remyelination, as it was observed that their ablation after chronic cuprizone administration (which prevents remyelination) increased the number of oligodendrocyte lineage cells [75]. However, it was not shown whether these were mature oligodendrocytes, nor whether remyelination was enhanced after astrocyte depletion. Another study demonstrated that, following focal demyelination and subsequent elimination of all endogenous OPCs and astrocytes by irradiation, co-transplant of OPCs with astrocytes reduced remyelination compared to that seen following injection of OPCs alone [76].

Astrocytes may inhibit remyelination through the production of factors that inhibit oligodendrocyte lineage cell responses. For instance, astrocytic expression of the extracellular matrix component fibronectin is correlated with disease severity in EAE [77] and inhibits remyelination [78]. Additionally, reactive astrocytes express high levels of endothelin-1 (ET-1) after demyelination, which impairs remyelination [79] by induction of Jagged1 expression in reactive astrocytes, leading to blockade of OPC differentiation through Notch signalling [80]. Furthermore, astrocytes may encourage demyelination by promoting a pro- inflammatory response. Transcriptomic analysis of astrocytes in EAE reveals upregulation of genes associated with inflammation [73]. Detachment of astrocyte end feet from the vasculature coincides with areas of inflammation and T lymphocyte infiltration [80]. Astrocytes can facilitate recruitment of peripheral immune cells through the release of chemokines (*e.g.* CCL2) [81], and expression of adhesion molecules (*e.g.* VCAM-1) at the BBB [82]. Recruitment of immune cells by astrocytes may be controlled by phagocytosis of myelin debris early after injury, which leads to NFκB signalling and chemokine secretion [83,84]. Additionally, astrocytes may directly regulate T lymphocyte activation by acting as antigen presenting cells [85].

Recent studies have suggested that damaging versus beneficial functions of astrocytes are regulated by distinct phenotypes. Akin to the simplified classification of microglia into ‘M1′ (pro-inflammatory) and ‘M2′ (pro-repair) microglia/ macrophages, astrocytes have been categorized as ‘A1′ and ‘A2′. The A1 phenotype results from exposure to bacterial peptide lipopolysaccharide (LPS), which induces a pro-inflammatory gene expression profile. The ‘A2′ phenotype is found in an ischemia model, where inflammation resolves, and gene expression relates to extracellular matrix and neurotrophic support [86]. However, recent work has revealed that markers associated with the A1 phenotype do not necessarily identify a damaging astrocyte, as inhibiting the appearance of A1 astrocytes in a model of prion disease leads to a mixed A1/A2 astrocyte phenotype associated with accelerated disease course and severity [87]. Therefore, astrocyte gene expression and activation may be highly context-dependent, and how these control their damaging versus regenerative functions in white matter injury remains to be fully elucidated.

3.3. Astrocytes in multiple sclerosis

MS is the prime example of a neurological disorder with extensive demyelination and, in early phases of disease, remyelination. Astrocytes can form a ‘glial scar’ that is a hallmark of demyelinating conditions like MS, and can have either beneficial or detrimental consequences. For instance, the glial scar may limit the migration of oligodendroglial cells into demyelinated areas, thereby impeding remyelination [88]. However, the glial scar may be beneficial for limiting inflammation within MS lesions [89]. It is required for axonal regrowth in a model of severe spinal cord injury, via secretion of repair-supporting molecules [90]. More recently, it was observed that in remyelinating lesions of rat EAE, astrocytes in the glial scar express factors known to have the capacity to induce oligodendrocyte differentiation [91].

In the normal-appearing white matter (NAWM) in MS, several

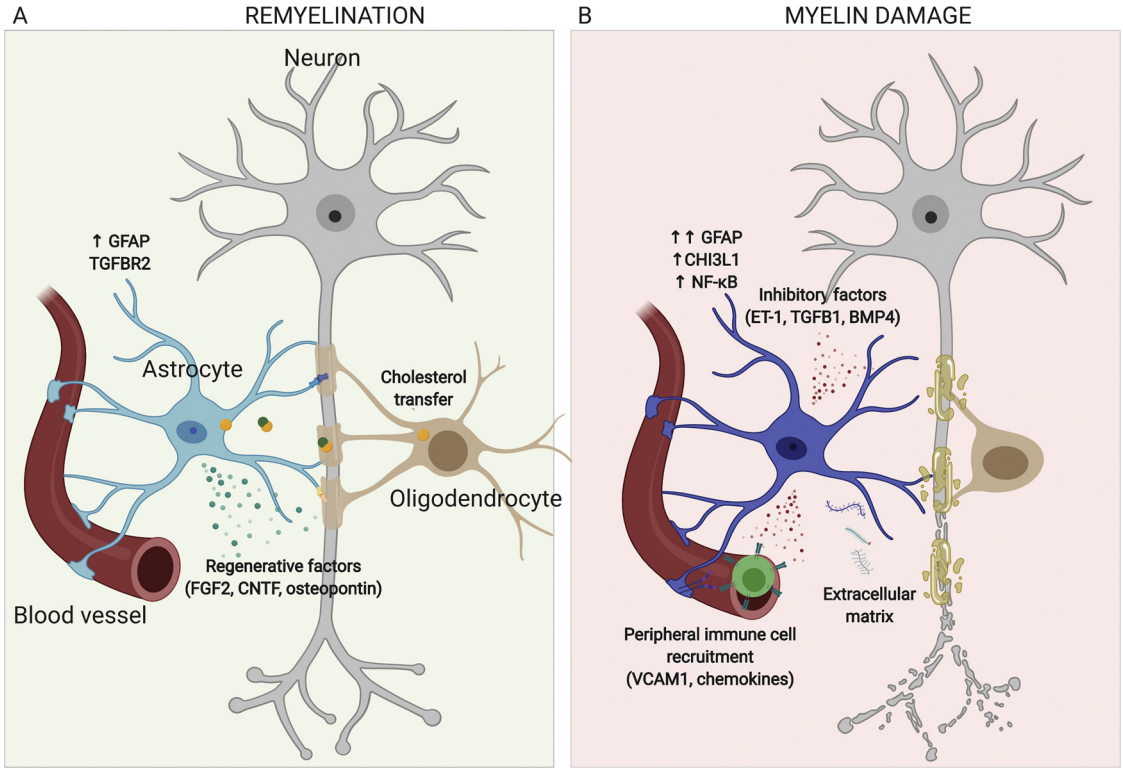

Fig. 2. Astrocytes regulate remyelination and demyelination.
A) Astrocytes support remyelination by cholesterol transfer (via ApoE) and secretion of regenerative factors such as fibroblast growth factor 2 (FGF2), ciliary neurotrophic factor (CNTF), and osteopontin. These regenerative astrocytes have increased expression of glial acidic fibrillary protein (GFAP) and transforming growth factor receptor beta 2 (TGFRβ2).
B) Astrocytes induce neural damage/ prevent repair by secretion of inhibitory factors like endothelin-1 (ET-1), transforming growth factor beta-1 (TGFβ1), and bone morphogenic protein-4 (BMP-4), facilitating recruitment of peripheral immune cells via chemokine secretion or expression of vascular cell adhesion protein 1(VCAM1), and release of inhibitory extracellular matrix components. These inhibitory astrocytes have increased expression of GFAP, chitinase 3 like 1 (CHI3L1), and increase signalling via nuclear factor kappa-light-chain enhancer or activated B cells (NFκB).

studies have suggested that astrocytes have supportive functions. Here, astrocytes upregulate genes involved in the control of iron homeostasis and neurotrophic support, indicating a neuroprotective role [92]. The regulation of iron metabolism by astrocytes is also important for remyelination; Conditional deletion of the iron efflux transporter ferroportin in all astrocytes decreases OPC proliferation and causes remyelination failure [93]. NAWM astrocytes in MS also upregulate genes that regulate oxidative responses [92]. Astrocytes have antioxidant functions mediated through the activation of the transcription factor nuclear factor E2-related factor 2 (Nrf2), which regulates the transcription of genes with antioxidant response elements (ARE) [94,95]. Nrf2 activation is neuroprotective in some neurological disorders [96]. In the cuprizone model, hyperactivation of Nrf2 in reactive astrocytes (driven by a GFAP promoter) prevents oligodendrocyte loss and demyelination [97]. However, the effects of Nrf2 signalling in remyelination have not been investigated. In the periplaque area in MS, transcriptomic analysis revealed transforming growth factor beta-1 (TGFβ1)-driven gene expression in astrocytes that may limit inflammation, yet induce astrocytosis and inhibit oligodendrocyte differentiation [98].

Within MS lesions, astrocytic responses may be lesion type-specific. For instance, astrocytes in remyelinated lesions express TGFβ-R2, but this is downregulated in chronic active lesions [99] which have poor remyelination at their core. Remyelination may also be impacted by disruption of astrocyte-oligodendrocyte connections via gap junctions [100]; In lesions in MS and NMO, a reduction of Cx43 was observed, associated with loss of astrocyte-to-oligodendrocyte connections via Cx43/Cx47 [101]. The loss of Cx43 was linked with actively progressive disease, oligodendrocyte pathology, and degenerating astrocytes, and was more often seen in patients with a rapid disease progression [101]. Remyelination may also be inhibited in MS by astrocytic expression of extracellular matrix components (such as fibronectin, chondroitin sulfate proteoglycans, and hyaluronic acid) that inhibit oligodendrocyte differentiation and impair remyelination [78,102–105]. In addition, reactive astrocytes in chronic MS lesions with poor remyelination (termed 'chronic inactive'), upregulate bone morphogenic protein (BMP)-4 [106,107], whose overexpression is known to decrease oligodendrocyte numbers in development [108]. Conversely, the BMP4 antagonist Noggin is upregulated in astrocytes in remyelinated MS lesions [106] and promotes oligodendrocyte differentiation and remyelination in the cuprizone model [107].

Astrocyte markers have been proposed as potential biomarkers for MS. For instance, CHI3L1has been suggested as an indicator for progressive MS [109], as it is expressed by astrocytes at the rim of chronic active lesions and downregulated in all other lesion types [99]. GFAP is a potential biomarker of highly active inflammation in relapse-remitting MS (RRMS) and in clinically isolated syndrome (CIS) [110]; GFAP levels are also elevated in the cerebrospinal fluid in primary progressive MS [111].

Therefore, astrocytes have been associated with both beneficial and detrimental functions in MS. Although their activation is being investigated as potential biomarkers for disease progression, a clearer indication of the roles of astrocytes at distinct stages of myelin damage and repair is needed in order to understand the biological processes associated with this activation, and how to potentially target this to enhance remyelination.

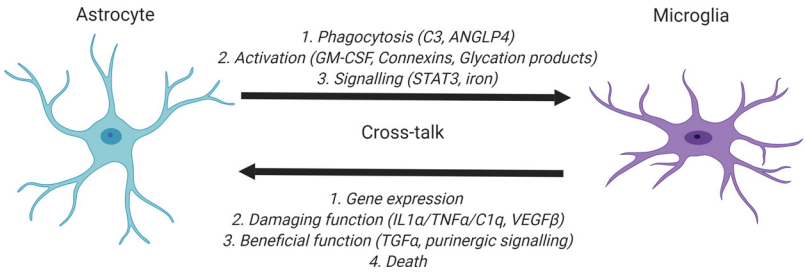

Fig. 3. Astrocyte-microglia crosstalk in white matter. Astrocytes can signal to microglia to regulate their phagocytic potential (via complement 3 (C3) and angiopoietin-like 4 (ANGLP4), activation [via granulocyte macrophage stimulating factor (GM-CSF), connexins, and glycation end products], and modulation of signalling (via STAT3 and iron pathways in astrocytes). Microglia can signal to astrocytes to alter their gene expression, induce damaging function [via secretion of interleukin-1 alpha (IL1-α), tumor necrosis factor alpha (TNFα), complement 1q (C1q), and vascular endothelial growth factor beta (VEGF-β)], induce beneficial function [via secretion of transforming growth factor alpha (TGF-α) or purinergic signalling], and induce death of astrocytes.

4. Astrocyte-microglia crosstalk following white matter injury

One cell type with which astrocytes communicate to regulate white matter health is the microglia (Fig. 3). The beneficial roles of microglia in myelination [112–114] and remyelination [68,115–117] have recently been uncovered [10]. Microglia-astrocyte interactions occur as early as in development, when microglia regulate astrocyte numbers in the retina by engulfment, which is critical for proper retinal network formation [118].

4.1. Astrocytes influencing microglia

Several studies have shown how astrocytes can regulate microglia function. First, they influence phagocytosis by microglia. Astrocytes can attract microglia through the release of CXCL10 [68,69,75], which is required for clearance of myelin debris and remyelination in the cuprizone model [68]. In a model of Alzheimer's disease, acute release of complement-3 (C3) by astrocytes promotes microglia phagocytosis, whereas chronic C3 release impairs phagocytosis and increases amyloid-beta (Aβ) pathology [119]. Astrocytes can also directly influence myelin debris clearance by microglia via expression of angiopoietin-like 4 (ANGLP4), an inhibitor of lipoprotein-lipase; reducing ANGLPL4 induces myelin debris clearance by microglia/ macrophages to enable remyelination [120].

Second, astrocytes can influence microglia activation. In EAE, transcriptomic analysis of astrocytes in the progressive phase revealed regulation of pathways that control expression of granulocyte-macrophage colony-stimulating factor (GM-CSF), which in turn modulates microglial activation [121]. In EAE, knockout of Cx30 (expressed by astrocytes) is associated with appearance of microglia with a protective phenotype (Arg-1 + , brain-derived neurotrophic factor (BDNF) + , reduced inducible nitric oxide synthase), associated with decreased neuronal death in the chronic phase [122]. On the contrary, mice lacking Cx47 have worse clinical outcome during EAE, associated with increased pro-inflammatory cytokine production by microglia and loss of myelin and axons [123]. This suggests that microglia phenotypes can be regulated by the coupling between astrocytes and oligodendrocytes. Astrocytes in MS release advanced glycation end-products, whose receptors are expressed by microglia and induce NFκB activation and pro-inflammatory cytokine release [124].

Third, astrocytes can regulate secretion of factors from microglia. In a developmental brain injury model induced by peripheral LPS injection, astrocytes restrict the production of TGFβ-1 by microglia through the activation of STAT3 signalling, which in turn regulates oligodendrocyte differentiation [58]. Additionally, iron transport regulation by astrocytes could influence microglia function, as a decrease in iron reduces microglial secretion of pro-inflammatory cytokines tumor necrosis factor alpha (TNFα) and interleukin-1 beta (IL1β) [93].

4.2. Microglia influencing astrocytes

On the other hand, microglia can influence astrocyte function. *in vitro* studies demonstrated that treatment of microglia with LPS increases secretion of IL-1α, TNFα, and complement 1q (C1q), which in turn alters astrocyte gene expression (*e.g.* upregulation of C3) and function such that they are less phagocytic, do not promote synapse formation, and are toxic to neurons and oligodendrocytes [125]. The gene expression associated with this astrocyte phenotype could be largely reproduced by LPS treatment of wildtype mice, but not in mice lacking microglia ($Csf1r^{-/-}$). This indicates the requirement of microglia-astrocyte crosstalk for these changes to take place [125].

Microglia can also induce a protective astrocyte phenotype in a traumatic brain injury model via purinergic signalling [126]. Additionally, Rothhammer and colleagues (2018) demonstrated that microglia can regulate damaging and protective astrocyte properties in EAE, where microglia-derived TGFα acting on the ErbB1 receptor on astrocytes reduces pathogenesis, whereas microglial VEGFβ triggers FLT1 signalling in astrocytes to worsen disease [127]. Microglia can also control astrocyte survival; in a model of spinal cord injury, pro-inflammatory microglia mediate astrocyte death, which is considered to be detrimental for repair [128] yet protective in dampening excessive astrogliosis [129].

5. Conclusions

In summary, astrocytes have both supportive and detrimental functions in myelination and remyelination, and their interaction with microglia may be important for controlling these processes. Future work could reveal how astrocyte heterogeneity regulates their roles in myelination and remyelination. Single-cell RNA sequencing has demonstrated subpopulations exist within specific regions [32], and after demyelination, differing levels of GFAP expression in astrocytes in brain versus spinal cord might indicate region-specific responses [37]. Furthermore, depletion of astrocytes in spinal cord cannot be rescued by astrocytes from neighbouring areas [14]. In addition, elucidating the interaction of astrocytes with other cell types, such as oligodendrocyte lineage cells and microglia, is needed prior to development of cell-type specific drugs aimed at enhancing myelin health in disease. Investigating how astrocytes can counteract damaging responses by microglia, for example via Nrf2 signalling to oppose oxidative stress– is of particular interest for the MS field due to existing drugs targeting this pathway. Given the emerging evidence for critical roles of astrocytes in white matter, further understanding of their contribution to myelin development and regeneration is pivotal for the identification of novel therapies for neurological disorders with impaired white matter integrity.

Declaration of Competing Interest

The authors have nothing to declare.

Acknowledgements

I.M.-G. is supported by a PhD studentship from the United Kingdom Multiple Sclerosis Society. V.E.M. is supported by a career development award from the Medical Research Council and the United Kingdom

Multiple Sclerosis Society [MR/M020827/1]. Diagrams were created using BioRender software.

References

[1] R.G. Almeida, D.A. Lyons, On myelinated axon plasticity and neuronal circuit formation and function, J. Neurosci. 37 (2017) 10023–10034, https://doi.org/10.1523/JNEUROSCI.3185-16.2017.

[2] C. Stadelmann, S. Timmler, A. Barrantes-freer, M. Simons, Myelin in the central nervous system: structure, function, and pathology, Physiol. Rev. 99 (2019) 1381–1431, https://doi.org/10.1152/physrev.00031.2018.

[3] R.J.M. Franklin, C. Ffrench-Constant, Regenerating CNS myelin — from mechanisms to experimental medicines, Nat. Rev. Neurosci. 18 (2017) 753–769, https://doi.org/10.1038/nrn.2017.136.

[4] I.D. Duncan, A. Brower, Y. Kondo, J.F. Curlee, R.D. Schultz, Extensive remyelination of the CNS leads to functional recovery, Proc. Natl. Acad. Sci. U. S. A. 106 (2009) 6832–6836, https://doi.org/10.1073/pnas.0812500106.

[5] M. Zawadzka, L.E. Rivers, S.P.J. Fancy, C. Zhao, R. Tripathi, K. Young, A. Goncharevich, H. Pohl, M. Rizzi, D.H. Rowitch, N. Kessaris, U. Suter, W.D. Richardson, R.J.M. Franklin, CNS-resident glial progenitor/stem cells produce schwann cells as well as oligodendrocytes during repair of CNS demyelination, Cell Stem Cell 6 (2008), https://doi.org/10.1016/j.stem.2010.04.002 678–590.

[6] T. Kuhlmann, V. Miron, Q. Cuo, C. Wegner, J. Antel, W. Brück, Differentiation block of oligodendroglial progenitor cells as a cause for remyelination failure in chronic multiple sclerosis, Brain. 131 (2008) 1749–1758, https://doi.org/10.1093/brain/awn096.

[7] S. Jäkel, E. Agirre, A.M. Falcão, D. Bruggen, K.W. Lee, I. Knuesel, D. Malhotra, A. Williams, G. Castelo-branco, Altered human oligodendrocyte heterogeneity in multiple sclerosis, Nature. 566 (2019) 543–547, https://doi.org/10.1038/s41586-019-0903-2.

[8] I.D. Duncan, A.B. Radcliff, M. Heidari, G. Kidd, B.K. August, L.A. Wierenga, The adult oligodendrocyte can participate in remyelination, PNAS. 115 (2018) 11807–11816, https://doi.org/10.1073/pnas.1808064115.

[9] M.S.Y. Yeung, M. Djelloul, E. Steiner, S. Bernard, M. Salehpour, G. Possnert, L. Brundin, J. Frisén, Dynamics of oligodendrocyte generation in multiple sclerosis, Nature. 566 (2019) 538–542, https://doi.org/10.1038/s41586-018-0842-3.

[10] V.E. Miron, Microglia-driven regulation of oligodendrocyte lineage cells, myelination, and remyelination, J. Leukoc. Biol. 101 (2017) 1103–1108, https://doi.org/10.1189/jlb.3RI1116-494R.

[11] L. Ben Haim, D. Rowitch, Functional diversity of astrocytes in neural circuit regulation, Nat. Publ. Gr. 18 (2016) 31–41, https://doi.org/10.1038/nrn.2016.159.

[12] B. Liu, A.G. Teschemacher, S. Kasparov, Neuroprotective potential of astroglia, J. Neurosci. Res. 95 (2017) 2126–2139, https://doi.org/10.1002/jnr.24140.

[13] V. Matyash, H. Kettenmann, Heterogeneity in astrocyte morphology and physiology, Brain Res. Rev. 63 (2009) 2–10, https://doi.org/10.1016/j.brainresrev.2009.12.001.

[14] H. Tsai, H. Li, L.C. Fuentealba, A.V. Molofsky, R. Taveira-marques, H. Zhuang, A. Tenney, A.T. Murnen, S.P.J. Fancy, F. Merkle, N. Kessaris, A. Alvarez-buylla, W.D. Richardson, D.H. Rowitch, Regional astrocyte allocation regulates CNS synaptogenesis and repair, Science. 337 (2012) 358–363, https://doi.org/10.1126/science.1222381.

[15] A. Araque, G. Carmignoto, P.G. Haydon, H.R. Oliet, R. Robitaille, A. Volterra, Perspective gliotransmitters travel in time and space, Neuron. 81 (2009) 728–739, https://doi.org/10.1016/j.neuron.2014.02.007.

[16] N.J. Abbott, L. Rönnbäck, E. Hansson, Astrocyte – endothelial interactions at the blood – brain barrier, Nat. Rev. Neurol. 7 (2006) 41–53, https://doi.org/10.1038/nrn1824.

[17] C. Howarth, The contribution of astrocytes to the regulation of cerebral blood flow, Front. Neurosci. 8 (2014) 1–9, https://doi.org/10.3389/fnins.2014.00103.

[18] B.A. MacVicar, E.A. Newman, Astrocyte regulation of blood flow in the brain, Cold Spring Harb. Perspect. Biol. 7 (2015) 1–15, https://doi.org/10.1101/cshpespect.at020388.

[19] A. Suzuki, S.A. Stern, O. Bozdagi, G.W. Huntley, R.H. Walker, P.J. Magistretti, C.M. Alberini, Astrocyte-neuron lactate transport is required for long-term memory formation, Cell. 144 (2011) 810–823, https://doi.org/10.1016/j.cell.2011.02.018.

[20] M.L. Olsen, B.S. Khakh, X.S.N. Skatchkov, M. Zhou, C.J. Lee, N. Rouach, New insights on astrocyte ion channels : critical for homeostasis and neuron-glia signaling, J. Neurosci. 35 (2015) 13827–13835, https://doi.org/10.1523/JNEUROSCI.2603-15.2015.

[21] A.M. Colangelo, L. Alberghina, M. Papa, Astrogliosis as a therapeutic target for neurodegenerative diseases, Neurosci. Lett. 565 (2014) 59–64, https://doi.org/10.1016/j.neulet.2014.01.014.

[22] A.V. Molofsky, B. Deneen, Astrocyte development : a guide for the perplexed, Glia. 63 (2015) 1320–1329, https://doi.org/10.1002/glia.22836.

[23] S.A. Liddelow, B.A. Barres, Reactive astrocytes: production, function, and therapeutic potential, Immunity. 46 (2017) 957–967, https://doi.org/10.1016/j.immuni.2017.06.006.

[24] E.J. Van Bodegraven, J.V. Van Asperen, P.A.J. Robe, E.M. Hol, Importance of GFAP isoform-specific analyses in astrocytoma, Glia. 67 (2019) 1417–1433, https://doi.org/10.1002/glia.23594.

[25] A.V. Molofsky, R. Krenick, E. Ullian, H. Tsai, B. Deneen, W.D. Richardson, B.A. Barres, D.H. Rowitch, Astrocytes and disease : a neurodevelopmental perspective, Genes Dev. 26 (2012) 891–907, https://doi.org/10.1101/gad.188326.112.tal.

[26] J.D. Cahoy, B. Emery, A. Kaushal, L.C. Foo, J.L. Zamanian, K.S. Christopherson, Y. Xing, J.L. Lubischer, P.A. Krieg, S.A. Krupenko, W.J. Thompson, B.A. Barres, A transcriptome database for astrocytes, neurons, and oligodendrocytes: a new resource for understanding brain development and function, J. Neurosci. 28 (2008) 264–278, https://doi.org/10.1523/JNEUROSCI.4178-07.2008.

[27] W. Sun, A. Cornwell, J. Li, S. Peng, M.J. Osorio, N. Aalling, S. Wang, A. Benraiss, N. Lou, S.A. Goldman, M. Nedergaard, Sox9 is an astrocyte-specific nuclear marker in the adult brain outside the neurogenic regions, J. Neurosci. 37 (2017) 4493–4507, https://doi.org/10.1523/JNEUROSCI.3199-16.2017.

[28] K. Reemst, S.C. Noctor, P.J. Lucassen, E.M. Hol, The indispensable roles of microglia and astrocytes during brain development, Front. Hum. Neurosci. 10 (2016) 1–28, https://doi.org/10.3389/fnhum.2016.00566.

[29] B. Deneen, R. Ho, A. Lukaszewicz, C.J. Hochstim, R.M. Gronostajski, D.J. Anderson, F. Hall, The transcription factor NFIA controls the onset of gliogenesis in the developing spinal cord, Neuron. 52 (2006) 953–968, https://doi.org/10.1016/j.neuron.2006.11.019.

[30] P. Kang, H.K. Lee, S.M. Glasgow, M. Finley, T. Donti, Z.B. Gaber, B.H. Graham, A.E. Foster, B.G. Novitch, R.M. Gronostajski, B. Deneen, Sox9 and NFIA coordinate a transcriptional regulatory cascade during the initiation of gliogenesis, Neuron. 74 (2012) 79–94, https://doi.org/10.1016/j.neuron.2012.01.024.

[31] M. Nagao, T. Ogata, Y. Sawada, Y. Gotoh, Zbtb20 promotes astrocytogenesis during neocortical development, Nat. Commun. 7 (2016) 1–14, https://doi.org/10.1038/ncomms11102.

[32] A. Zeisel, A.B. Muñoz-Manchado, S. Codeluppi, P. Lonnerberg, G. La Manno, A. Juréus, S. Marques, H. Munguba, L. He, C. Betsholtz, C. Rolny, G. Castelo-Branco, J. Hjerling-Leffler, S. Linnarsson, Brain structure. cell types in the mouse cortex and hippocampus revealed by single-cell RNA-seq, Science 347 (2015) 1138–1142, https://doi.org/10.1126/science.aaa1934.

[33] A. Zeisel, H. Hochgerner, P. Lönnerberg, A. Johnsson, F. Memic, J. der Zwan, M. Häring, E. Braun, L.E. Borm, G.L. Manno, S. Codeluppi, A. Furlan, K. Lee, N. Skene, K.D. Harris, J. Hjerling-Leffler, E. Arenas, P. Ernfors, U. Marklund, S. Linnarsson, Molecular architecture of the mouse nervous system, Cell. 174 (2018) 999–1014, https://doi.org/10.1016/j.cell.2018.06.021.

[34] C. Hochstim, B. Deneen, Q. Zhou, D.J. Anderson, Identification of positionally distinct astrocyte subtypes whose identities are specified by a homeodomain code, Cell. 133 (2008) 510–522, https://doi.org/10.1016/j.cell.2008.02.046.

[35] I. Lundgaard, M.J. Osório, B.T. Kress, S. Sanggaard, M. Nedergaard, White matter astrocytes in health and disease, Neuroscience. 276 (2014) 161–173, https://doi.org/10.1016/j.neuroscience.2013.10.050.

[36] H. Tabata, Diverse subtypes of astrocytes and their development during corticogenesis, Front. Neurosci. 9 (2015) 1–7, https://doi.org/10.3389/fnins.2015.00114.

[37] H. Yoon, G. Walters, A.R. Paulsen, I.A. Scarisbrick, Astrocyte heterogeneity across the brain and spinal cord occurs developmentally, in adulthood and in response to demyelination, PLoS Biol. (2017) 1–19, https://doi.org/10.1371/journal.pone.0180697.

[38] B. Nash, C.E. Thomson, C. Linington, A.T. Arthur, J.D. McClure, M.W. McBride, S.C. Barnett, Functional duality of astrocytes in myelination, J. Neurosci. 31 (2011) 13028–13038, https://doi.org/10.1523/JNEUROSCI.1449-11.2011.

[39] A. Meyer-Franke, S. Shen, B.A. Barres, Astrocytes induce oligodendrocyte processes to align with and adhere to axons, Mol. Cell. Neurosci. 14 (1999) 385–397.

[40] P. Jiang, C. Chen, X. Liu, D.E. Pleasure, Y. Liu, W. Deng, Human iPSC-derived immature astroglia promote oligodendrogenesis by increasing TIMP-1 secretion, Cell Rep. 15 (2016) 1303–1315, https://doi.org/10.1016/j.celrep.2016.04.011.

[41] B. Stankoff, M.S. Aigrot, F. Föet, A. Wattilliaux, B. Zalc, C. Lubetzi, Ciliary neurotrophic factor (CNTF) enhances myelin formation : a novel role for CNTF and CNTF-related molecules, J. Neurosci. 22 (2002) 9221–9227.

[42] K. Modi, S. Michael, K. Pahan, Up-regulation of ciliary neurotrophic factor in astrocytes by aspirin, J. Biol. Chem. 288 (2013) 18533–18545, https://doi.org/10.1074/jbc.M112.447268.

[43] D.A. Padovani-Claudio, L. Liu, R.M. Ransohoff, R.H. Miller, Alterations in the oligodendrocyte lineage, myelin, and white matter in adult mice lacking the chemokine receptor CXCR2, Glia. 54 (2006) 471–483, https://doi.org/10.1002/glia.20383.

[44] N. Camargo, A. Goudriaan, A.L.F. van Deijk, W.M. Otte, J.F. Brouwers, H. Lodder, D.H. Gutmann, K.A. Nave, R.M. Dijkhuizen, H.D. Mansvelder, R. Chrast, A.B. Smit, M.H.G. Verheijen, Oligodendroglial myelination requires astrocyte-derived lipids, PLoS Biol. 15 (2017) 1–24, https://doi.org/10.1371/journal.pbio.1002605.

[45] J.L. Orthmann-Murphy, Gap junctions couple astrocytes and oligodendrocytes, J. Mol. Neurosci. 35 (2009) 101–116, https://doi.org/10.1007/s12031-007-9027-5.

[46] J.E. Rash, T. Yasumura, F.E. Dudek, J.I. Nagy, Cell-specific expression of connexins and evidence of restricted gap junctional coupling between glial cells and between neurons, J.Neurosci 21 (2001) 1983–2000, https://doi.org/10.1523/JNEUROSCI.21-06-01983.2001.

[47] J. Niu, T. Li, C. Yi, N. Huang, A. Koulakoff, C. Weng, C. Li, C.J. Zhano, C. Giaume, L. Xiao, Connexin-based channels contribute to metabolic pathways in the oligodendroglial lineage, J. Cell. Sci. 129 (2016) 1902–1914, https://doi.org/10.1242/jcs.178731.

[48] O. Tress, M. Maglione, D. May, T. Pivneva, N. Richter, J. Seyfarth, S. Binder, A. Zlomuzica, G. Seifert, M. Theis, E. Dere, H. Kettenmann, K. Willecke, Panglial gap junctional communication is essential for maintenance of myelin in the CNS, J. Neurosci. 32 (2012) 7499–7518, https://doi.org/10.1523/JNEUROSCI.0392-12.2012.

[49] R. Biancheri, C. Rosano, L. Denegri, E. Lamantea, F. Pinto, F. Lanza, M. Severino, M. Filocamo, Expanded spectrum of Pelizaeus–merzbacher-like disease: literature revision and description of a novel GJC2 mutation in an unusually severe form, Eur. J. Hum. Genet. 21 (2012) 34–39, https://doi.org/10.1038/ejhg.2012.93.
[50] J.L. Orthmann-Murphy, A.D. Enriquez, C.K. Abrams, S.S. Scherer, Loss-of-function GJA12/Connexin47 mutations cause pelizaeus–merzbacher-like disease, Mol. Cell. Neurosci. 34 (2007) 629–641, https://doi.org/10.1016/j.mcn.2007.01.010.
[51] A. Lanciotti, M.S. Brignone, E. Bertini, T.C. Petrucci, F. Aloisi, E. Ambrosini, Astrocytes: emerging stars in leukodystrophy pathogenesis, Transl. Neurosci. 4 (2013) 1–37, https://doi.org/10.2478/s13380-013-0118-1.
[52] R. Von Bernhardi, Glial cells in health and disease of the CNS, Advances in Experimental Medicine, 8th ed., Cham: Springer International Publishing, 2016, https://doi.org/10.1007/978-3-319-40764-7.
[53] B. Bu, J. Li, P. Davies, I. Vincent, Deregulation of cdk5, hyperphosphorylation, and cytoskeletal pathology in the Niemann – pick type C murine model, J. Neurosci. 22 (2002) 6515–6525, https://doi.org/10.1523/JNEUROSCI.22-15-06515.2002.
[54] M. Zhang, D. Strnatka, C. Donohue, J. Hallows, I. Vincent, R.P. Erickson, Astrocyte-only Npc1 reduces neuronal cholesterol and triples life span of Npc1 −/− mice, J. Neurosci. Res. 86 (2009) 2848–2856, https://doi.org/10.1002/jnr.21730.
[55] S. Jitrapakdee, M.S. Maurice, I. Rayment, W.W. Cleland, C. Wallace, P.V. Attwood, Structure, mechanism and regulation of pyruvate carboxylase, Biochem. J. 413 (2008) 369–387, https://doi.org/10.1042/BJ20080709.
[56] E.G. Coci, V. Gapsys, N. Shur, Y. Shin-Podskarbi, B.L. de Groot, N. Shur, K. Miller, R. Ganetzky, P. Freisinger, Pyruvate carboxylase deficiency type a and type c: characterization of five novel pathogenic variants in PC and analysis of the genotype – phenotype correlation, Hum. Mutat. 40 (2019) 816–827, https://doi.org/10.1002/humu.23742.
[57] I. Marin-Valencia, C.R. Roe, J.M. Pascual, Pyruvate carboxylase deficiency : mechanisms, mimics and anaplerosis, Mol. Genet. Metab. 101 (2010) 9–17, https://doi.org/10.1016/j.ymgme.2010.05.004.
[58] H. Nobuta, C.A. Ghiani, P.M. Paez, H. Dong, R.A. Korsak, A. Manukyan, J. Li, H.V. Vinters, E.J. Huang, D.H. Rowitch, M.V. Sofroniew, A.T. Campagnoni, J. de Vellis, J.A. Waschek, STAT3-mediated astrogliosis protects myelin development in neonatal brain injury, Ann. Neurol. 72 (2012) 750–765, https://doi.org/10.1002/ana.23670.
[59] I. Fasciani, P. Pluta, D.G. Paloma, J. Molano, C.L. Paíno, O. Millet, L.C. Barrio, Directional coupling of oligodendrocyte connexin-47 and astrocyte connexin-43 gap junctions, Glia. 66 (2018) 2340–2352, https://doi.org/10.1002/glia.23471.
[60] S. Dooves, P.S. Leferink, S. Krabbenborg, N. Breeuwsma, S. Bots, A.E.J. Hillen, G. Jacobs, M.S. Van Der Knaap, V.M. Heine, Cell replacement therapy improves pathological hallmarks in a mouse model of leukodystrophy vanishing white matter, Stem Cell Reports 12 (2019) 441–450, https://doi.org/10.1016/j.stemcr.2019.01.018.
[61] A. Varela-Echevarría, V. Vargas-Barroso, C. Lozano-Flores, J. Larriva-Sahd, Is there evidence for myelin modeling by astrocytes in the normal adult brain? Front. Neuroanat. 11 (2017) 1–23, https://doi.org/10.3389/fnana.2017.00075.
[62] D.J. Dutta, D. Ho, P.R. Lee, S. Pajevic, O. Bukalo, W.C. Huffman, H. Wake, P.J. Basser, S. SheikhBahaei, V. Lazarevic, J.C. Smith, R.D. Fields, Regulation of myelin structure and conduction velocity by perinodal astrocytes, PNAS. 115 (2018) 11832–11837, https://doi.org/10.1073/pnas.1811013115.
[63] V.A. Lennon, T.J. Kryzer, S.J. Pittock, A.S. Verk, S.R. Hinson, IgG marker of opic-spinal multiple sclerosis binds to the aquaporin-4 water channel, JEM. 202 (2005) 473–477, https://doi.org/10.1084/jem.20050304.
[64] T. Vincent, P. Saikali, R. Cayrol, A.D. Roth, A. Bar-Or, A. Prat, J.P. Antel, Functional consequences of neuromyelitis optica-IgG astrocyte interactions on blood-brain barrier permeability and granulocyte recruitment, J. Immunol. 181 (2008) 5730–5737, https://doi.org/10.4049/jimmunol.181.8.5730.
[65] S.R. Hinson, I.C. Clift, N. Luo, T.J. Kryzer, V.A. Lennon, Autoantibody-induced internalization of CNS AQP4 water channel and EAAT2 glutamate transporter astrocytic Fc receptor, PNAS. 114 (2017) 5491–5496.
[66] T. Misu, K. Fujihara, S. Kakita, H. Konno, M. Nakamura, S. Watanabe, T. Takahashi, I. Nakashima, H. Takahashi, Y. Itoyama, Loss of aquaporin 4 in lesions of neuromyelitis optica: distinction from multiple sclerosis, Brain. 130 (2007) 1224–1234, https://doi.org/10.1093/brain/awm047.
[67] R.J.M. Franklin, A.J. Crang, W.F. Blakemore, Transplanted type-1 astrocytes facilitate repair of demyelinating lesions by host oligodendrocytes in adult rat spinal cord, J. Neurocytol. 20 (1991) 420–430, https://doi.org/10.1007/BF01355538.
[68] T. Skripuletz, D. Hackstette, K. Bauer, V. Gudi, R. Pul, E. Voss, K. Berger, M. Kipp, W. Baumgärtner, M. Stangel, Astrocytes regulate myelin clearance through recruitment of microglia during cuprizone-induced demyelination, Brain. 136 (2013) 147–167, https://doi.org/10.1093/brain/aws262.
[69] N. Kramann, L. Menken, R. Pförtner, S.N. Schmid, C. Wegner, W. Brück, Glial fibrillary acidic protein expression alters astrocytic chemokine release and protects mice from cuprizone-induced demyelination, Glia. 67 (2019) 1308–1319, https://doi.org/10.1002/glia.23605.
[70] P.J. Albrecht, J.C. Murtie, J.K. Ness, J.M. Redwine, J.R. Enterline, R.C. Armstrong, S.W. Levison, Astrocytes produce CNTF during the remyelination phase of viral-induced spinal cord demyelination to stimulate FGF-2 production, Neurobiol. Dis. 13 (2003) 89–101, https://doi.org/10.1016/S0969-9961(03)00019-6.
[71] R. Selvaraju, L. Bernasconi, C. Losberger, P. Graber, L. Kadi, V. Avellana-Adalid, N. Picard-Riera, A.B. Van Evercooren, R. Cirillo, M. Kosco-Vilbois, G. Feger, R. Papoian, U. Boschert, Osteopontin is upregulated during in vivo demyelination and remyelination and enhances myelin formation in vitro, Mol. Cell. Neurosci. 25 (2004) 707–721, https://doi.org/10.1016/j.mcn.2003.12.014.
[72] S.A. Berghoff, N. Gerndt, J. Winchenbach, S.K. Stumpf, L. Hosang, F. Odoardi, T. Ruhwedel, C. Böhler, B. Barrette, R. Stassart, D. Liebetanz, P. Dibaj, W. Möbius, J.M. Edgar, G. Saher, Dietary cholesterol promotes repair of demyelinated lesions in the adult brain, Nat. Commun. 8 (2017) 14241, https://doi.org/10.1038/ncomms14241.
[73] N. Itoh, Y. Itoh, A. Tassoni, E. Ren, M. Kaito, A. Ohno, Y. Ao, V. Farkhondeh, H. Johnsonbaugh, J. Burda, M.V. Sofroniew, R.R. Voskuhl, Cell-specific and region-specific transcriptomics in the multiple sclerosis model : focus on astrocytes, PNAS. 115 (2017) E302–E309, https://doi.org/10.1073/pnas.1716032115.
[74] J. Zhang, Q. Liu, Cholesterol metabolism and homeostasis in the brain, Protein Cell 6 (2015) 254–264, https://doi.org/10.1007/s13238-014-0131-3.
[75] S. Madadi, P. Pasbakhsh, F. Tahmasebi, K. Mortezaee, M. Khanehzad, F.B. Boroujeni, G. Noorzehi, I.R. Kashani, Astrocyte ablation induced by la-aminoadipate (L-AAA) potentiates remyelination in a cuprizone demyelinating mouse model, Metab. Brain Dis. 34 (2019) 593–603.
[76] W.F. Blakemore, J.M. Gilson, A.J. Crang, The presence of astrocytes in areas of demyelination influences remyelination following transplantation of oligodendrocyte progenitors, Exp. Neurol. 184 (2003) 955–963, https://doi.org/10.1016/S0014-4886(03)00347-9.
[77] K. Kamizato, S. Sato, K. Shil, B.A. Umaru, Y. Kagawa, Y. Yamamoto, M. Ogata, Y. Yasumoto, Y. Okuyama, N. Ishii, Y. Owada, H. Miyazaki, The role of fatty acid binding protein 7 in spinal cord astrocytes in a mouse model of experimental autoimmune encephalomyelitis, Neuroscience. 409 (2019) 120–129, https://doi.org/10.1016/j.neuroscience.2019.03.050.
[78] J.M.J. Stoffels, J.C. De Jonge, M. Stancic, A. Nomden, O. Maier, M.E. Van Strien, D. Ma, S. Zuzana, R.J.M. Franklin, D. Hoekstra, C. Zhao, W. Baron, Fibronectin aggregation in multiple sclerosis lesions impairs remyelination, Brain. 136 (2013) 116–131, https://doi.org/10.1093/brain/aws313.
[79] T.R. Hammong, A. Gadea, J. Dupree, C. Kerninon, B. Nait-Oumesmar, A. Aguirre, V. Gallo, Astrocyte-derived endothelin-1 inhibits remyelination through notch activation, Neuron. 81 (2014) 588–602, https://doi.org/10.1016/j.neuron.2013.11.015.
[80] R. Eilam, M. Segal, R. Malach, M. Sela, R. Arnon, R. Aharoni, Astrocyte disruption of neurovascular communication is linked to cortical damage in an animal model of multiple sclerosis, Glia. 66 (2018) 1098–1117, https://doi.org/10.1002/glia.23304.
[81] R.Y. Kim, A.S. Hoffman, N. Itoh, Y. Ao, R. Spence, M.V. Sofroniew, R.R. Voskuhl, Astrocyte CCL2 sustains immune cell infiltration in chronic experimental autoimmune encephalomyelitis, J. Neuroimmunol. 274 (2014) 53–61, https://doi.org/10.1016/j.jneuroim.2014.06.009.
[82] M.A.T. Gimenez, J.E. Sim, J.H. Russell, TNFR1-dependent VCAM-1 expression by astrocytes exposes the CNS to destructive inflammation, J. Neuroimmunol. 151 (2004) 116–125, https://doi.org/10.1016/j.jneuroim.2004.02.012.
[83] K.I. Claycomb, K.M. Johnson, P.N. Winokur, A.V. Sacino, S.J. Crocker, Astrocyte regulation of CNS inflammation and remyelination, Brain Sci. 3 (2013) 1109–1127, https://doi.org/10.3390/brainsci3031109.
[84] G. Ponath, S. Ramanan, M. Mubarak, W. Housley, S. Lee, F.R. Sahinkaya, A. Vortmeyer, C.S. Raine, D. Pitt, Myelin phagocytosis by astrocytes after myelin damage promotes lesion pathology, Brain. 140 (2017) 399–413, https://doi.org/10.1093/brain/aww298.
[85] A. Waisman, L. Johann, Antigen-presenting cell diversity for T cell reactivation in central nervous system autoimmunity, J. Mol. Med. 96 (2018) 1279–1292, https://doi.org/10.1007/s00109-018-1709-7 REVI.
[86] J. Zamanian, L. Xu, L. Foo, N. Nouri, L. Zhou, R.G. Giffard, B.A. Barres, Genomic analysis of reactive astrogliosis, J. Neurosci. 32 (2012) 6391–6410, https://doi.org/10.1523/JNEUROSCI.6221-11.2012.Genomic.
[87] K. Hartmann, D. Sepulveda-falla, I.V.L. Rose, C. Madore, C. Muth, J. Matschke, O. Butovsky, S. Liddelow, M. Glatzel, S. Krasemann, Complement 3 + -astrocytes are highly abundant in prion diseases, but their abolishment led to an accelerated disease course and early dysregulation of microglia, Acta Neuropathol. 7 (2020) 1–15, https://doi.org/10.1186/s40478-019-0735-1.
[88] P. Bannerman, A. Hahn, A. Soulika, V. Gallo, D. Pleasure, Astrogliosis in EAE spinal cord : derivation from radial glia, and relationships to oligodendroglia, Glia. 64 (2007) 57–64, https://doi.org/10.1002/glia.
[89] G. Ponath, C. Park, D. Pitt, The role of astrocytes in multiple sclerosis, Front. Immunol. 9 (2018) 1–12, https://doi.org/10.3389/fimmu.2018.00217.
[90] M.A. Anderson, J.E. Burda, Y. Ren, Y. Ao, T.M. O'Shea, R. Kawaguchi, G. Coppola, B.S. Khakh, T.J. Deming, M.V. Sofroniew, Astrocyte scar formation aids central nervous system axon regeneration, Nature. 522 (2016) 195–200, https://doi.org/10.1038/nature17623.
[91] M.H. Haindl, U. Köck, M. Zeitelhofer-Adzemovic, F. Fazekas, S. Hochmeister, The formation of a glial scar does not prohibit remyelination in an animal model of multiple sclerosis, Glia. 67 (2019) 467–481, https://doi.org/10.1002/glia.23556.
[92] R. Waller, M.N. Woodroofe, S.B. Wharton, P.G. Ince, S. Francese, P.R. Heath, A. Cudzich-Madry, R.H. Thomas, N. Rounding, B. Sharrack, J.E. Simpson, Gene expression profiling of the astrocyte transcriptome in multiple sclerosis normal appearing white matter reveals a neuroprotective role, J. Neuroimmunol. 299 (2016) 139–146, https://doi.org/10.1016/j.jneuroim.2016.09.010.
[93] K. Schulz, A. Kroner, S. David, Iron efflux from astrocytes plays a role in remyelination, J. Neurosci. 32 (2012) 4841–4847, https://doi.org/10.1523/JNEUROSCI.5328-11.2012.
[94] S.M. Ahmed, L. Luo, A. Namani, X.J. Wang, X. Tang, Nrf2 signaling pathway: pivotal roles in inflammation, Biochim. Biophys. Acta 1863 (2017) 585–597, https://doi.org/10.1016/j.bbadis.2016.11.005.
[95] M.R. Vargas, J.A. Johnson, The Nrf2 – ARE cytoprotective pathway in astrocytes, Expert Rev. Mol. Med. 11 (2009) 1–20, https://doi.org/10.1017/S1462399409001094.

[96] J.R. Liddell, Are astrocytes the predominant cell type for activation of Nrf2 in aging and neurodegeneration? Antioxidants. 6 (2017) 1–35, https://doi.org/10.3390/antiox6030065.
[97] T. Draheim, A. Liessem, M. Scheld, F. Wilms, M. Weißflog, B. Denecke, T.W. Kensler, A. Zendedel, C. Beyer, M. Kipp, C.J. Wruck, A. Fragoulis, T. Clarner, Activation of the astrocytic Nrf2 / ARE system ameliorates the formation of demyelinating lesions in a multiple sclerosis animal model, Glia. 64 (2016) 2219–2230, https://doi.org/10.1002/glia.23058.
[98] S. Nataf, M. Barritault, L. Pays, A unique TGFB1-driven genomic program links astrocytosis, low-grade inflammation and partial demyelination in spinal cord periplaques from progressive multiple sclerosis patients, Int. J. Mol. Sci. 18 (2017) 2097, https://doi.org/10.3390/ijms18102097.
[99] M.L. Elkjaer, T. Frisch, R. Reynolds, T. Kacprowski, M. Burton, T.A. Kruse, M. Thomassen, J. Baumbach, Z. Illes, Unique RNA signature of different lesion types in the brain white matter in progressive multiple sclerosis, Acta Neuropathol. Commun. 7 (2019) 1–17, https://doi.org/10.1186/s40478-019-0709-3.
[100] K.A. Kleopa, I. Sargiannidou, K. Markoullis, Connexin pathology in chronic multiple sclerosis and experimental autoimmune encephalomyelitis, Clin. Exp. Neuroimmunol. 4 (2013) 45–58, https://doi.org/10.1111/cen3.12055.
[101] K. Masaki, S.O. Suzuki, T. Matsushita, T. Matsuoka, S. Imamura, R. Yamasaki, M. Suzuki, T. Suenega, T. Iwaki, J. Kira, Connexin 43 astrocytopathy linked to rapidly progressive multiple sclerosis and neuromyelitis optica, PLoS One 8 (2013) 1–21, https://doi.org/10.1371/journal.pone.0072919.
[102] D.E. Harlow, K.E. Saul, C.M. Culp, E.M. Vesely, W.B. Macklin, Expression of proteolipid protein gene in spinal cord stem cells and early oligodendrocyte progenitor cells is dispensable for normal cell migration and myelination, J. Neurosci. 34 (2014) 1333–1343, https://doi.org/10.1523/JNEUROSCI.2477-13.2014.
[103] J.A. Sloane, C. Batt, Y. Ma, Z.M. Harris, B. Trapp, T. Vartanian, Hyaluronan blocks oligodendrocyte progenitor maturation and remyelination through TLR2, PNAS. 107 (2010) 11555–11560, https://doi.org/10.1073/pnas.1006496107.
[104] S.A. Back, T.M. Tuohy, H. Chen, N. Wallingford, A. Craig, J. Struve, N.L. Luo, F. Banine, Y. Liu, A. Chang, B.D. Trapp, B.F. Bebo, M.S. Rao, L.S. Sherman, Hyaluronan accumulates in demyelinated lesions and inhibits oligodendrocyte progenitor maturation, Nat. Me. 11 (2005) 966–972, https://doi.org/10.1038/nm1279.
[105] M. Bugiani, N. Postma, E. Polder, N. Dieleman, P.G. Scheffer, F.J. Sim, M.S. Van Der Knaap, I. Boor, Hyaluronan accumulation and arrested oligodendrocyte progenitor maturation in vanishing white matter disease, Brain. 136 (2013) 209–222, https://doi.org/10.1093/brain/aws320.
[106] K. Harnisch, S. Teuber-hanselmann, N. Macha, F. Mairinger, L. Fritsche, D. Soub, E. Meinl, A. Junker, Myelination in multiple sclerosis lesions is associated with regulation of bone morphogenetic protein 4 and its antagonist Noggin, Int. J. Mol. Sci. 20 (2019) 1–13, https://doi.org/10.3390/ijms20010154.
[107] J.K. Sabo, T.D. Aumann, D. Merlo, T.J. Kilpatrick, H.S. Cate, Remyelination is altered by bone morphogenic protein signaling in demyelinated lesions, J. Neurosci. 31 (2011) 4504–4510, https://doi.org/10.1523/JNEUROSCI.5859-10.2011.
[108] W.A. Gomes, M.F. Mehler, J.A. Kessler, Transgenic overexpression of BMP4 increases astroglial and decreases oligodendroglial lineage commitment, Dev. Biol. 255 (2003) 164–177, https://doi.org/10.1016/S0012-1606(02)00037-4.
[109] E. Cantó, F. Reverter, F. Matesanz, O. Fernández, G. Izquierdo, K. Vandenbroeck, A. Rodríguez-Antigüedad, E. Urcelay, R. Arroyo, D. Otaegui, J. Olascoaga, A. Saíz, A. Navarro, A. Sánchez, C. Domínguez, A. Caminero, A. Horga, M. Tintoré, X. Montalban, M. Comabella, Chitinase 3-like 1 plasma levels are increased in patients with progressive forms of multiple sclerosis, Mult. Scler. J. 18 (2012) 983–990, https://doi.org/10.1177/1352458511433063.
[110] R. Kassubek, M. Gorges, M. Schocke, V.A.M. Hagenston, A. Huss, A.C. Ludolph, J. Kassubek, H. Tumani, GFAP in early multiple sclerosis: a biomarker for inflammation, Neurosci. Lett. 657 (2017) 166–170, https://doi.org/10.1016/j.neulet.2017.07.050.
[111] M.A. Mañé-Martínez, B. Olsson, L. Bau, E. Matas, Á. Cobo-Calvo, U. Andreasson, K. Blennow, L. Romero-Pinel, S. Martínez-Yélamos, H. Zetterberg, Glial and neuronal markers in cerebrospinal fluid in different types of multiple sclerosis, J. Neuroimmunol. 299 (2016) 112–117, https://doi.org/10.1016/j.jneuroim.2016.08.004.
[112] B. Erblich, L. Zhu, A.M. Etgen, K. Dobrenis, J.W. Pollard, Absence of colony stimulation factor-1 receptor results in loss of microglia, disrupted brain development and olfactory deficits, PLoS One 6 (2011) 1–13, https://doi.org/10.1371/journal.pone.0026317.
[113] N. Hagemeyer, K.M. Hanft, M.A. Akriditou, N. Unger, E.S. Park, E.R. Stanley, O. Staszewski, L. Dimou, M. Prinz, Microglia contribute to normal myelinogenesis and to oligodendrocyte progenitor maintenance during adulthood, Acta Neuropathol. 134 (2017) 441–458, https://doi.org/10.1007/s00401-017-1747-1.
[114] A. Wlodarczyk, I.R. Holtman, M. Krueger, N. Yogev, J. Bruttger, R. Khorooshi, A. Benmamar-badel, J.J. de Boer-Bergsma, N.A. Martin, K. Karram, I. Kramer, E.W. Boddeke, A. Waisman, B.J. Eggen, T. Owens, A novel microglial subset plays a key role in myelinogenesis in developing brain, EMBO J. 36 (2017) 3292–3308, https://doi.org/10.15252/embj.201696056.
[115] M. Olah, S. Amor, N. Brouwer, J. Vinet, B. Eggen, K. Biber, H.W. Boddeke, Identification of a microglia phenotype supportive of remyelination, Glia. 60 (2012) 306–321, https://doi.org/10.1002/glia.21266.
[116] V.E. Miron, A. Boyd, J.W. Zhao, T.J. Yuen, J.M. Ruckh, J.L. Shadrach, P. van Wijngaarden, A.J. Wagers, A. Williams, R.J.M. Franklin, C. Ffrench-Constant, M2 microglia and macrophages drive oligodendrocyte differentiation during CNS remyelination, Nat. Neurosci. 16 (2013) 1211–1218, https://doi.org/10.1038/nn.3469.
[117] A. Lampron, A. Larochelle, N. Laflamme, P. Préfontaine, M.M. Plante, M.G. Sánchez, V.W. Yong, P.K. Stys, M.È. Tremblay, S. Rivest, Inefficient clearance of myelin debris by microglia impairs remyelinating processes, J. Exp. Med. 212 (2015) 481–495, https://doi.org/10.1084/jem.20141656.
[118] V.M. Puñal, C.E. Paisley, F.S. Brecha, M.A. Lee, R.M. Perelli, E.G.O. Koren, R. Caroline, D.R. Saban, B.E. Reese, J.N. Kay, Large-scale death of retinal astrocytes during normal development mediated by microglia, bioRxiv. (2019) 1–12, https://doi.org/10.1101/593731.
[119] H. Lian, A. Litvinchuk, A.C.-A. Chiang, N. Aithmitti, J.L. Jankowsky, H. Zheng, Astrocyte-microglia cross talk through complement activation modulates amyloid pathology in mouse models of alzheimer's disease, J. Neurosci. 36 (2016) 577–589, https://doi.org/10.1523/JNEUROSCI.2117-15.2016.
[120] A. Kamermans, M. Rijnsburger, A. Chakraborty, S. Van Der Pol, H.E. de Vries, J. van Horssen, Reduced angiopoietin-like 4 expression in multiple sclerosis lesions facilitates lipid uptake by phagocytes via modulation of lipoprotein-lipase activity, Front. Immunol. 10 (2019) 1–8, https://doi.org/10.3389/fimmu.2019.00950.
[121] L. Mayo, S.A. Trauger, M. Blain, M. Nadeau, B. Patel, J.I. Alvarez, I.D. Mascanfroni, A. Yeste, P. Kivisäkk, K. Kallas, B. Ellezam, R. Bakshi, A. Prat, J.P. Antel, H.L. Weiner, F.J. Quintana, Regulation of astrocyte activation by glycolipids drives chronic CNS inflammation, Nat. Med. 20 (2014) 1147–1156, https://doi.org/10.1038/nm.3681.
[122] M. Fang, R. Yamasaki, G. Li, K. Masaki, H. Yamaguchi, A. Fujita, N. Isobe, J. Kira, Connexin 30 deficiency attenuates chronic but not acute phases of experimental autoimmune encephalomyelitis through induction of neuroprotective microglia, Front. Immunol. 9 (2018) 1–19, https://doi.org/10.3389/fimmu.2018.02588.
[123] C.P. Papaneophytou, E. Georgiou, C. Karaiskos, I. Sargiannidou, K. Markoullis, M.M. Freidin, C.K. Abrams, K.A. Kleopa, Regulatory role of oligodendrocyte gap junctions in inflammatory demyelination, Glia. 66 (2018) 2589–2603, https://doi.org/10.1002/glia.23513.
[124] S. Wetzels, T. Vanmierlo, J.L.J.M. Scheijen, J. Van Horssen, S. Amor, V. Somers, C.G. Schalwijk, J.J.A. Hendriks, K. Wouters, Methylglyoxal-derived advanced glycation endproducts accumulate in multiple sclerosis lesions, Front. Immunol. 10 (2019) 1–9, https://doi.org/10.3389/fimmu.2019.00855.
[125] S.A. Liddelow, K.A. Guttenplan, L.E. Clarke, F.C. Bennett, C.J. Bohlen, L. Schirmer, M.L. Bennett, A.E. Münch, W.-S. Chung, T.C. Peterson, D.K. Wilton, A. Frouin, B.A. Napier, N. Panicker, M. Kumar, M.S. Buckwalter, D.H. Rowitch, V.L. Dawson, T.M. Dawson, B. Stevens, B.A. Barres, Neurotoxic reactive astrocytes are induced by activated microglia, Nature. 541 (2017) 481–487, https://doi.org/10.1038/nature21029.
[126] Y. Shinozaki, K. Shibata, K. Yoshida, E. Shigetomi, C. Gachet, K. Ikenaka, K.F. Tanaka, S. Koizumi, Transformation of astrocytes to a neuroprotective phenotype by microglia via P2Y1 receptor downregulation, Cell Rep. 19 (2017) 1151–1164, https://doi.org/10.1016/j.celrep.2017.04.047.
[127] V. Rothhammer, D.M. Borucki, E.C. Tjon, M.C. Takenaka, C. Chao, A. Ardura-fabregat, K.A. De Lima, C. Gutiérrez-Vázquez, P. Hewson, O. Staszewski, M. Blain, L. Healy, T. Neziraj, M. Borio, M. Wheeler, L.L. Dragin, D.A. Laplaud, J. Antel, J.I. Alvarez, M. Prinz, F.J. Quintana, Microglial control of astrocytes in response to microbial metabolites, Nature. 557 (2018) 724–728, https://doi.org/10.1038/s41586-018-0119-x.
[128] H. Fan, K. Zhang, L. Shan, F. Kuang, K. Chen, K. Zhu, H. Ma, G. Ju, Y.Z. Wang, Reactive astrocytes undergo M1 microglia/macrohpages-induced necroptosis in spinal cord injury, Mol. Neurodegener. 11 (2016) 14, https://doi.org/10.1186/s13024-016-0081-8.
[129] C. Quintas, D. Pinho, C. Pereira, L. Saraiva, J. Gonçalves, G. Queiroz, Microglia P2Y6 receptors mediate nitric oxide release and astrocyte apoptosis, J. Neuroinflammation 11 (2014) 141, https://doi.org/10.1186/s12974-014-0141-3.